The Electrohydraulic Effect On The Fracture of Rock

by

Philip Edward Haskell

June 1971

Department of Mining and Mineral Technology

Royal School of Mines

Imperial College of Science and Technology

University of London

CORRECTIONS

The text should be corrected in the following places:

Page 13 - Paragraph 3: The second sentence should read:

The program does not agree precisely with the observations by Smith below although the trend is similar. It is thought that the observations are the best practical guide available as the discrepancy is due to the assumptions in the model (see appendix 2).

Page 16: add:

t = time

where t = 0 at the time of arrival of the stress pulse at the joint.

Page 20: add:

Capacity = .1 uf Voltage = 35 KV

Page 37 - Paragraph 7: . . . optimum spark machines for grinding

Page 51 Section 6.5, insert:-

It should be noted that the following use of tensor technique is treated tentatively and is based on analogy rather than rigid proof. It has been used because, insofar as it is valid, it facilitates manipulation of the matrices involved in the process models.

Page 86: End of paragraph 1, and in all following text: delete pseudo in pseudo eluclidean space.

"Abstract"

Studies were carried out on the fracture of rock by the electrohydraulic effect: considering the electrohydraulic effect from the basis of its operation to the development of its use in a complete plant.

A theoretical model of the breakdown of water is developed and shows reasonable agreement with experimental values of the breakdown time-lag field relationship.

The spark pressure on a solid was measured and found to be of the order of 12,500 atmospheres.

A new comminution mechanism by surface waves is considered for electrohydraulic comminution and computer techniques to study dynamic stress analysis and fractures are developed.

The performance of electrohydraulic crushers is considered and design criteria defined. Bond's Index and Kick's Constant were found to be correlated with uniaxial compressive strength but not with point load strength. Bond's Index and Kick's Constant were found to be independent of water conductivity.

A tensor method of describing mineral processes is developed and examples given for the analysis of shape in jaw crushing, the analysis of a complete plant and the dynamics of grinding circuits.

An extensive bibliography of the fields considered is appended.

Index

		Page
	Abstract	1
	Index	2
1	Introduction	5
	1.1 Acknowledgements	7
2	The Breakdown of Water	9
	2.1 Introduction	9
	2.2 Experiments	9
	2.3 Theory	12
3	The Generation of Pressure by the Spark	15
	3.1 Introduction	15
	3.2 Momentum Experiment	15
4	Stress Analysis	21
	4.1 Introduction	21
	4.2 Surface Waves	22
	4.3 Numerical Methods and Results	31
	4.4 Criteria of Efficiency	32
	4.5 Fractures	33
5	Comminution	35
	5.1 Introduction	35
	5.2 Electrohydraulic Comminution Efficiency	35
	5.3 Discharge Parameters	36
	5.4 Optimum Coupling Design Principles	38
	5.5 Experiments	39
6	Mineral Process Models	44
	6.1 Introduction	44

(Continued .....)

		Page
6.2	Novel features of electrohydraulic comminution	44
6.3	The traditional approach to modelling	48
6.4	The philosophy of plant modelling	50
6.5	Size and Shape - An example of the tensor method	51
6.6	Shape Experiments	58
6.7	Notation and Algebra	61
	6.7.1 Reduction of primary axes	89
	6.7.2 The Process	90
	6.7.3 Control	92
	6.7.4 Plant Dynamics	93
	6.7.5 Non-Linearity	95
	6.7.6 Constraint	95
6.8	Addition of flows	98
6.9	Simplification in the time domain	99
6.10	Primary and secondary spaces and the basis set	100
6.11	Control of the incompletely observed process	102
6.12	A tensor approach to the unit process	103
	6.12.1 Design by empirical methods	104
	6.12.2 Design by first principles	105
6.13	Examples	106
	6.13.1 Complete plant analysis	106
	6.13.2 Dynamics of grinding	107
	6.13.3 Dynamics of a change of grindability	111
7	Suggestions for further work	113

(Continued .....)

Appendices

		Page
1	Apparatus for the measurement of the breakdown time-lag in water	115
2	Computer model of the breakdown process in water	118
3	Dynamic relaxation	135
4	Capacitor charging	147
5	Switching techniques	152
6	Electrohydraulic crushing technique	156
7	Einstein's Convention	158
8	Bibliography	159
9	List of figures	212

Part 1 - Introduction

When a high voltage is applied to a pair of underwater electrodes there is a short period of ionic conduction until the water gap breaks down. When the gap has broken down a high-temperature, high-pressure, conducting plasma is formed. This plasma expands and generates a fast rise-time load upon the rock. Stress waves are induced into the rock and fracture may occur. Rock crushing machines may be constructed using this principle and offer many novel features. The use of these features must be evaluated by considering the crusher as part of a mineral processing system.

When the research work on this thesis was begun it was found that there was a great deal of qualitative data available. The author was not able to decide in which field he should concentrate his research as there was no indication of the relative significance of the various phenomena. The author has therefore studied each of the processes involved and considers that this work will enable future researchers to concentrate their efforts on the more significant features of electrohydraulic comminution.

It is considered that this thesis will be of use in related fields, particularly in high voltage engineering, blasting and process control.

The thesis is in seven major sections.

(Continued .....)

Section 1 introduces the thesis and abstracts the whole work.

Section 2 considers the electrical breakdown of water both experimentally and theoretically.

Section 3 considers the generation of shock waves and determines the spark pressure on surfaces experimentally.

Section 4 considers the propagation of stresses through rock and the generation of fractures.

Section 5 discusses the design of electrohydraulic crushers and evaluates the performance of a simple optimum coupling crusher.

Section 6 describes a new theoretical approach to the modelling of mineral processes.

Section 7 makes suggestions for further work.

1.1 Acknowledgements

The author would like to thank all persons and organisations who have helped in this research project and in the preparation of this thesis.

In particular:

Messrs Atlas Copco AB Stockholm, Sweden	Who generously sponsored this work and who have taken a lively interest in it.
Mr. H. A. Johnston Dept. Mining & Mineral Technology Imperial College, London	My supervisor, for his guidance which, with his long experience of electro-hydraulic comminution and of mining generally, has been of great value.
Mr. C. H. J. Beaven Dept. Mining & Mineral Technology Imperial College, London	For the many conversations during which the basis for the breakdown theory, process modelling and other mathematical aspects of the thesis were evolved.
Mr. M. P. Jones Dept. Mining & Mineral Technology Imperial College, London	For his help in mineral dressing problems.
Mr. H. Fairbrother Dept. Mathematics Imperial College, London	For his help with statistical theory.
Dr. J. Franklin Dept. Rock Mechanics Imperial College, London	For supplying rock and measuring rock strengths.
Dr. B. Lundqvist and Dr. N. H. Hall Taylor Atlas Copco AB Stockholm, Sweden	For their suggestions, advice and friendly cooperation.

(Continued .....)

Professor R. N. Pryor and Professor M. G. Fleming Dept. Mining & Mineral Technology Imperial College, London	For the use of the facilities of the Department of Mining and Mineral Technology
The Imperial College Computer Centre and University of London Computer Centre	For the use of their computers and the help of their staff.
Messrs Shawki, Sullivan and Soussmann and the staffs of their respective workshops	For their help in constructing and conducting experiments.
Mrs. J. Smith and Mr. B. Holt	Who respectively typed and reproduced this thesis.

2 - The Electrical Breakdown of Water

2.1 Introduction

Photographic work (reference 99) has shown that water breaks down by a streamer mechanism. When voltage is applied to a water gap, streamers start out from each electrode; when either two streamers meet or a streamer crosses the gap, a conducting path is established between the electrodes and the main discharge begins. The streamer velocity is dependant on the field, the positive streamer moving approximately twice as fast as the negative streamer (reference 169).

Because of the streamer mechanism, water exhibits a breakdown time-lag. During the time-lag energy is lost by ionic conduction in the water and it has been postulated by Carley-Macauly et al (reference 44) that this lost energy causes a significant part of the inefficiency in electrohydraulic comminution. This section of the thesis reports some experiments, and analyses theoretically the breakdown time-lags in water.

2.2 Experimental Work

The breakdown time-lag in a sphere-plane (+ve sphere) gap was measured using the apparatus described in Appendix 1. Some 200 observations were made at each voltage. The sphere was 2.5 cms in diameter and the gap was 3.17 mms. The field was calculated from:-

(Continued .....)

$$F_{max} = \frac{v\left(\frac{x}{2r} + 1 + \sqrt{\left(\frac{x}{2r} + 1\right)^2 + 8}\right)}{4x}$$

r = radius of sphere

x = gap length

v = voltage

Fmax = maximum electric field

The results are tabulated in Table 2/1.

The voltage-breakdown time relation is plotted in Figure 2/1. The standard deviation of breakdown time-lag is plotted against breakdown time in Figure 2/2. Histograms of the breakdown time-lags are plotted in Figures 2/3 to 2/6.

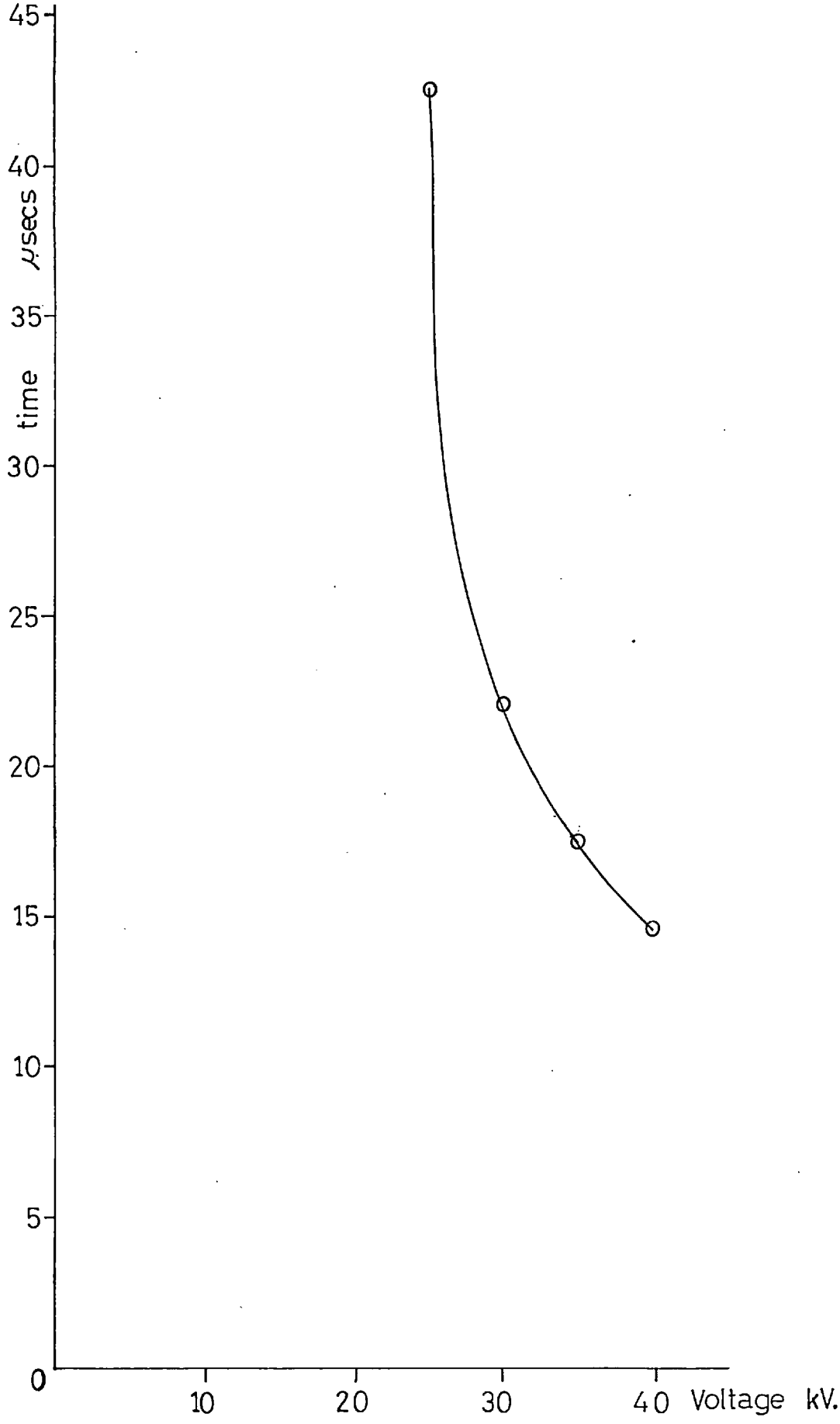
The water used was clean, demineralized water having a conductivity of 12 micromhos per centimetre. Mild steel electrodes were used.

It was found that at the lower voltages breakdown did not always occur. However, if, after trying at 25kv the gap did not break down, the voltage was raised to 40kv and the gap fired, thereafter attempting a 25kv breakdown was nearly always successful. The gap would then break down for the next 5 or so trials and then would cease to break down until a 40kv shot had been fired.

Discussion of Results

The breakdown time-lags showed considerable variation; this feature is well known in the breakdown of liquids. The breakdown time-lag decreased with increasing voltage as was expected. A

(Continued .....)



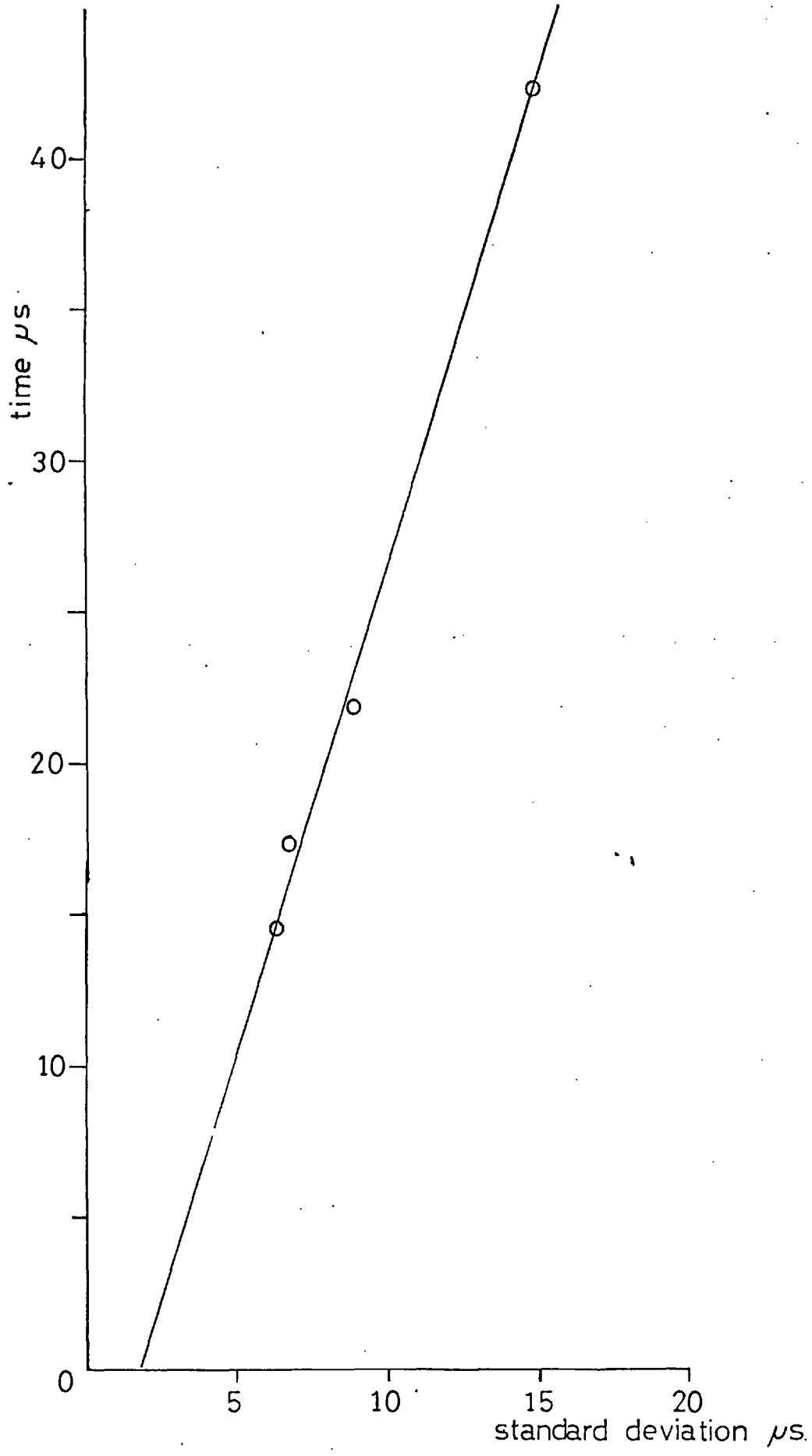
Breakdown time-lag versus voltage

figure 2/1

Table 2/1

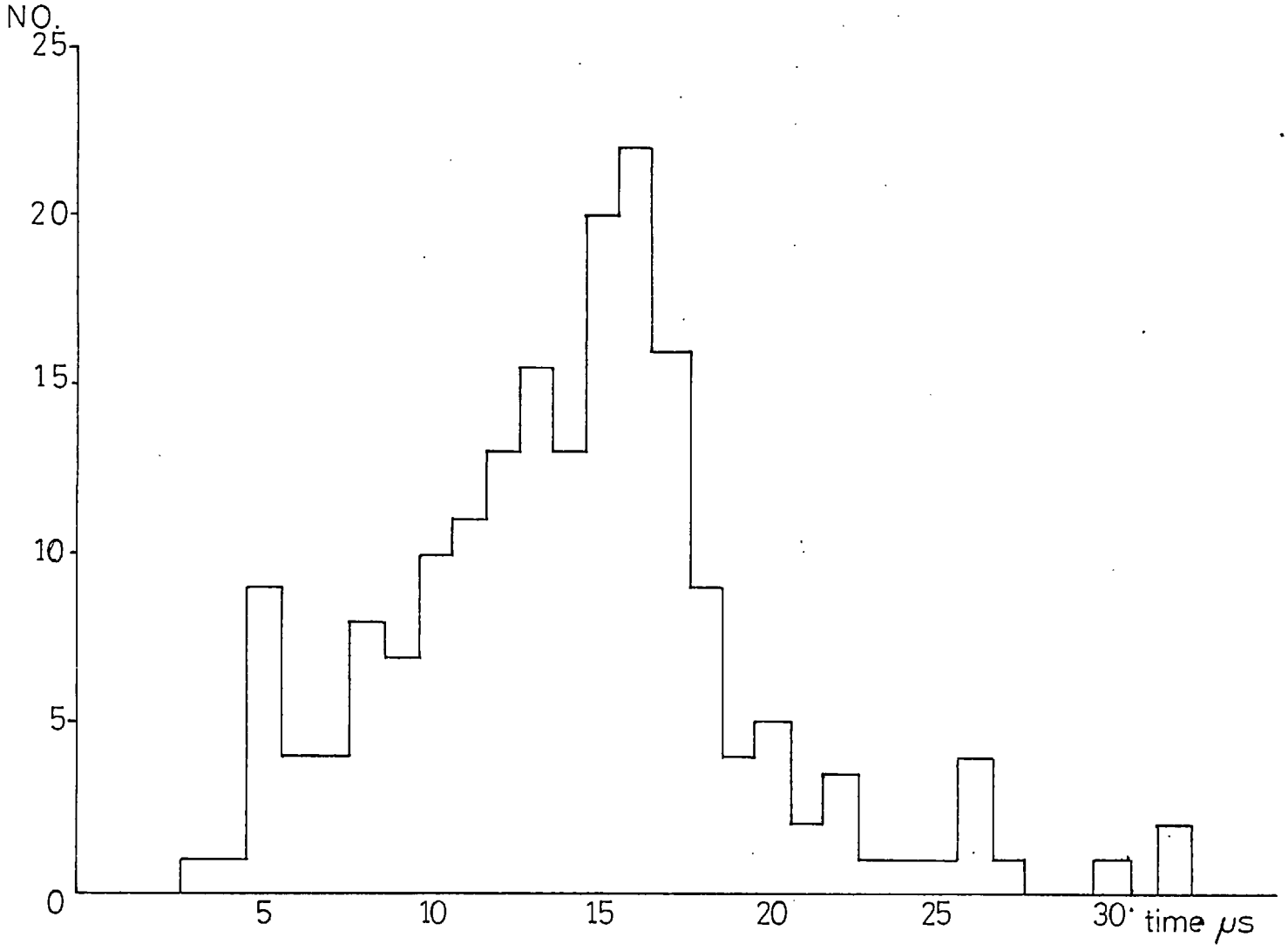
Breakdown Time-Lags in a Sphere Plane Gap

Voltage KV	Field MV/m	Time-Lag μSec	Standard Deviation of Time μSec
40	13·15	14·6	6·3
35	11·5	17·4	6·7
30	9·86	22·1	9·1
25	8·22	42·5	14·9



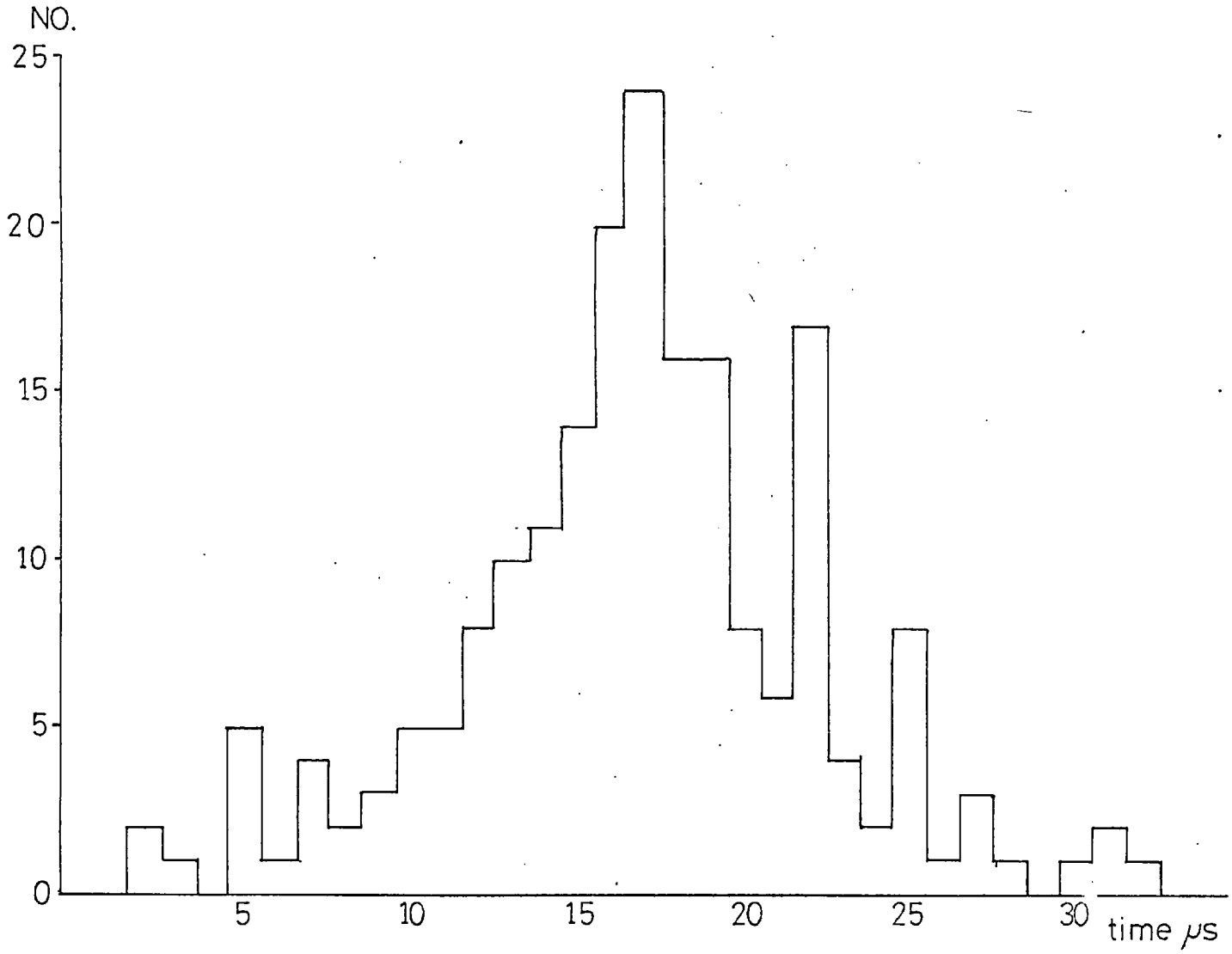
Time lag versus standard deviation of time lag

figure 2/2



Distribution of breakdown time lags at 40 kV.

figure 2/3



Distribution of breakdown time lags at 35 kV.

figure 2/4

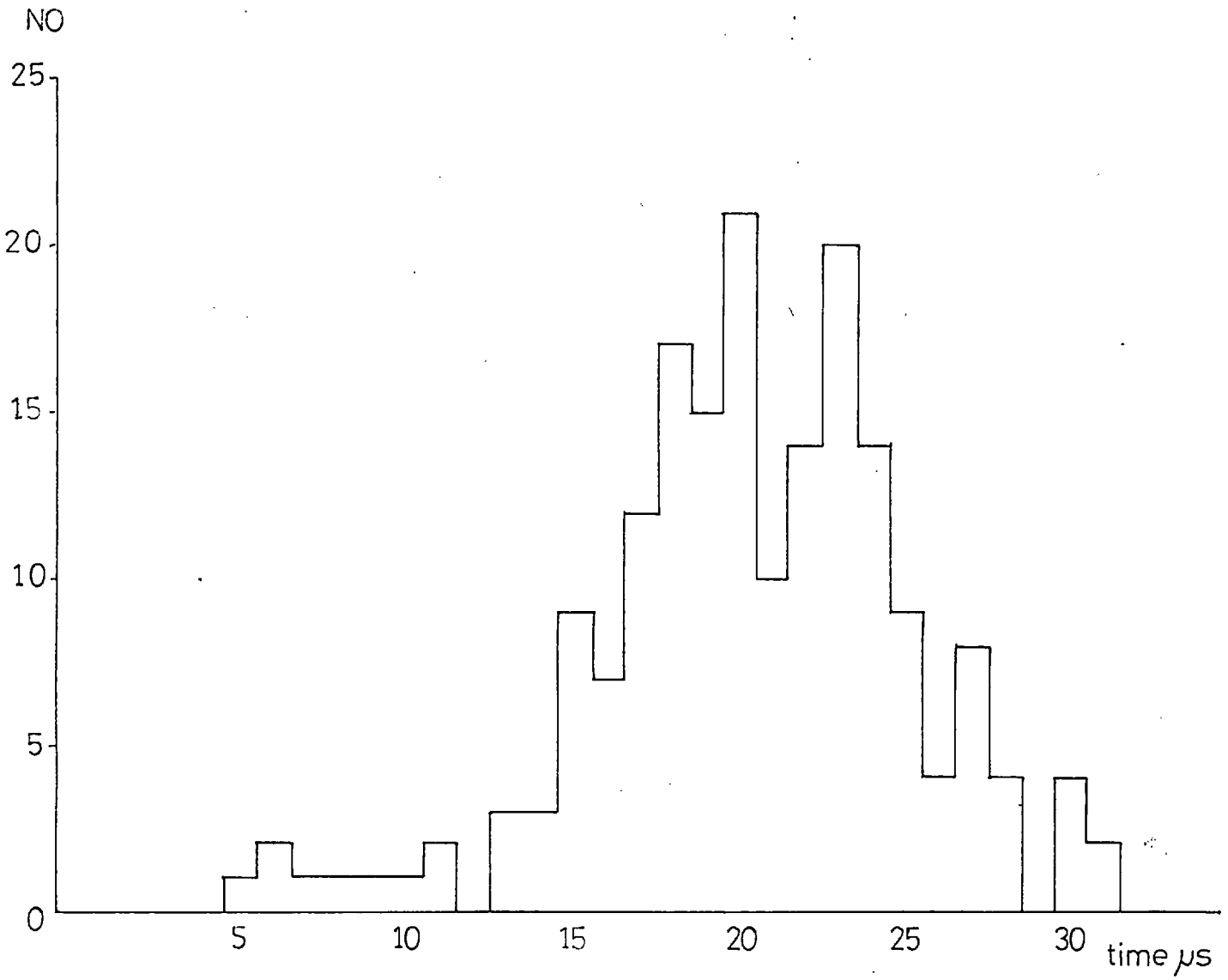
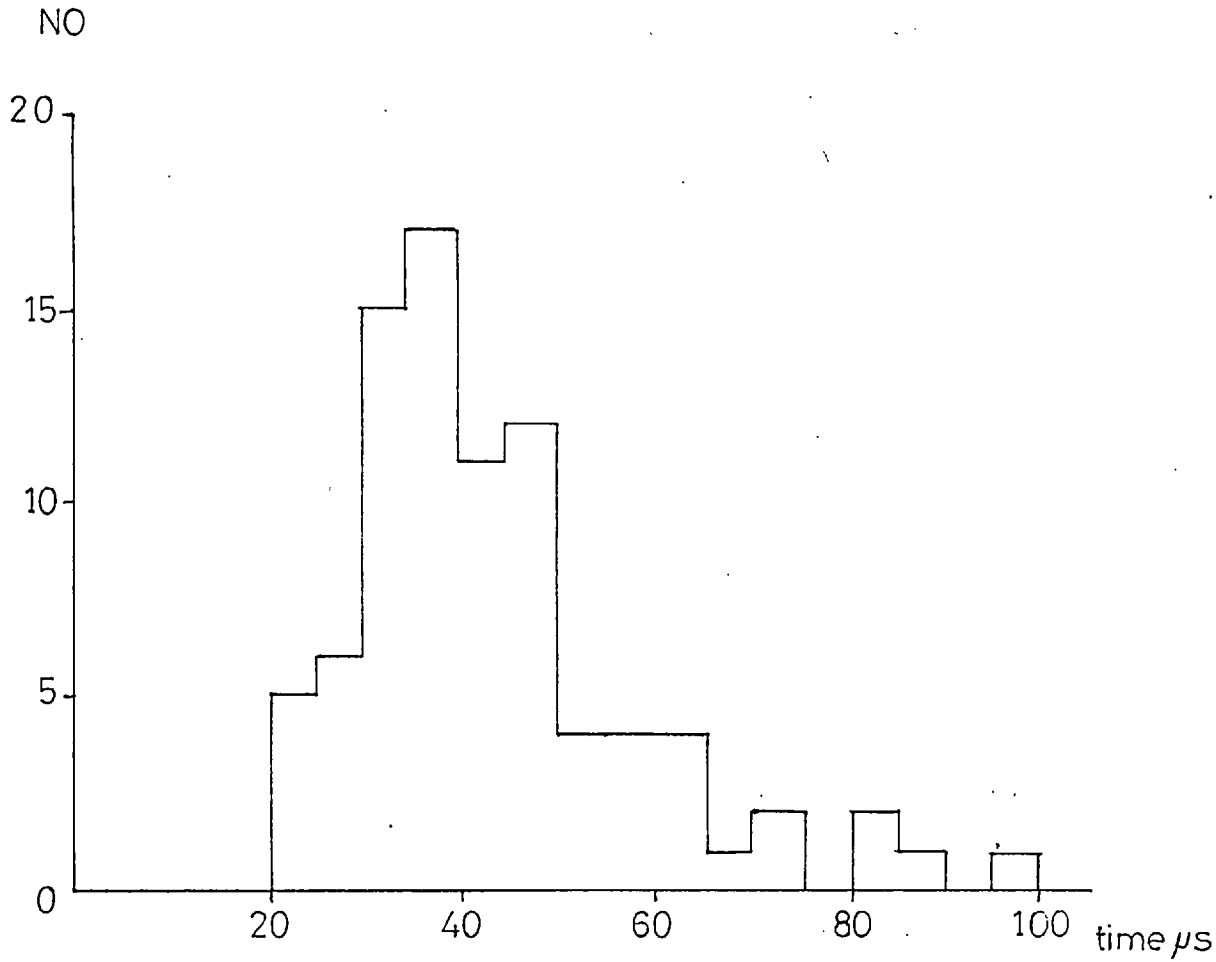


figure 2/5

Distribution of breakdown time lags at 30 kV



Distribution of breakdown times at 25 kV.

figure 2/6

linear correlation between the breakdown time-lags and the standard deviations of the breakdown times was found. This interesting statistical result is a feature of processes in which catastrophies occur.

2.3 Theory

Many alternative theories of the breakdown mechanism of water have been suggested. It is possible that any or any combination of the effects listed below may be responsible.

a) Electron Emission

High electric fields will exist at the water-cathode interface before breakdown. Field emission of electrons from the cathode may occur. This local electron input may be increased by charged dust particles or non-neutralized positive ions generating local intense electron beams. The electrons emitted by the cathode will be accelerated and collide with water molecules, transferring considerable quantities of energy to the water.

b) Ion Movement

Water contains various ion species, e.g. OH^-, H^+, H_3O^+, $H_9O_4^+$, which will move under the influence of the field and may collide with water molecules generating more ions.

(Continued .....)

c) Thermal Breakdown

The pre-breakdown currents will cause heating of the water which may be localized (due to cathode irregularities, etc). This energy input may vapourise some water giving off gas bubbles and these may break down by a gas discharge mechanism.

It is the author's opinion that breakdown is due to an ionic mechanism and a computer model of the process was devised. The model is fully discussed in Appendix 2. The model agrees reasonably with the experimental results. The statistical probability of the agreement, between the experiments and the prediction, arising by chance is better than 1 in 20 which is a statistically significant result.

The model shows that the breakdown time-lag at constant electric field is independant of the gap length which agrees with the work of Smith (reference 169). However the programme does not agree with the observations:

$$\tau \propto \frac{1}{E^3}$$

or

$$\tau \propto \frac{1}{\sigma}$$

τ = breakdown lag

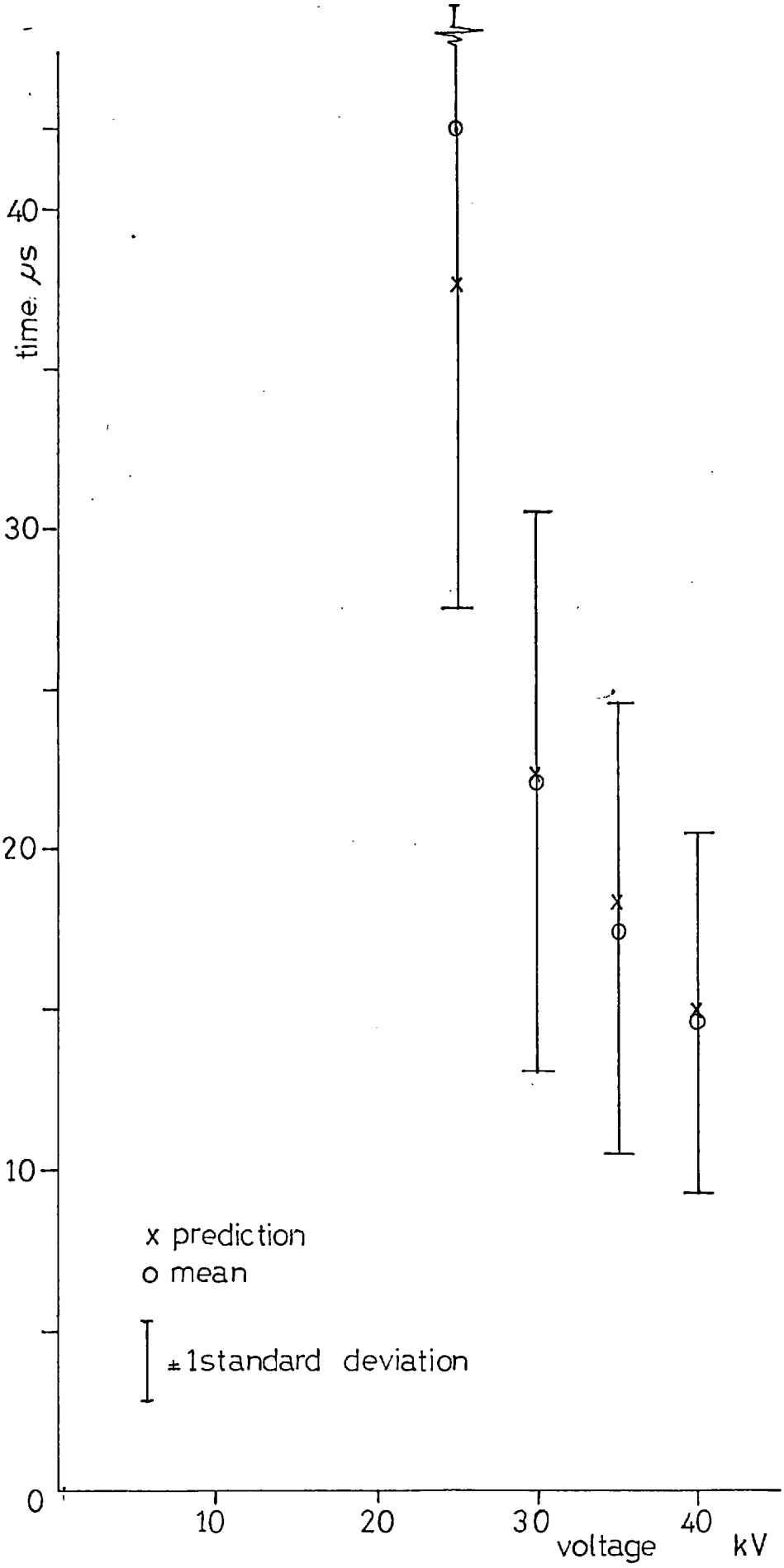
E = field

σ = conductivity

The relationships found by the programme are less non-linear. The discrepancy between programme and data is also of this form, indicating that the postulated model is not completely correct.

(Continued .....)

It is thought that all these errors arise from assumptions made about the ion molecule collision processes. (See Appendix 2). Time was not available to refine the model further but as a trial attempt the results are encouraging and it is thought that further work would confirm the hypothesis that breakdown is due to ionic processes. Figure 2/7 shows the predicted curve and the experimental results.



Predicted breakdown time - lags

figure 2/7

Part 3 - The Generation of Pressure by the Spark

3.1 Introduction

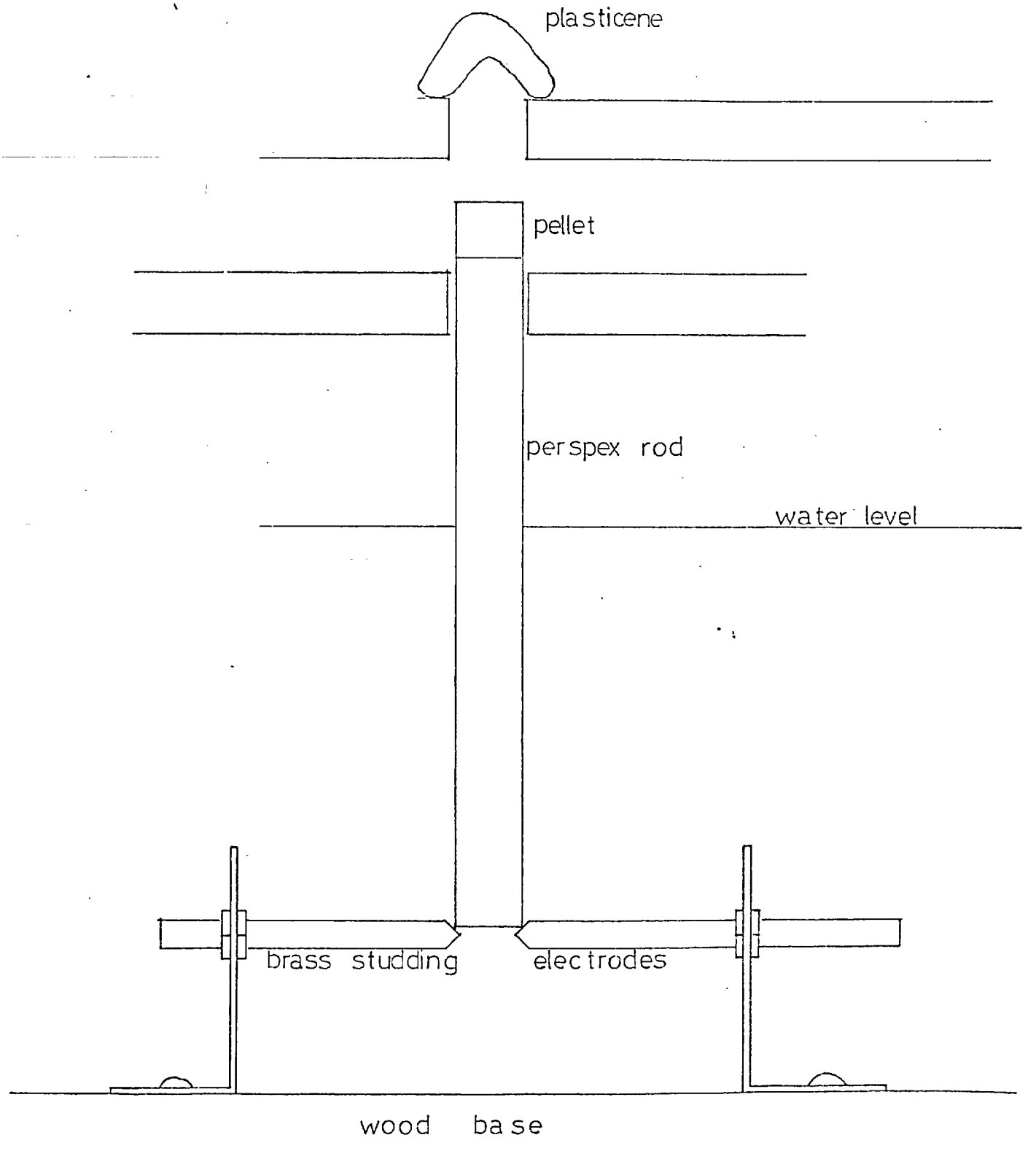
There have been many studies (references 39, 40, 75, 76, 143) of the underwater spark and of exploding wires which have calculated, or measured directly, the pressure in the spark. Typically pressures of the order of 25,000 atmospheres were found. However, none of these studies have attempted to measure the spark pressure when the spark is travelling on a solid surface; a situation of considerable importance in comminution. This part of the thesis describes an experimental method of determining the pressure generated by a spark on a surface, and demonstrates the form of the inductance - pressure relationship. (At a given spark energy, the circuit inductance is of major importance in determining the peak value of spark pressure.)

3.2 The Momentum Range Experiment

A spark was generated using the apparatus described in Appendix 1. The electrode system used (shown in Figure 3/1) was a point-point gap of 1 centimetre length. The gap was bridged by a 12 centimetre long vertical perspex rod. When the spark is fired it travels across the end surface of the rod. A pellet in the form of a short perspex rod sits on top of the main rod, good acoustic contact being assured by wetting the adjacent surfaces.

The stress wave caused by the spark pressure travels up the

(Continued .....)



Momentum range experiment

figure 3/1

perspex rod through the joint and into the pellet. When the stress wave reaches the far surface of the pellet it is reflected in tension. The joint has no tensile strength and so, when the returning tensile wave reaches the joint, the pellet flies off vertically. The momentum of the pellet is given by:-

$$mv = \int_0^{\frac{2l}{V_s}} A\bar{\sigma}\, dt \qquad \text{(by Newtons Laws)}$$

m = mass of pellet.

v = velocity of pellet.

l = length of pellet.

A = area of rod and pellet.

$\bar{\sigma}$ = mean stress travelling up the rod.

t = time.

V_s = velocity of sound in the rod and the pellet.

When the experiment was first carried out it was found (for reasonably short pellets) that the momentum of the pellet was too great to measure directly.

In order to measure the pellet momentum, it was allowed, after travelling about 1 centimetre, to impact into a piece of plasticine to which it adhered. The momentum of the pellet was thus transferred to a pellet-plasticine combination which had much greater mass and hence (as momentum is conserved) travelled more slowly.

(Continued .....)

The height which the pellet-plasticine combination attained was recorded using a television camera and a video tape recorder. Its initial velocity was calculated from:-

$$v^2 = u^2 + 2gs$$

u = initial velocity

v = o = final velocity

g = acceleration due to gravity = $-9{\cdot}81\ m/s^2$

The rod and plasticine were weighed and their momentum calculated.

In order to evaluate the pressure as a function of time, the experiment was repeated for 11 different rod lengths. Each experiment was repeated to increase the accuracy.

The circuit inductance was found by measuring the circuit impedance, as seen by the spark gap, with the air gap shorted. The lowest frequency (fr) at which the impedance was at a minima was noted and the inductance calculated from:-

$$L = \frac{1}{C(2\pi fr)^2}$$

fr = resonant frequency

C = capacity = $\cdot 5\mu f$

L = inductance

The inductance was increased by a small coil in the return circuit and the experiment was repeated for 4 different values of inductance.

(Continued .....)

Results

A function of the form:-

$$Y = Yo\ (1 - e^{\frac{-\ell}{\ell o}})$$

Y = pellet momentum

ℓ = pellet length

Yo ℓo = constants

was found to be a reasonable fit for the relationship between pellet momentum and pellet length.

Values of Yo and ℓo to give least squares error were found for each value of inductance. The experimental results with the fitted curves are plotted in Figures 3/2 to 3/5.

The momentum length relationship is converted to a momentum time relationship by the transform:-

$t = 2\ell / V_s$ t = time ℓ, ℓo, V_s as above

$\tau = 2\ell o / V_s$ τ = time constant

hence

$$Y = Yo\ (1 - e^{\frac{-t}{\tau}})$$

$$Yo\ (1 - e^{\frac{-t}{\tau}}) = \int_{o}^{\frac{2\ell}{V_s}} A\sigma\, dt$$

(Continued .....)

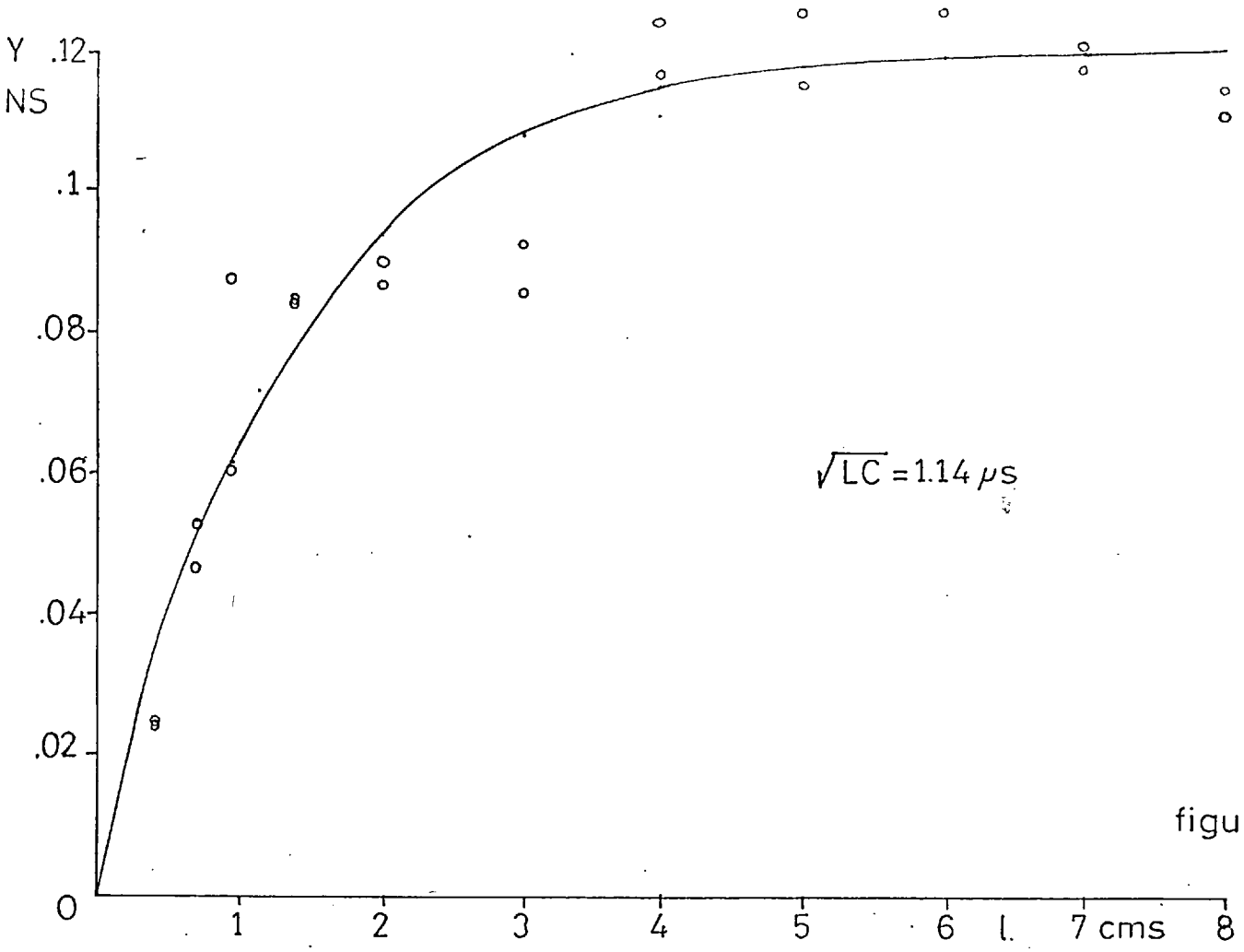
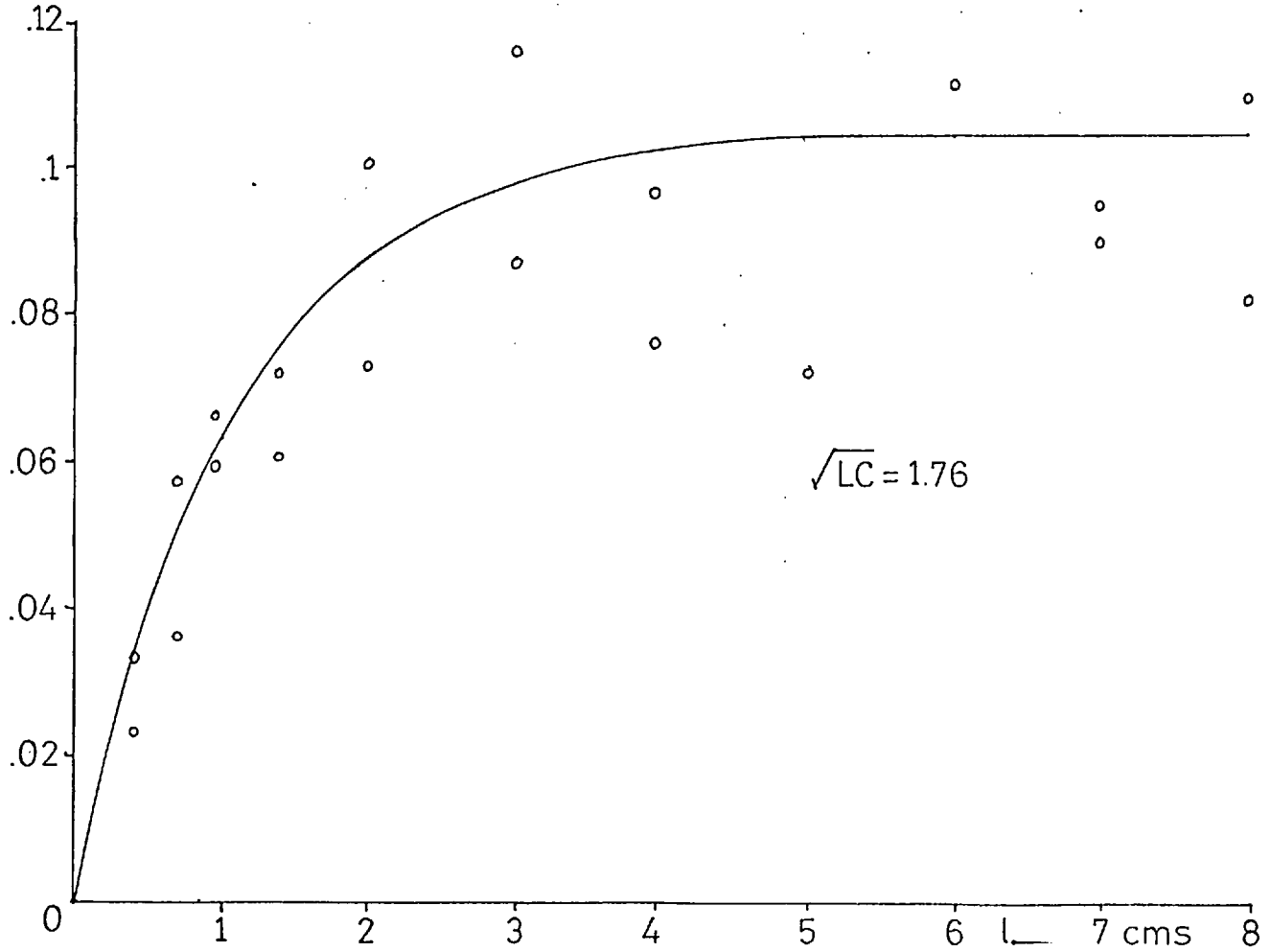


figure 3/2



Impulse versus pellet length

figure 3/3

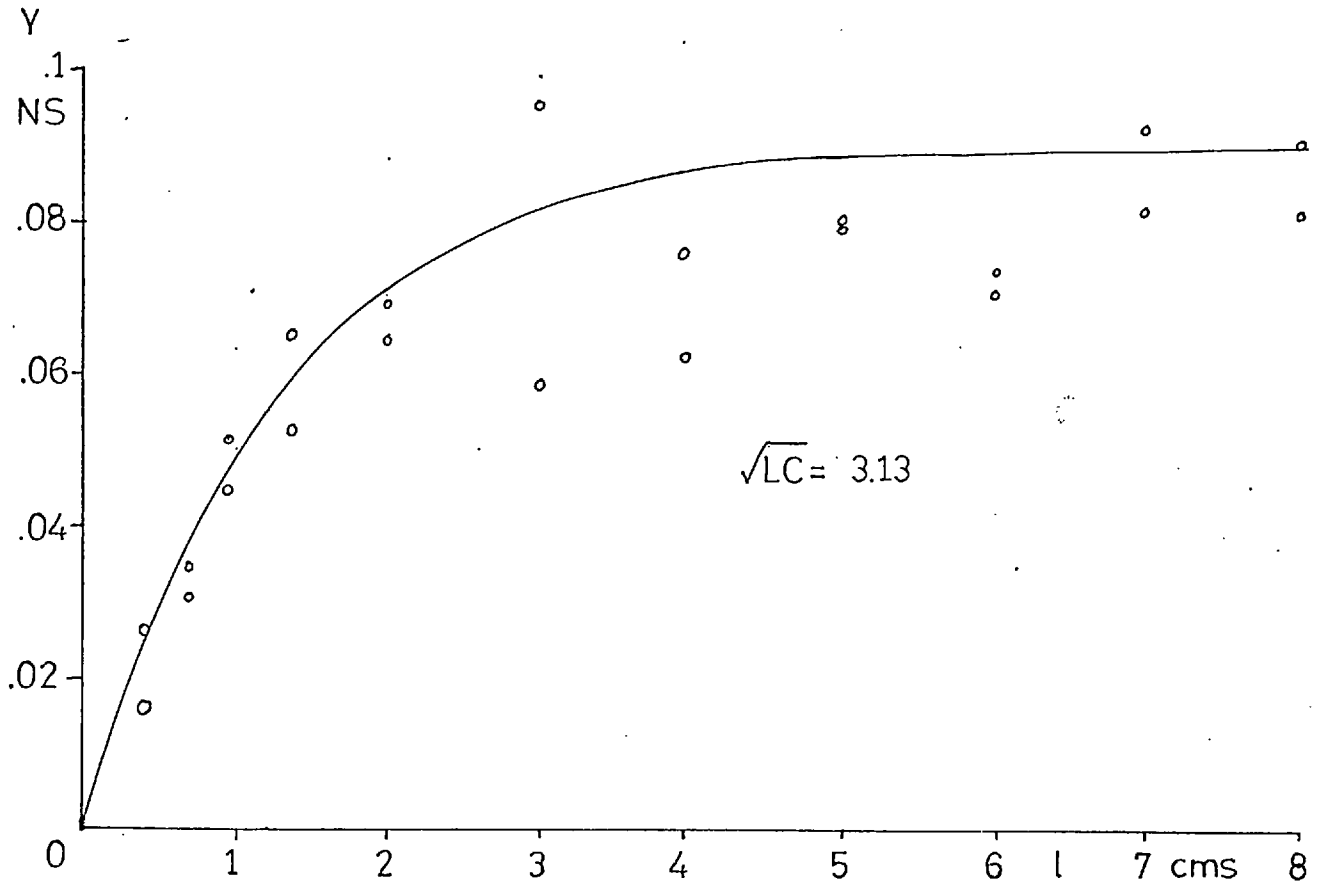
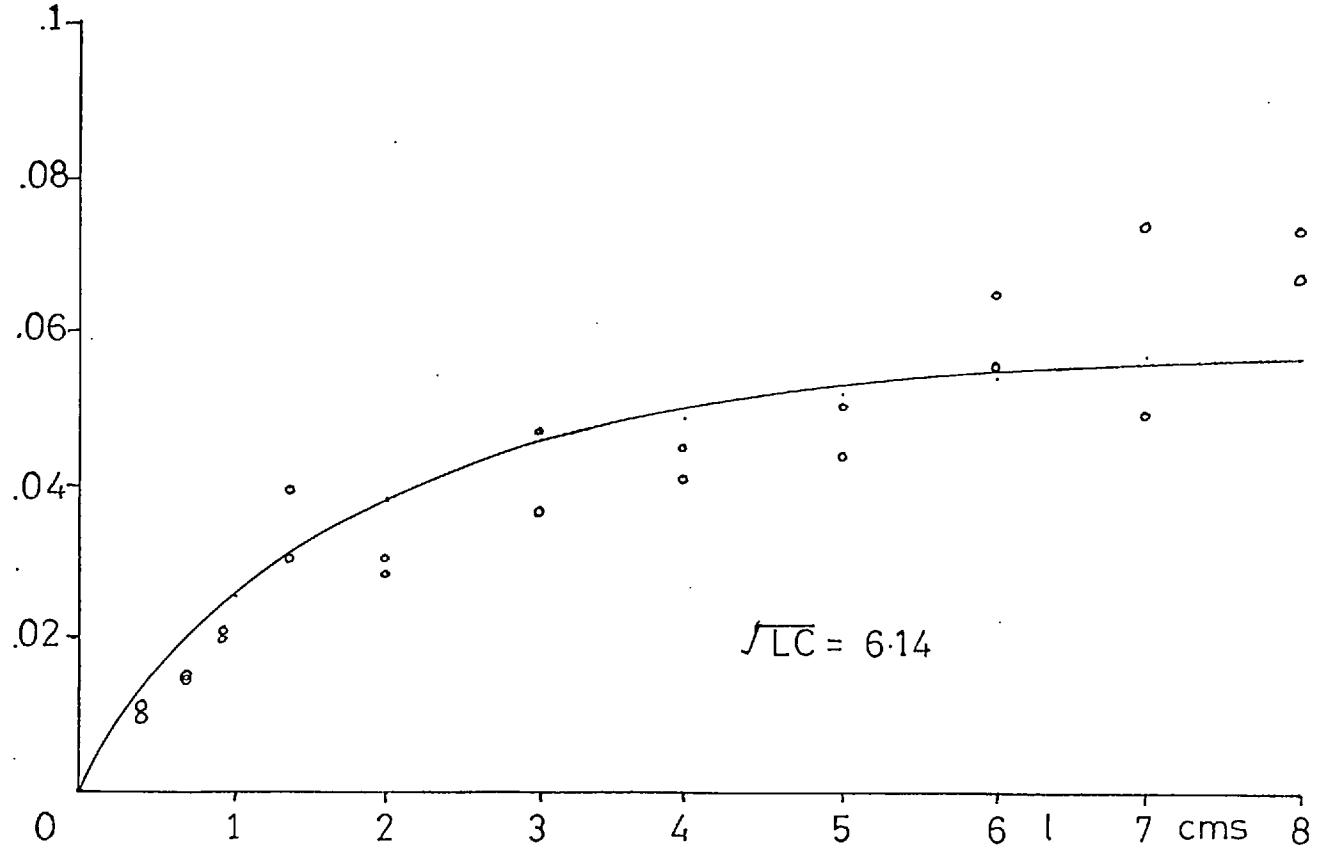


figure 3/4



Impulse versus pellet length

figure 3/5

$$Yo\ (1 - e^{\frac{-t}{\tau}}) = \int_0^t A\sigma\ dt$$

Solving,

$$\frac{Yo}{\tau} e^{\frac{-t}{\tau}} = A\sigma \qquad t > 0$$

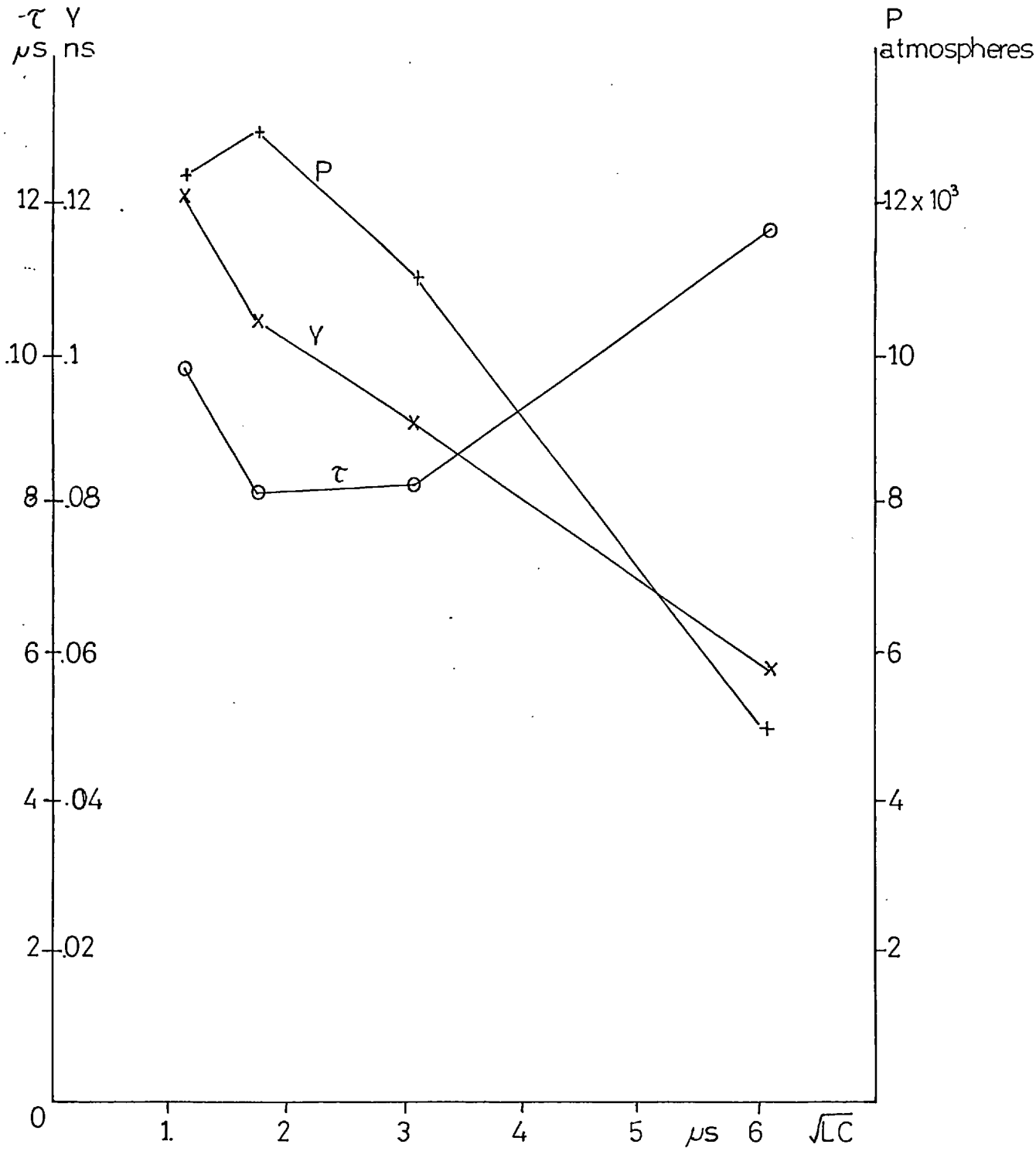
$$\sigma = 0 \qquad t < 0$$

Thus the force transmitted up the rod ($A\sigma$) is exponentially decaying with time constant τ and amplitude Yo/τ.

The peak force in the rod (Yo/τ), the specific impulse (Yo) and the stress wave time constant (τ) are plotted in Figure 3/6 against $\sqrt{LC}$. The peak force remained approximately constant until $\pi\sqrt{LC} > \tau$ a result which a simple model would predict.

In order to calculate the pressure Ps in the spark it is necessary to assume a value for the contact area of the spark with the rod. An assumption of this type is inevitable if the pressure is measured outside the plasma. It is assumed that the mean spark contact area is approximately $10^{-5} m^2$ (i.e. 1 cm x 1 mm)(reference 39,) and this gives spark pressures of the order of 12,500 atmospheres. Table 3/1 summarizes the results.

The result of 12,500 atmospheres is comparable with the results of Martin, reference 39, but the pulse time constants are larger than those he found. This discrepancy is almost certainly due to the different acoustic environment (perspex has a higher acoustic impedance than water).



Time constant, impulse and pressure versus $\sqrt{LC}$

figure 3/6

Table 3/1

Spark Pressures

Fr	$\sqrt{LC}$	L	τ	Yo	Pressure
kH_2	μS	μH	μS	NS	Atmospheres
140	1·14	2·6	9·8	1·21	12,400
89	1·76	6·2	8·1	1·05	13,000
51	3·13	19·6	8·2	0·90	11,000
26	6·14	75·4	11·5	0·58	5,000

Part 4 - Stress Analysis

Introduction

Earlier workers (references 36, 37, 44, 136) have considered two principle fracture mechanisms in electrohydraulic comminution. These mechanisms are, respectively, tensile stresses generated by surface release waves and tensile stresses generated by reflection at boundaries. These mechanisms will be considered briefly.

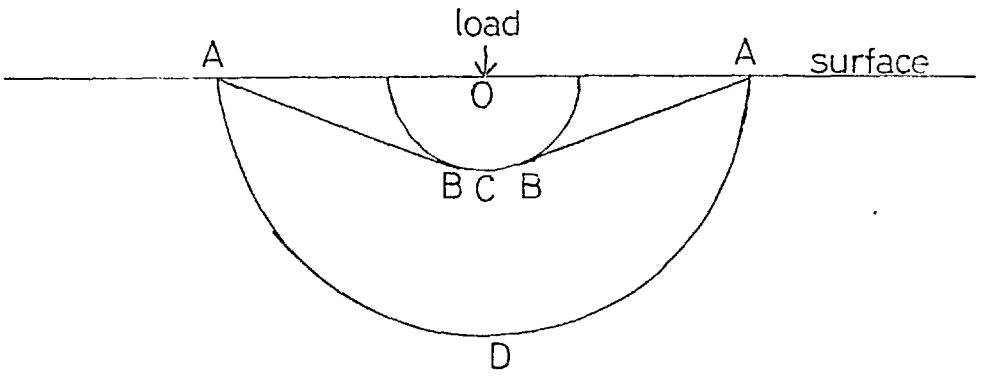
Release Wave Stresses

When a surface is loaded at a point a dilatational wave is propagated (Figure 4/1). Immediately behind the dilatational wave front A D A there is a zone in circumferential compression due to the Poisson's Ratio effect. This compression is released by movements of the surface. The surface movement generates a shear wave of front A B B A. When the transverse compression is relieved the surface still has upward momentum and this momentum generates tensile forces behind the shear wave front.

Reflected Stresses

When a compressive dilatational wave in a solid arrives at a fluid boundary a tensile dilatational wave is reflected into the solid. The magnitude of the reflected wave depends on the solid and liquid properties and the angle of incidence. Fracture occurs when the reflected tensile stress exceeds the incident compressive stress by a magnitude greater than the tensile strength of the solid.

(Continued .....)



Release wavefront diagram

figure 4/1

Figure 4/2 shows the mechanism diagramatically.

The earlier workers have ignored a third mechanism of comminution arising from surface waves.

4.2 Surface Waves

When a dilatational wave in a solid meets a fluid boundary a shear wave, a dilatational wave and a surface wave are generated in the solid.

The theory of such waves will now be explained.

Consider an infinite half space with the boundary as the xy plane and z positive downwards into the solid. The space above the solid is assumed to be vacuum. Consider a plane wave propagating in the x direction. Displacements will be independent of y axis and so the potential functions ϕ and ψ are defined such that

$$u = \frac{\partial \phi}{\partial x} + \frac{\partial \psi}{\partial z}$$

$$w = \frac{\partial \phi}{\partial z} - \frac{\partial \psi}{\partial x} \qquad (1)$$

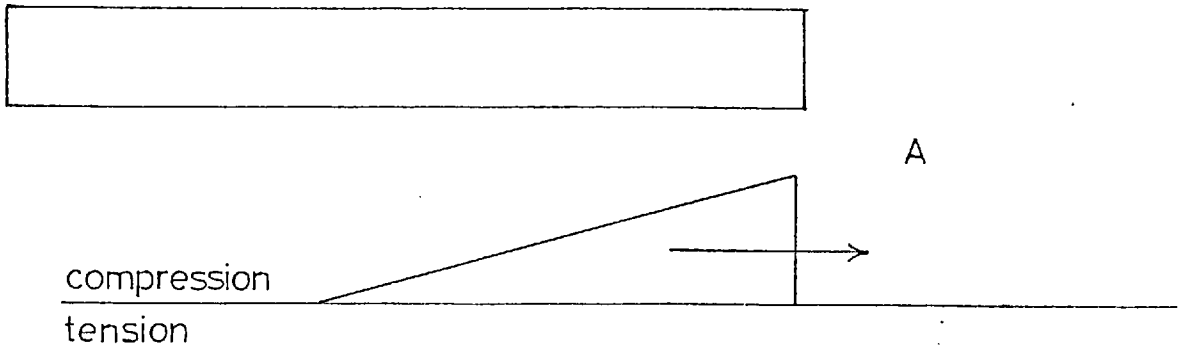
the dilatation Δ is therefore

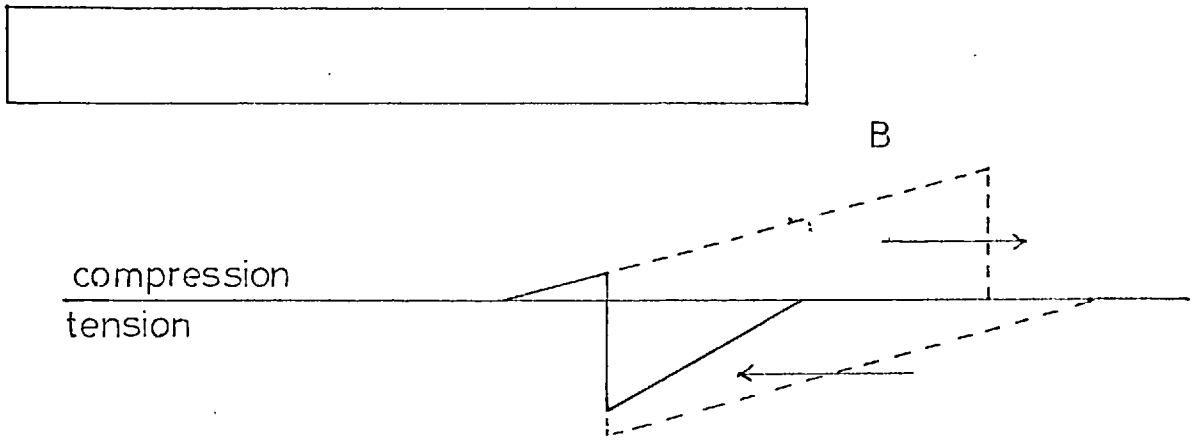
$$\Delta = \frac{\partial u}{\partial x} + \frac{\partial w}{\partial z} = \nabla^2 \phi \qquad (2)$$

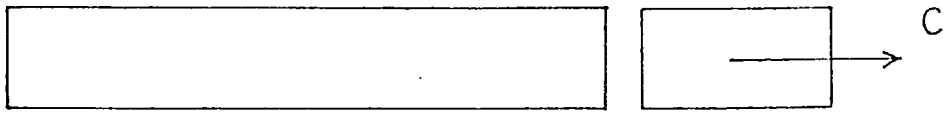
(u, v, w are the displacements caused by the wave)

and $\bar{w}$ the rotation in the x z plane is

$$\bar{w}y = \frac{\partial u}{\partial z} - \frac{\partial w}{\partial x} = \nabla^2 \psi \qquad (3)$$







Failure by reflected stresses

figure 4/2

The equation of motion becomes

$$\rho \frac{\partial^2}{\partial t}(u,v,w) = (\lambda+\mu)\left(\frac{\partial \Delta}{\partial x}, \frac{\partial \Delta}{\partial y}, \frac{\partial \Delta}{\partial z}\right) + \mu \nabla^2 (u,v,w) \qquad (4)$$

Substituting ϕ and ψ and eliminating terms involving $\frac{\partial}{\partial y}$ as the displacements are independent of y

$$\rho \frac{\partial}{\partial x}\left(\frac{\partial^2 \phi}{\partial t^2}\right) + \rho \frac{\partial}{\partial z}\left(\frac{\partial^2 \psi}{\partial t^2}\right) = (\lambda+2\mu)\frac{\partial}{\partial x}(\nabla^2 \phi) + \mu \frac{\partial}{\partial z}(\nabla^2 \psi) \qquad (5)$$

and

$$\rho \frac{\partial}{\partial z}\left(\frac{\partial^2 \phi}{\partial t^2}\right) - \rho \frac{\partial}{\partial x}\left(\frac{\partial^2 \psi}{\partial t^2}\right) = (\lambda+2\mu)\frac{\partial}{\partial z}(\nabla^2 \phi) - \mu \frac{\partial}{\partial x}(\nabla^2 \psi) \qquad (6)$$

These equations are satisfied if

$$\frac{\partial^2 \phi}{\partial t^2} = \left((\lambda+2\mu)/\rho\right)\nabla^2 \phi \qquad (7)$$

$$\frac{\partial^2 \psi}{\partial t^2} = (\mu/\rho)\nabla^2 \psi \qquad (8)$$

but $C_1^2 = \lambda + 2\mu/\rho$ $\quad C_1$ = velocity of propagation of dilatation

and $C_2^2 = \mu/\rho$ $\quad C_2$ = velocity of propagation of distortion

therefore

$$\frac{\partial^2 \phi}{\partial t^2} = C_1^2 \nabla^2 \phi \qquad (9)$$

$$\frac{\partial 2 \psi}{\partial t^2} = C_2^2 \nabla^2 \psi \qquad (10)$$

Consider a sinusoidal wave of frequency $p/2\pi$ propagated in the x direction with velocity C and wave length $2\pi/f$

i.e. $C = p/f$.

(Continued .....)

A solution is

$$\phi = F(z) \exp (i (pt - fx)) \qquad (11)$$

$$\psi = G(z) \exp (i (pt - fx)) \qquad (12)$$

Where $i = \sqrt{-1}$ and F and G are functions which determine the way in which the amplitude varies with depth.

Substituting

$$\frac{-p^2}{C_1^2} F(z) = -f^2 F(z) + F''(z)$$

where $F''(z) = \frac{\partial^2 F(z)}{\partial z}$

or

$$F''(z) - (f^2 - h^2) F(z) = 0 \qquad (13)$$

where $h = p/C_1$

The general solution is

$$F(z) = A \exp (-qz) + A' \exp (qz) \qquad (14)$$

where $q^2 = f^2 - h^2$

The term $A' \exp (qz)$ increases as z increases and for a surface wave A' must be zero.

Similarly for ψ

$$G(z) = B \exp (-sz) \qquad s = f^2 - k^2 \qquad (15)$$

$$k = \frac{p}{C_2}$$

(Continued .....)

Thus the equations for Ψ and ϕ are

$$\phi = A \exp (-qz + i(pt - fx)) \quad (16)$$

$$\Psi = B \exp (-sz + i(pt - fx)) \quad (17)$$

at the boundary z = 0

and

$$\begin{aligned} \sigma_z &= 0 \\ \tau_{xz} &= 0 \\ \tau_{zy} &= 0 \end{aligned} \quad (18)$$

Now $\sigma_z = \lambda \Delta + 2\mu \frac{\partial w}{\partial z}$

from 1 and 2

$$\sigma_z = (\lambda + 2\mu) \frac{\partial^2 \phi}{\partial x^2} + \lambda \frac{\partial^2 \phi}{\partial x^2} - 2\mu \frac{\partial^2 \Psi}{\partial x \partial z} \quad (19)$$

Substituting into 17 at z = 0

$$A ((\lambda + 2\mu) q^2 - \lambda f^2) - 2B \mu isf = 0 \quad (20)$$

Similarly

$$\tau_{zx} = \mu \left(\frac{\partial u}{\partial z} + \frac{\partial w}{\partial x}\right)$$

$$\tau_{zx} = \mu \left(2\frac{\partial^2 \phi}{\partial x \partial z} - \frac{\partial^2 \Psi}{\partial x^2} + \frac{\partial^2 \Psi}{\partial z^2}\right)$$

at z = 0

$$2iqf A + (s^2 + f^2) B = 0 \quad (21)$$

Eliminating A/B from 20 and 21

$$4\mu qsf^2 = ((\lambda + 2\mu)q^2 - \lambda f^2) (s^2 + f^2) \quad (22)$$

(Continued .....)

Simplifying and substituting for p and s gives

$$16\,(1 - h^2/f^2)\,(1 - k^2/f^2) = (2 - (\lambda + 2\mu)\mu^{-1}\, h^2/f^2)^2\,(2 - k^2/f^2)^2$$

$$h = \frac{p}{C_1} \qquad k = \frac{p}{C_2}$$

so $h^2/k^2 = \mu/(\lambda + 2\mu) = \frac{1 - 2\nu}{2 - 2\nu} = \alpha_1^2$ (say)

ν = Poisson's ratio

and $h = \alpha_1 k$

Substituting

$$16\,(1 - \alpha_1^2 k^2/f^2)\,(1 - k^2/f^2) = (2 - k^2/f^2)^4$$

put $k_1 = k/f$ and rearrange

$$k_1^6 - 8k_1^4 + (24 - 16\alpha_1^2)\,k_1^2 + (16\alpha_1^2 - 16) = 0$$

This is a cubic in k_1^2 and if α_1 is known, i.e. if Poisson's Ratio is known, may be solved for k_1.

but

$$k_1 = k/f = p/fc_2$$

p/f is the velocity of the surface wave, C_2 is the velocity of distortion waves and thus k_1 is the ratio of surface wave velocity to shear wave velocity. The velocity of propagation is independent of frequency and thus pulse shape is preserved.

The rate of decay with depth depends on the values of q and s

$$\frac{q^2}{f^2} = 1 - \alpha_1^2 k_1^2$$

$$\frac{s^2}{f^2} = 1 - k_1^2$$

(Continued .....)

Let $\nu = \frac{1}{4}$ for a rock

then $\alpha_1^2 = 1/3$

and

$$3k_1^6 - 24k_1^4 + 56k_1^2 - 32 = 0$$

$$k_1^2 = 4, \quad 2 + \frac{2}{\sqrt{3}}, \quad 2 - \frac{2}{\sqrt{3}}$$

$k_1^2 = 4$ and $k_1 = 2 + \frac{2}{\sqrt{3}}$ lead to imaginary $^q/_f$ and hence do not correspond to surface waves.

$$k_1 = 2 - \frac{2}{\sqrt{3}} \text{ gives } k_1 = \cdot 9194$$

and the velocity of a surface wave is ·9194 of that of a shear wave.

Now:

$$u = \frac{\partial \phi}{\partial x} + \frac{\partial \Psi}{\partial z} \text{ and } w = \frac{\partial \phi}{\partial z} - \frac{\partial \Psi}{\partial x}$$

therefore

$$u = -(Aife^{-qz} + Bse^{-sz})e^{i(pt-fx)}$$

$$w = -(Aqe^{-qz} - Bif\, e^{sz})e^{i(pt-fx)}$$

Substituting for B and simplifying

$$u = Af(e^{-qz} - 2qs\,(s^2 + f^2)^{-1}e^{-sz}) \sin (pt-fx)$$

$$w = Aq(e^{-qz} - 2f^2\,(s^2 + f^2)^{-1}e^{-sz}) \cos (pt-fx)$$

$$\frac{q^2}{f^2} = 1 - \alpha_1^2 k_1^2 = 1 - \frac{1}{3} \times \cdot 9194$$

$$\frac{q}{f} = \cdot 8475$$

Similarly s/f = ·3933

(Continued .....)

The rate of attenuation of displacements along the direction of propagation with depth depends on

$$e^{-qz} - 2qs\,(s^2 + f^2)^{-1}\, e^{-sz}$$

Substituting numerical values of q/f and s/f this becomes

$$e^{(-\cdot 8475fz)} - \cdot 5773 e^{(-\cdot 3933fz)}$$

Similarly for the transverse displacements the factor is

$$e^{-\cdot 8475fz} - 1\cdot 7321\, e^{(-\cdot 3933fz)}$$

Consider an exponentially decaying pulse of time constant 10^{-6} Secs. This will have a Fourier spectrum of large amplitude in the region of 1 MHz

$p/2\pi \simeq 10^6$

$p \simeq 6\cdot 28 \times 10^6$

$p \simeq 6 \times 10^6$

A typical shear wave velocity in rock is about 2,000 m/s

therefore surface wave velocity = $\cdot 9194 \times 2 \times 10^3$

$C \simeq 1\cdot 8 \times 10^3$ m/s

$C = p/f$

$$f = \frac{p}{C} = \frac{6 \times 10^6}{1\cdot 8 \times 10^3} = 3\cdot 3 \times 10^3 \text{ per metre}$$

The magnitude of the factor, for motion parallel to the surfaces, decreases rapidly with depth and becomes zero for fz = 1·210.

$3\cdot 3 \times 10^3\ z = 1\cdot 210$

$z = 3\cdot 6 \times 10^{-4}$ metres

$= 360$ microns

(Continued.....)

Below this depth the factor is negative indicating the body at depth is moving in opposite phase to the surface.

The magnitude of the factor, for motion transverse, first increases reaching a maximum at ·076 wave lengths.

$$\frac{fz}{2} = \cdot 076$$

$$z = \frac{\cdot 076 \times 2}{3 \cdot 3 \times 10^{3}}$$

$$= \cdot 076 \times 2 \times 3 \times 10^{-4}$$

$$= 1 \cdot 44 \times 10^{-4} \text{ metres}$$

$$= 144 \text{ microns.}$$

The grain size of some rocks is of this order. For example the Pennant Sandstone used in the crushing experiments described below has a grain size of some 50 microns. As the grain size is comparable with the phase inversion depth the rock cannot be considered an isotropic homogeneous body and thus the analysis is necessarily incorrect. It is probable that surface waves generated by the spark will cause individual grains to resonate. Although the damping coefficient in the bulk rock is high, it is likely to be very low within a single grain. Consequently the resonance of single grains will generate large forces on the grain boundaries thus liberating the grain. Evidence for this failure mechanism is also shown in the size distribution for Pennant Sandstone (see below) where the virtual absence of particles in the 75 - 105 micron size range indicates that particles are liberated at grain size. This hypothesis of failure

(Continued .....)

requires more detailed investigation as comminution devices which break rock into single grains would be of considerable value, if economic in power consumption, in the mineral dressing field. It is considered that it would be possible to devise surface wave generators suitable for this application.

4.3 Numerical Methods and Results

As analytical methods of dynamic stress analysis are impracticable with realistic boundary conditions, the author has used numerical methods to study the stresses generated by underwater sparks. The method of analysis used is described in Appendix 3.

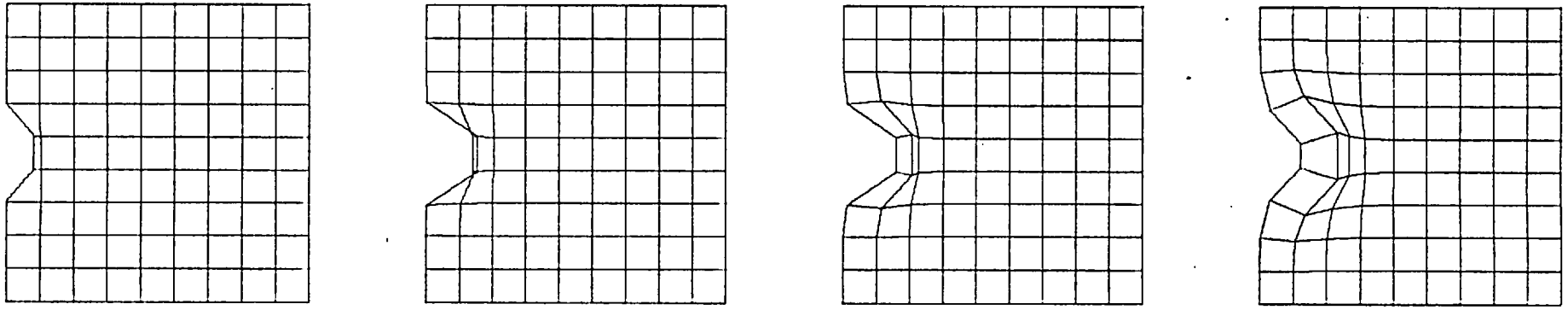
It is assumed that the rock is linear elastic, homogeneous and isotropic. The load applied is a point load with zero rise-time and an exponential decay.

It is realised that these assumptions are not very realistic considering the pressure and time scales of the loads but more realistic data was not available. However the analysis provides a first attempt at a quantitative solution and given suitable data can be modified to produce more accurate solutions.

Figures 4/3 to 4/18 show the distortion, with time, of a square when loaded by a spark. The graphs are generated by adding the displacement of the grid points, greatly scaled up, to their rest points. The analysis is two dimensional, the z stress is assumed zero. This situation is a reasonable approximation to the centre of a cube loaded by a line shock on one edge face. The full three dimensional analysis is possible but uses a large amount of computer time.

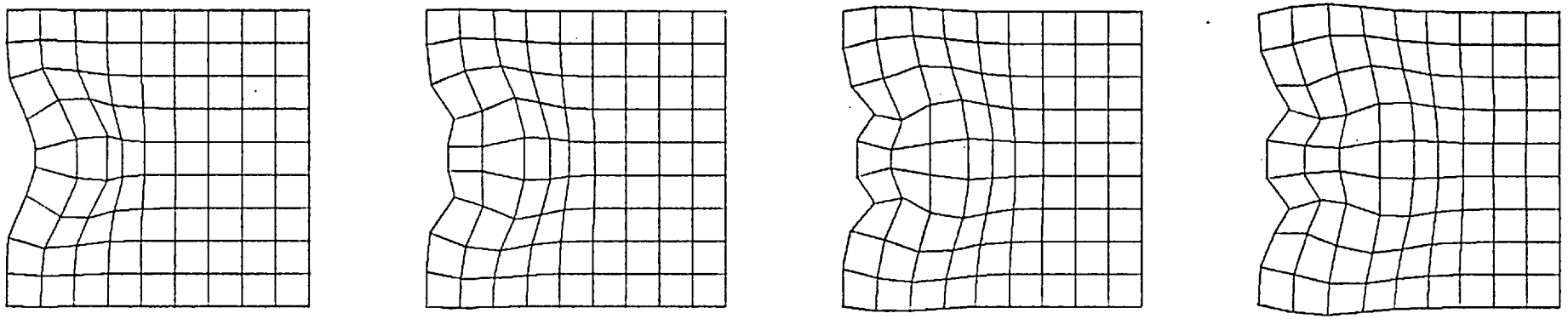
Figure 4/19 shows the locus of each of the grid points during the process.

(Continued .....)



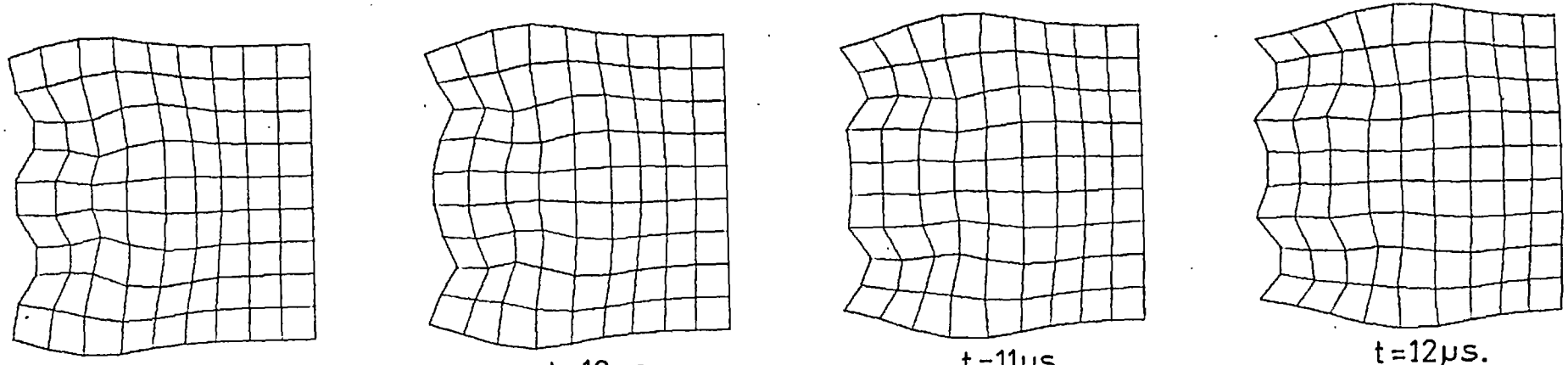
Distortion grids

figure 4/3



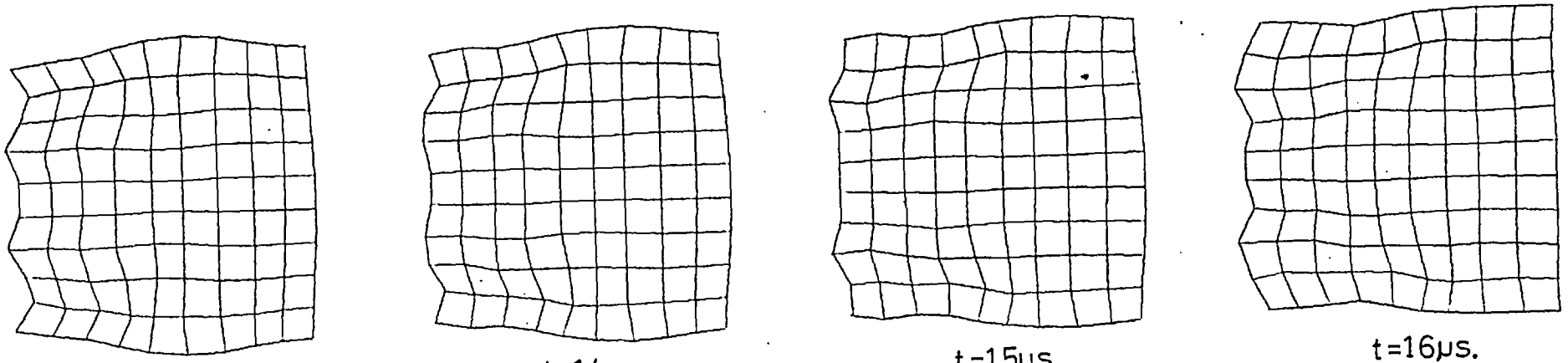
Distortion grids

figure 4/4



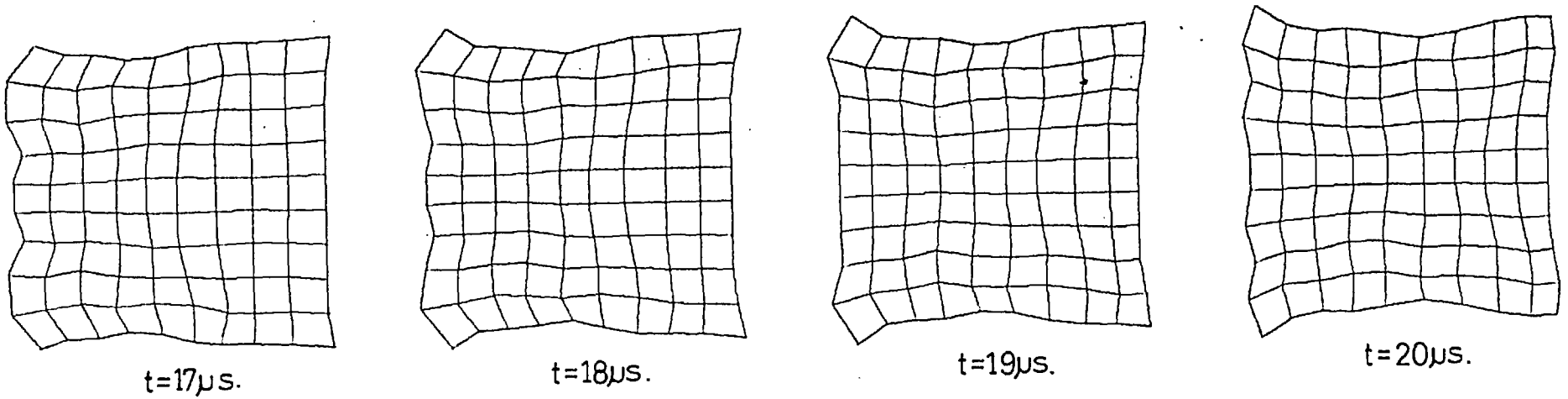
Distortion grids

figure 4/5



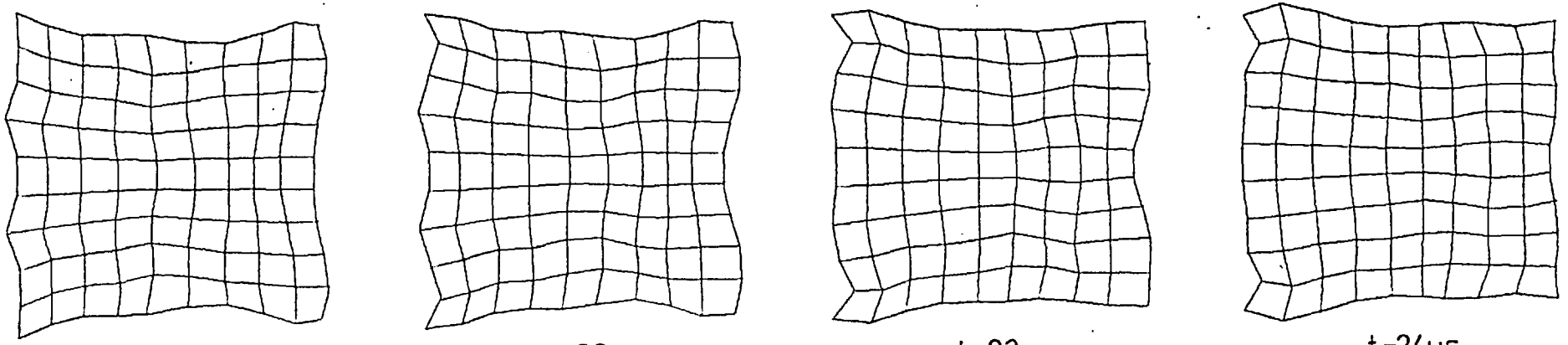
Distortion grids

figure 4/6



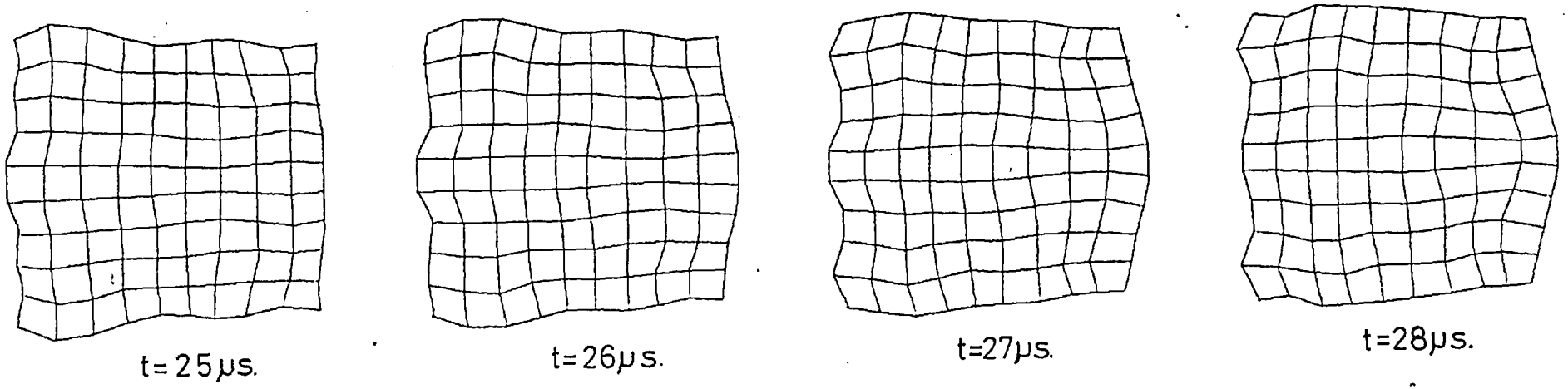
Distortion grids

figure 4/7



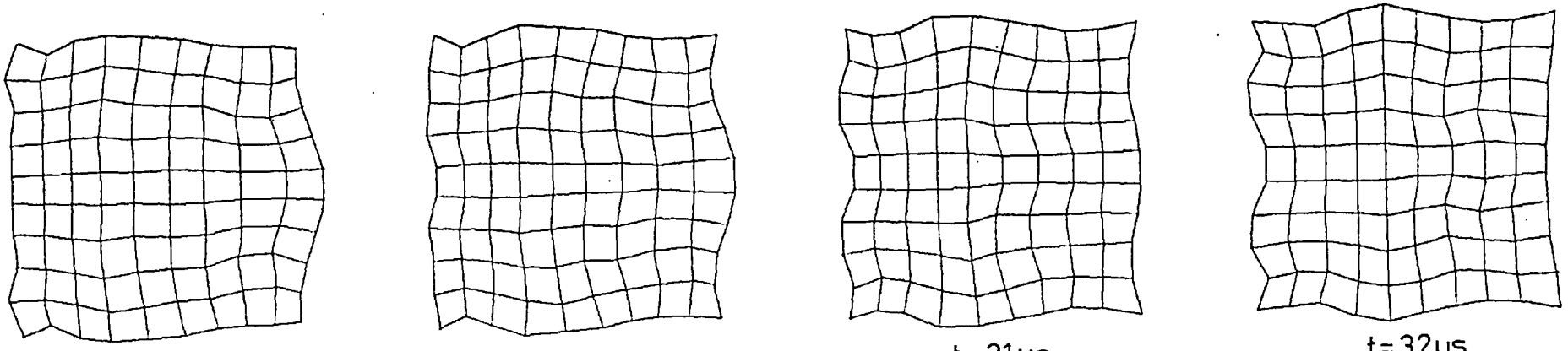
Distortion grids

figure 4/8



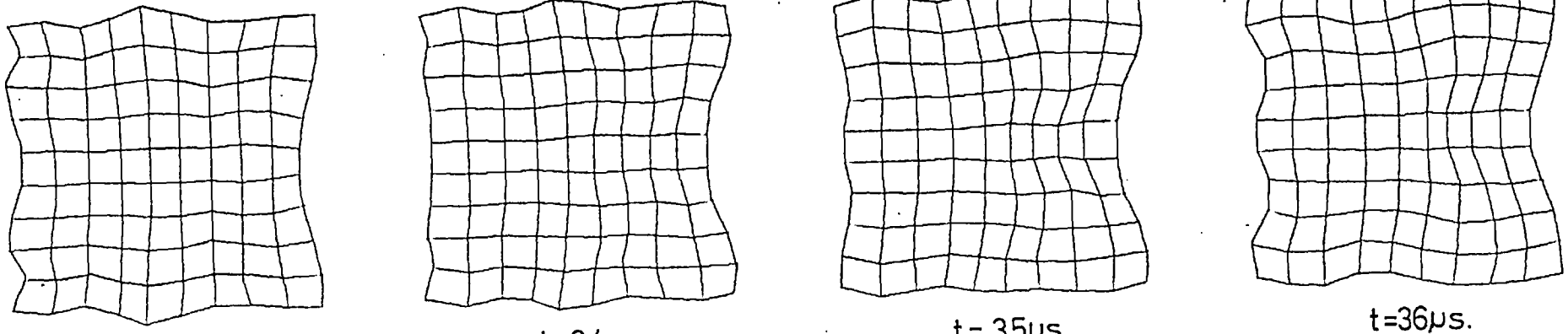
Distortion grids

figure 4/9



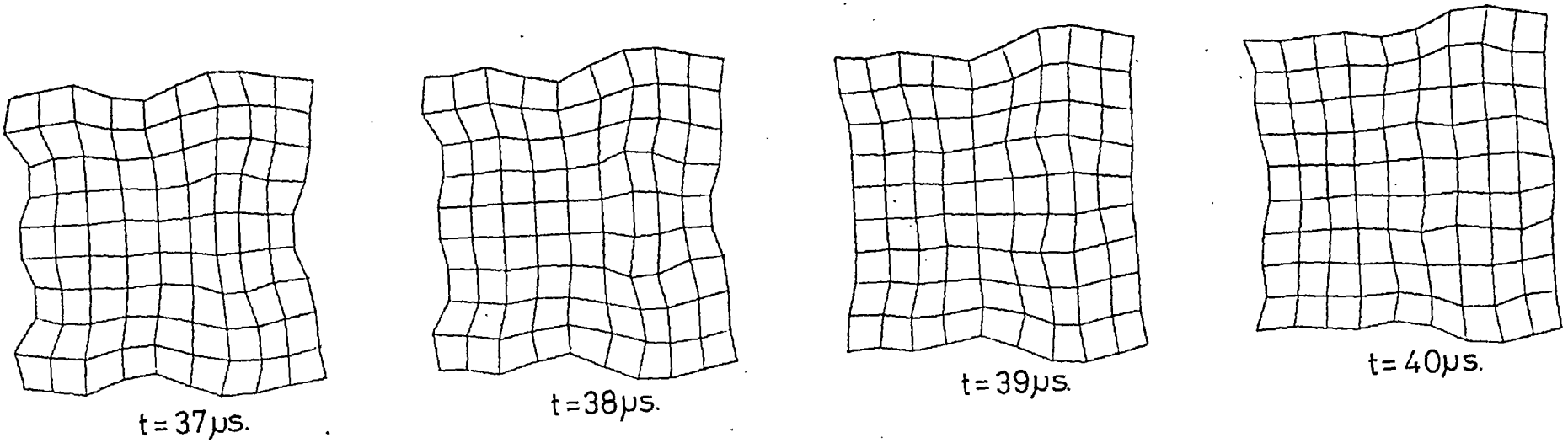
Distortion grids

figure 4/10



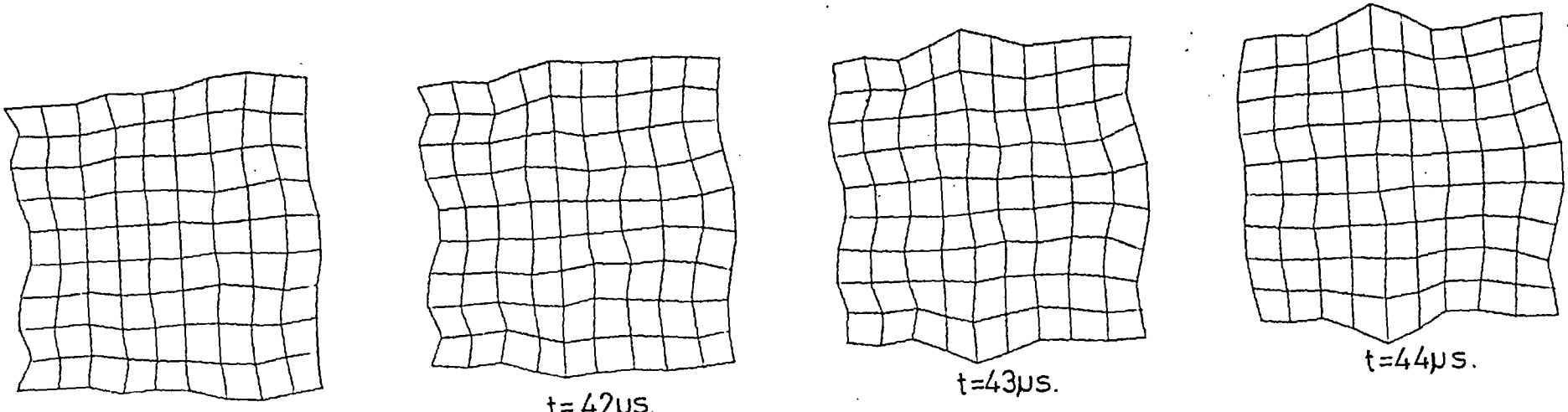
Distortion grids

figure 4/11



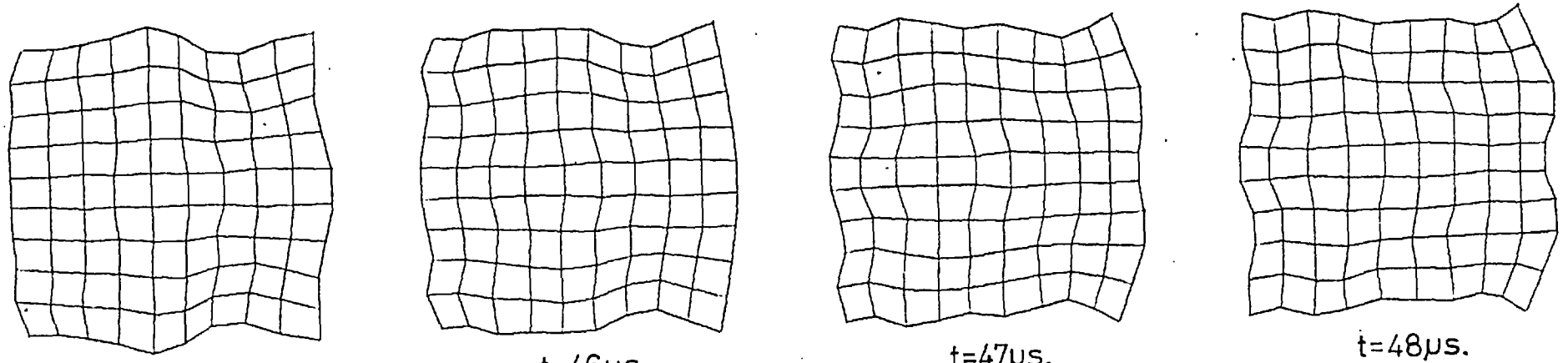
Distortion grids

figure 4/12



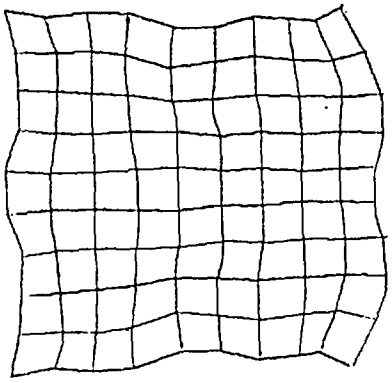
Distortion grids

figure 4/13

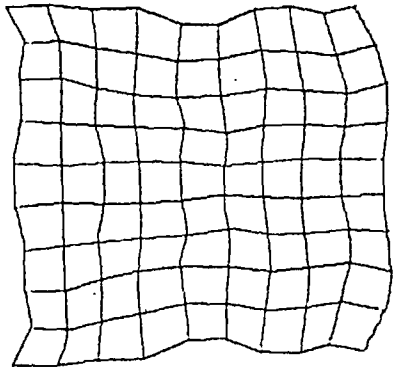


Distortion grids

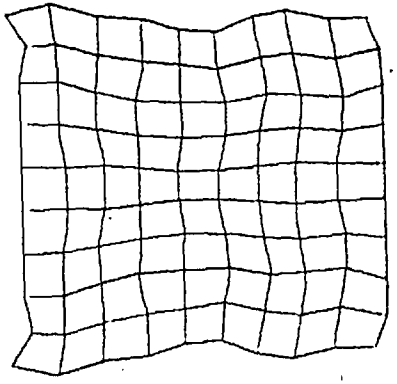
figure 4/14



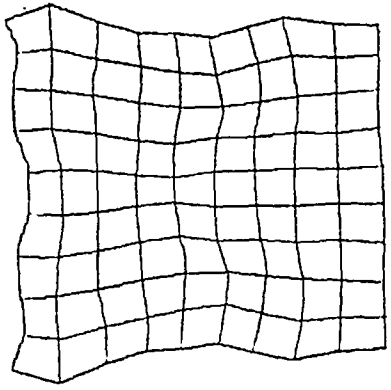
t = 49μs.



t = 50μs.



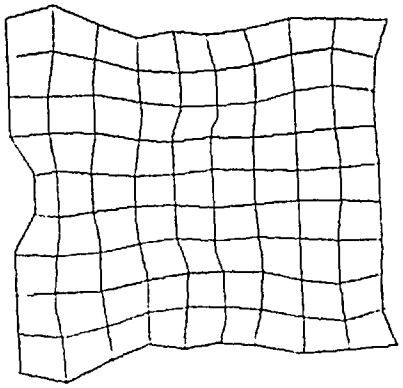
t = 51μs.



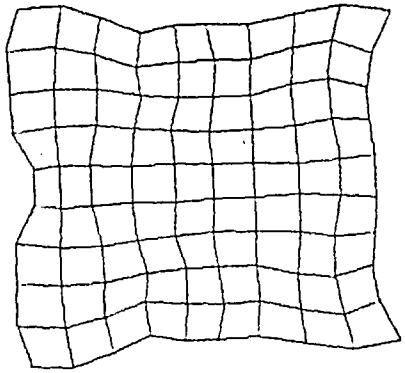
t = 52μs.

Distlortion grids

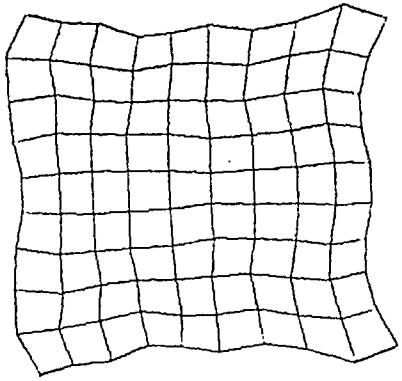
figure 4/15



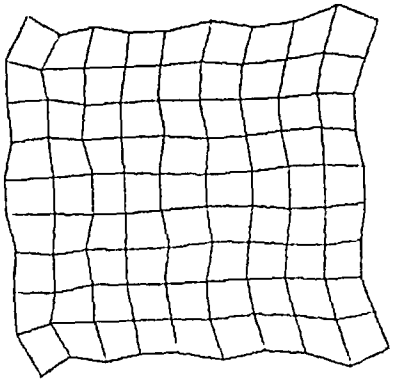
t= 53μs.



t= 54μs.



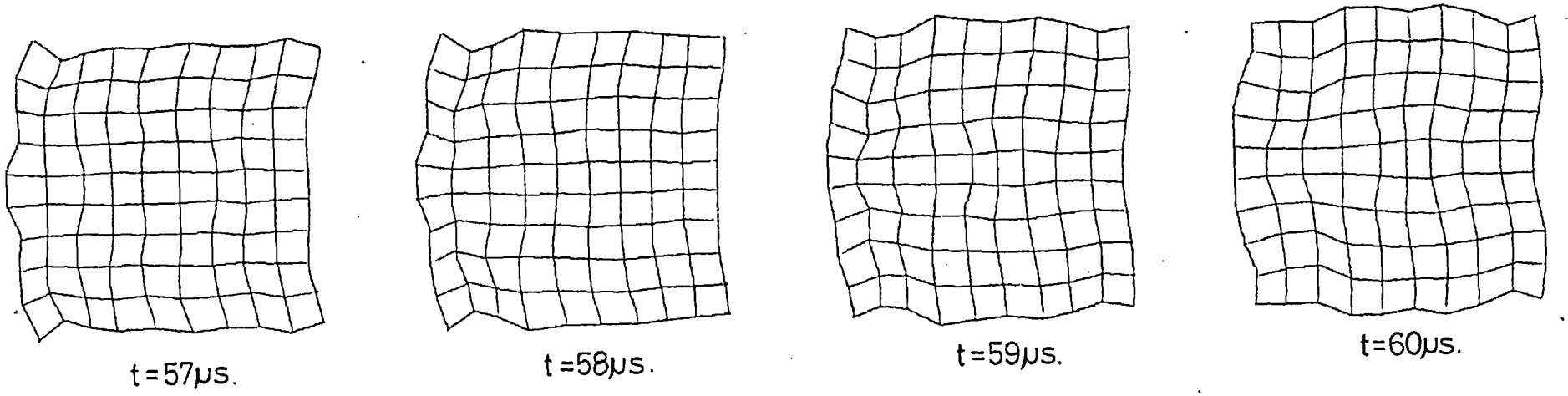
t=55μs.



t=56μs.

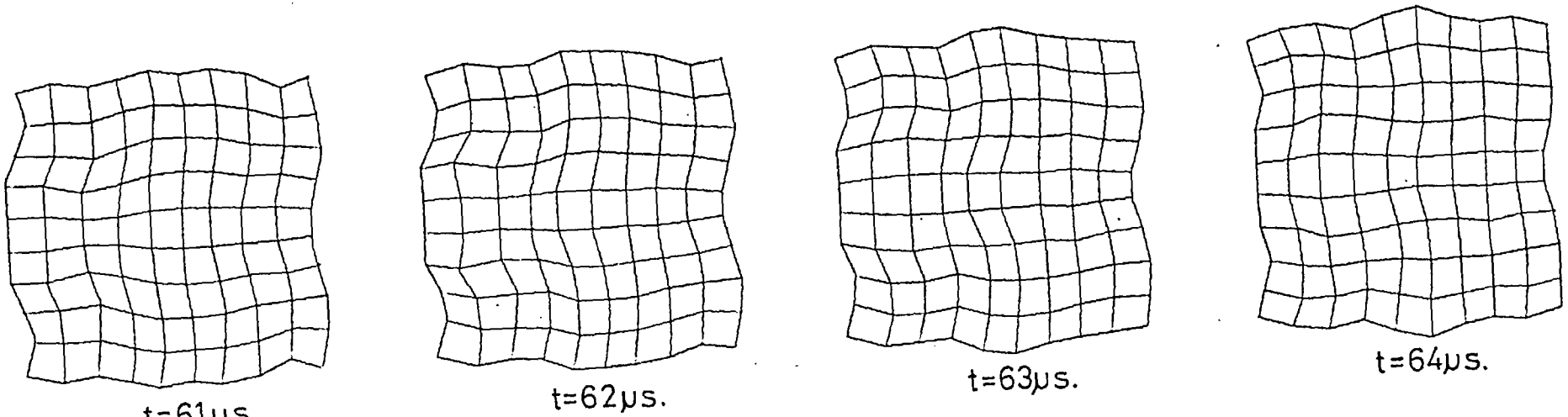
Distortion grids

figure 4/16



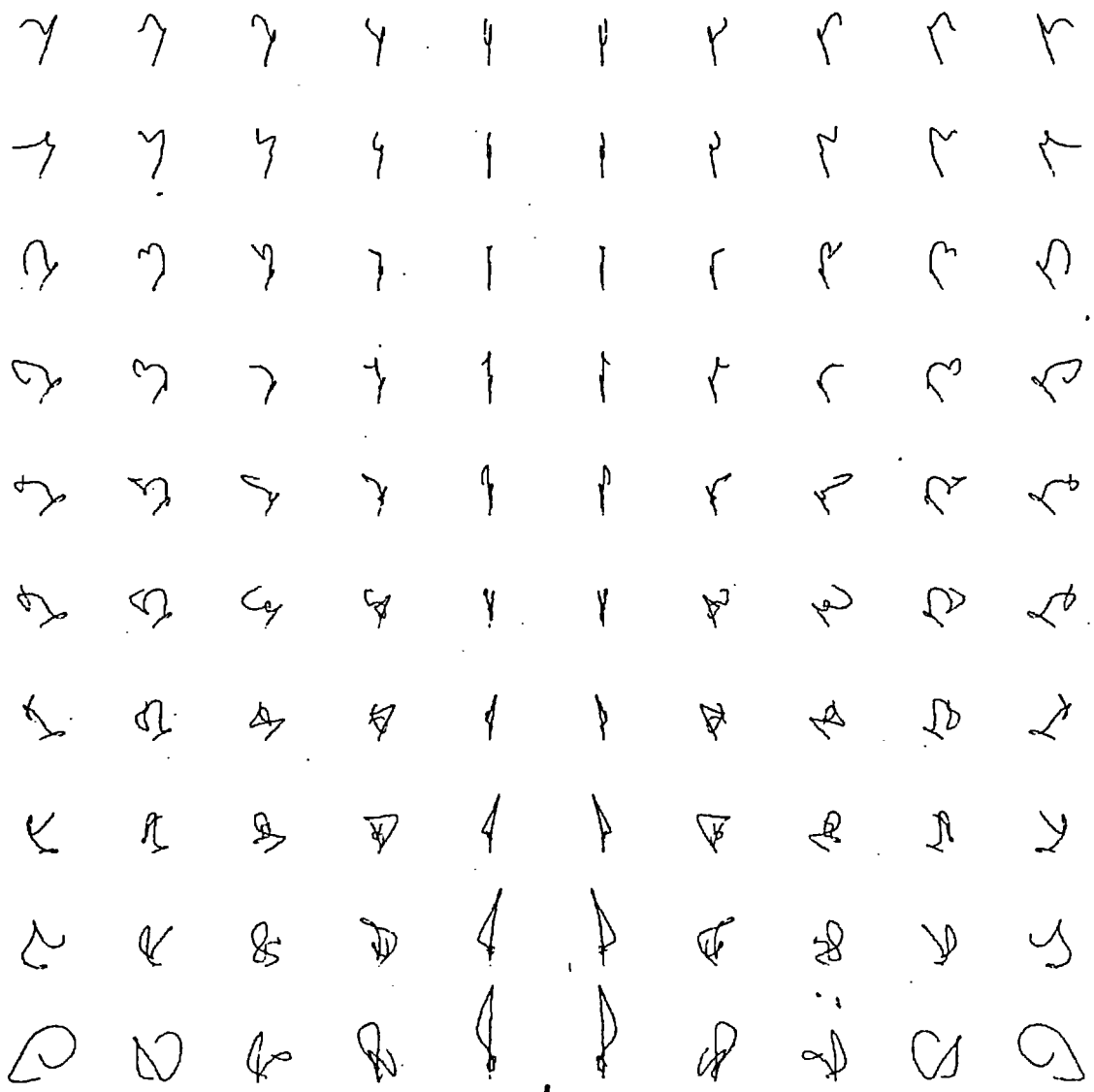
Distortion grids

figure 4/17



Distor tion grids

figure 4/18



Trajectories of points on a dynamically loaded square

Figures 4/20 to 4/39 show the principle major stress σ_1, the principle minor stress σ_3 and the shear stress τ as a function of time in the same situation. In the first few graphs the release waves can be clearly seen. In the later graphs the reflected waves can be seen interferring with the forward travelling waves.

4.4 Criteria of Efficiency

By using the numerical analysis programme, the effects of the stress-wave time constant were studied. Failure of the specimen will occur when σ_3 is tensile and has a magnitude greater than the tensile strength of the material.

The ratio S_R is defined as follows:

$$S_R = \frac{\text{Maximum Tensile Value of } \sigma_3}{\text{Maximum Applied Stress}}$$

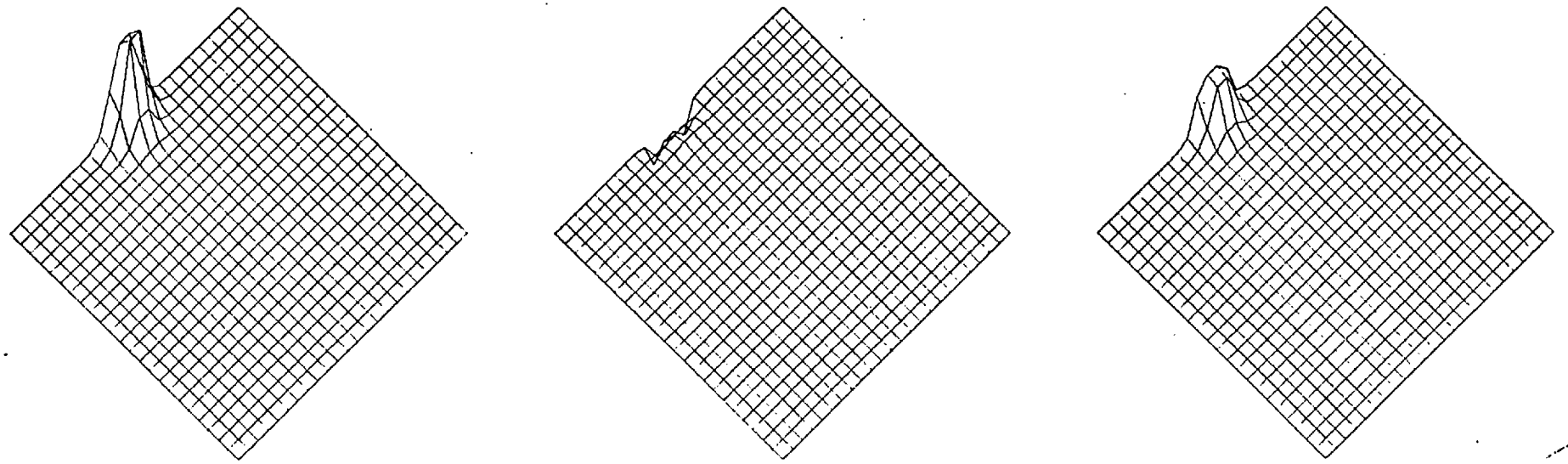
This ratio is a measure of the acoustic gain of the rock specimen as it describes the stress increase generated by geometrical and pulse shape considerations only.

The ratio η_r is defined as follows:

$$\eta_r = \frac{S_R}{Si} \qquad Si = \text{specific impulse of load}$$

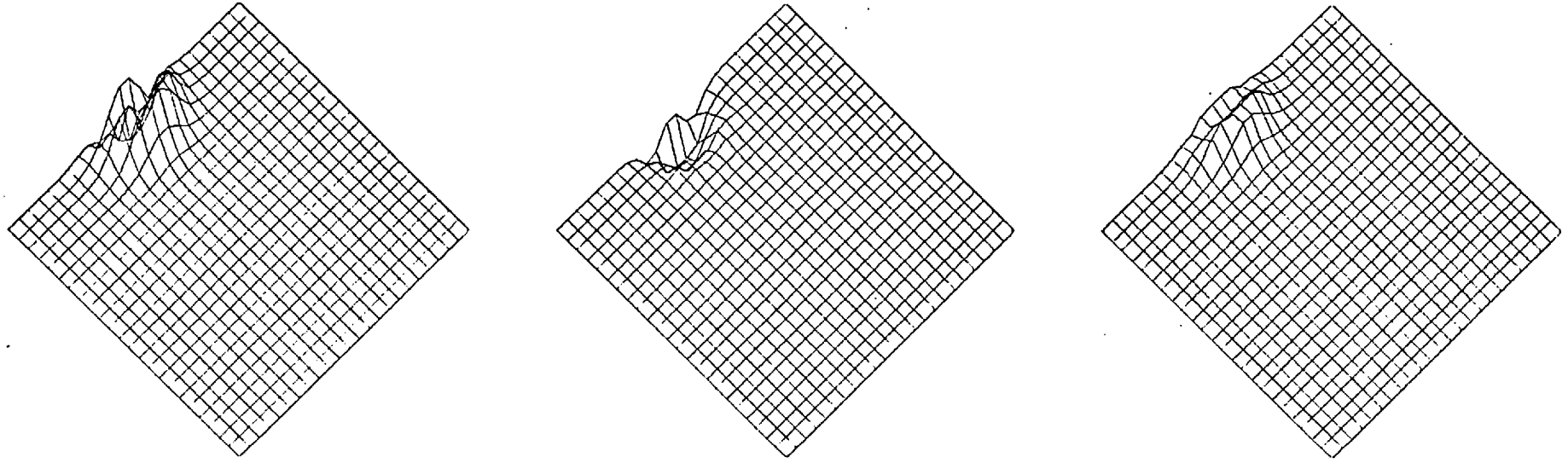
This is a measure of the efficiency of converting acoustic energy into fractures.

(Continued .....)



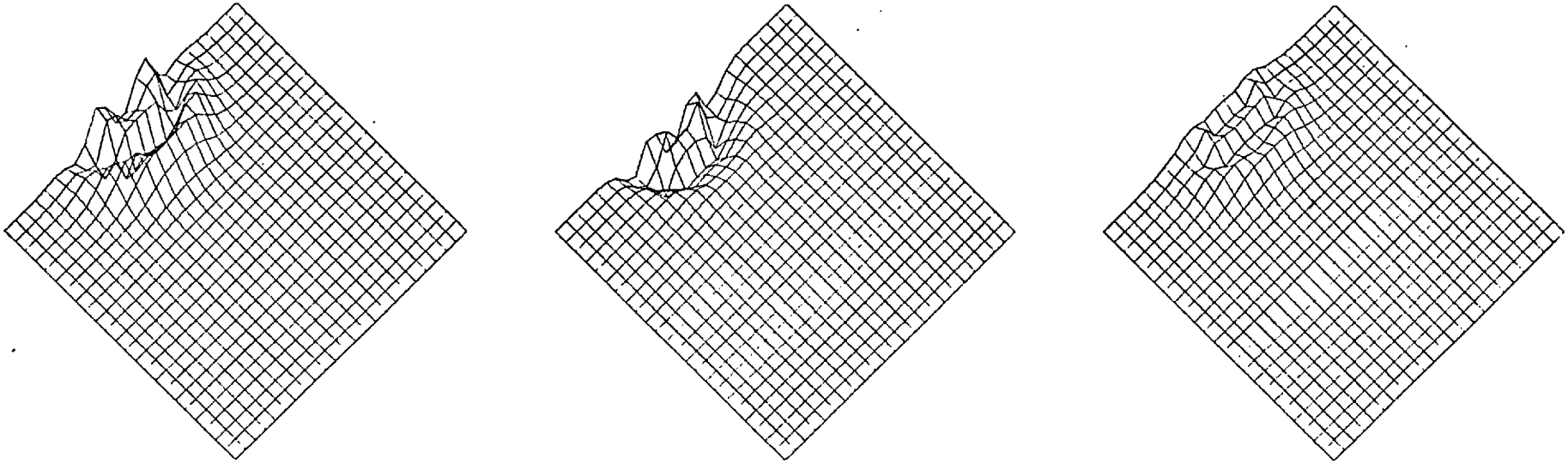
Stress isometric time = 1μs.

figure 4 / 20



Stress isometric time = 2μs.

figure 4/21



Stress isometric time = 3 μs.

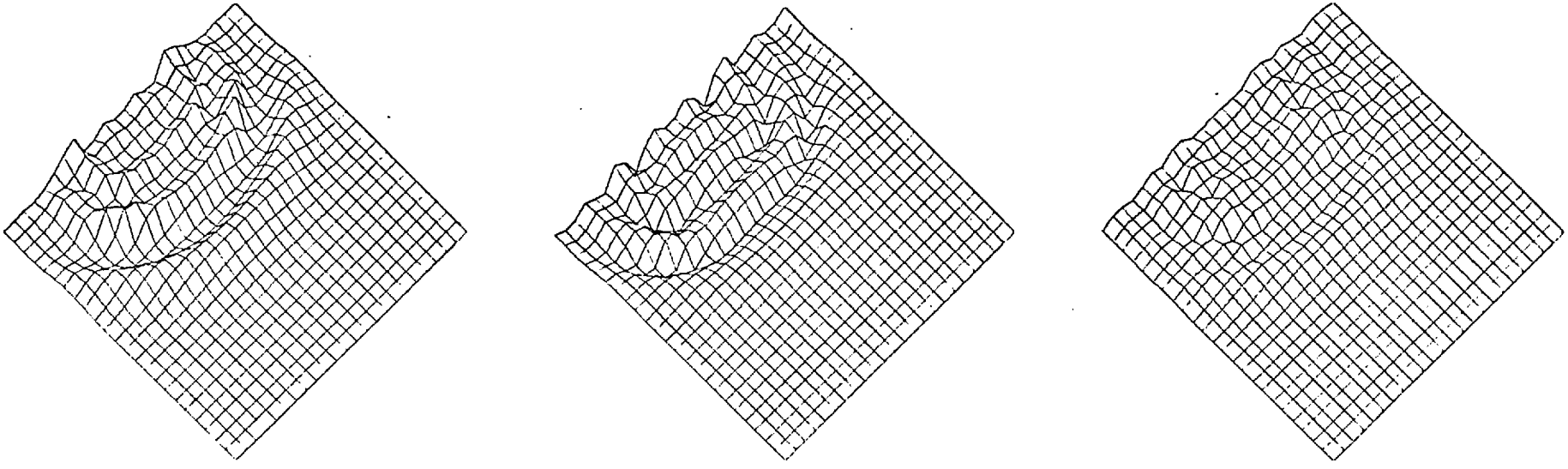
figure 4/22

Stress isometric time = 4μs.

figure 4/23

Stress isometric time = 5μs

figure 4/24

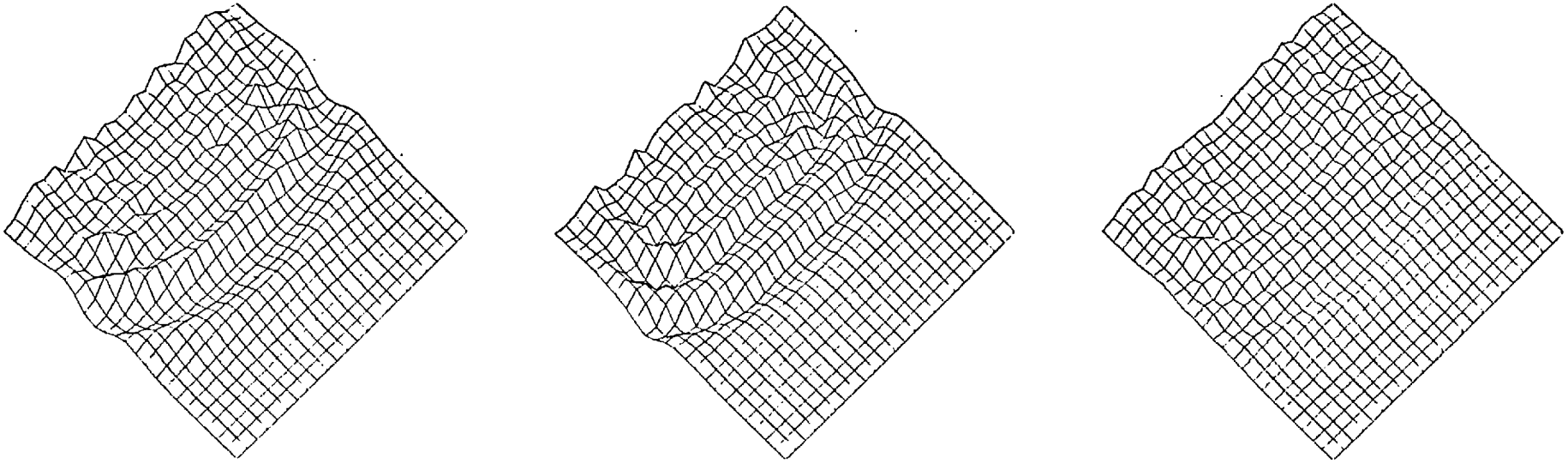


Stress isometric time=6μs.

figure 4/25

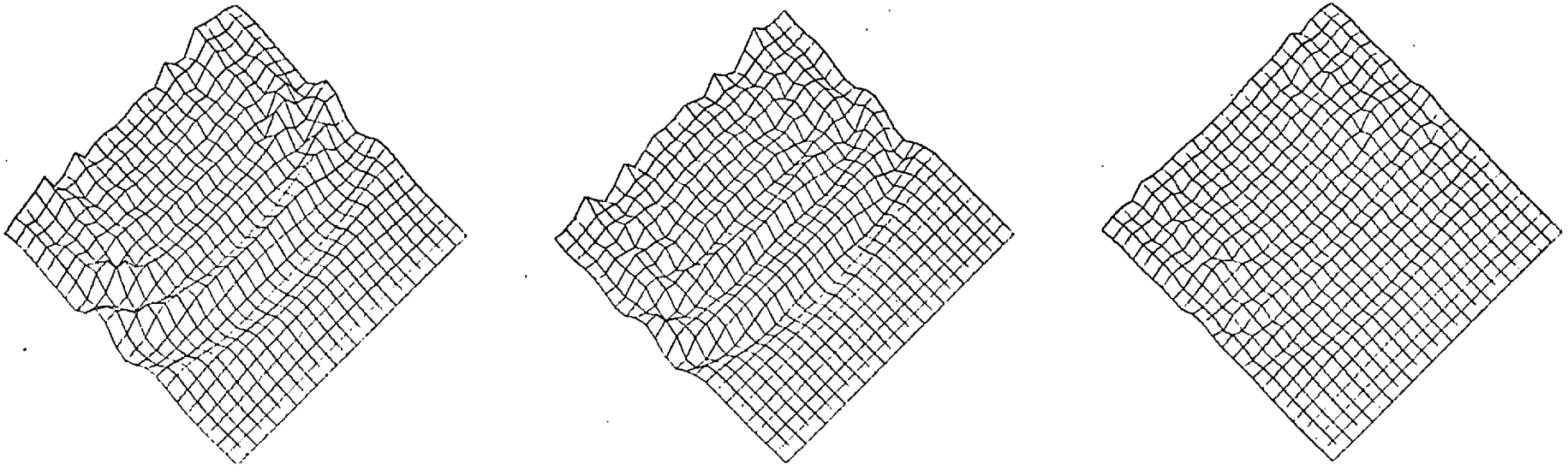
Stress isometric time = 7 μs.

figure 4/26



Stress isometric time = 8μs.

figure 4/27

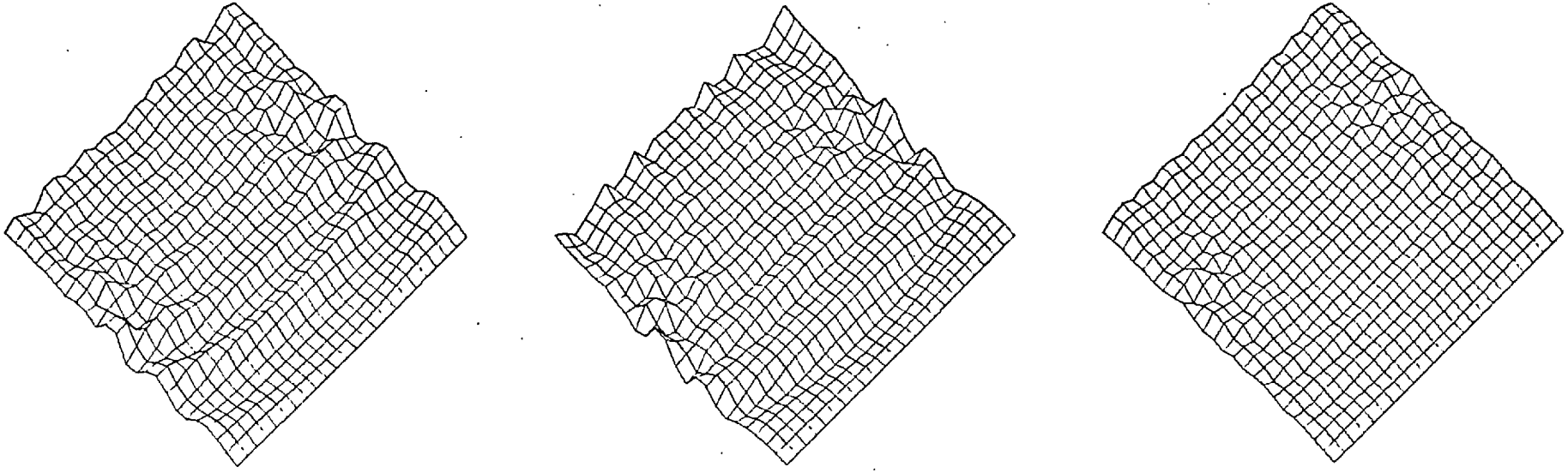


Stress isometric time=9μs.

figure 4/28

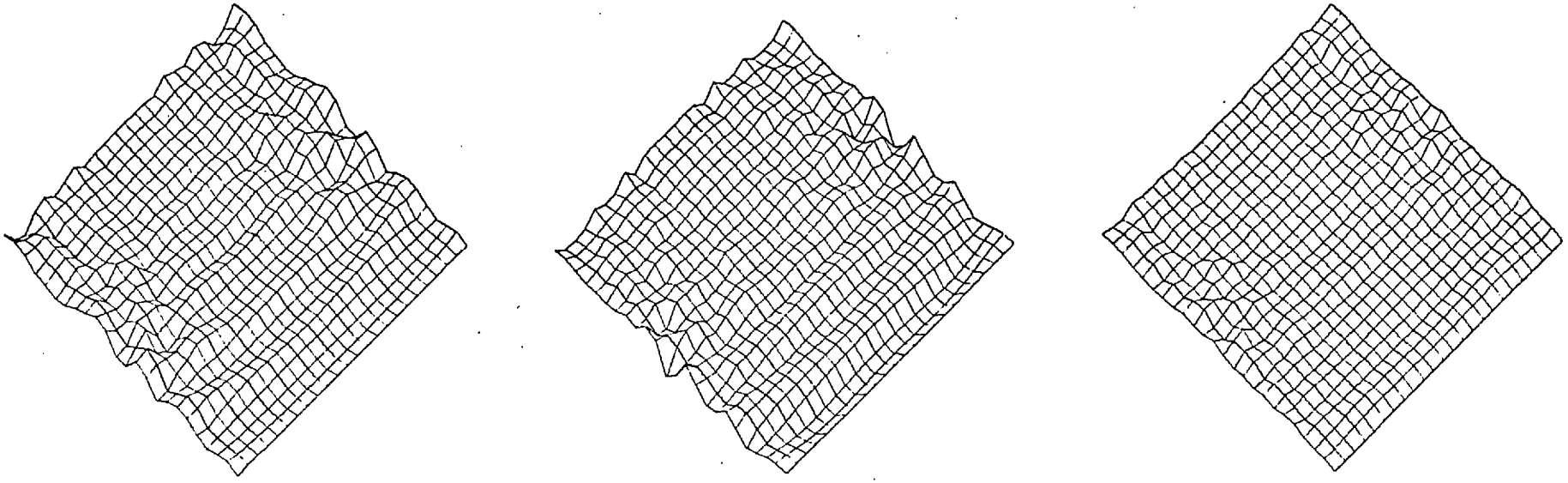
Stress isometric time=10μs.

figure 4/29



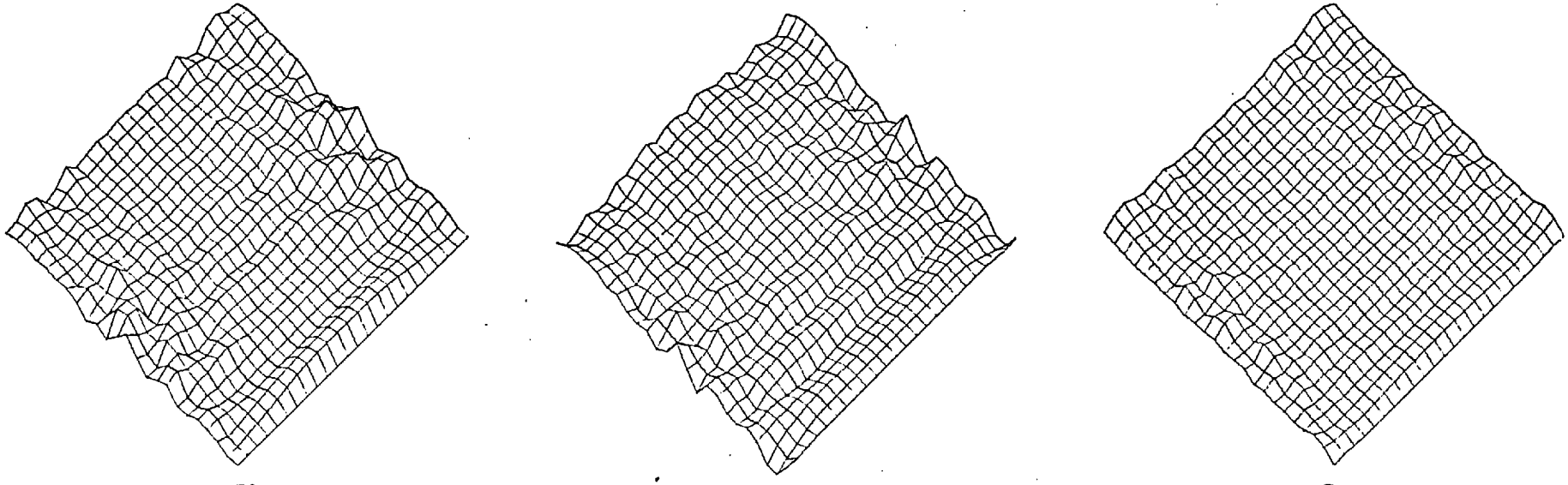
Stress isometric time=11μs.

figure 4/30



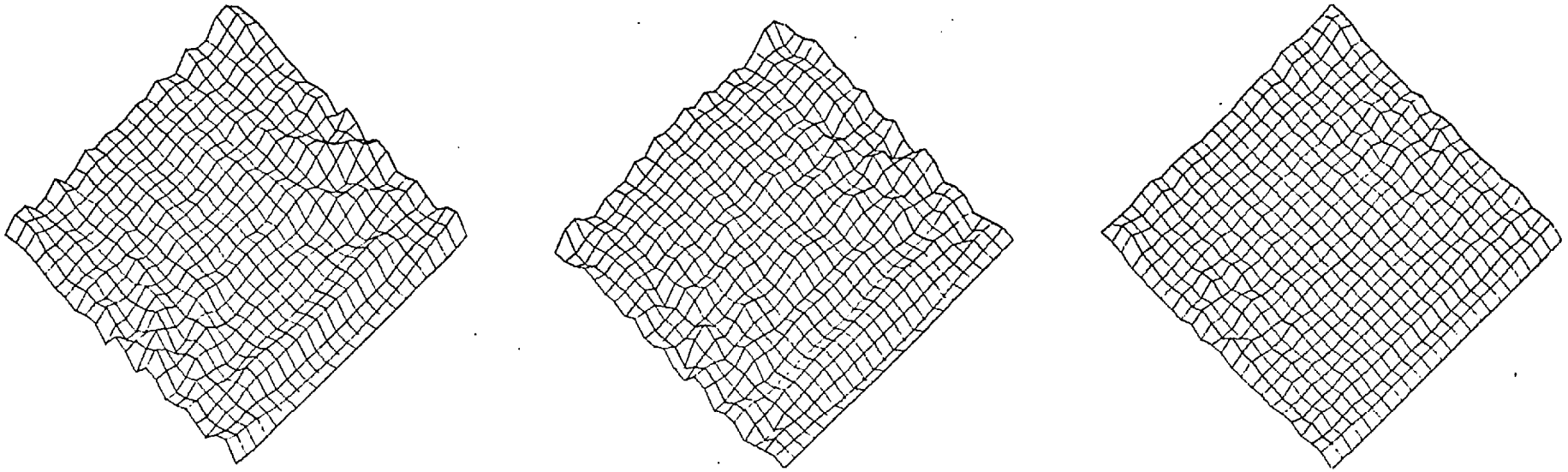
Stress isometric time = 12 μs

figure 4/31



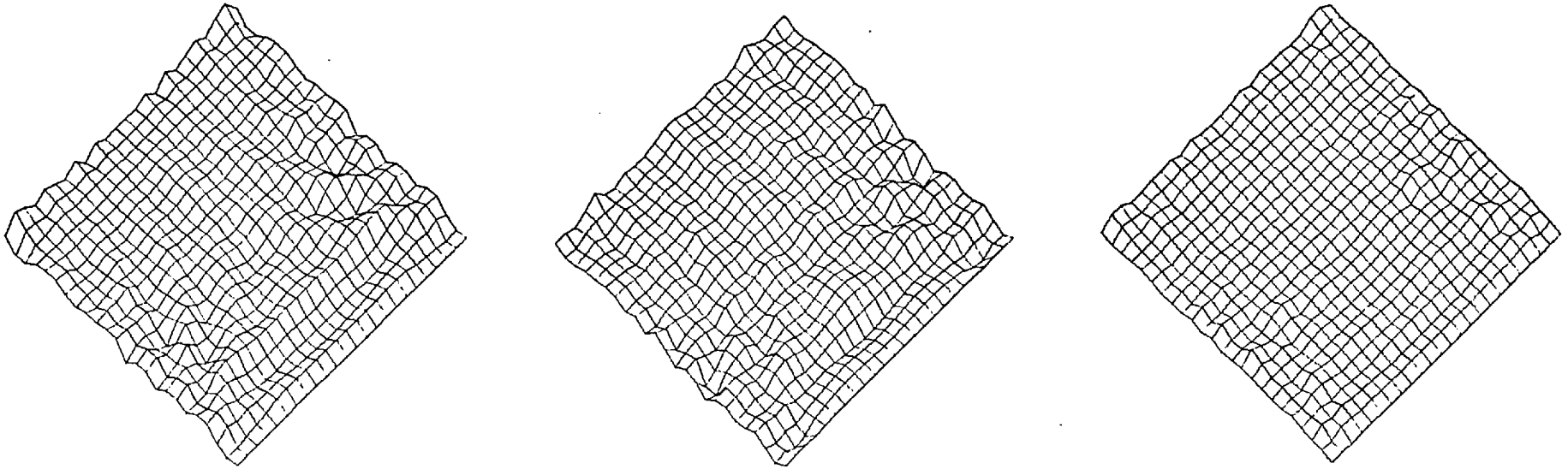
Stress isometric time = 13μ s.

figure 4/32



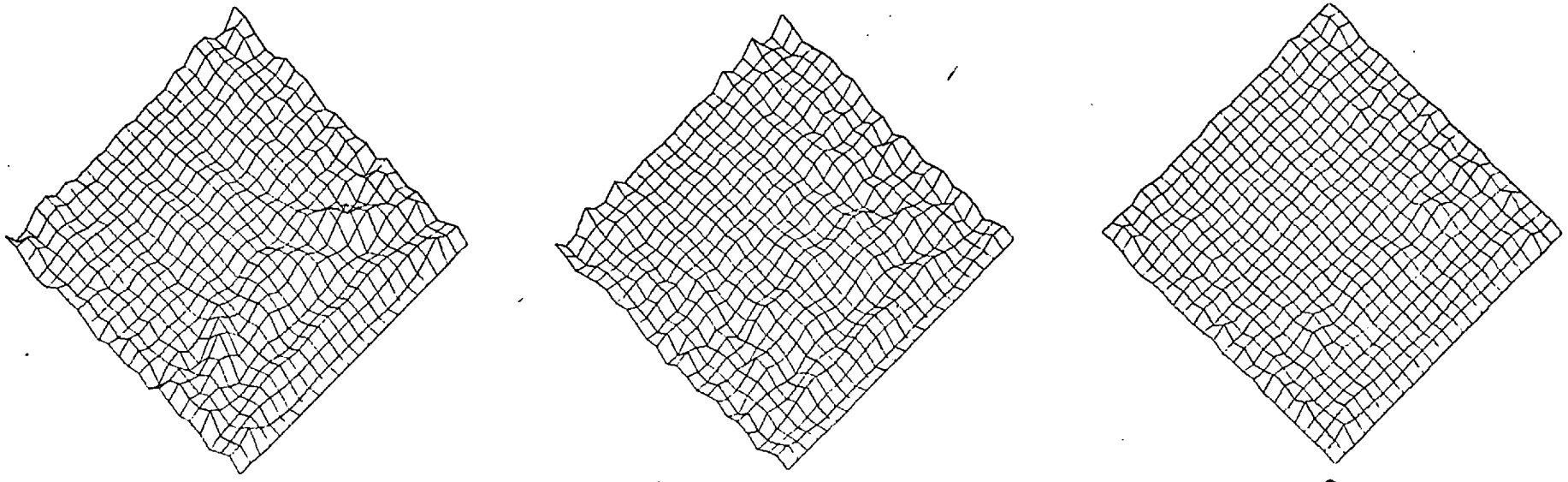
Stress isometric time = 14 μ s.

figure 4/33



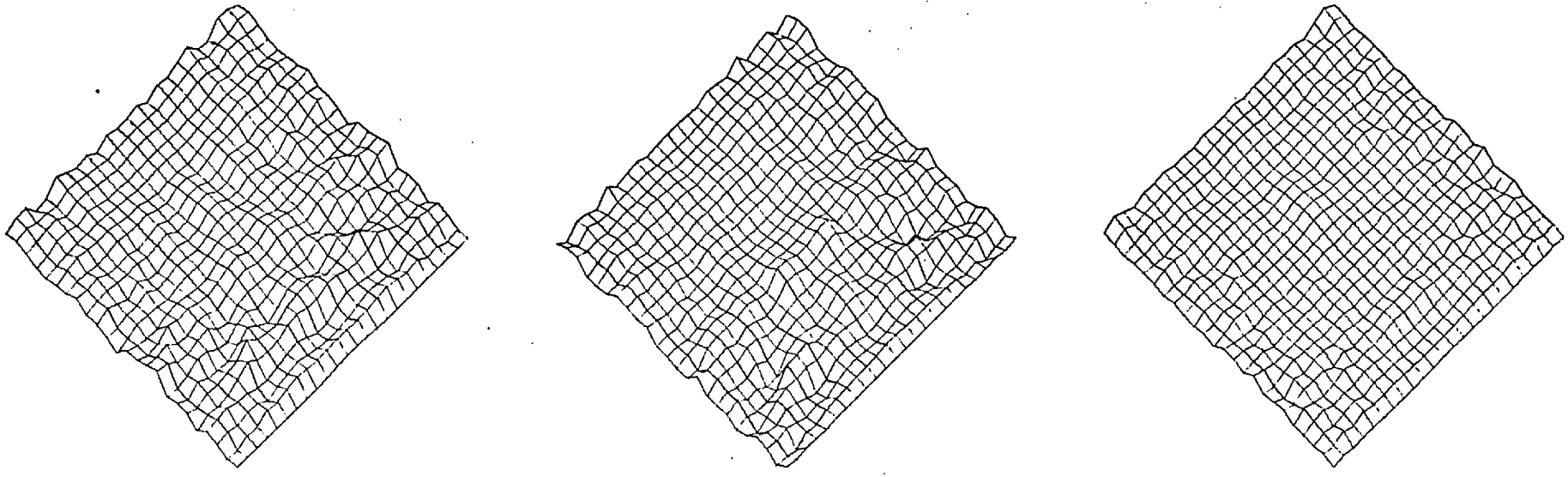
Stress isometric time = 15 μ s.

figure 4/34



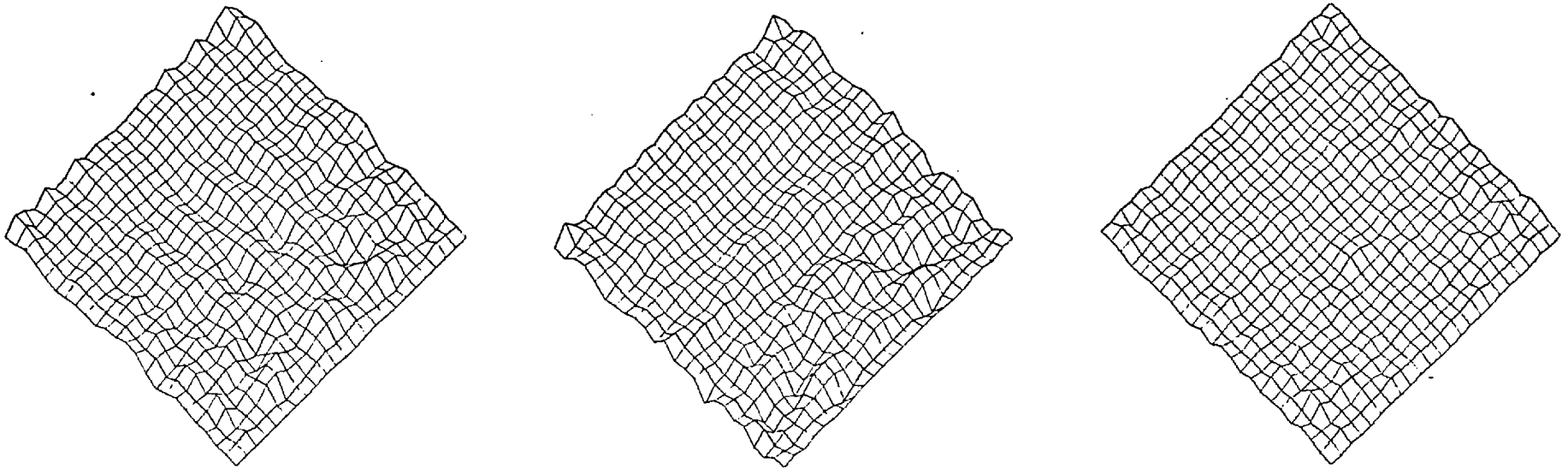
Stress isometric time = 16μs.

figure 4/35



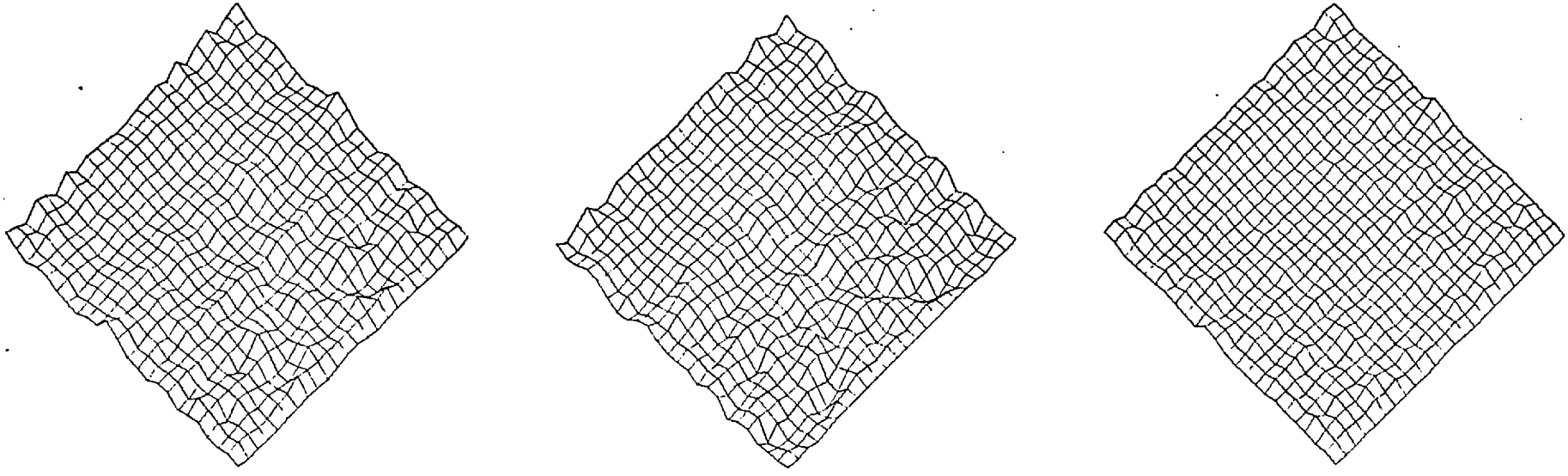
Stress isometric time = 17μs.

figure 4/36



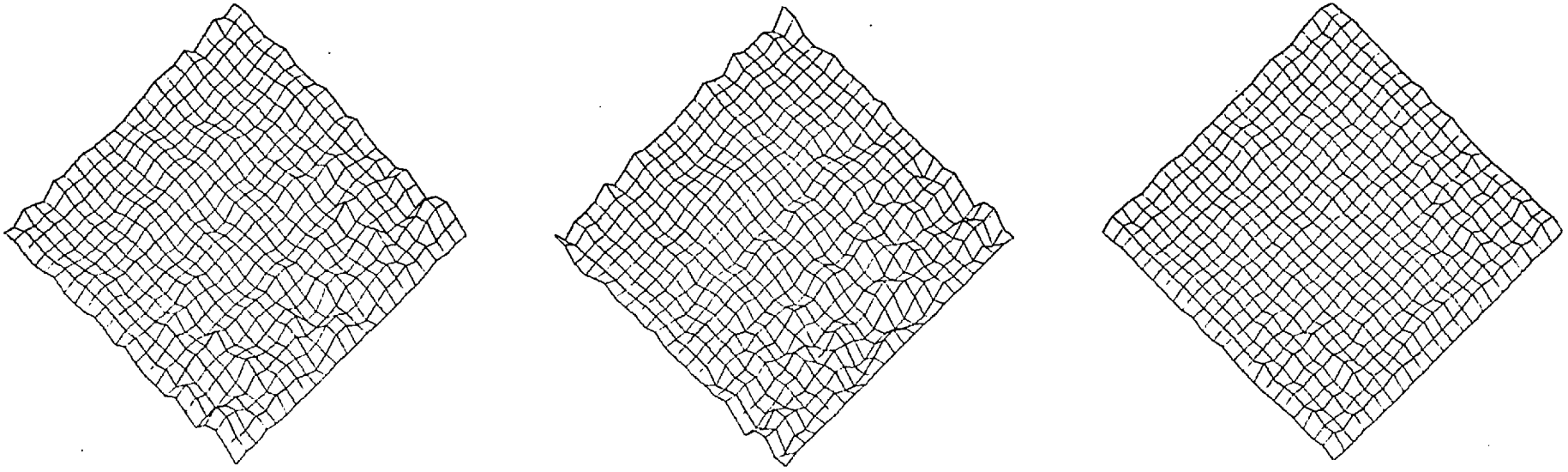
Stress isometric time = 18 μs.

figure 4/37



Stress isometric time = 19 μs.

figure 4/38



Stress isometric time = 20 μ s

figure 4/39

S_R, η_r and Si are plotted in Figure 4/40 against the time constant of the applied stress. The initial value of the applied load is assumed equal to one unit stress.

The specific impulse increases linearly with time constant. (This is implicit as the load decays exponentially.)

The ratio S_R increases rapidly at first and then more slowly as time constant increases. The increase is due to the increase of specific impulse.

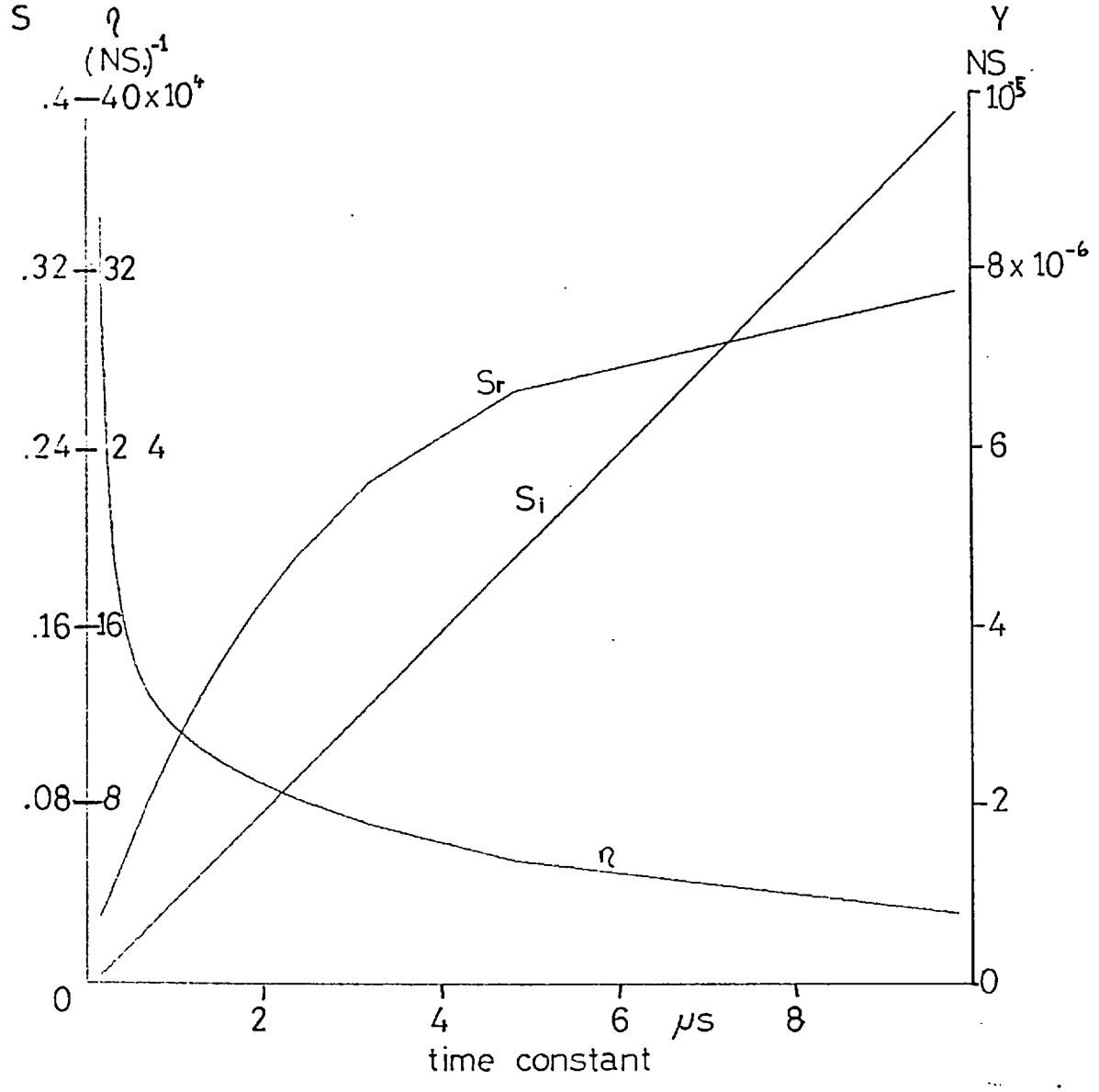
The ratio η_r decreases rapidly with increasing time constant showing that loads of short time constant are liable to cause fracture more efficiently than those of long time constant. This is in good agreement with the experimental observation that low inductance crushers are more efficient than high inductance crushers.

4.5 Fractures

An attempt was made to model the fracture process in electro-hydraulic comminution. Again the simple square two-dimensional analysis was used. The fracture criterion of Figure 4/41 was assumed. (This is a realistic static failure criterion : its validity at the strain rates considered is unknown.)

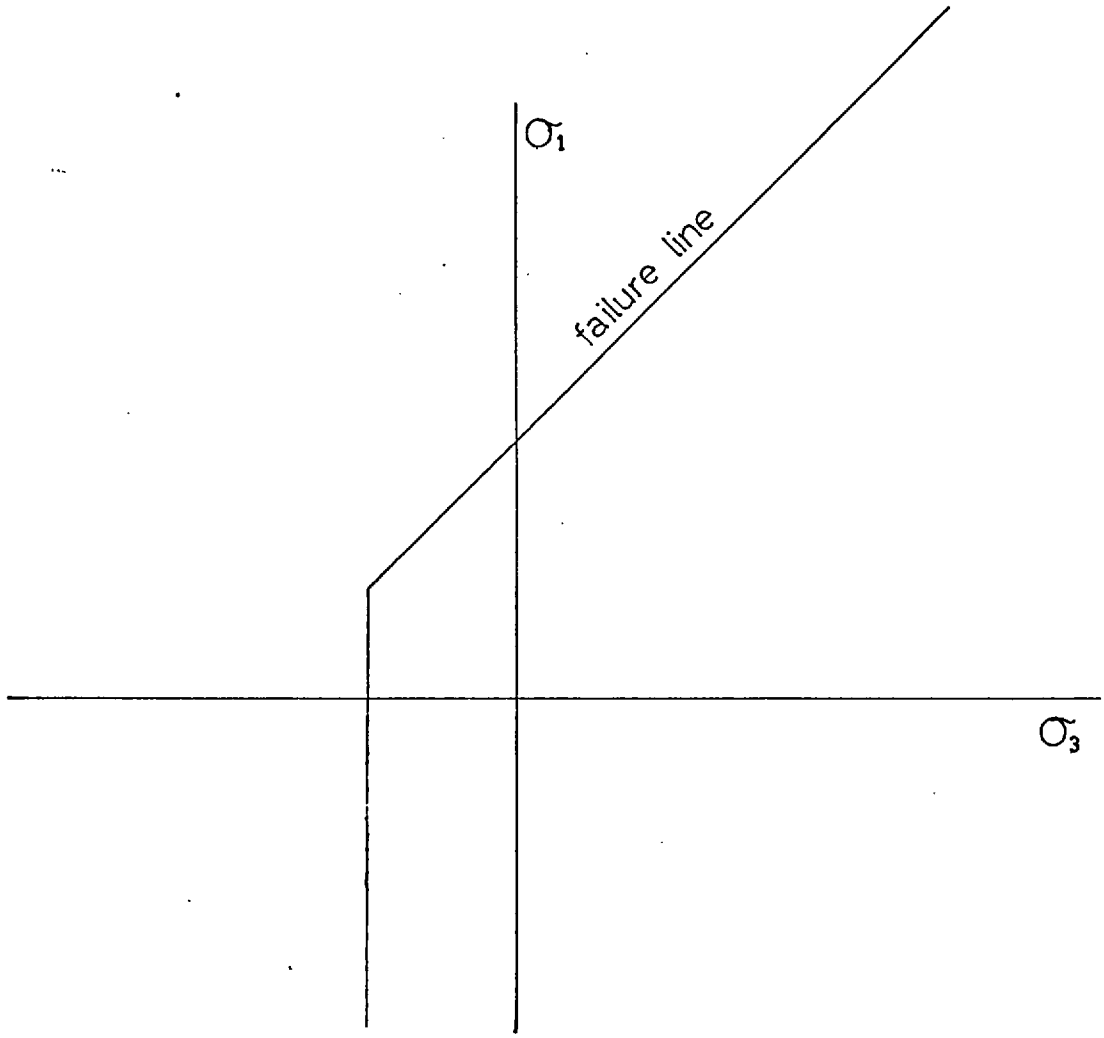
The fracture was assumed to have taken place when the stress state had crossed the fracture line of Figure 4/41. The fracture was assumed not to affect in any way the stress state. This assumption is not strictly valid; the crack tip will act as a stress

(Continued .....)



Impulse(S_i), stress ratio (S_r) and stress ratio per impulse (η) versus time constant

figure 4/40



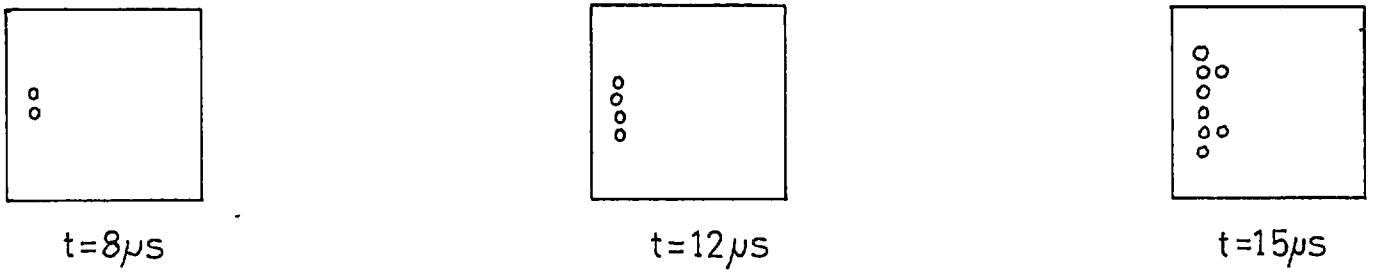
Fracture critierion

figure 4/41

raiser and radiate its own stresses, the crack will act as a new boundary and its propagation will absorb energy. However, the modelling needed to describe the true situation is complex and, interesting though it would have been, time was not available.

This simple model predicted the fracture patterns of Figure 4/42. The result is in good agreement with the radial fractures observed in experimental work, references 36, 37, 44, 136.

This result shows also that the spalling mechanism is unlikely to occur in electrohydraulic comminution as the radial fractures occur earlier and require lower stresses than spalls. The spalling mechanism will only be observed when the specimen geometry and boundary conditions are particularly favourable (i.e. a long bar).



Computed fracture patterns

figure 4/42

Part 5 - Comminution

5.1 Introduction

Full scale electrohydraulic comminution studies were originally started by Russian workers, notably Yutkin (reference 38). Some work was also carried out at the laboratories of Allis Chalmers Ltd, U.S.A. in 1952 (reference 97). The most important work in recent years has been that carried out at the United Kingdom Atomic Energy Research Establishment at Harwell, where new designs have increased the efficiency of the process principally by reduction of the circuit inductance (references 44, 37, 36).

5.2 Electrohydraulic Comminution Efficiency

The efficiency of an electrohydraulic crusher can be described by the formula:-

$$\eta o = \eta a \quad \eta f \quad \eta c$$

ηo = overall efficiency.

ηf = efficiency of converting acoustic energy into fractures.

ηa = efficiency of converting electrical energy into acoustic energy.

ηc = efficiency of capacitor charging.

The expression can be factorized:-

$$\eta o = (\eta f \quad \eta a) \quad \eta c$$

as ηc is independent of ηf and ηa.

(Continued .....)

The optimisation of ηc, the capacitor charging efficiency, is considered in Appendix 4. In simple systems, however, it is unlikely to be greater than 50%.

5.3 Discharge Parameters

The optimisation of ηf ηa leads to conflicting constraints in that some parameters increase ηf and decrease ηa.

ηf depends on:-

- The distance of the spark to the mineral to be crushed.
- The stress wave time constant.
- The stress wave amplitude.

ηa depends on:-

- Voltage.
- Electric field.
- Gap length.
- Inductance.
- Resistance.
- Capacitance.
- Water conductivity.
- Presence of nearby minerals.

Now if ηf is maximised electrodes should be designed in such a way that the spark travels over the rock surface. This ensures the minimum distance from spark to rock, the shortest time constant wave and the highest wave amplitude. However in order to ensure the

(Continued .....)

spark occurs on the rock surface the electrode area must be large in comparison with the rock size.

This will mean that the pre-breakdown conduction losses, the inductance and the resistance will all be greater.

If the electrodes are small in area (essentially a point-point electrode system) the inductance, resistance and pre-breakdown losses will be reduced but the spark may not always be on the surface of the rock thereby reducing the wave amplitude and increasing the wave time constant.

Electrohydraulic crushers can thus be classified into two types:-

Optimum coupling crushers in which the electrodes are designed to ensure that the spark travels on a rock surface; and

Optimum spark crushers in which the electrodes are designed to maximise the spark pressures by having the smallest possible area.

It is the author's opinion that optimum coupling machines should be used for coarse crushing and optimum ~~coupling~~ spark machines for grinding.

As the properties of optimum spark machines are well described by Carley Macauly et al (references 36, 37, 44) only optimum coupling machines will be considered.

(Continued .....)

5.4 Optimum Coupling Design Principles

a) The electrode area should be great enough that at the design flow rate there is at least one piece of rock sitting on the electrodes. If the area is too small then the feeder will be unable to place the rock accurately enough to ensure that all sparks do some useful work. If, however, the electrode area is large then the pre-spark breakdown losses may be considerable.

b) In the absence of a piece of rock the maximum value of electric field across the gap should be the same throughout the length of the gap. This ensures that when a rock is present the spark will travel across the rock surface.

c) The circuit inductance should be minimised. Experiments, reported in part 3 of this thesis, and in the literature, show that the peak pressure and the specific impulse of the shock wave decrease with increasing inductance if $\pi \sqrt{LC} > \tau$.

L = inductance.

C = capacity.

τ = time constant of stress wave.

d) Circuit resistance should be minimised. Circuit resistance reduces the energy available for crushing and may in large crushers cause unwanted heating of components. It should be noted that conductor resistance is principally due to skin effects because of the high frequencies involved. The minimisation of both inductance and skin resistance demand large conductor areas with small

(Continued .....)

spaces between "go" and "return" conductors. The choice of best switching techniques is discussed in Appendix 5 where it is shown that spark gaps, preferably of the field distortion type, offer the best properties.

e) The circuit should be approximately critically damped; this has been shown to give maximum spark pressures and hence best crushing performance (reference 36).

f) Voltage should be optimised. The relationship between voltage and efficiency is complex but the following are important:-

Pre-spark loss power increases with increasing voltage.
Breakdown time decreases with increasing voltage.
Air-gap resistance decreases with increasing voltage.

It is considered that there is an optimum voltage for a given crusher design.

5.5 Experiments

In order to provide some information about the performance of optimum coupling crushers, some experiments were carried out using the crusher developed by Yigit (reference 136). The experimental technique and apparatus are described in Appendix 6.

5.5.1 Effect of Rock Strength

Seven different rock types were crushed starting with three

(Continued .....)

different sizes. Bond's Index and Kick's Constant were calculated. Rock strengths were measured by the uniaxial unconfined compression test and by the point load test. Graphs 5/1 to 5/4 show the relationships between crushing efficiency and rock strength.

It was initially thought that there should be a good correlation between point load strength and crushing efficiency as the point load strength is essentially a measure of tensile strength. The experiments did not show this. The crushing efficiency was partially correlated with the uniaxial compression strength. It is probable that further factors such as acoustic impedance would enable accurate predictions of crushing efficiency.

5.5.2 Crushing of Ores

As a crusher is also likely to be used for the crushing of ores some four ore types were also crushed. These showed no marked difference to the rocks except in the case of a nickel ore which had a Bond's Index of 800 kwh/tonne, far in excess of any of the other power consumptions. It is thought that this result is due to the high conductivity of the nickel ore.

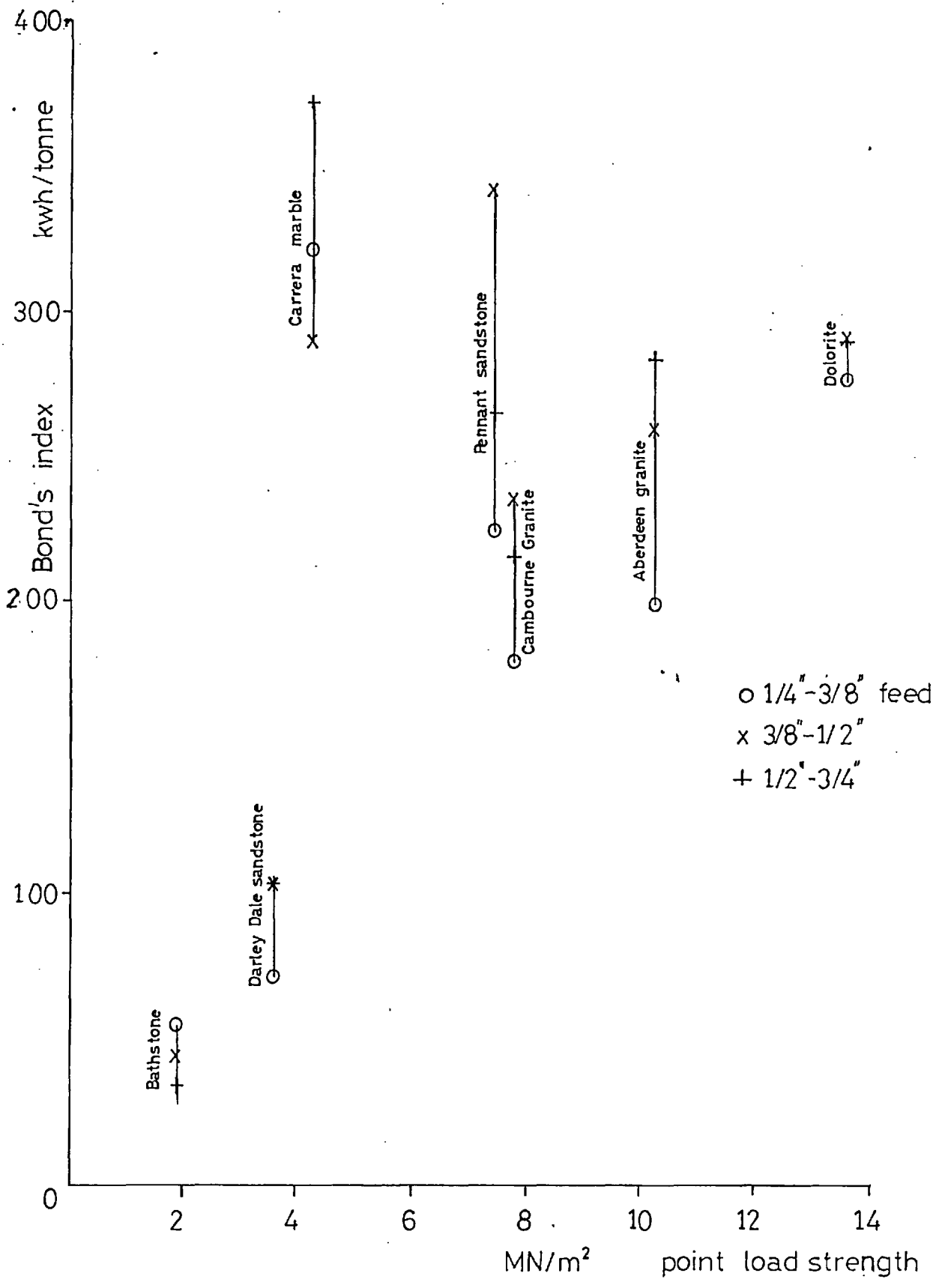
5.5.3 Starting Size

It was considered that the work indices should change with starting size as the ratio

$$\frac{\text{Stress pulse wavelength}}{\text{Body size}}$$

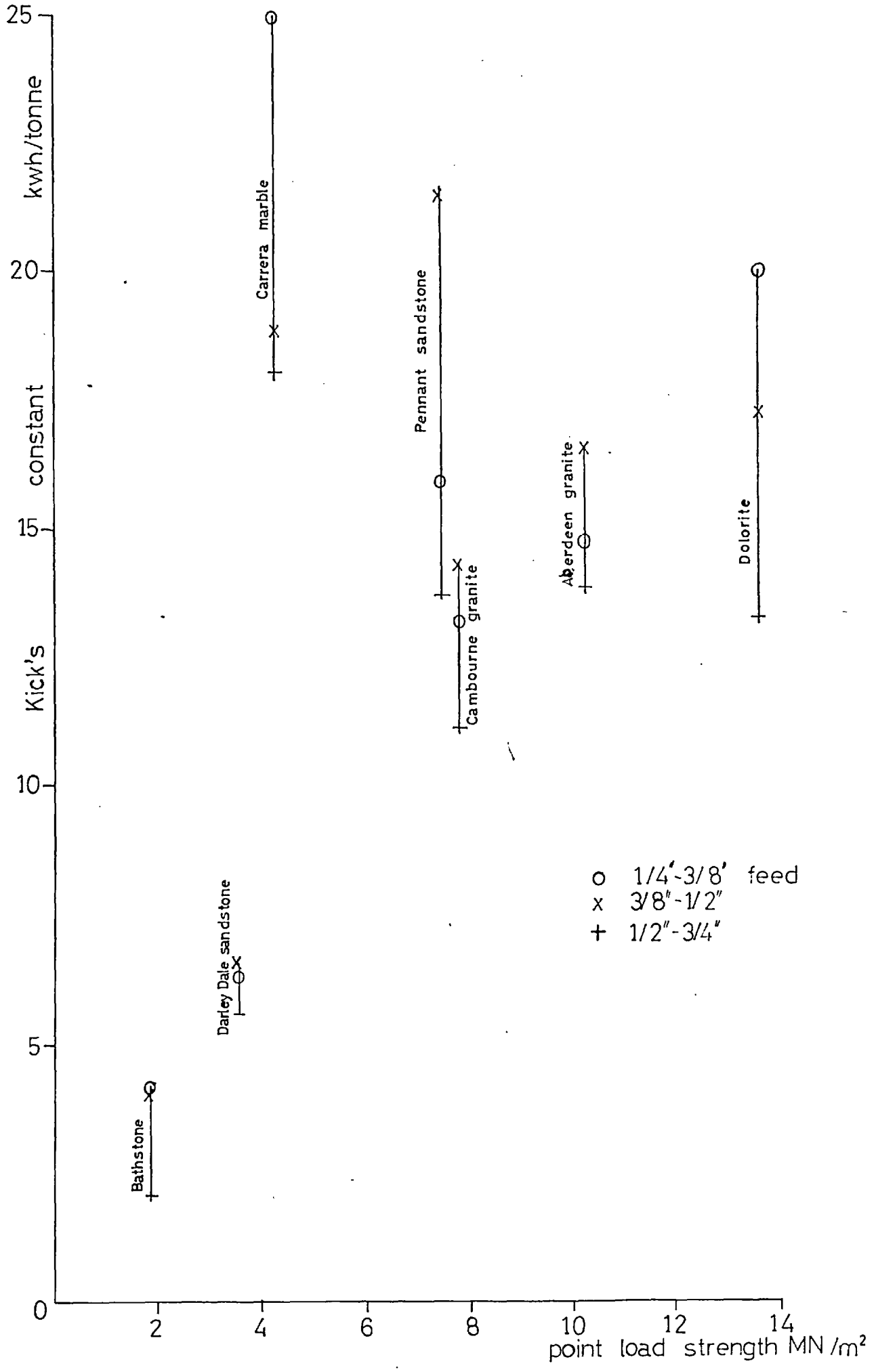
would change. Each of the rock samples tested were crushed at

(Continued .....)



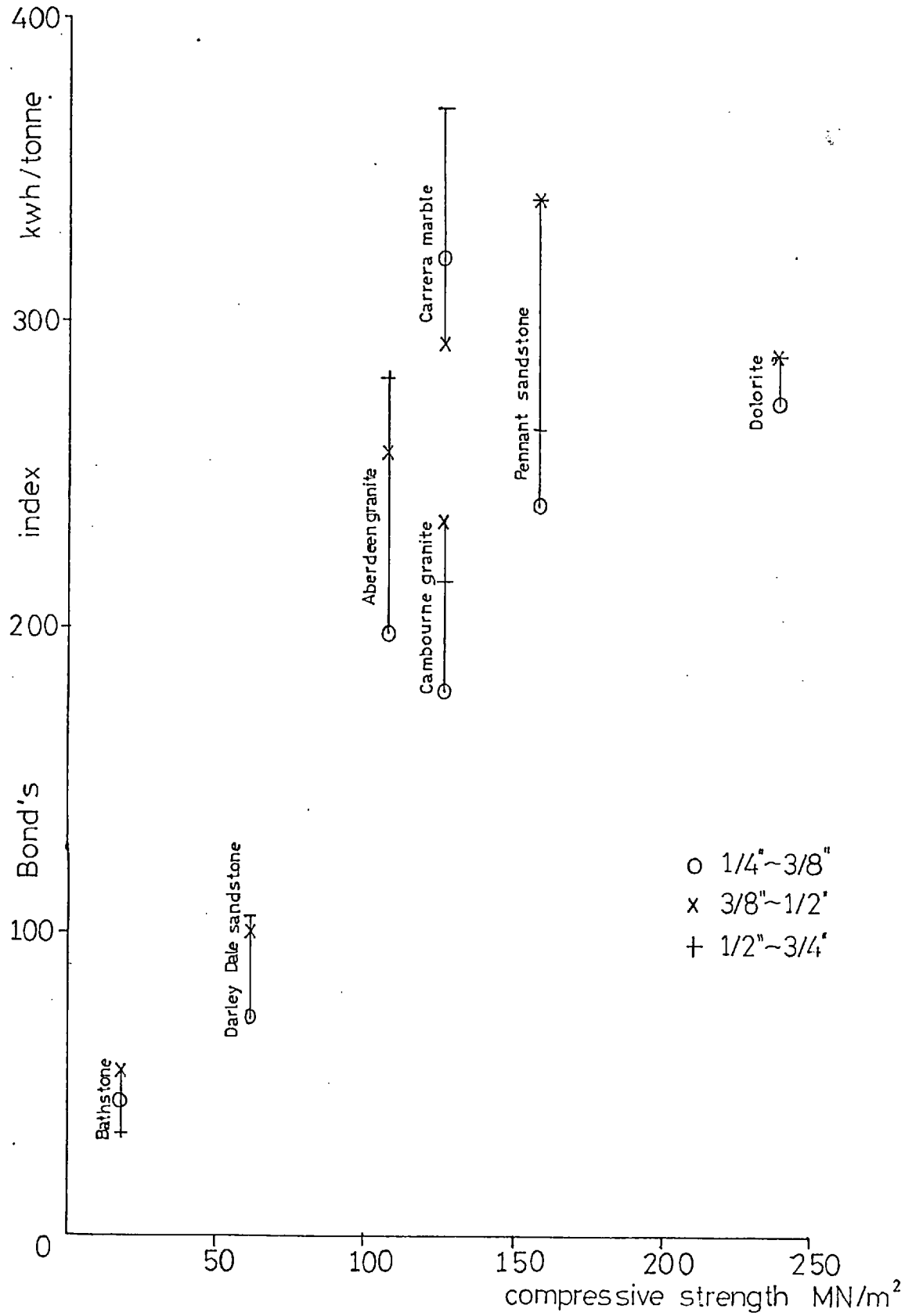
Crushing efficiency versus point load strength

figure 5/1



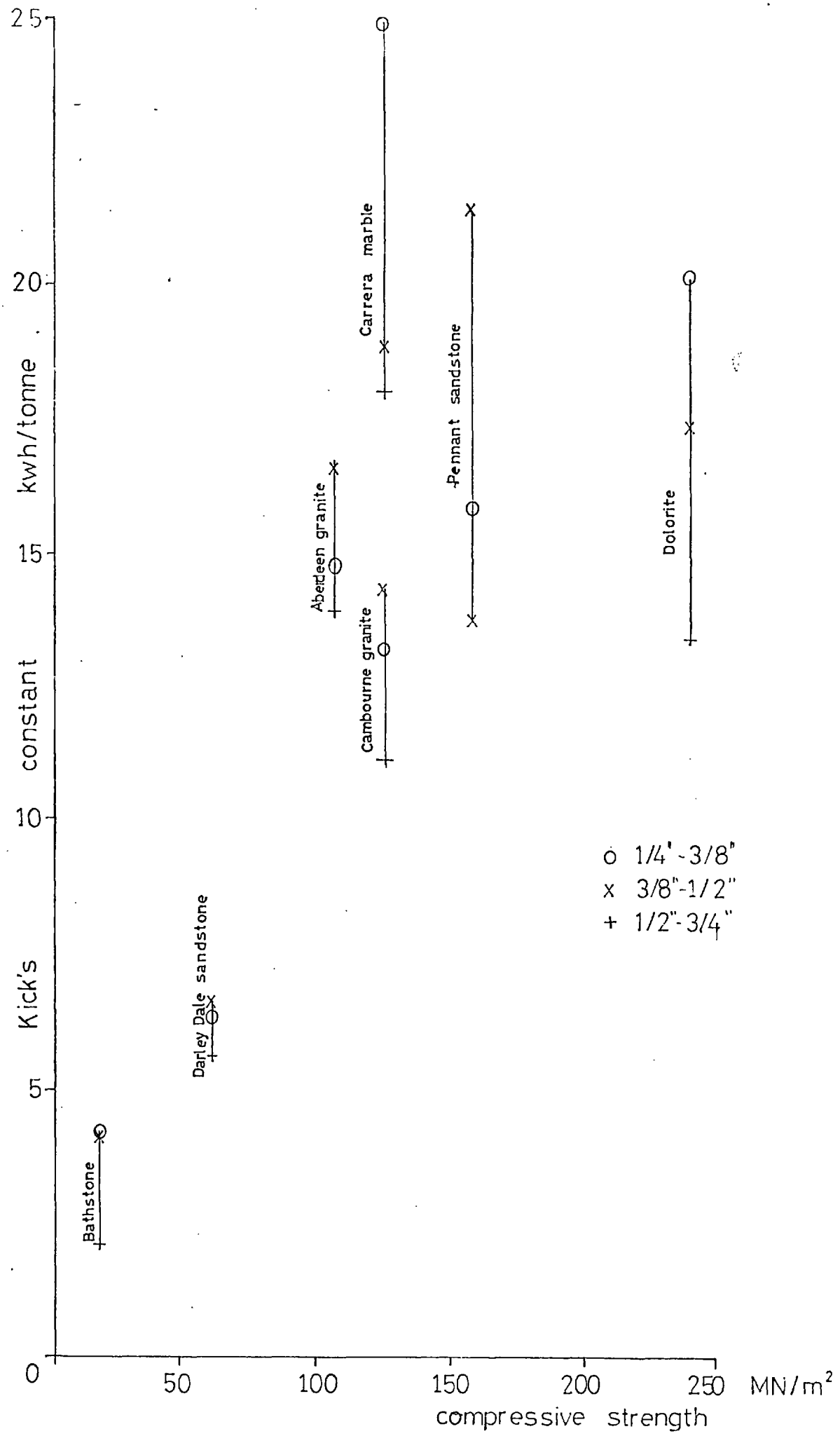
Kick's constant versus point load strength

figure 5/2



Bond's index versus compressive strength

figure 5/3



Kick's constant versus compressive strength

figure 5/4

Table 5/1

Electrohydraulic Crushing

	Bond's Index kwh/ton			Kick's Constant kwh/ton			Rock Strength MN/m^2		Porosity %	Comments	Sample Number
	¼-⅜ Feed	⅜-½ Feed	½-¾ Feed	¼-⅜ Feed	⅜-½ Feed	½-¾ Feed	Uni Axial	Point Load			
Pennant Sandstone	224	341	265	15·9	21.4	13.7	159	7.5	.22		219
Darley dale Sandstone	71	103	103	6·3	6·6	5·6	62	3·6	12.6	Strength less when wet	215
Dolorite	275	290	288	20·1	17·3	13·3	244	13·7	·03		217
Bathstone	44	54	34	4·2	4·1	2·1	17·9	1·9	8	These porosities are only estimates not measured values. Data on rocks supplied by Rock Mechanics Group	216
Aberdeen Granite	198	258	282	14·8	16·6	13·9	108·7	10·3	3		207
Cambourne Granite	179	235	215	13·2	14·3	11·1	127	7·8	3		218
Carrera Marble	321	289	371	24·8	18·8	18·0	127	4·31	·07		213
Derbyshire Granite	339	393	383	24·2	23·4	18·1	-	-	-	This rock was used for conductivity measurements	-
Turkish Chromite	59	51	44	4·7	3·6	2·7	-	-	-	Very weak mechanically slightly conductive at D.C.	-
Gold Ore (South Africa)	138	110	142	10·2	6·5	7·2	-	-	-	Mechanically competent Insulating at D.C.	-
Beryillium Ore	189	281	242	15·0	17·9	12·8	-	-	-	Mechanically competent Insulating at D.C.	-
Nickel Ore (Australia)	455	814	940	33·2	45·0	40·1	-	-	-	Very brittle and weak Conductive at D.C.	-

three different starting sizes but no consistent trend could be observed. This is because both the Bond's Index and Kick's Constant formulae involve the starting size and the effect is masked.

Table 5/1 summarizes the results of all the crushing experiments.

5.5.4 Water Conductivity

A Derbyshire granite was crushed with water flowing through the crusher. Bond's Index and Kick's Constant were measured for six different values of water conductivity.

Neither Bond's Index nor Kick's Constant changed (within the limits of experimental error). However the power consumption was lower when water flowed through the crusher than when it was stationary in the crusher. Figure 5/5 shows the experimental results.

In section 2 it was shown that:

$$\tau \propto \frac{1}{\sigma}$$

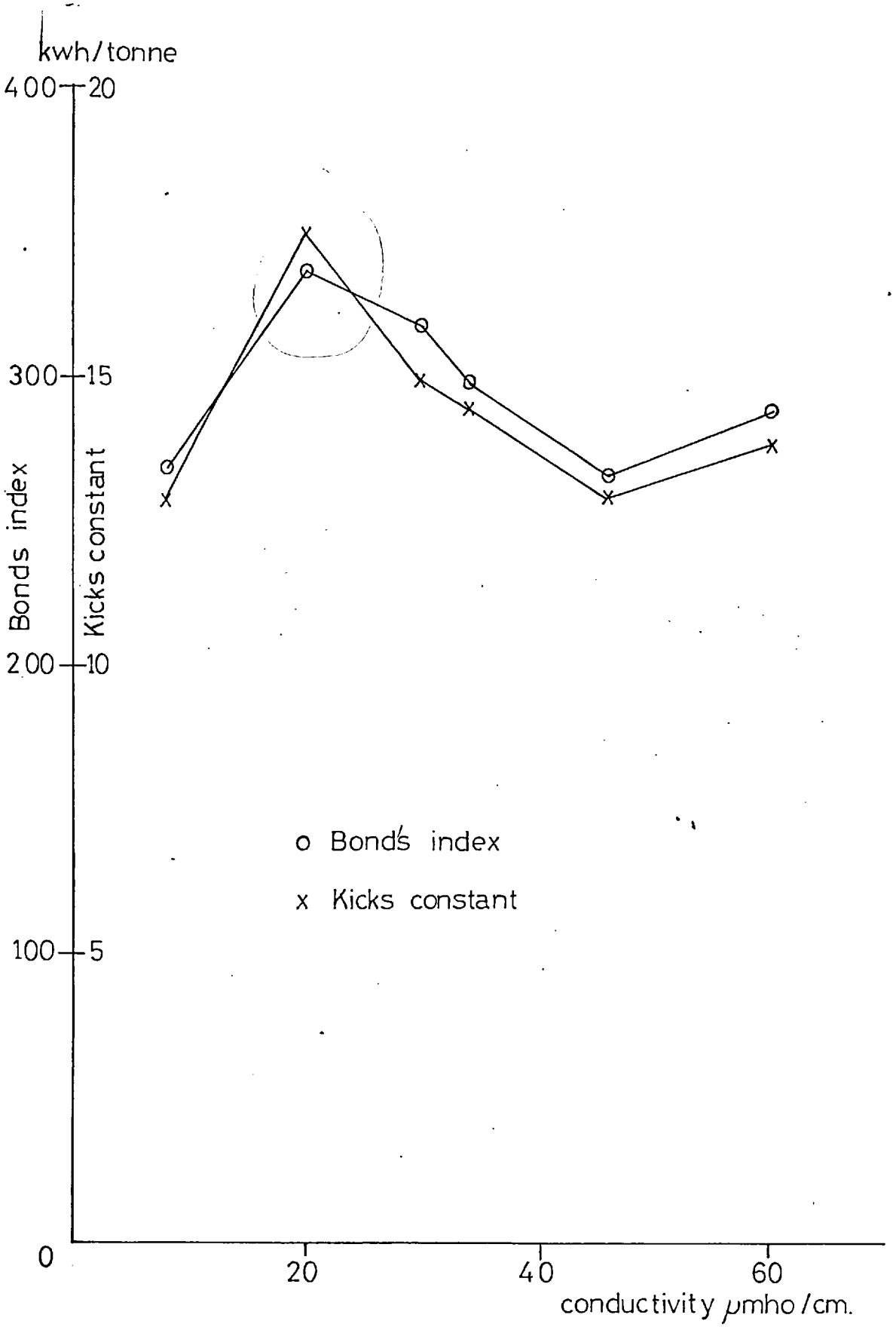
τ = breakdown time

σ = water conductivity

Pre-spark losses $\propto \tau\sigma$

Therefore pre-spark losses are independent of conductivity and hence crushing efficiency does not depend on water conductivity over the range considered. It is considered that the lower efficiency with stationary water is due to the less efficient removal of crushed pieces.

(Continued .....)

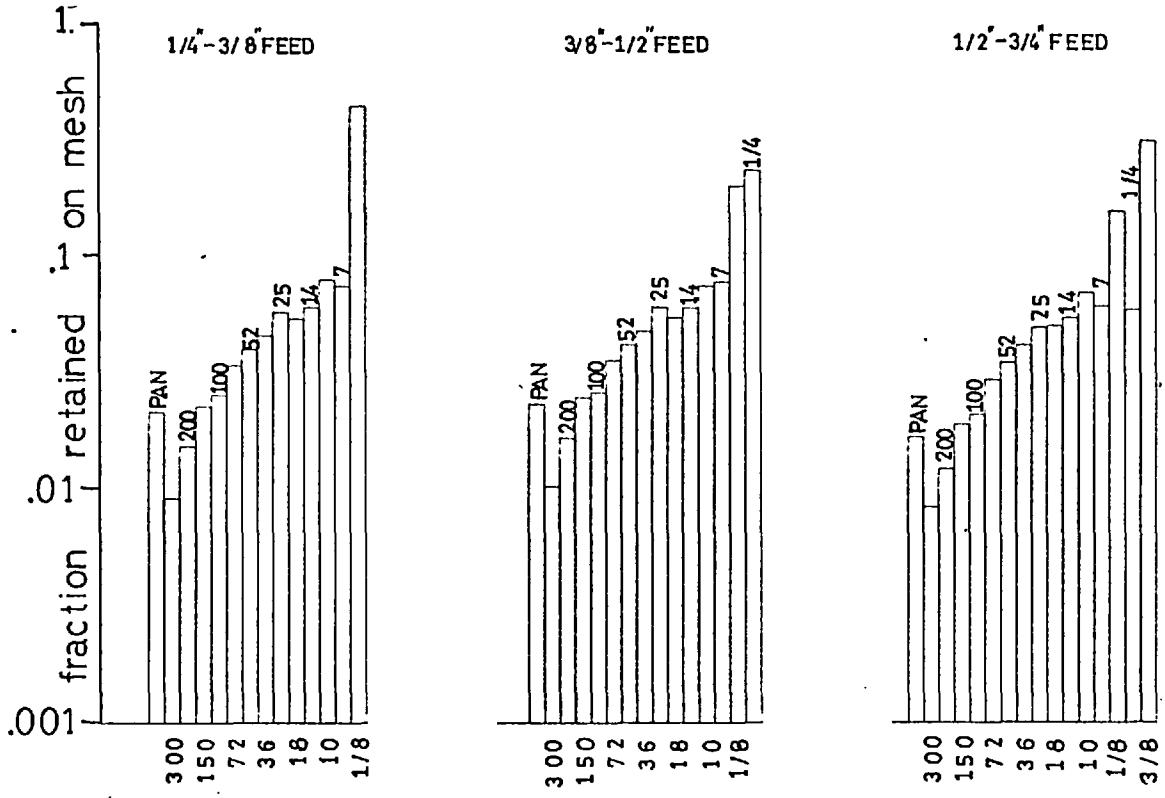


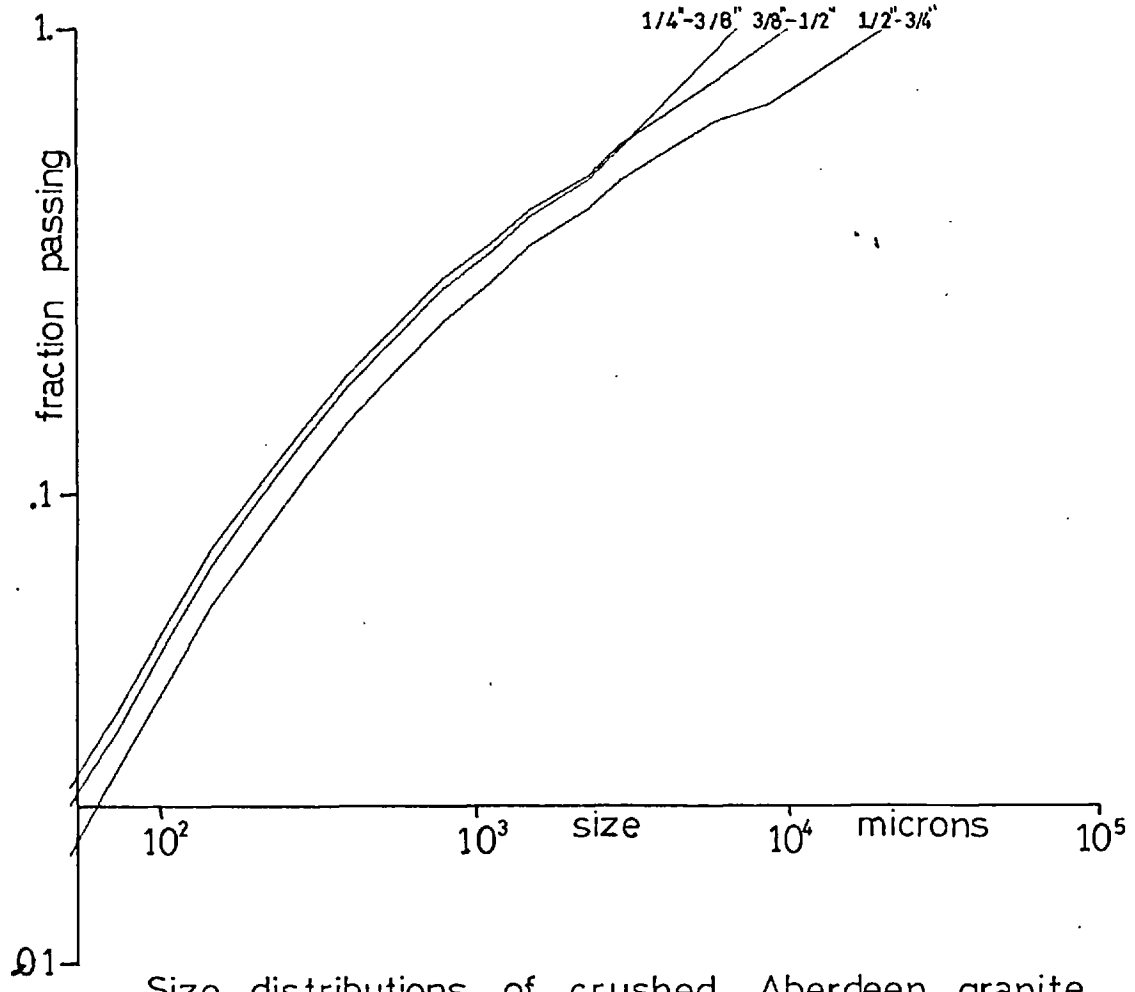
Crushing power consumption versus water conductivity

figure 5/5

5.5.5 Size Distributions

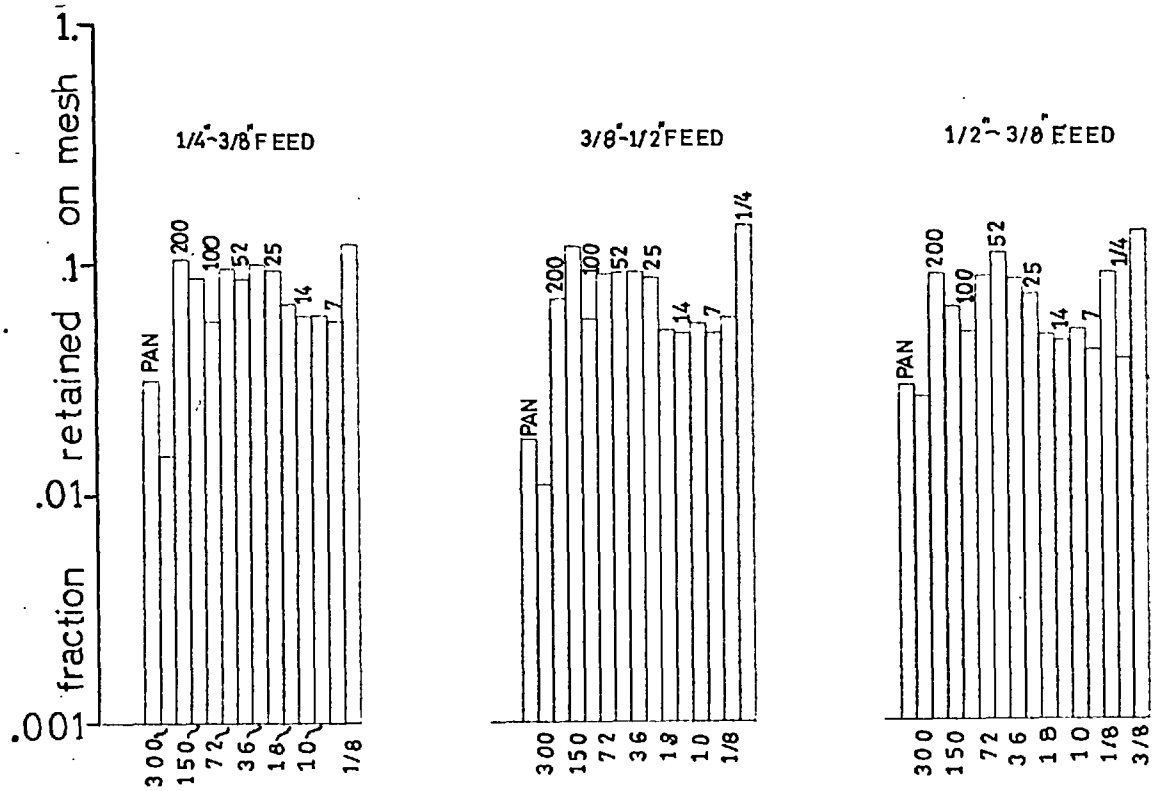
Size distributions for the product of each crushing experiment are given in Figures 5/6 to 5/17. It is interesting to note that some rocks (in particular the Pennant Sandstone) exhibit grain size effects showing that electrohydraulic comminution can be efficient in liberation. This effect may be due to surface wave phenomena discussed in part 4 of this thesis.

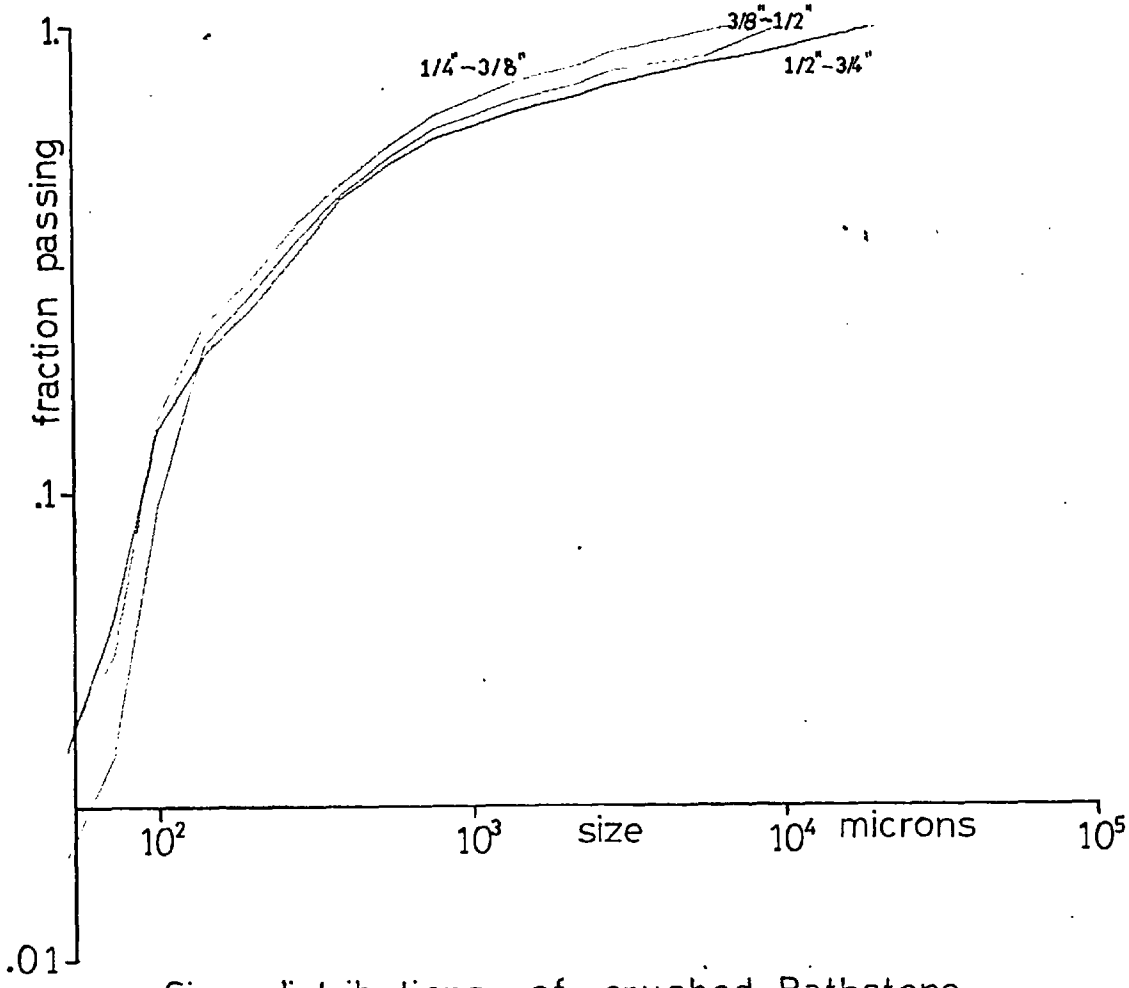




Size distributions of crushed Aberdeen granite

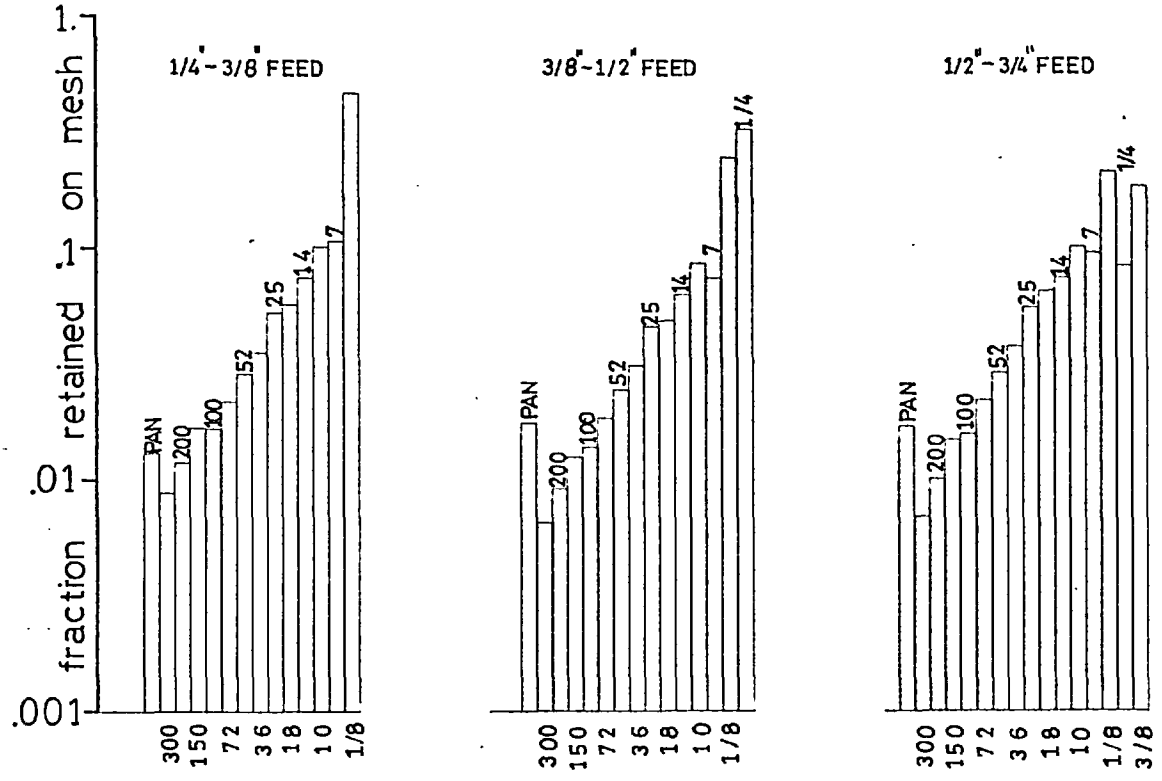
figure 5/6

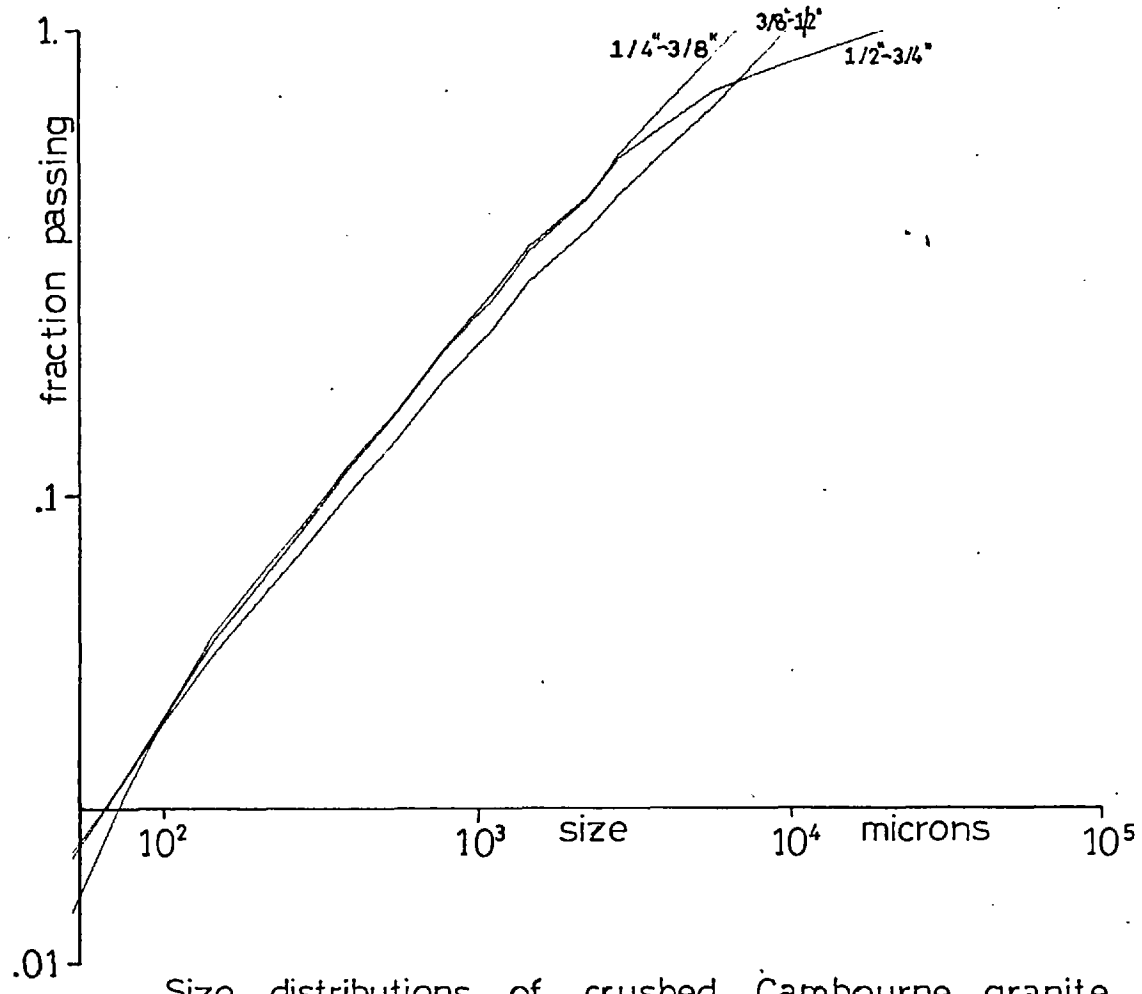




Size distributions of crushed Bathstone

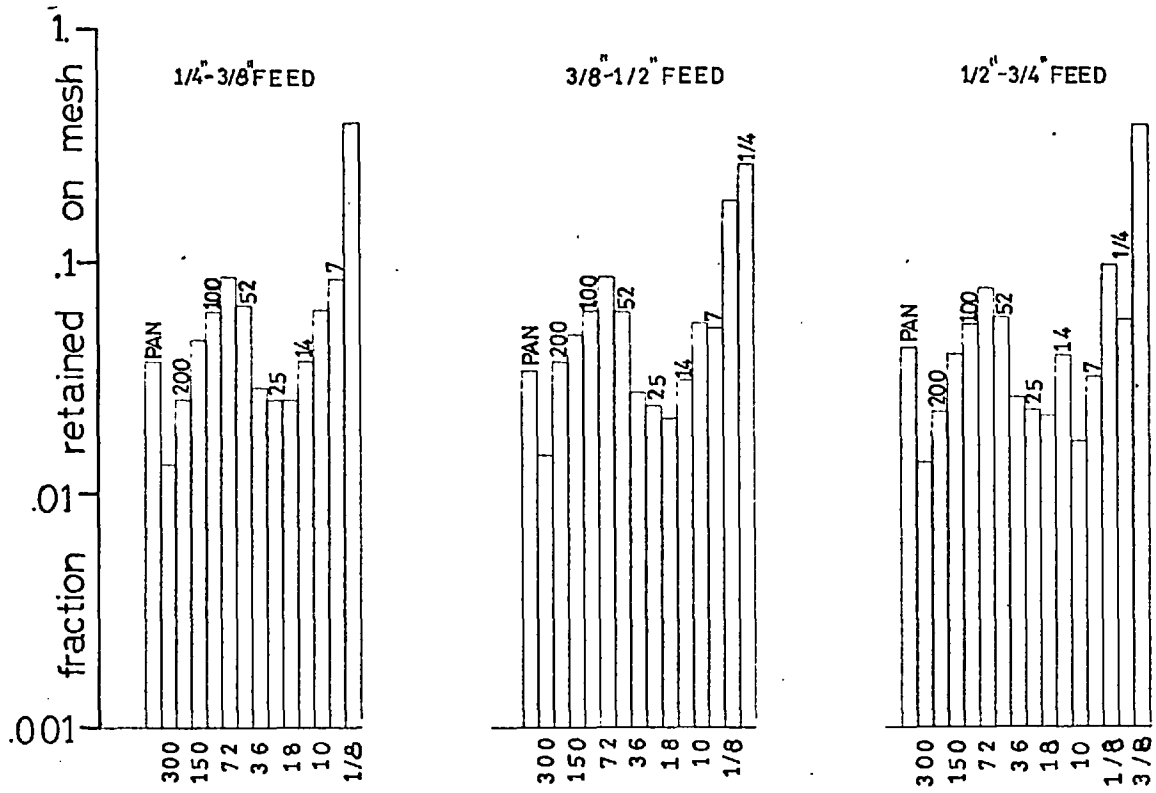
figure 5/7

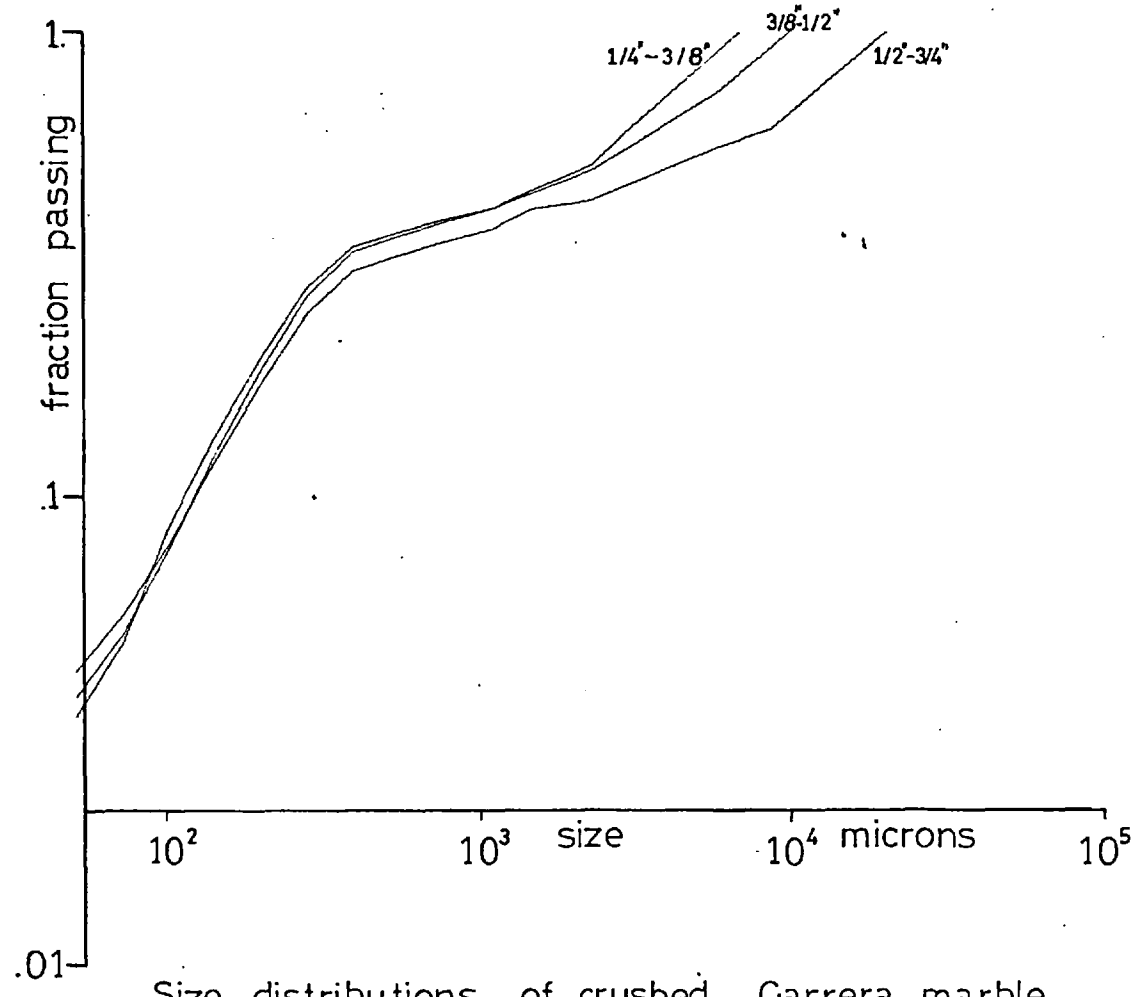




Size distributions of crushed Cambourne granite

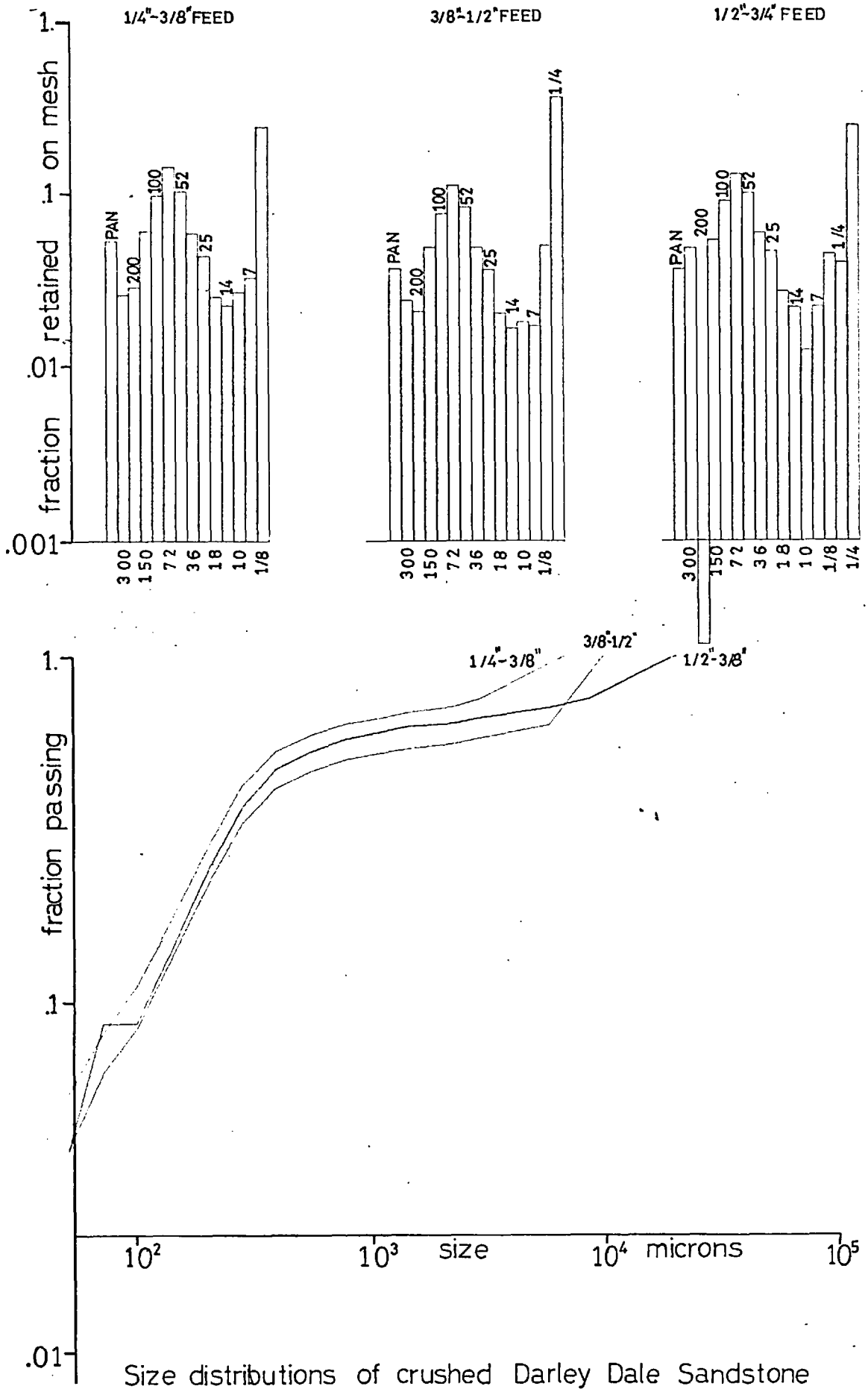
figure 5/8





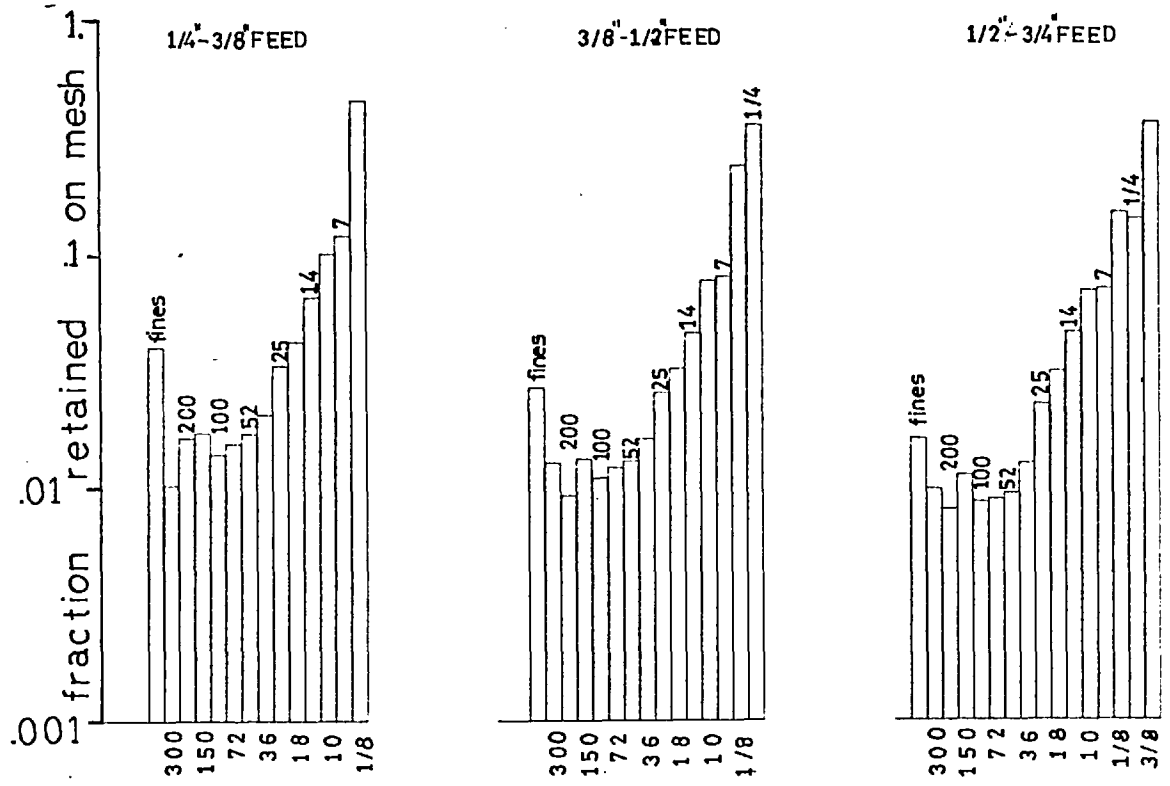
Size distributions of crushed Carrera marble

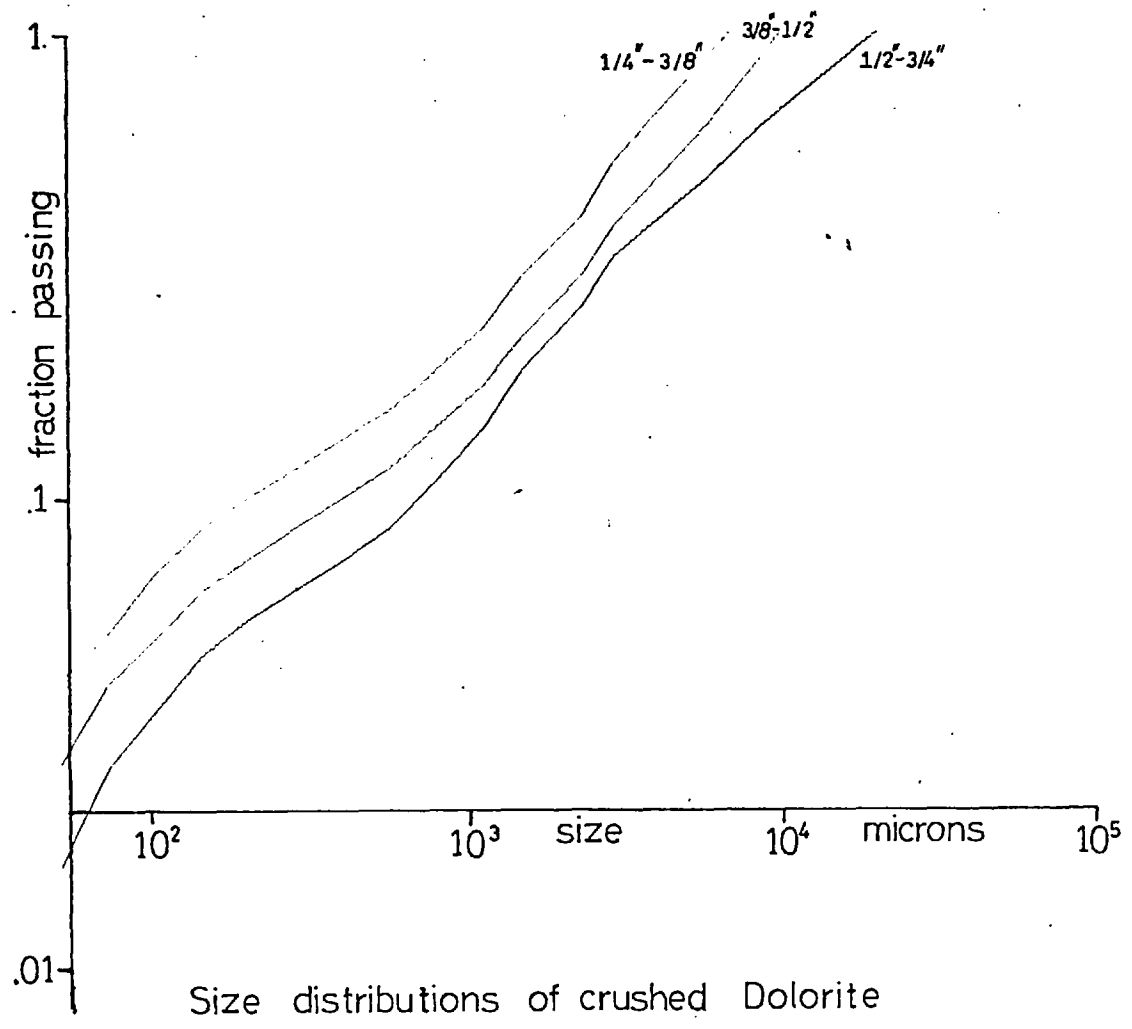
figure 5/9



Size distributions of crushed Darley Dale Sandstone

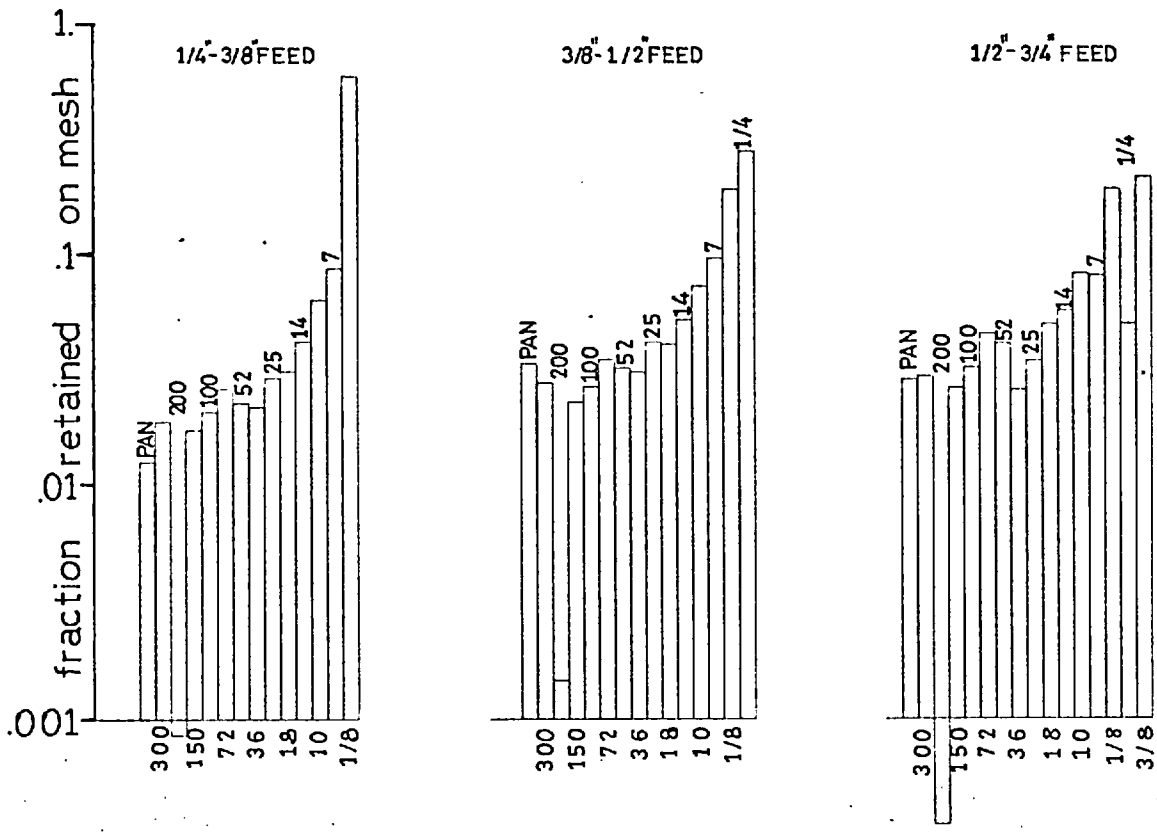
figure 5/10

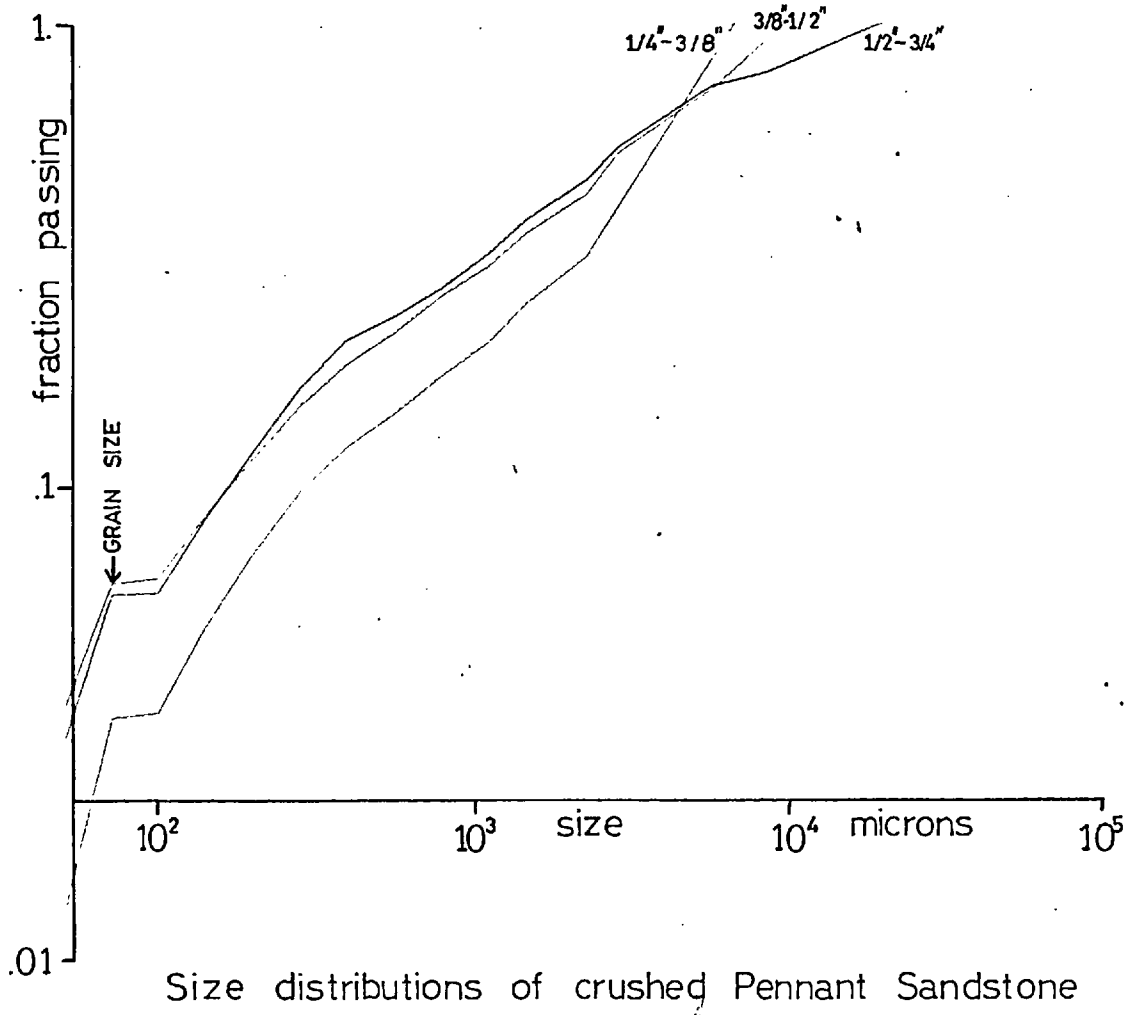




Size distributions of crushed Dolorite

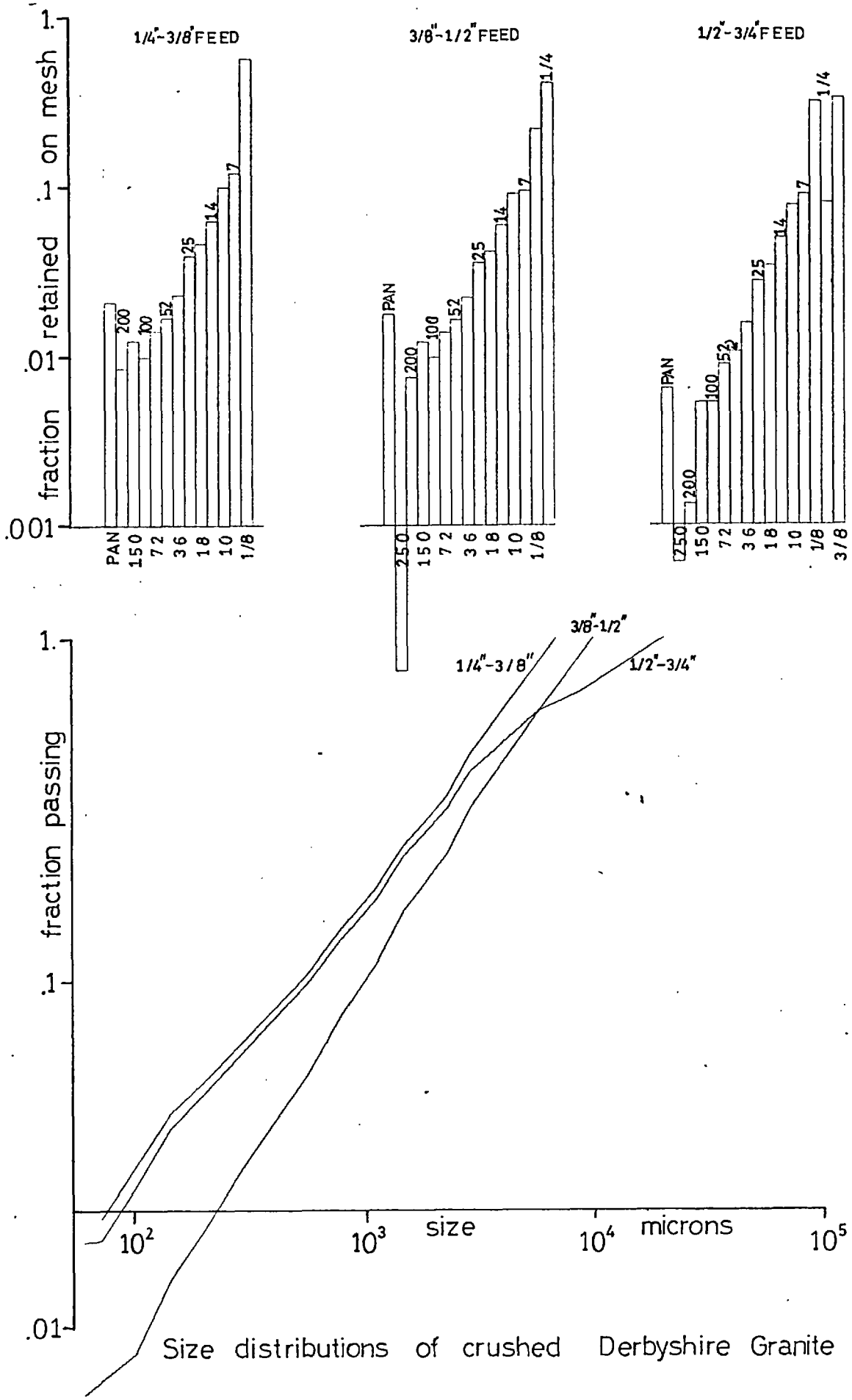
figure 5/11





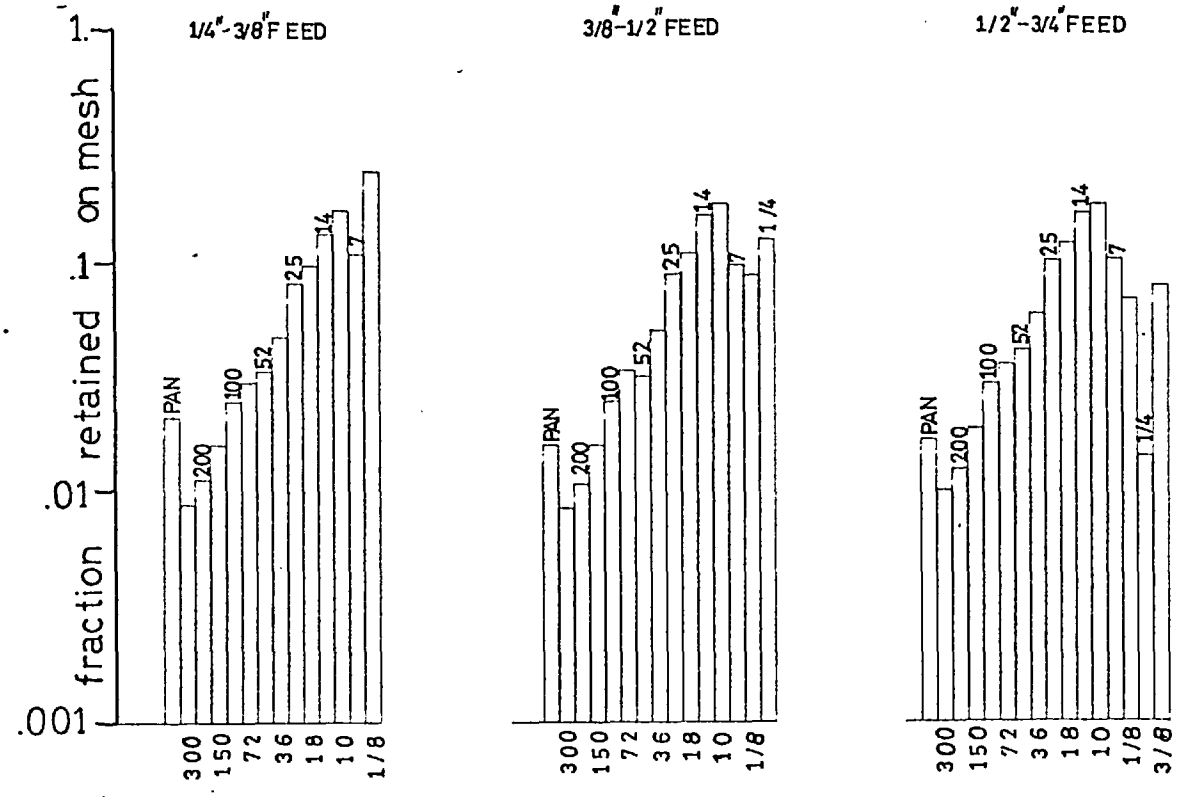
Size distributions of crushed Pennant Sandstone

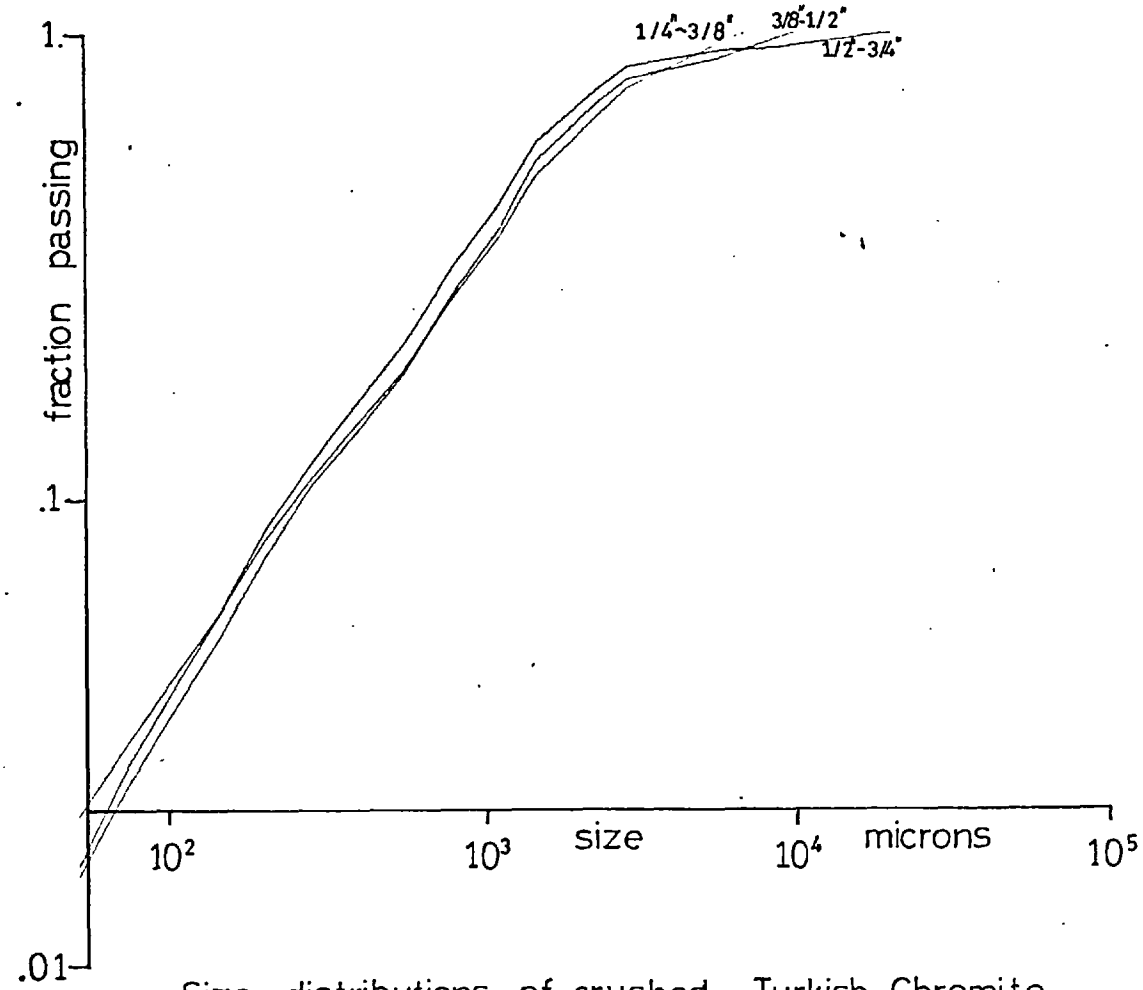
figure 5/12



Size distributions of crushed Derbyshire Granite

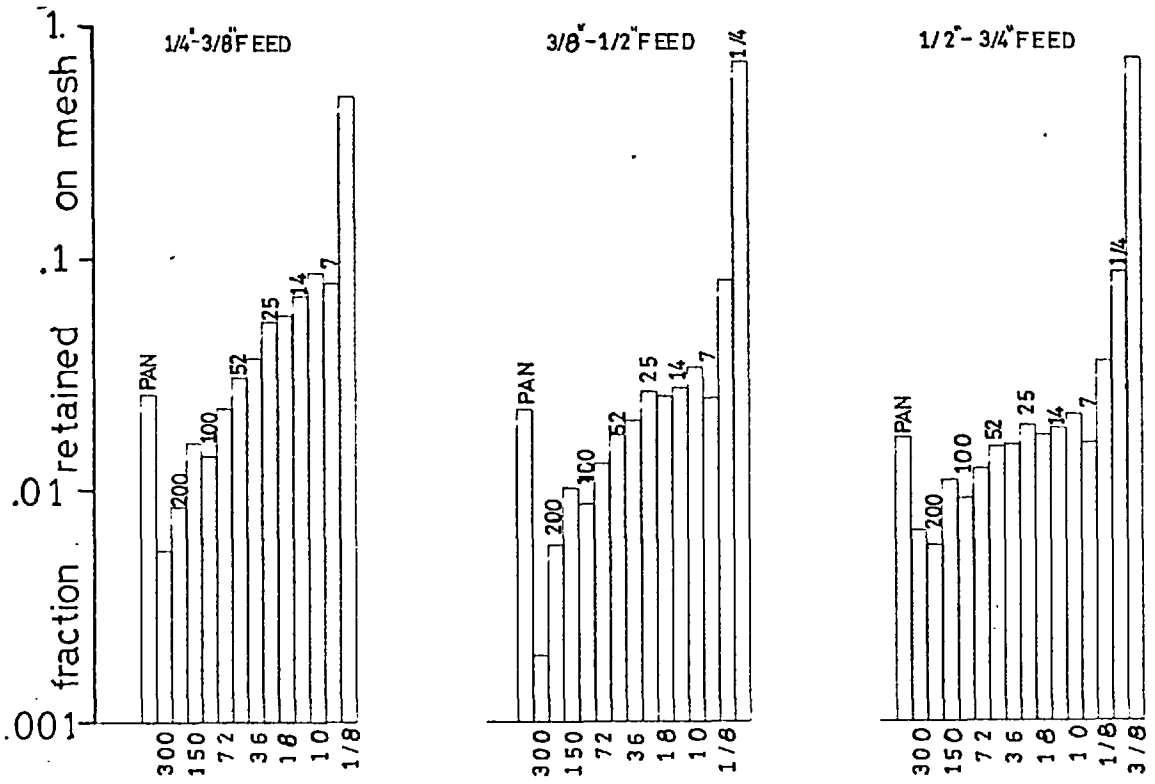
figure 5/13

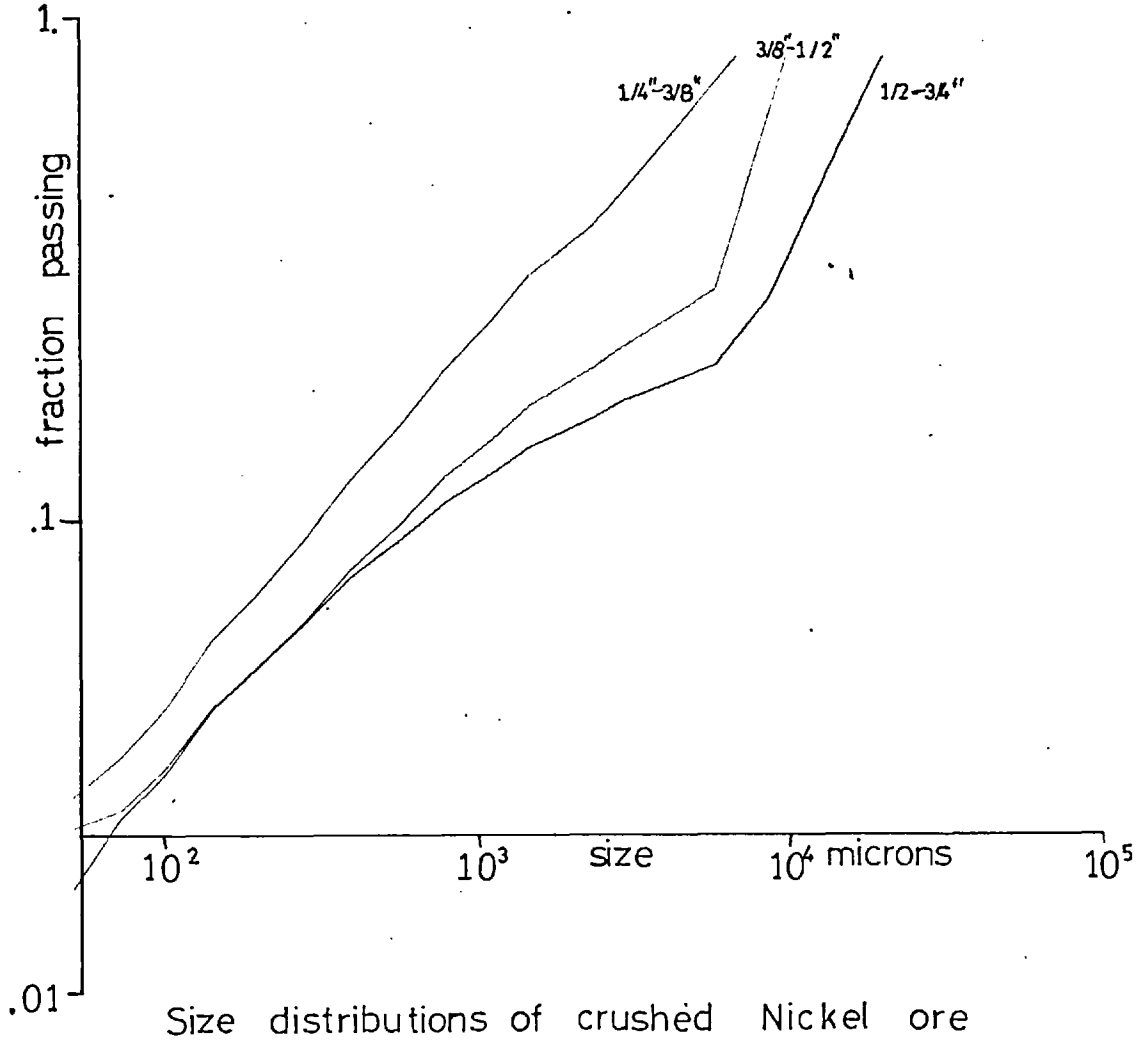




Size distributions of crushed Turkish Chromite

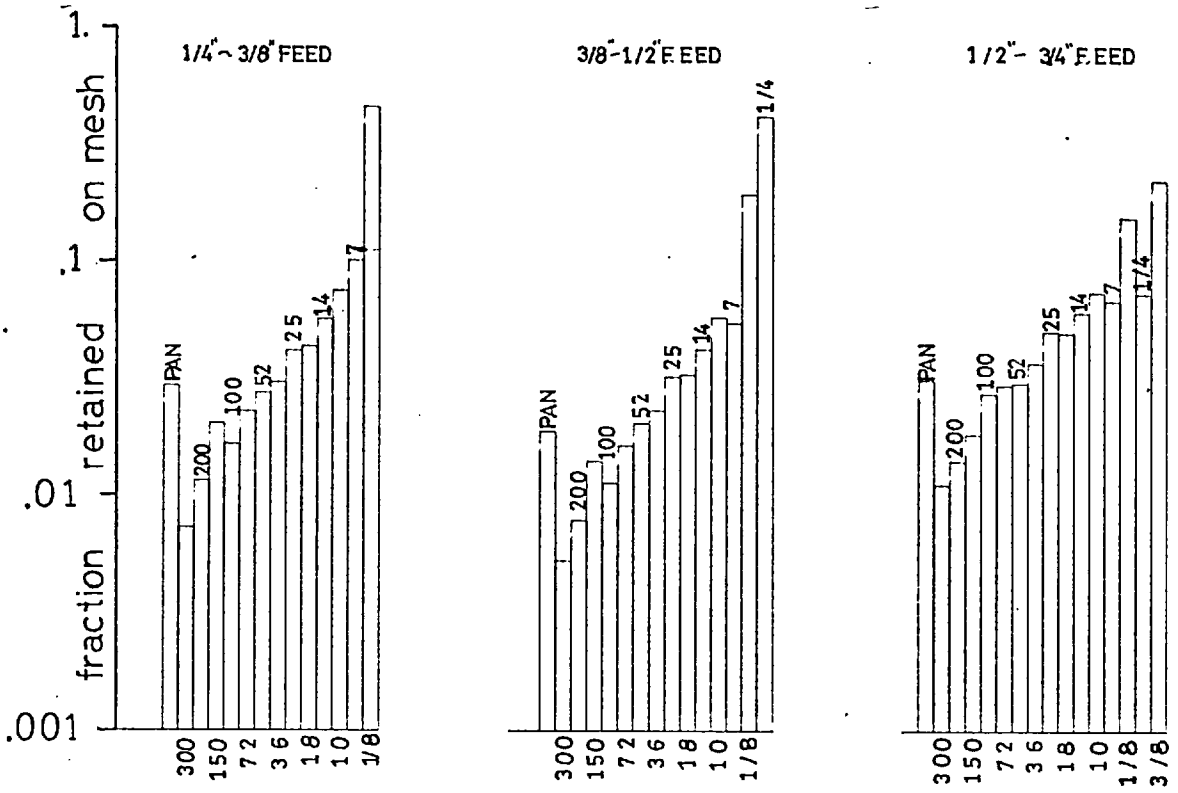
figure 5/14

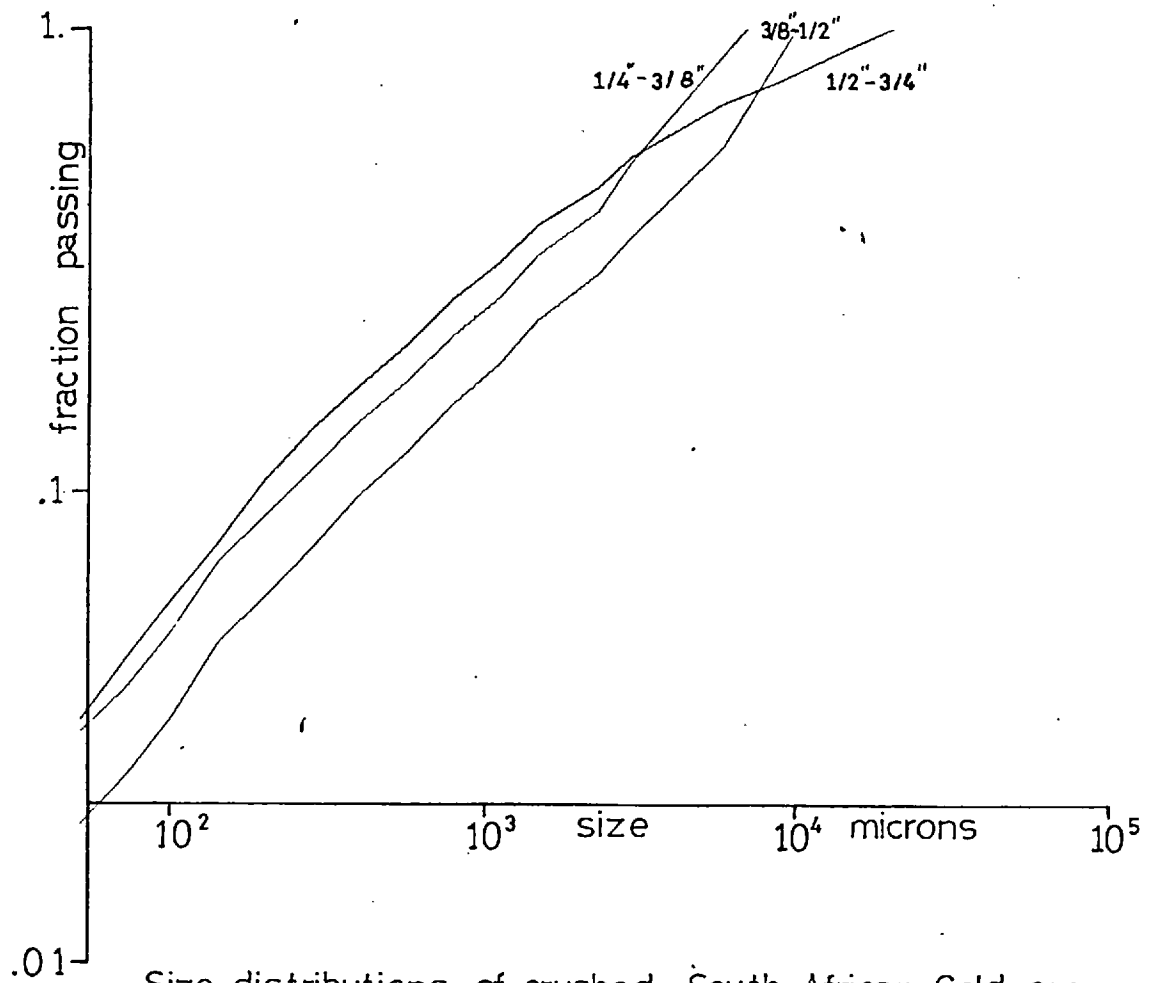




Size distributions of crushed Nickel ore

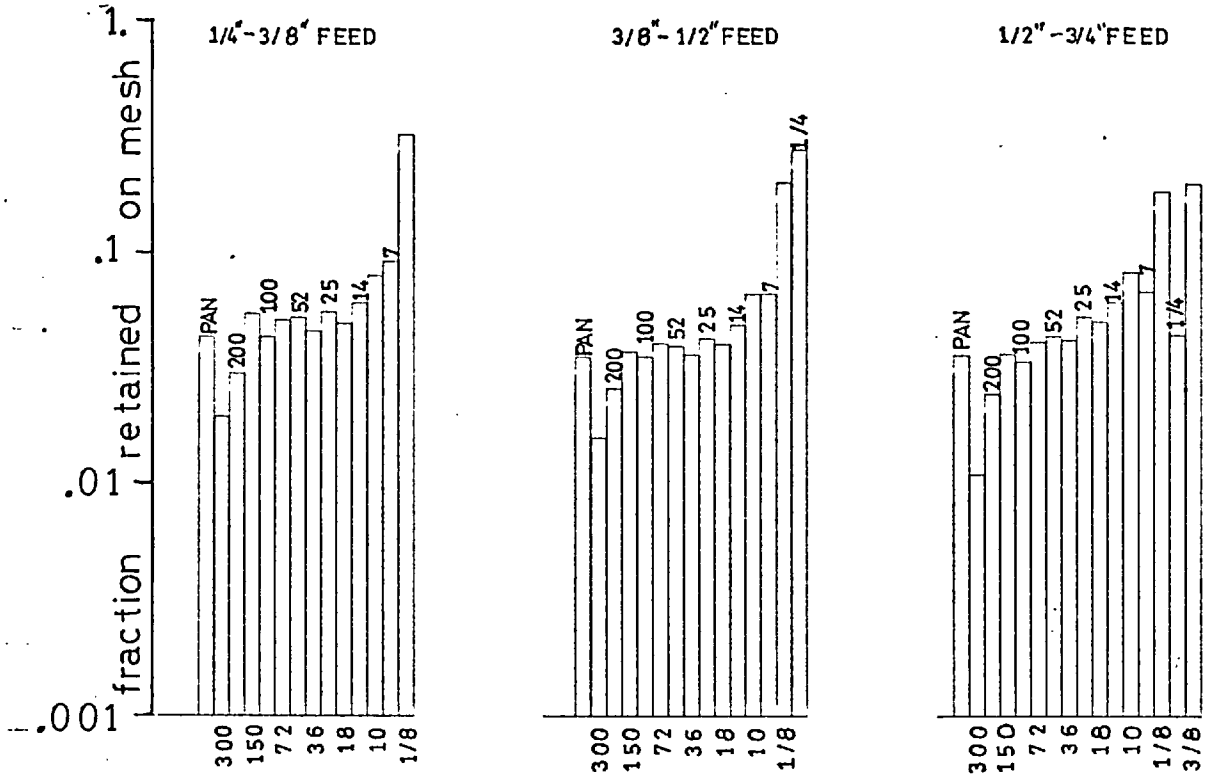
figure 5/15

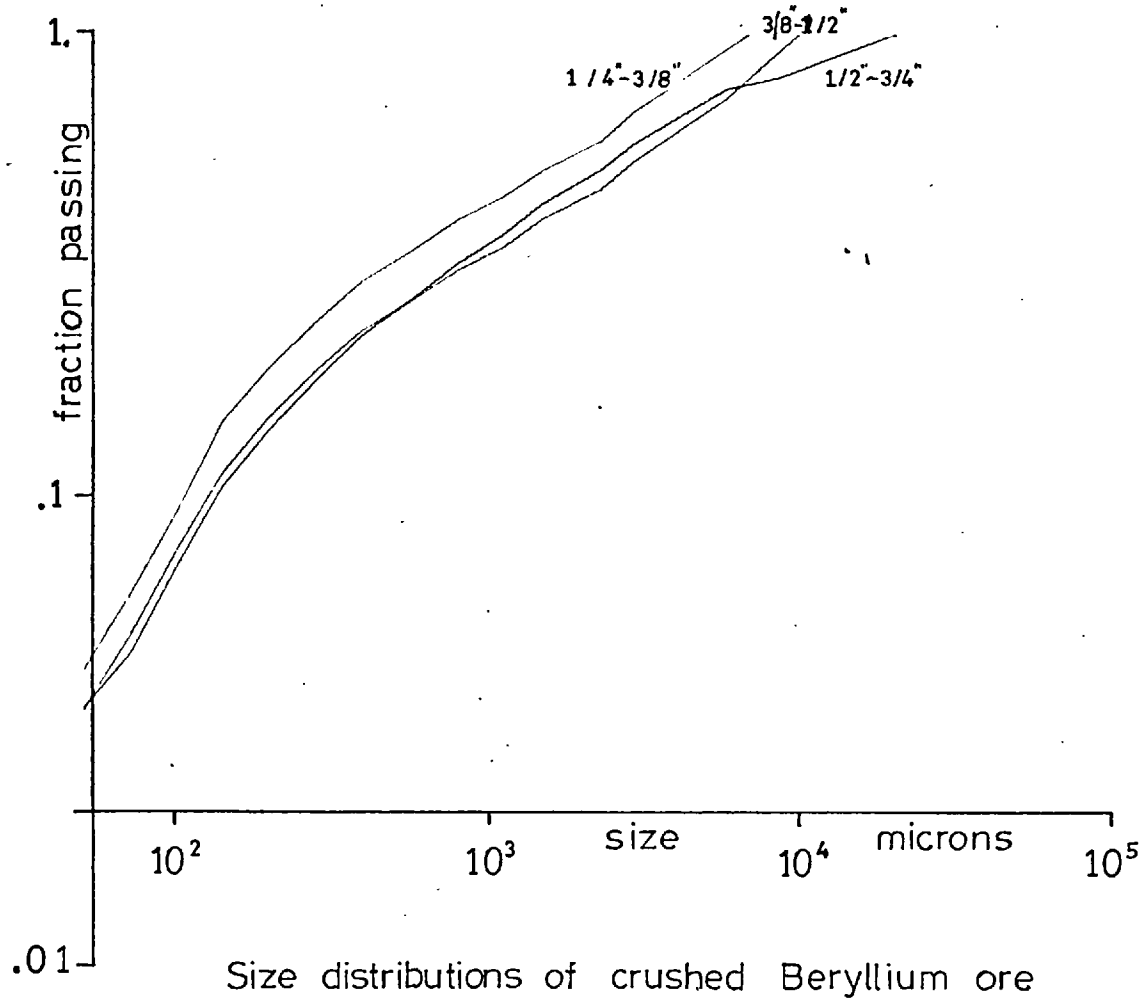




Size distributions of crushed South African Gold ore

figure 5/16





Size distributions of crushed Beryllium ore

figure 5/17

Part 6 - The Description of Mineral Processes

6.1 Introduction

The earlier work at the R.S.M. on electrohydraulic comminution showed that the process had markedly different properties to the more conventional processes. In order to gain maximum economic advantage from these novel features, the electrohydraulic crusher should not be used as a straightforward substitute for a conventional crusher. However the economic evaluation of such new systems requires a method for describing complete plant behaviour; such a method is not as yet available. This part of the thesis reviews the unusual properties of electrohydraulic comminution, the traditional methods of plant analysis and the philosophy of plant modelling. It then goes on to devise a new notation and algebra designed to facilitate plant description and gives some representative examples from the field of mineral engineering. The examples given are for conventional devices. These were chosen as considerable data and operating experience were available from the literature and the experimentation necessary to derive similar data for electrohydraulic processes would have been too time consuming.

6.2 Novel Features of the Electrohydraulic Process

1. Shape

In the construction industry considerable quantities of crushed stone are used, principally in the manufacture of concrete and road dressings.

(Continued .....)

In the manufacture of concrete both strength and workability decrease with increasing aggregate flakiness.

If the average flakiness of the aggregate could be reduced from 40% to 0% a saving of some 100lb of cement per cubic yard of concrete could be realized: the product would have the same strength and workability.

In the manufacture of coated roadstone an improvement in stone shape would reduce the surface area of the aggregate and hence the binder content could be reduced: a further advantage of non-flaky stones is that after the road surface has worn, the chippings, because of their cubic shape, are less likely to flake off and create dangerous surfaces.

A comparison of flakiness and elongation indices between products of jaw and electrohydraulically crushed stone from a range of British quarries (Table 6/1) shows that the electrohydraulically crushed stone is very much more cubical in shape; the flakiness ranges from 0 - 15% compared with 19 - 100% from a jaw crusher. (Reference 136).

As both cement and roadstone binders are considerably more expensive than crushed stone the economic advantages of the process may be large.

2. Power Consumption and Wear

Experiment has shown that the power consumption of an electrohydraulic crusher is very much greater (5 to 10 times) than

(Continued .....)

Table 6/1

Comparison of Flakiness and Elongation Indices of Products from Electrohydraulic Comminution and Jaw Crushing

Material	Size range, in	Flakiness index,%		Elongation index,%	
		E.H.C.	Jaw Crusher	E.H.C.	Jaw Crusher
FELSITE	¾-½	2·6	38·5	0·0	18·8
	½-⅜	2·3	25·0	6·0	40·1
	⅜-¼	1·2	32·0	8·5	42·6
	Mean	2·0	31·8	4·8	33·8
QUARTZITE	¾-½	0·0	71·4	8·6	41·2
	½-⅜	5·8	19·1	0·0	30·9
	⅜-¼	0·0	26·2	16·4	40·6
	Mean	2·0	38·9	8·3	37·6
ALBITIZED OLIVINE DOLERITE (Criggion Quarry)	¾-½	0·0	45·3	0·0	16·6
	½-⅜	1·9	29·5	16·8	24·8
	⅜-¼	10·3	48·5	12·3	37·6
	Mean	4·1	41·1	9·7	26·3
PYROXENE ANDESITE (Moon's Hill Quarry)	¾-½	2·9	37·0	18·9	25·0
	½-⅜	2·4	47·9	0·0	37·8
	⅜-¼	15·3	49·4	3·2	50·0
	Mean	6·9	44·7	7·4	37·6
OLIVINE BASALT (Dumbuck Hill Quarry)	¾-½	0·0	40·0	9·4	57·8
	½-⅜	0·0	51·0	13·0	36·6
	⅜-¼	7·0	46·1	12·0	38·9
	Mean	2·3	46·4	11·4	44·4
FLINT	¾-½	5·0	98·5	1·5	2·0
	½-⅜	2·5	25·9	5·0	32·1
	⅜-¼	0·0	19·3	14·3	31·6
	Mean	2·5	47·9	7·0	21·9
LIMESTONE	¾-½	1·4	95·5	11·8	14·6
	½-⅜	3·8	19·6	0·0	38·2
	⅜-¼	3·0	40·8	18·5	33·7
	Mean	2·7	51·6	10·1	28·8
QUARTZITE-DIORITE PORPHYRITE (Enderby Quarry)	¾-½	0·0	100·0	6·5	27·3
	½-⅜	2·8	39·3	10·7	25·7
	⅜-¼	7·7	52·6	19·7	39·7
	Mean	3·5	63·9	12·3	30·9

From Ph.D Thesis by Yigit

that of conventional devices. However the metal wear of the device is very much lower, possibly as low as one hundreth of that in a ball mill. The wear is localized to the electrodes and surfaces on which the rock slides. The remaining components involve no moving parts and could have lives of the order of 30 years. In areas where maintenance skill is expensive and power cheap the electrohydraulic crusher may be economically worthwhile.

3. Size and Volume

Design studies have indicated that the volume and weight of electrohydraulic crushers are considerably lower than conventional plant. Estimated performances are:-

Volume efficiency 100 tonnes/hour/cubic metre of crusher

Weight efficiency 50 tonnes/hour/tonne of crusher

Applications which may make use of these properties are:-

1) for mobile equipment.

2) for underground equipment.

3) for use in hydraulic transport systems following continuous miners or tunnel boring machines.

4. Selective Crushing

If a feed, consisting of two different rock types, is crushed in an optimum-coupling electrohydraulic crusher then the sparks will travel preferentially over one rock type and the rock which attracts

(Continued .....)

the sparks will be crushed. A schematic diagram of a selective crusher is shown in Figure 6/1. Experiments by Yigit (reference 136) with artificial feeds showed good separation efficiency - see Table 6/2. Such properties could be exploited where waste and ore are mixed and only ore is crushed.

Conclusion

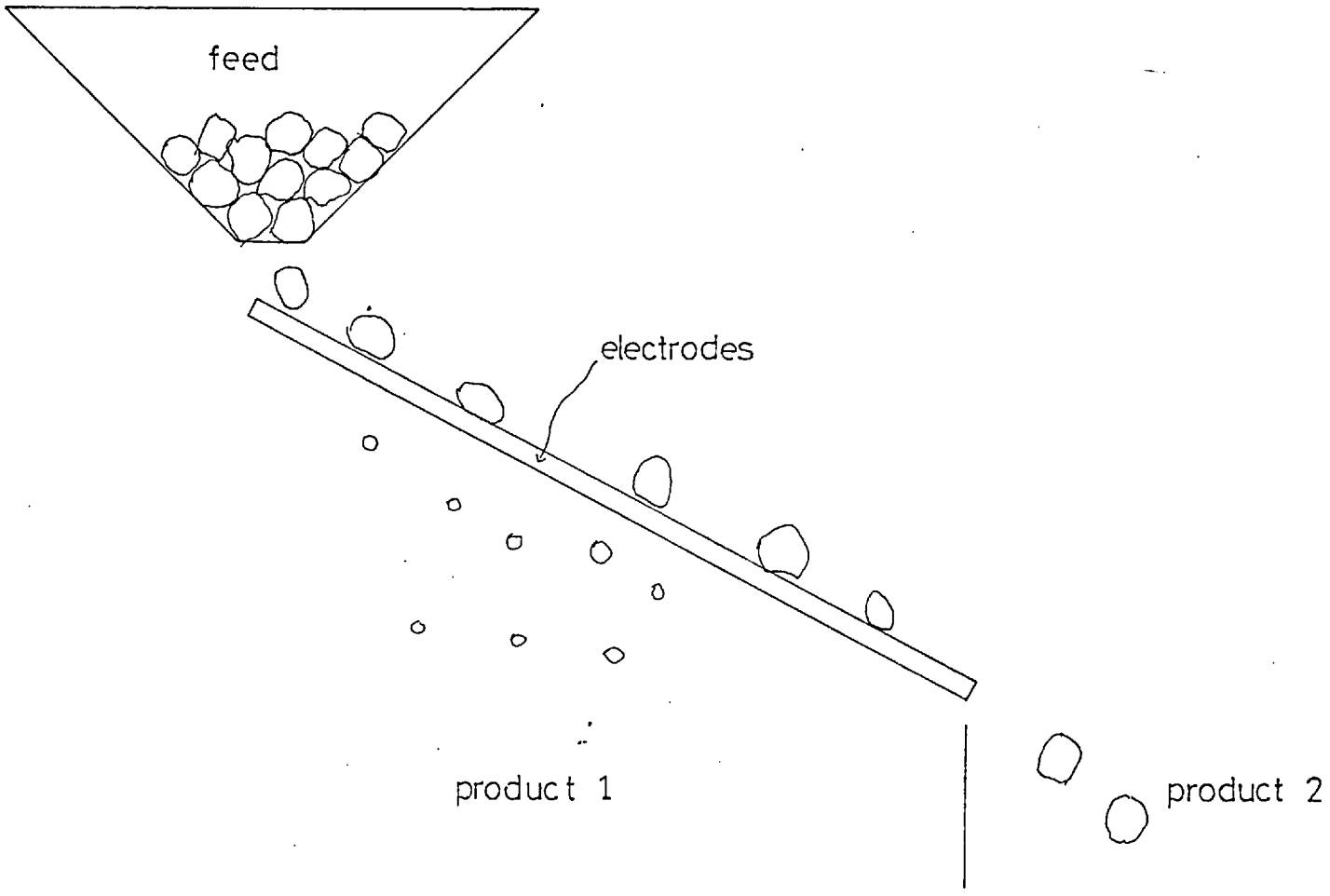
Electrohydraulic crushing offers advantages in several applications: however to estimate whether these advantages outweigh the high power consumption it is necessary to be able to predict the performance of whole systems, as straightforward replacement of conventional devices would not realize the possible advantages.

6.3 The Traditional Approach to Plant Modelling

Mineral processes are complex and, in the past, design and performance tests have been based on single-number indices (e.g. Bond's Index, Kick's Constant, B.S.S.flakiness). The use of such indices was, in the past, necessary because manual calculations were too time consuming to permit more complex methods. With these limitations considerably reduced by the computing facilities now available, more complex and accurate description techniques can be developed.

The method used below is related to the earlier matrix method of Callcott and the sizing-sorting assay tests. The matrix method

(Continued .....)



Separating crusher

figure 6/1

Table 6/2

Selective Electrohydraulic Breakage and Resultant Concentration with some Artificially Prepared Feeds

(·1 μf, 35KV, 1 pulse/2 seconds)

Mixture (A - B)	%B Feed 1½"	%B Product - ¼
Pyrrhotine-flint	60	98·3
Flint-Granite	50	98·7
Limestone-felsite	50	72·0

of Callcott has the disadvantages that it cannot solve problems of control, or of time variation. The size-sorting assay test generally does not consider the distribution of assay within a single size, nor does it solve any problems in processing. Much of the research into mineral dressing has attempted to build models in terms of physical or chemical laws rather than by cybernetic methods.

6.4 The Philosophy of Modelling

Process models are essentially required for three reasons:-

a) To relate the properties of a unit process to its design and the fundamental physical and chemical laws of its operation.

b) To relate the properties of a system to its elements.

c) To control a system, or an element of a system.

In mineral process development, research is largely oriented towards models of the first kind. As the processes concerned are complex, major simplifications and assumptions are necessary in order to render the mathematics tractible. Earlier parts of this thesis attempt to build such models for electrohydraulic processes. Many attempts have been made to model systems in terms of fundamental laws but, in general, the models evolved this way have been unwieldy.

In other disciplines, control and system models have used a "black box" or cybernetic approach. This approach makes system and control modelling simpler at the expense of physical reality. In the "black box" method a model of an element is made in terms of cause

(Continued .....)

and effect, as observed by an external observer, without reference to the internal mechanism of the element. By this approach a system can be described mathematically without any requirements of internal laws being satisfied; the description has only to define an input-output relationship.

Having defined each element of a system in a "black box" manner, modelling reduces to two principle classes:-

a) Describing system performance in terms of the "black box" elements.

b) The justification of the "black box" elements in terms of physical laws.

This part of the thesis attempts to put forward a "black box" notation with an associated algebra for use in mineral process description. Before deriving the notation and algebra formally a simple example will be given.

6.5 Size and Shape : An Example of the Tensor Technique

In principle the size and shape of a particle can be defined by comparison with a standard set of particles. A mathematically elegant set of particles is the family of ellipsoids: with such reference particles some parameters can be defined.

1. "Ideal Size"

A particle has size $\dagger$ if the sphere to which it most accurately corresponds has radius $\dagger$. That is to say that $\dagger$ is the best

(Continued .....)

value which can be obtained in fitting the surface

$$x^2 + y^2 + z^2 = \dagger^2$$

to the particle.

2. "First Order Ellipticity"

A particle has first order ellipticity e if the ellipsoid of revolution to which it most accurately fits has ellipticity e.

That is to say that e is the best value which can be obtained in fitting the surface

$$\frac{x^2}{(1+e)^2} + y^2 + z^2 = a^2$$

to the particle.

Obviously it is possible to carry on in this manner generating higher order reference particles and gaining more and more accurate descriptions.

However there is a major difficulty, with any definition based on these concepts; that is to define a measurement method to find the most accurate fit.

Consider the "ideal size". The value for † could be calculated by any of the following methods each of which would be valid in some context.

1. If the volume of the particle is V; then

(Continued .....)

$$\sqrt[3]{\frac{3V}{4\pi}} = r$$

2. If the surface area of the particle is A; then

$$\sqrt{\frac{A}{4\pi}} = r$$

3. If the average distance across the particle is D; then

$$r = D/2$$

Because of the impracticability of such measurements the minerals industry has adopted the sieve sizes as the size of a particle. This has the advantages of being practical and economic.

However if a collection of particles all having the same sieve size is examined carefully it will be found that their sizes as judged intuitively will be very varied. The action of a sieve in sorting is not only size dependent but also shape dependent. The shape dependence causes the disagreement between measured and intuitive concepts.

Similarly particle shape is assessed by the ability of a particle to pass through a standard slot (reference 241).

Because of the inadequacies of measurement by these techniques it is difficult to describe plant performance in anything but the crudest terms.

(Continued .....)

4. The Tensor Approach

As it is difficult to separate size and shape it is useful to choose a two parameter system which:

a) is measurable; and

b) sorts particles into shapes and sizes as effectively as possible.

In the experiments described below the parameters chosen were:

a) particle mass; and

b) maximum length of the particle.

These parameters were chosen as they are very simple to measure and have no uncertainty. Other parameters can be measured but usually involve some uncertainty in measurement.

An additional advantage is that the measurement accuracy can be very high without any sophisticated equipment.

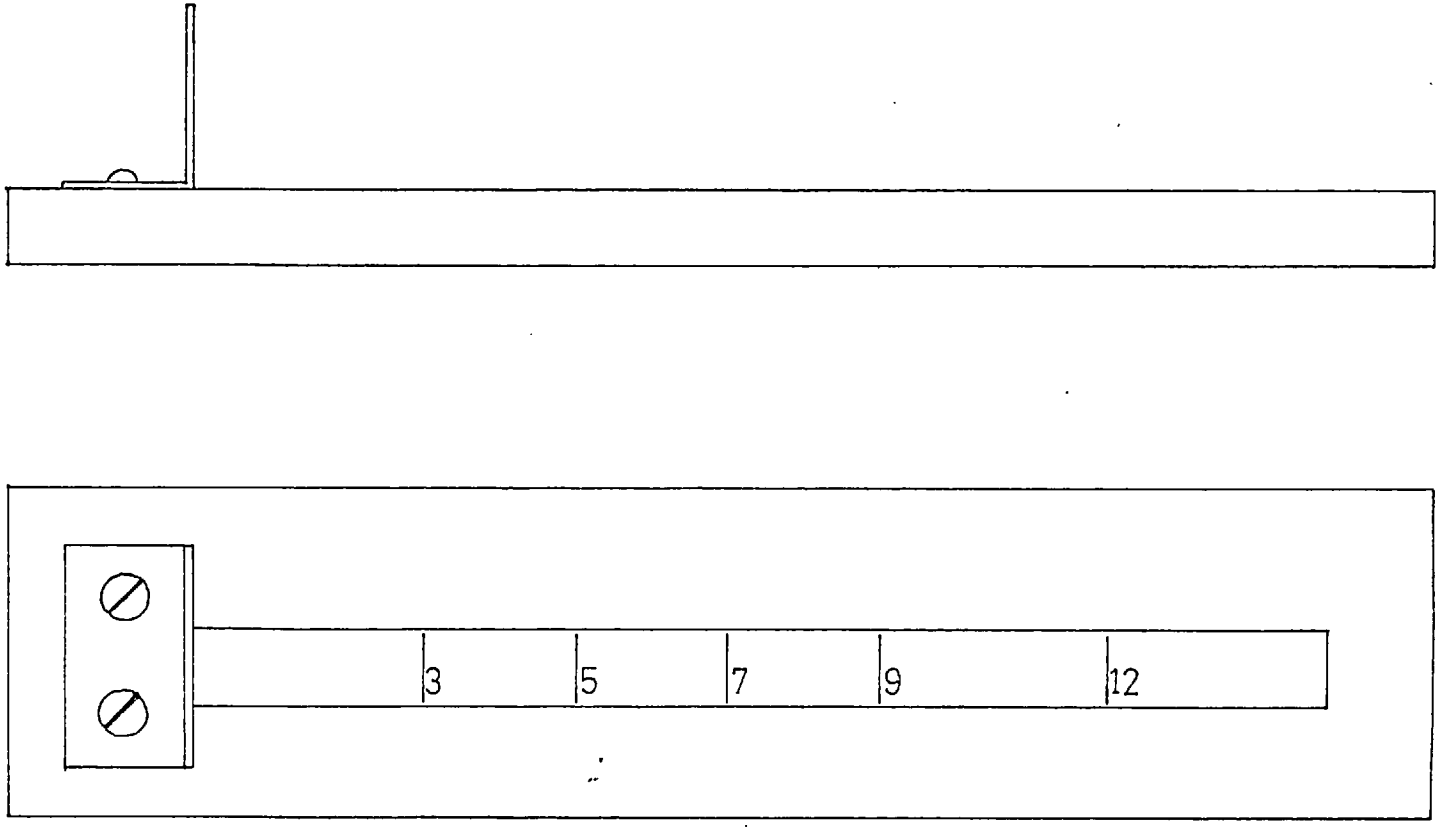
In practice particles were weighed with a spring balance and their length was measured with a simple jig (Figure 6/2).

A particle can now be described by a point in a weight-length plane - see Figure 6/3. This plane in the tensor notation being used is called the primary space.

A large collection of particles could be described by a probability density in the weight-length plane, i.e. the collection is described by a function

$$\psi(w, \ell)$$

(Continued .....)



Length jig

figure 6/2

Now to fit such a function accurately over the surface would be a lengthy and tedious exercise. If such a function were found it would be extremely complex to describe its transformation into a new function after the collection of particles has been crushed.

In order to simplify the description of a collection the primary axes are divided into ranges, see Figure 6/4.

This divides the primary space into a series of rectangles. These rectangles are called the apertures of the primary space.

Each range is numbered, see Figure 6/5.

The aperture marked with a star is known as aperture 4 - 3 as it corresponds to weight range 3 and length range 4.

(Continued .....)

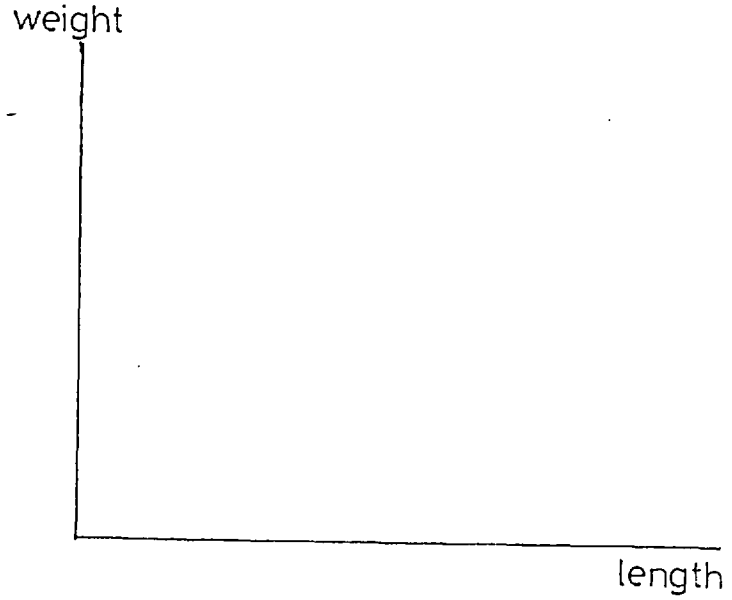


figure 6/3

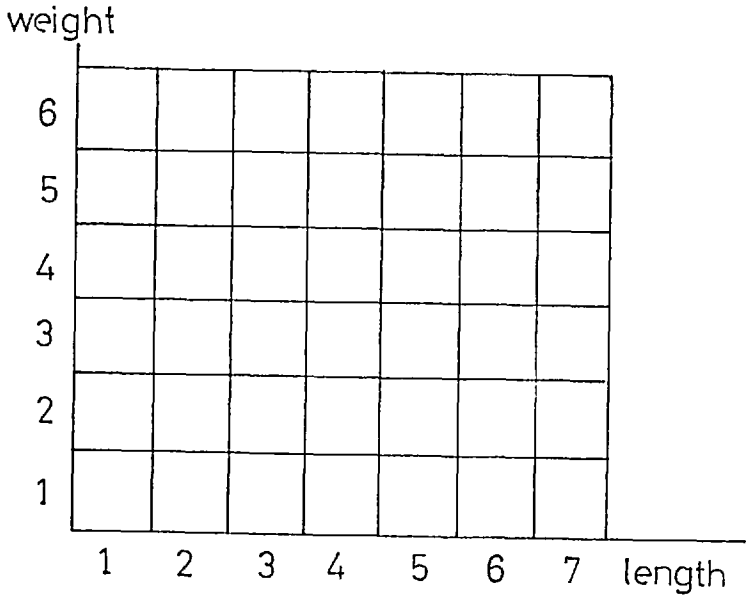


figure 6/4

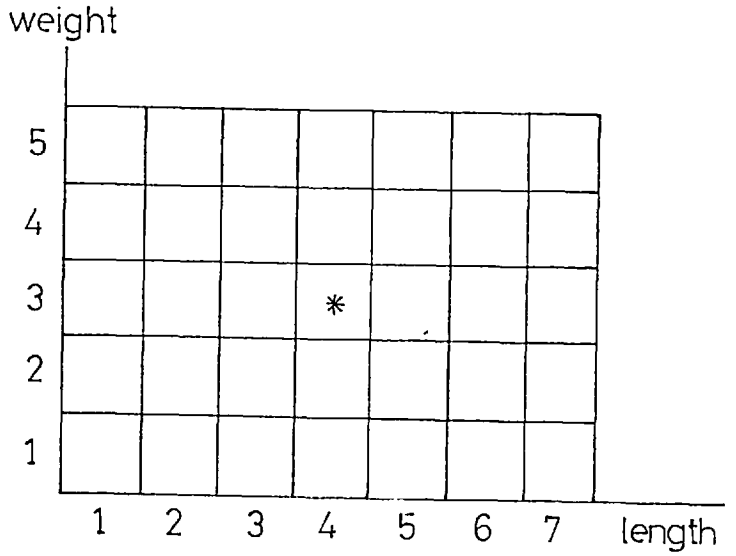


figure 6/5

Development of the aperture concept

The collection of particles can now be sorted into groups; each group of particles corresponding to an aperture.

Let the total weight of the group of particles in aperture ij be m_{ij}.

If there are a weight ranges and b length ranges there are ab apertures and hence ab elements of the type m_{ij}. It can be shown that the ordered set of elements M_{ab} having elements m_{ij} is a tensor.

This tensor describes the particle collection. In essence it is the discrete form of the probability function

$$\Psi(w, \ell)$$

Having defined the tensor notation for particle collections it is now possible to consider comminution.

Firstly it will be assumed that the crushing action on a given particle is unaffected by the presence of any other particles. This approximation is valid at low feed rates but at high feed rates must be modified.

Consider a flow of particles, belonging to one aperture, fed to a crusher. This feed will be crushed and produce a product flow which can be described by a tensor. For this system the following equation can be written:

$$P_{ab} = Q_{ab}\, m_{ij} \quad \text{(Linearity is assumed)}$$

(Continued .....)

where

P_{ab} is the product flow tensor

m_{ij} is the flow of particles in the feed

Q_{ab} is an operator.

By repeating this process for each feed aperture ab equations are formed.

These equations are combined as follows:

$$P_{ab} = \sum_{\substack{i=1 \to a \\ j=1 \to b}} Q_{ab}^{ij} \; m_{ij}$$

giving a tensor equation

$$P_{ab} = G_{ab}^{rs} \; F_{rs}$$

using the Einstein Summation Convention. See Appendix 7 . (From the product theorum G_{ab}^{rs} is a tensor).

In the particular case of crushing with weight-length as the primary space, it is noted that particles do not become larger and the additional constraint exists

$$g_{wy}^{uv} = 0 \quad \text{for} \quad w > u$$

$$\text{or} \quad y > v$$

where g_{wy}^{uv} is an element of G_{wy}^{uv}

It is known that the product size and shape distribution of a jaw crusher vary with the setting and so the tensor equation

$$P_{ab} = G_{ab}^{rs} \; F_{rs}$$

(Continued .....)

is expanded by Taylor's Theorum

$$g_{wy}^{uv} = h_{wy}^{uv} + \frac{\partial g_{wy}^{uv}}{\partial x} \partial x$$

where h_{wy}^{uv} is the value of g_{wy}^{uv} at some fixed value x_o,(x is the jaw crusher setting,)and g_{wy}^{uv} is the value at $x_o + \delta x$.

By combining such equations the tensor equation

$$P_{ab} = (H_{ab}^{rs} + M_{ab}^{rs} x) F_{rs}$$

is derived

where P_{ab} is the product tensor.

H_{ab}^{rs} is the crusher tensor measured at x_o.

M_{ab}^{rs} is the central tensor having elements $\frac{\partial g_{wy}^{uv}}{\partial x}$

x is the deviation from the crusher setting x_o; and

F_{rs} is the feed tensor.

6.6 Experiments

The tensors for a 1 H.P. Laboratory jaw crusher were measured by the following procedure.

The weight ranges were:

0 - 25 grams

25 - 35 "

35 - 50 "

50 - 75 "

75 - 100 "

(Continued .....)

100 - 150 grams

150 - 225 "

The length ranges were:

0 - 3 cm

3 - 5 "

5 - 7 "

7 - 9 "

9 - 12 "

This gives the primary space diagram of Figure 6/6.

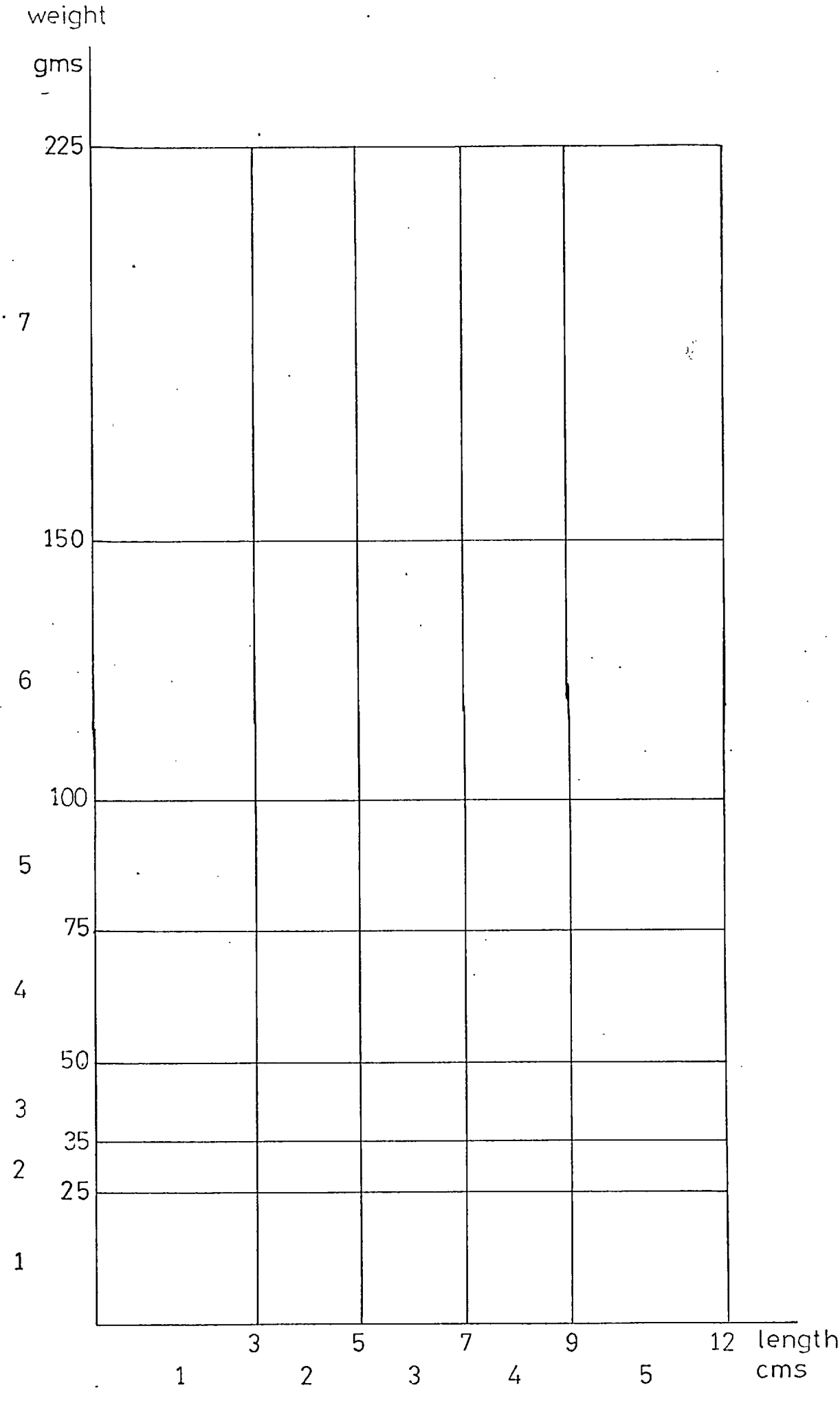
A Derbyshire granite was used for the experiments.

Because of the measurement inconvenience, all particles in weight range 1 and length range 1 were combined as fines. This approximation is reasonable as particles of length greater than 3 cms and weight less than 25 grams are so flaky that they are extremely rare and particles of weight greater than 30 grams but shorter than 3 cms would have to be more dense than the material. Particles could exist with weight 25 - 30 grams and length less than 3 cms but would be very nearly spheres and thus are also rare.

Similarly no particles were found or could be manufactured in the apertures:-

2 - 5	Too high density or too nearly spherical.
2 - 6	
2 - 7	
3 - 7	

(Continued .....)



Basic aperture set for shape experiments

figure 6/6

5 - 2)
)
5 - 3) Too flaky
)
5 - 4)

See Figure 6/7.

A batch of each feed category was made up, weighed and crushed; the product particles were sorted into categories and a tensor calculated. The experiment was carried out for two crusher settings, ¾" and 1".

Let T(¾) be the tensor measured at the ¾" setting;

and T(1) be the tensor measured at the 1" setting.

Linearity over the setting range ¾" - 1" is assumed and hence in the equation:

$$Pab = (H_{ab}^{rs} + M_{ab}^{rs}\ x)\ Frs$$

$$H_{ab}^{rs} = \frac{T(1) + T(¾)}{2}$$

and

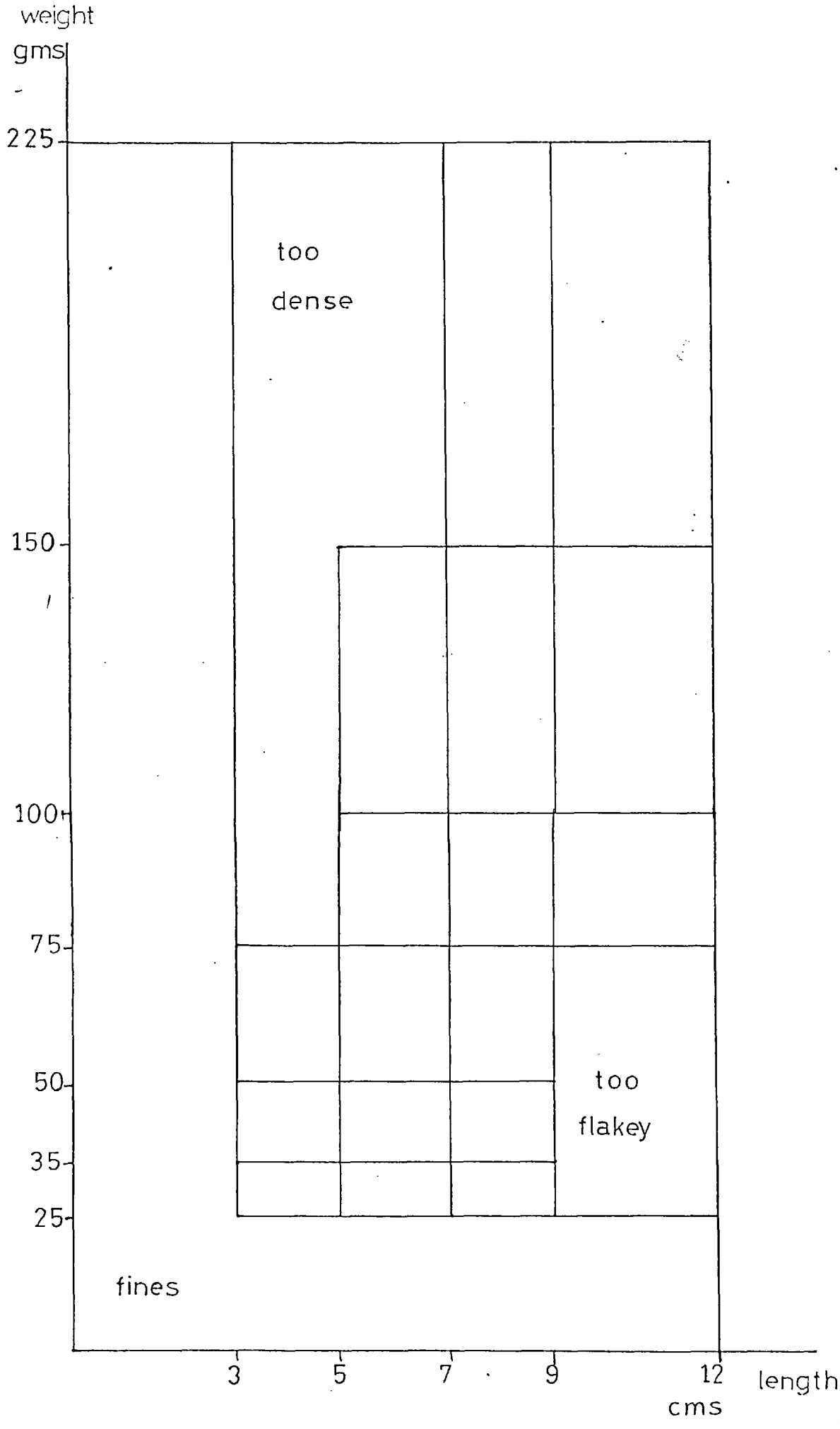
$$M_{ab}^{rs} = \frac{T(1) - T(¾)}{¼}$$

if x is in inches.

The tensors T(¾), T(1), H and M are tabulated - Table 6/3.

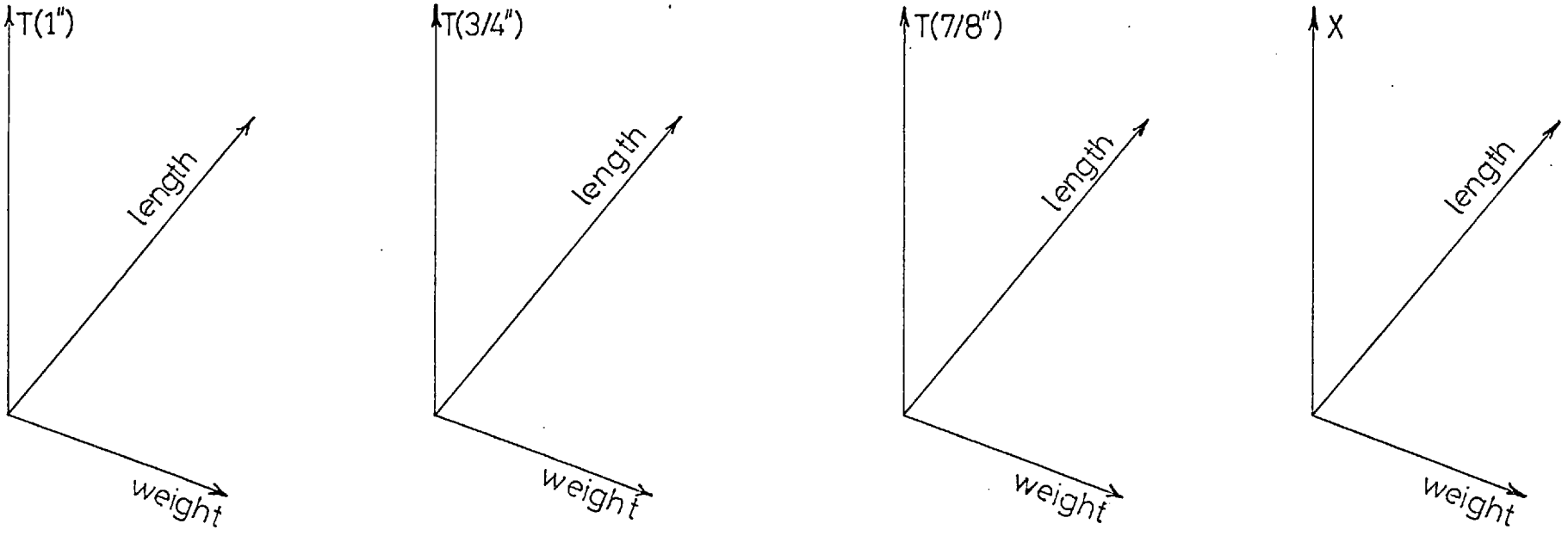
Because the tabulated form of the results is difficult to comprehend, the results are plotted graphically. Here for each feed category the output tensor is plotted as a pseudo-isometric with the axes as in Figure 6/8.

(Continued .....)



Final primary space for shape experiment

figure 6/7



Axes for shape isometrics

figure 6/8

The tensors T(¾), T(1), H and M are shown in this way in Figures 6/9 to 6/26.

Discussion of Results

The results show that the product shape after jaw crushing is dependent on input shape, size and crusher setting. The mass-length method of describing particles sorts particles effectively by shape; particles having large mass to length ratio have a cubic shape and those of low mass to length ratio are flaky. The tensor method permits both a systematic description of particle flows and of processes.

The jaw crusher process tensor shows when plotted graphically a saddle shape with high areas around the feed aperture and the fines aperture. With flaky particles the feed aperture is dominant and with chunky particles the fines aperture is dominant. With very flaky particles the output may be solely in the feed aperture because the crusher action aligns the particles parallel to the jaws and they drop straight through.

6.7 Notation and Algebra

This part formally derives the notation and algebra. Consider a particle uniquely defined by its size. It can be described by defining a point on a size axis. For practical reasons it is not possible to measure each particle exactly and so the size axis is divided into a finite number of ranges. Each range is defined by an upper size limit and a lower size limit. The method of size measurement is not of significance at this stage.

(Continued .....)

Table 6/3

Feed Size 9 to 12 Cms 70 to 100 Grams

1 Inch Tensor

Lengths	12 To 9	9 To 7	7 To 5	5 To 3	3 To 0
Weights					
150 to 225 Grams	0·000	0·000	0·000	0·000	0·000
100 to 150 "	0·000	0·000	0·000	0·000	0·000
75 to 100 "	·373	0·000	0·000	0·000	0·000
50 to 75 "	0·000	0·000	0·000	0·000	0·000
35 to 50 "	0·000	·036	·036	·061	0·000
25 to 35 "	0·000	0·000	·053	·073	0·000
0 to 25 "	0·000	0·000	0·000	0·000	·368

⅞ Inch Tensor

Lengths	12 To 9	9 To 7	7 To 5	5 To 3	3 To 0
Weights					
150 to 225 Grams	0·000	0·000	0·000	0·000	0·000
100 to 150 "	0·000	0·000	0·000	0·000	0·000
75 to 100 "	·186	0·000	0·000	0·000	0·000
50 to 75 "	0·000	0·000	0·000	0·000	0·000
35 to 50 "	0·000	·032	·018	·030	0·000
25 to 35 "	0·000	0·000	·049	·055	0·000
0 to 25 "	0·000	0·000	0·000	0·000	·627

¾ Inch Tensor

Lengths	12 To 9	9 To 7	7 To 5	5 To 3	3 To 0
Weights					
150 to 225 Grams	0·000	0·000	0·000	0·000	0·000
100 to 150 "	0·000	0·000	0·000	0·000	0·000
75 to 100 "	0·000	0·000	0·000	0·000	0·000
50 to 75 "	0·000	0·000	0·000	0·000	0·000
35 to 50 "	0·000	·029	0·000	0·000	0·000
25 to 35 "	0·000	0·000	·046	·038	0·000
0 to 25 "	0·000	0·000	0·000	0·000	·887

Control Tensor

Lengths	12 To 9	9 To 7	7 To 5	5 To 3	3 To 0
Weights					
150 to 225 Grams	0·000	0·000	0·000	0·000	0·000
100 to 150 "	0·000	0·000	0·000	0·000	0·000
75 to 100 "	1·492	0·000	0·000	0·000	0·000
50 to 75 "	0·000	0·000	0·000	0·000	0·000
35 to 50 "	0·000	·028	·144	·244	0·000
25 to 35 "	0·000	0·000	·028	·140	0·000
0 to 25 "	0·000	0·000	0·000	0·000	-2·076

Feed Size 9 to 12 Cms 100 to 150 Grams

1 Inch Tensor

Lengths	12 To 9	9 To 7	7 To 5	5 To 3	3 To 0
Weights					
150 to 225 Grams	0·000	0·000	0·000	0·000	0·000
100 to 150 "	·284	0·000	0·000	0·000	0·000
75 to 100 "	0·000	0·000	0·000	0·000	0·000
50 to 75 "	0·000	·023	·038	0·000	0·000
35 to 50 "	0·000	0·000	·058	·070	0·000
25 to 35 "	0·000	0·000	·034	·078	0·000
0 to 25 "	0·000	0·000	0·000	0·000	·415

⅜ Inch Tensor

Lengths	12 To 9	9 To 7	7 To 5	5 To 3	3 To 0
Weights					
150 to 225 Grams	0·000	0·000	0·000	0·000	0·000
100 to 150 "	·142	0·000	0·000	0·000	0·000
75 to 100 "	0·000	0·000	0·000	0·000	0·000
50 to 75 "	0·000	·012	·019	0·000	0·000
35 to 50 "	0·000	0·000	·031	·035	0·000
25 to 35 "	0·000	0·000	·023	·070	0·000
0 to 25 "	0·000	0·000	0·000	0·000	·698

¾ Inch Tensor

Lengths	12 To 9	9 To 7	7 To 5	5 To 3	3 To 0
Weights					
150 to 225 Grams	0·000	0·000	0·000	0·000	0·000
100 to 150 "	0·000	0·000	0·000	0·000	0·000
75 to 100 "	0·000	0·000	0·000	0·000	0·000
50 to 75 "	0·000	0·000	0·000	0·000	0·000
35 to 50 "	0·000	0·000	·004	0·000	0·000
25 to 35 "	0·000	0·000	·012	·062	0·000
0 to 25 "	0·000	0·000	0·000	0·000	·982

Control Tensor

Lengths	12 To 9	9 To 7	7 To 5	5 To 3	3 To 0
Weights					
150 to 225 Grams	0·000	0·000	0·000	0·000	0·000
100 to 150 "	1.136	0·000	0·000	0·000	0·000
75 to 100 "	0·000	0·000	0·000	0·000	0·000
50 to 75 "	0·000	·092	·152	0·000	0·000
35 to 50 "	0·000	0·000	·216	·280	0·000
25 to 35 "	0·000	0·000	·088	·064	0·000
0 to 25 "	0·000	0·000	0·000	0·000	-2.268

Feed Size 9 to 12 Cms 150 to 225 Grams

1 Inch Tensor

Lengths	12 To 9	9 To 7	7 To 5	5 To 3	3 To 0
Weights					
150 to 225 Grams	·066	0·000	0·000	0·000	0·000
100 to 150 "	·095	0·000	0·000	0·000	0·000
75 to 100 "	·037	·094	·037	0·000	0·000
50 to 75 "	0·000	0·000	0·000	·021	0·000
35 to 50 "	0·000	·015	·065	·034	0·000
25 to 35 "	0·000	0·000	·024	·035	0·000
0 to 25 "	0·000	0·000	0·000	0·000	·477

⅞ Inch Tensor

Lengths	12 To 9	9 To 7	7 To 5	5 To 3	3 To 0
Weights					
150 to 225 Grams	·033	0·000	0·000	0·000	0·000
100 to 150 "	·048	0·000	0·000	0·000	0·000
75 to 100 "	·018	·047	·018	0·000	0·000
50 to 75 "	0·000	0·000	0·000	·011	0·000
35 to 50 "	0·000	·008	·032	·017	0·000
25 to 35 "	0·000	0·000	·016	·029	0·000
0 to 25 "	0·000	0·000	0·000	0·000	·723

¾ Inch Tensor

Lengths	12 To 9	9 To 7	7 To 5	5 To 3	3 To 0
Weights					
150 to 225 Grams	0·000	0·000	0·000	0·000	0·000
100 to 150 "	0·000	0·000	0·000	0·000	0·000
75 to 100 "	0·000	0·000	0·000	0·000	0·000
50 to 75 "	0·000	0·000	0·000	0·000	0·000
35 to 50 "	0·000	0·000	0·000	0·000	0·000
25 to 35 "	0·000	0·000	·007	·023	0·000
0 to 25 "	0·000	0·000	0·000	0·000	·970

Control Tensor

Lengths	12 To 9	9 To 7	7 To 5	5 To ·3	3 To 0
Weights					
150 to 225 Grams	·264	0.000	0.000	0.000	0.000
100 to 150 "	·380	0·000	0·000	0.000	0.000
75 to 100 "	·148	·376	·148	0·000	0.000
50 to 75 "	0·000	0·000	0·000	·084	0.000
35 to 50 "	0·000	·060	·260	·136	0.000
25 to 35 "	0·000	0·000	·068	·048	0.000
0 to 25 "	0·000	0·000	0·000	0.000	-1.972

Feed Size 7 to 9 Cms 25 to 35 Grams

1 Inch Tensor

Lengths	12 To 9	9 To 7	7 To 5	5 To 3	3 To 0
Weights					
150 to 225 Grams	0.000	0.000	0.000	0.000	0.000
100 to 150 "	0.000	0.000	0.000	0.000	0.000
75 to 100 "	0.000	0.000	0.000	0.000	0.000
50 to 75 "	0.000	0.000	0.000	0.000	0.000
35 to 50 "	0.000	0.000	0.000	0.000	0.000
25 to 35 "	0.000	1.000	0.000	0.000	0.000
0 to 25 "	0.000	0.000	0.000	0.000	0.000

⅞ Inch Tensor

Lengths	12 To 9	9 To 7	7 To 5	5 To 3	3 To 0
Weights					
150 to 225 Grams	0.000	0.000	0.000	0.000	0.000
100 to 150 "	0.000	0.000	0.000	0.000	0.000
75 to 100 "	0.000	0.000	0.000	0.000	0.000
50 to 75 "	0.000	0.000	0.000	0.000	0.000
35 to 50 "	0.000	0.000	0.000	0.000	0.000
25 to 35 "	0.000	1.000	0.000	0.000	0.000
0 to 25 "	0.000	0.000	0.000	0.000	0.000

¾ Inch Tensor

Lengths	12 To 9	9 To 7	7 To 5	5 To 3	3 To 0
Weights					
150 to 225 Grams	0.000	0.000	0.000	0.000	0.000
100 to 150 "	0.000	0.000	0.000	0.000	0.000
75 to 100 "	0.000	0.000	0.000	0.000	0.000
50 to 75 "	0.000	0.000	0.000	0.000	0.000
35 to 50 "	0.000	0.000	0.000	0.000	0.000
25 to 35 "	0.000	1.000	0.000	0.000	0.000
0 to 25 "	0.000	0.000	0.000	0.000	0.000

Control Tensor

Lengths	12 To 9	9 To 7	7 To 5	5 To 3	3 To 0
Weights					
150 to 225 Grams	0.000	0.000	0.000	0.000	0.000
100 to 150 "	0.000	0.000	0.000	0.000	0.000
75 to 100 "	0.000	0.000	0.000	0.000	0.000
50 to 75 "	0.000	0.000	0.000	0.000	0.000
35 to 50 "	0.000	0.000	0.000	0.000	0.000
25 to 35 "	0.000	0.000	0.000	0.000	0.000
0 to 25 "	0.000	0.000	0.000	0.000	0.000

Feed Size 7 to 9 Cms 35 to 50 Grams

1 Inch Tensor

Lengths	12 To 9	9 To 7	7 To 5	5 To 3	3 To 0
Weights					
150 to 225 Grams	0·000	0·000	0·000	0·000	0·000
100 to 150 "	0·000	0·000	0·000	0·000	0·000
75 to 100 "	0·000	0·000	0·000	0·000	0·000
50 to 75 "	0·000	0·000	0·000	0·000	0·000
35 to 50 "	0·000	·497	·140	0·000	0·000
25 to 35 "	0·000	·107	·049	0·000	0·000
0 to 25 "	0·000	0·000	0·000	0·000	·207

⅞ Inch Tensor

Lengths	12 To 9	9 To 7	7 To 5	5 To 3	3 To 0
Weights					
150 to 225 Grams	0·000	0·000	0·000	0·000	0·000
100 to 150 "	0·000	0·000	0·000	0·000	0·000
75 to 100 "	0·000	0·000	0·000	0·000	0·000
50 to 75 "	0·000	0·000	0·000	0·000	0·000
35 to 50 "	0·000	·523	·177	0·000	0·000
25 to 35 "	0·000	·054	·024	·028	0·000
0 to 25 "	0·000	0·000	0·000	0·000	·192

¾ Inch Tensor

Lengths	12 To 9	9 To 7	7 To 5	5 To 3	3 To 0
Weights					
150 to 225 Grams	0·000	0·000	0·000	0·000	0·000
100 to 150 "	0·000	0·000	0·000	0·000	0·000
75 to 100 "	0·000	0·000	0·000	0·000	0·000
50 to 75 "	0·000	0·000	0·000	0·000	0·000
35 to 50 "	0·000	·550	·215	0·000	0·000
25 to 35 "	0·000	0·000	0·000	·057	0·000
0 to 25 "	0·000	0·000	0·000	0·000	·178

Control Tensor

Lengths	12 To 9	9 To 7	7 To 5	5 To 3	3 To 0
Weights					
150 to 225 Grams	0·000	0·000	0·000	0·000	0·000
100 to 150 "	0·000	0·000	0·000	0·000	0·000
75 to 100 "	0·000	0·000	0·000	0·000	0·000
50 to 75 "	0·000	0·000	0·000	0·000	0·000
35 to 50 "	0·000	-·212	-·300	0·000	0·000
25 to 35 "	0·000	·428	·196	-·228	0·000
0 to 25 "	0·000	0·000	0·000	0·000	·116

Feed Size 7 to 9 Cms 50 to 70 Grams

1 Inch Tensor

Lengths / Weights	12 To 9	9 To 7	7 To 5	5 To 3	3 To 0
150 to 225 Grams	0·000	0·000	0·000	0·000	0·000
100 to 150 "	0·000	0·000	0·000	0·000	0·000
75 to 100 "	0·000	0·000	0·000	0·000	0·000
50 to 75 "	0·000	·225	0·000	0·000	0·000
35 to 50 "	0·000	0·000	·103	·015	0·000
25 to 35 "	0·000	·013	·068	·130	0·000
0 to 25 "	0·000	0·000	0·000	0·000	·446

⅞ Inch Tensor

Lengths / Weights	12 To 9	9 To 7	7 To 5	5 To 3	3 To 0
150 to 225 Grams	0.000	0·000	0.000	0.000	0.000
100 to 150 "	0·000	0·000	0·000	0·000	0·000
75 to 100 "	0·000	0·000	0·000	0·000	0·000
50 to 75 "	0·000	·112	0·000	0·000	0·000
35 to 50 "	0·000	0·000	·052	·008	0·000
25 to 35 "	0·000	·007	·053	·065	0·000
0 to 25 "	0·000	0·000	0·000	0·000	·704

¾ Inch Tensor

Lengths / Weights	12 To 9	9 To 7	7 To 5	5 To 3	3 To 0
150 to 225 Grams	0·000	0·000	0·000	0·000	0·000
100 to 150 "	0·000	0·000	0·000	0·000	0·000
75 to 100 "	0·000	0·000	0·000	0·000	0·000
50 to 75 "	0·000	0·000	0·000	0·000	0·000
35 to 50 "	0·000	0·000	0·000	0·000	0·000
25 to 35 "	0·000	0·000	·038	0·000	0·000
0 to 25 "	0·000	0·000	0·000	0·000	·962

Control Tensor

Lengths / Weights	12 To 9	9 To 7	7 To 5	5 To 3	3 To 0
150 to 225 Grams	0·000	0·000	0·000	0·000	0·000
100 to 150 "	0·000	0·000	0·000	0·000	0·000
75 to 100 "	0·000	0·000	0·000	0·000	0·000
50 to 75 "	0·000	·900	0·000	0·000	0·000
35 to 50 "	0·000	0·000	·412	·060	0·000
25 to 35 "	0·000	·052	·120	·520	0·000
0 to 25 "	0·000	0·000	0·000	0·000	-2·064

Feed Size 7 to 9 Cms 70 to 100 Grams

1 Inch Tensor

Lengths	12 To 9	9 To 7	7 To 5	5 To 3	3 To 0
Weights					
150 to 225 Grams	0·000	0·000	0·000	0·000	0·000
100 to 150 "	0·000	0·000	0·000	0·000	0·000
75 to 100 "	0·000	·050	·021	0·000	0·000
50 to 75 "	0·000	0·000	·102	·014	0·000
35 to 50 "	0·000	0·000	·077	·032	0·000
25 to 35 "	0·000	0·000	·031	·093	0·000
0 to 25 "	0·000	0·000	0·000	0·000	·580

⅜ Inch Tensor

Lengths	12 To 9	9 To 7	7 To 5	5 To 3	3 To 0
Weights					
150 to 225 Grams	0·000	0·000	0·000	0·000	0·000
100 to 150 "	0·000	0·000	0·000	0·000	0·000
75 to 100 "	0·000	·032	·011	0·000	0·000
50 to 75 "	0·000	·019	·055	·007	0·000
35 to 50 "	0·000	0·000	·050	·016	0·000
25 to 35 "	0·000	0·000	·022	·053	0·000
0 to 25 "	0·000	0·000	0·000	0·000	·734

¾ Inch Tensor

Lengths	12 To 9	9 To 7	7 To 5	5 To 3	3 To 0
Weights					
150 to 225 Grams	0·000	0·000	0·000	0·000	0·000
100 to 150 "	0·000	0·000	0·000	0·000	0·000
75 to 100 "	0·000	·015	0·000	0·000	0·000
50 to 75 "	0·000	·038	·009	0·000	0·000
35 to 50 "	0·000	0·000	·023	0·000	0·000
25 to 35 "	0·000	0·000	·014	·013	0·000
0 to 25 "	0·000	0·000	0·000	0·000	·888

Control Tensor

Lengths	12 To 9	9 To 7	7 To 5	5 To 3	3 To 0
Weights					
150 to 225 Grams	0·000	0·000	0·000	0·000	0·000
100 to 150 "	0·000	0·000	0·000	0·000	0·000
75 to 100 "	0·000	·140	·084	0·000	0·000
50 to 75 "	0·000	-·152	·372	·056	0·000
35 to 50 "	0·000	0·000	·216	·128	0·000
25 to 35 "	0·000	0·000	·068	·320	0·000
0 to 25 "	0·000	0·000	0·000	0·000	-1·232

Feed Size 7 to 9 Cms 100 to 150 Grams

1 Inch Tensor

Lengths	12 To 9	9 To 7	7 To 5	5 To 3	3 To 0
Weights					
150 to 225 Grams	0.000	0.000	0.000	0.000	0.000
100 to 150 "	0.000	.064	0.000	0.000	0.000
75 to 100 "	0.000	.042	0.000	0.000	0.000
50 to 75 "	0.000	0.000	.032	0.000	0.000
35 to 50 "	0.000	0.000	.105	.019	0.000
25 to 35 "	0.000	0.000	.016	.044	0.000
0 to 25 "	0.000	0.000	0.000	0.000	.680

⅞ Inch Tensor

Lengths	12 To 9	9 To 7	7 To 5	5 To 3	3 To 0
Weights					
150 to 225 Grams	0.000	0.000	0.000	0.000	0.000
100 to 150 "	0.000	.032	0.000	0.000	0.000
75 to 100 "	0.000	.040	0.000	0.000	0.000
50 to 75 "	0.000	0.000	.027	0.000	0.000
35 to 50 "	0.000	0.000	.062	.017	0.000
25 to 35 "	0.000	0.000	.020	.027	0.000
0 to 25 "	0.000	0.000	0.000	0.000	.775

¾ Inch Tensor

Lengths	12 To 9	9 To 7	7 To 5	5 To 3	3 To 0
Weights					
150 to 225 Grams	0.000	0.000	0.000	0.000	0.000
100 to 150 "	0.000	0.000	0.000	0.000	0.000
75 to 100 "	0.000	.038	0.000	0.000	0.000
50 to 75 "	0.000	0.000	.022	0.000	0.000
35 to 50 "	0.000	0.000	.019	.016	0.000
25 to 35 "	0.000	0.000	.024	.011	0.000
0 to 25 "	0.000	0.000	0.000	0.000	.871

Control Tensor

Lengths	12 To 9	9 To 7	7 To 5	5 To 3	3 To 0
Weights					
150 to 225 Grams	0.000	0.000	0.000	0.000	0.000
100 to 150 "	0.000	.256	0.000	0.000	0.000
75 to 100 "	0.000	.016	0.000	0.000	0.000
50 to 75 "	0.000	0.000	.040	0.000	0.000
35 to 50 "	0.000	0.000	.344	.012	0.000
25 to 35 "	0.000	0.000	-.032	.132	0.000
0 to 25 "	0.000	0.000	0.000	0.000	-.764

Feed Size 7 to 9 Cms 150 to 225 Grams

1 Inch Tensor

Lengths	12 To 9	9 To 7	7 To 5	5 To 3	3 To 0
Weights					
150 to 225 Grams	0·000	·046	0·000	0·000	0·000
100 to 150 "	0·000	0·000	·033	0·000	0·000
75 to 100 "	0·000	·020	0·000	0·000	0·000
50 to 75 "	0·000	·069	·030	0·000	0·000
35 to 50 "	0·000	·027	·053	·013	0·000
25 to 35 "	0·000	0·000	·027	·062	0·000
0 to 25 "	0·000	0·000	0·000	0·000	·620

⅞ Inch Tensor

Lengths	12 To 9	9 To 7	7 To 5	5 To 3	3 To 0
Weights					
150 to 225 Grams	0·000	·023	0·000	0·000	0·000
100 to 150 "	0·000	0·000	·016	0·000	0·000
75 to 100 "	0·000	·010	0·000	0·000	0·000
50 to 75 "	0·000	·034	·015	0·000	0·000
35 to 50 "	0·000	·014	·031	·007	0·000
25 to 35 "	0·000	0·000	·017	·031	0·000
0 to 25 "	0·000	0·000	0·000	0·000	·800

¾ Inch Tensor

Lengths	12 To 9	9 To 7	7 To 5	5 To 3	3 To 0
Weights					
150 to 225 Grams	0·000	0·000	0·000	0·000	0·000
100 to 150 "	0·000	0·000	0·000	0·000	0·000
75 to 100 "	0·000	0·000	0·000	0·000	0·000
50 to 75 "	0·000	0·000	0·000	0·000	0·000
35 to 50 "	0·000	0·000	·010	0·000	0·000
25 to 35 "	0·000	0·000	·008	0·000	0·000
0 to 25 "	0·000	0·000	0·000	0·000	·981

Control Tensor

Lengths	12 To 9	9 To 7	7 To 5	5 To 3	3 To 0
Weights					
150 to 225 Grams	0·000	·184	0·000	0·000	0·000
100 to 150 "	0·000	0·000	·132	0·000	0·000
75 to 100 "	0·000	·080	0·000	0·000	0·000
50 to 75 "	0·000	·276	·120	0·000	0·000
35 to 50 "	0·000	·108	·172	·052	0·000
25 to 35 "	0·000	0·000	·076	·248	0·000
0 to 25 "	0·000	0·000	0·000	0·000	-1·444

Feed Size 5 to 7 Cms 35 to 50 Grams

1 Inch Tensor

Lengths	12 To 9	9 To 7	7 To 5	5 To 3	3 To 0
Weights					
150 to 225 Grams	0·000	0·000	0·000	0·000	0·000
100 to 150 "	0·000	0·000	0·000	0·000	0·000
75 to 100 "	0·000	0·000	0·000	0·000	0·000
50 to 75 "	0·000	0·000	0·000	0·000	0·000
35 to 50 "	0·000	0·000	·571	·081	0·000
25 to 35 "	0·000	0·000	·029	·047	0·000
0 to 25 "	0·000	0·000	0·000	0·000	·272

⅞ Inch Tensor

Lengths	12 To 9	9 To 7	7 To 5	5 To 3	3 To 0
Weights					
150 to 225 Grams	0·000	0·000	0·000	0·000	0·000
100 to 150 "	0·000	0·000	0·000	0·000	0·000
75 to 100 "	0·000	0·000	0·000	0·000	0·000
50 to 75 "	0·000	0·000	0·000	0·000	0·000
35 to 50 "	0·000	0·000	·297	·040	0·000
25 to 35 "	0·000	0·000	·021	·039	0·000
0 to 25 "	0·000	0·000	0·000	0·000	·602

¾ Inch Tensor

Lengths	12 To 9	9 To 7	7 To 5	5 To 3	3 To 0
Weights					
150 to 225 Grams	0·000	0·000	0·000	0·000	0·000
100 to 150 "	0·000	0·000	0·000	0·000	0·000
75 to 100 "	0·000	0·000	0·000	0·000	0·000
50 to 75 "	0·000	0·000	0·000	0·000	0·000
35 to 50 "	0·000	0·000	·023	0·000	0·000
25 to 35 "	0·000	0·000	·013	·031	0·000
0 to 25 "	0·000	0·000	0·000	0·000	·933

Control Tensor

Lengths	12 To 9	9 To 7	7 To 5	5 To 3	3 To 0
Weights					
150 to 225 Grams	0·000	0·000	0·000	0·000	0·000
100 to 150 "	0·000	0·000	0·000	0·000	0·000
75 to 100 "	0·000	0·000	0·000	0·000	0·000
50 to 75 "	0·000	0·000	0·000	0·000	0·000
35 to 50 "	0·000	0·000	2·192	·324	0·000
25 to 35 "	0·000	0·000	·064	·064	0·000
0 to 25 "	0·000	0·000	0·000	0·000	-2·644

Feed Size 5 to 7 Cms 25 to 35 Grams

1 Inch Tensor

Lengths	12 To 9	9 To 7	7 To 5	5 To 3	3 To 0
Weights					
150 to 225 Grams	0·000	0·000	0·000	0·000	0·000
100 to 150 "	0·000	0·000	0·000	0·000	0·000
75 to 100 "	0·000	0·000	0·000	0·000	0·000
50 to 75 "	0·000	0·000	0·000	0·000	0·000
35 to 50 "	0·000	0·000	0·000	0·000	0·000
25 to 35 "	0·000	0·000	·304	·128	0·000
0 to 25 "	0·000	0·000	0·000	0·000	·568

⅜ Inch Tensor

Lengths	12 To 9	9 To 7	7 To 5	5 To 3	3 To 0
Weights					
150 to 225 Grams	0·000	0·000	0·000	0·000	0·000
100 to 150 "	0·000	0·000	0·000	0·000	0·000
75 to 100 "	0·000	0·000	0·000	0·000	0·000
50 to 75 "	0·000	0·000	0·000	0·000	0·000
35 to 50 "	0·000	0·000	0·000	0·000	0·000
25 to 35 "	0·000	0·000	·189	·071	0·000
0 to 25 "	0·000	0·000	0·000	0·000	·739

¾ Inch Tensor

Lengths	12 To 9	9 To 7	7 To 5	5 To 3	3 To 0
Weights					
150 to 225 Grams	0·000	0·000	0·000	0·000	0·000
100 to 150 "	0·000	0·000	0·000	0·000	0·000
75 to 100 "	0·000	0·000	0·000	0·000	0·000
50 to 75 "	0·000	0·000	0·000	0·000	0·000
35 to 50 "	0·000	0·000	0·000	0·000	0·000
25 to 35 "	0·000	0·000	·075	·014	0·000
0 to 25 "	0·000	0·000	0·000	0·000	·911

Control Tensor

Lengths	12 To 9	9 To 7	7 To 5	5 To 3	3 To 0
Weights					
150 to 225 Grams	0·000	0·000	0·000	0·000	0·000
100 to 150 "	0·000	0·000	0·000	0·000	0·000
75 to 100 "	0·000	0·000	0·000	0·000	0·000
50 to 75 "	0·000	0·000	0·000	0·000	0·000
35 to 50 "	0·000	0·000	0·000	0·000	0·000
25 to 35 "	0·000	0·000	·916	·456	0·000
0 to 25 "	0·000	0·000	0·000	0·000	-1·372

Feed Size 5 to 7 Cms 50 to 70 Grams

1 Inch Tensor

Lengths	12 To 9	9 To 7	7 To 5	5 To 3	3 To 0
Weights					
150 to 225 Grams	0·000	0·000	0·000	0·000	0·000
100 to 150 "	0·000	0·000	0·000	0·000	0·000
75 to 100 "	0·000	0·000	0·000	0·000	0·000
50 to 75 "	0·000	0·000	·277	0·000	0·000
35 to 50 "	0·000	0·000	·047	·055	0·000
25 to 35 "	0·000	0·000	·022	·069	0·000
0 to 25 "	0·000	0·000	0·000	0·000	·530

⅞ Inch Tensor

Lengths	12 To 9	9 To 7	7 To 5	5 To 3	3 To 0
Weights					
150 to 225 Grams	0·000	0·000	0·000	0·000	0·000
100 to 150 "	0·000	0·000	0·000	0·000	0·000
75 to 100 "	0·000	0·000	0·000	0·000	0·000
50 to 75 "	0·000	0·000	·183	0·000	0·000
35 to 50 "	0·000	0·000	·046	·027	0·000
25 to 35 "	0·000	0·000	·019	·049	0·000
0 to 25 "	0·000	0·000	0·000	0·000	·715

¾ Inch Tensor

Lengths	12 To 9	9 To 7	7 To 5	5 To 3	3 To 0
Weights					
150 to 225 Grams	0·000	0·000	0·000	0·000	0·000
100 to 150 "	0·000	0·000	0·000	0·000	0·000
75 to 100 "	0·000	0·000	0·000	0·000	0·000
50 to 75 "	0·000	0·000	·090	0·000	0·000
35 to 50 "	0·000	0·000	·045	0·000	0·000
25 to 35 "	0·000	0·000	·016	·029	0·000
0 to 25 "	0·000	0·000	0·000	0·000	·901

Control Tensor

Lengths	12 To 9	9 To 7	7 To 5	5 To 3	3 To 0
Weights					
150 to 225 Grams	0·000	0·000	0·000	0·000	0·000
100 to 150 "	0·000	0·000	0·000	0·000	0·000
75 to 100 "	0·000	0·000	0·000	0·000	0·000
50 to 75 "	0·000	0·000	·748	0·000	0·000
35 to 50 "	0·000	0·000	·008	·220	0·000
25 to 35 "	0·000	0·000	·024	·160	0·000
0 to 25 "	0·000	0·000	0·000	0·000	-1·484

Feed Size 5 to 7 Cms 70 to 100 Grams

1 Inch Tensor

Lengths	12 To 9	9 To 7	7 To 5	5 To 3	3 To 0
Weights					
150 to 225 Grams	0·000	0·000	0·000	0·000	0·000
100 to 150 "	0·000	0·000	0·000	0·000	0·000
75 to 100 "	0·000	0·000	·053	0·000	0·000
50 to 75 "	0·000	0·000	·011	0·000	0·000
35 to 50 "	0·000	0·000	·035	·032	0·000
25 to 35 "	0·000	0·000	·015	·092	0·000
0 to 25 "	0·000	0·000	0·000	0·000	·762

⅜ Inch Tensor

Lengths	12 To 9	9 To 7	7 To 5	5 To 3	3 To 0
Weights					
150 to 225 Grams	0·000	0·000	0·000	0·000	0·000
100 to 150 "	0·000	0·000	0·000	0·000	0·000
75 to 100 "	0·000	0·000	·026	0·000	0·000
50 to 75 "	0·000	0·000	·009	0·000	0·000
35 to 50 "	0·000	0·000	·020	·016	0·000
25 to 35 "	0·000	0·000	·011	·050	0·000
0 to 25 "	0·000	0·000	0·000	0·000	·867

¼ Inch Tensor

Lengths	12 To 9	9 To 7	7 To 5	5 To 3	3 To 0
Weights					
150 to 225 Grams	0·000	0·000	0·000	0·000	0·000
100 to 150 "	0·000	0·000	0·000	0·000	0·000
75 to 100 "	0·000	0·000	0·000	0·000	0·000
50 to 75 "	0·000	0·000	·007	0·000	0·000
35 to 50 "	0·000	0·000	·005	0·000	0·000
25 to 35 "	0·000	0·000	·006	·009	0·000
0 to 25 "	0·000	0·000	0·000	0·000	·973

Control Tensor

Lengths	12 To 9	9 To 7	7 To 5	5 To 3	3 To 0
Weights					
150 to 225 Grams	0·000	0·000	0·000	0·000	0·000
100 to 150 "	0·000	0·000	0·000	0·000	0·000
75 to 100 "	0·000	0·000	·212	0·000	0·000
50 to 75 "	0·000	0·000	·016	0·000	0·000
35 to 50 "	0·000	0·000	·120	·128	0·000
25 to 35 "	0·000	0·000	·036	·332	0·000
0 to 25 "	0·000	0·000	0·000	0·000	-·844

Feed Size 5 to 7 Cms 100 to 150 Grams

1 Inch Tensor

Lengths	12 To 9	9 To 7	7 To 5	5 To 3	3 To 0
Weights					
150 to 225 Grams	0·000	0·000	0·000	0·000	0·000
100 to 150 "	0·000	0·000	0·000	0·000	0·000
75 to 100 "	0·000	0·000	·025	0·000	0·000
50 to 75 "	0·000	0·000	·066	0·000	0·000
35 to 50 "	0·000	0·000	·041	·040	0·000
25 to 35 "	0·000	0·000	·020	·075	0·000
0 to 25 "	0·000	0·000	0·000	0·000	·733

⅞ Inch Tensor

Lengths	12 To 9	9 To 7	7 To 5	5 To 3	3 To 0
Weights					
150 to 225 Grams	0.000	0.000	0.000	0.000	0.000
100 to 150 "	0.000	0.000	0.000	0.000	0.000
75 to 100 "	0.000	0.000	.013	0.000	0.000
50 to 75 "	0.000	0.000	.033	0.000	0.000
35 to 50 "	0.000	0.000	.020	.020	0.000
25 to 35 "	0.000	0.000	.010	.038	0.000
0 to 25 "	0.000	0.000	0.000	0.000	.866

¾ Inch Tensor

Lengths	12 To 9	9 To 7	7 To 5	5 To 3	3 To 0
Weights					
150 to 225 Grams	0·000	0·000	0·000	0·000	0·000
100 to 150 "	0·000	0·000	0·000	0·000	0·000
75 to 100 "	0·000	0·000	0·000	0·000	0·000
50 to 75 "	0·000	0·000	0·000	0·000	0·000
35 to 50 "	0·000	0·000	0·000	0·000	0·000
25 to 35 "	0·000	0·000	0·000	0·000	0·000
0 to 25 "	0·000	0·000	0·000	0·000	1·000

Control Tensor

Lengths	12 To 9	9 To 7	7 To 5	5 To 3	3 To 0
Weights					
150 to 225 Grams	0·000	0·000	0·000	0·000	0·000
100 to 150 "	0·000	0·000	0·000	0·000	0·000
75 to 100 "	0·000	0·000	·100	0·000	0·000
50 to 75 "	0·000	0·000	·264	0·000	0·000
35 to 50 "	0·000	0·000	·164	·160	0·000
25 to 35 "	0·000	0·000	·080	·300	0·000
0 to 25 "	0·000	0·000	0·000	0·000	-1·068

Feed Size 3 to 5 Cms 50 to 70 Grams

1 Inch Tensor

Lengths / Weights	12 To 9	9 To 7	7 To 5	5 To 3	3 To 0
150 to 225 Grams	0·000	0·000	0·000	0·000	0·000
100 to 150 "	0·000	0·000	0·000	0·000	0·000
75 to 100 "	0·000	0·000	0·000	0·000	0·000
50 to 75 "	0·000	0·000	0·000	·019	0·000
35 to 50 "	0·000	0·000	0·000	·134	0·000
25 to 35 "	0·000	0·000	0·000	·076	0·000
0 to 25 "	0·000	0·000	0·000	0·000	·771

⅜ Inch Tensor

Lengths / Weights	12 To 9	9 To 7	7 To 5	5 To 3	3 To 0
150 to 225 Grams	0·000	0·000	0·000	0·000	0·000
100 to 150 "	0·000	0·000	0·000	0·000	0·000
75 to 100 "	0·000	0·000	0·000	0·000	0·000
50 to 75 "	0·000	0·000	0·000	·010	0·000
35 to 50 "	0·000	0·000	0·000	·067	0·000
25 to 35 "	0·000	0·000	0·000	·038	0·000
0 to 25 "	0·000	0·000	0·000	0·000	·886

¼ Inch Tensor

Lengths / Weights	12 To 9	9 To 7	7 To 5	5 To 3	3 To 0
150 to 225 Grams	0·000	0·000	0·000	0·000	0·000
100 to 150 "	0·000	0·000	0·000	0·000	0·000
75 to 100 "	0·000	0·000	0·000	0·000	0·000
50 to 75 "	0·000	0·000	0·000	0·000	0·000
35 to 50 "	0·000	0·000	0·000	0·000	0·000
25 to 35 "	0·000	0·000	0·000	0·000	0·000
0 to 25 "	0·000	0·000	0·000	0·000	1·000

Control Tensor

Lengths / Weights	12 To 9	9 To 7	7 To 5	5 To .3	3 To 0
150 to 225 Grams	0·000	0·000	0·000	0·000	0·000
100 to 150 "	0·000	0·000	0·000	0·000	0·000
75 to 100 "	0·000	0·000	0·000	0·000	0·000
50 to 75 "	0·000	0·000	0·000	·076	0·000
35 to 50 "	0·000	0·000	0·000	·536	0·000
25 to 35 "	0·000	0·000	0·000	·304	0·000
0 to 25 "	0·000	0·000	0·000	0·000	-·916

Feed Size 3 to 5 Cms 25 to 35 Grams

1 Inch Tensor

Lengths	12 To 9	9 To 7	7 To 5	5 To 3	3 To 0
Weights					
150 to 225 Grams	0·000	0·000	0·000	0·000	0·000
100 to 150 "	0·000	0·000	0·000	0·000	0·000
75 to 100 "	0·000	0·000	0·000	0·000	0·000
50 to 75 "	0·000	0·000	0·000	0·000	0·000
35 to 50 "	0·000	0·000	0·000	0·000	0·000
25 to 35 "	0·000	0·000	0·000	·490	0·000
0 to 25 "	0·000	0·000	0·000	0·000	·510

⅞ Inch Tensor

Lengths	12 To 9	9 To 7	7 To 5	5 To 3	3 To 0
Weights					
150 to 225 Grams	0·000	0·000	0·000	0·000	0·000
100 to 150 "	0·000	0·000	0·000	0·000	0·000
75 to 100 "	0·000	0·000	0·000	0·000	0·000
50 to 75 "	0·000	0·000	0·000	0·000	0·000
35 to 50 "	0·000	0·000	0·000	0·000	0·000
25 to 35 "	0·000	0·000	0·000	·269	0·000
0 to 25 "	0·000	0·000	0·000	0·000	·730

¾ Inch Tensor

Lengths	12 To 9	9 To 7	7 To 5	5 To 3	3 To 0
Weights					
150 to 225 Grams	0·000	0·000	0·000	0·000	0·000
100 to 150 "	0·000	0·000	0·000	0·000	0·000
75 to 100 "	0·000	0·000	0·000	0·000	0·000
50 to 75 "	0·000	0·000	0·000	0·000	0·000
35 to 50 "	0·000	0·000	0·000	0·000	0·000
25 to 35 "	0·000	0·000	0·000	·049	0·000
0 to 25 "	0·000	0·000	0·000	0·000	·951

Control Tensor

Lengths	12 To 9	9 To 7	7 To 5	5 To .3	3 To 0
Weights					
150 to 225 Grams	0.000	0.000	0.000	0.000	0.000
100 to 150 "	0·000	0·000	0·000	0·000	0·000
75 to 100 "	0·000	0·000	0·000	0·000	0·000
50 to 75 "	0·000	0·000	0·000	0·000	0·000
35 to 50 "	0·000	0·000	0·000	0·000	0·000
25 to 35 "	0·000	0·000	0·000	1·764	0·000
0 to 25 "	0·000	0·000	0·000	0·000	-1·764

Feed Size 3 to 5 Cms 35 to 50 Grams

1 Inch Tensor

Lengths	12 To 9	9 To 7	7 To 5	5 To 3	3 To 0
Weights					
150 to 225 Grams	0.000	0.000	0.000	0.000	0.000
100 to 150 "	0.000	0.000	0.000	0.000	0.000
75 to 100 "	0.000	0.000	0.000	0.000	0.000
50 to 75 "	0.000	0.000	0.000	0.000	0.000
35 to 50 "	0.000	0.000	0.000	.112	0.000
25 to 35 "	0.000	0.000	0.000	.178	0.000
0 to 25 "	0.000	0.000	0.000	0.000	.712

⅞ Inch Tensor

Lengths	12 To 9	9 To 7	7 To 5	5 To 3	3 To 0
Weights					
150 to 225 Grams	0.000	0.000	0.000	0.000	0.000
100 to 150 "	0.000	0.000	0.000	0.000	0.000
75 to 100 "	0.000	0.000	0.000	0.000	0.000
50 to 75 "	0.000	0.000	0.000	0.000	0.000
35 to 50 "	0.000	0.000	0.000	.056	0.000
25 to 35 "	0.000	0.000	0.000	.093	0.000
0 to 25 "	0.000	0.000	0.000	0.000	.851

¾ Inch Tensor

Lengths	12 To 9	9 To 7	7 To 5	5 To 3	3 To 0
Weights					
150 to 225 Grams	0.000	0.000	0.000	0.000	0.000
100 to 150 "	0.000	0.000	0.000	0.000	0.000
75 to 100 "	0.000	0.000	0.000	0.000	0.000
50 to 75 "	0.000	0.000	0.000	0.000	0.000
35 to 50 "	0.000	0.000	0.000	0.000	0.000
25 to 35 "	0.000	0.000	0.000	.009	0.000
0 to 25 "	0.000	0.000	0.000	0.000	.991

Control Tensor

Lengths	12 To 9	9 To 7	7 To 5	5 To 3	3 To 0
Weights					
150 to 225 Grams	0.000	0.000	0.000	0.000	0.000
100 to 150 "	0.000	0.000	0.000	0.000	0.000
75 to 100 "	0.000	0.000	0.000	0.000	0.000
50 to 75 "	0.000	0.000	0.000	0.000	0.000
35 to 50 "	0.000	0.000	0.000	.448	0.000
25 to 35 "	0.000	0.000	0.000	.676	0.000
0 to 25 "	0.000	0.000	0.000	0.000	-1.116

Feed Size 0 to 3 Cms 0 to 25 Grams

1 Inch Tensor

Lengths	12 To 9	9 To 7	7 To 5	5 To 3	3 To 0
Weights					
150 to 225 Grams	0·000	0·000	0·000	0·000	0·000
100 to 150 "	0·000	0·000	0·000	0·000	0·000
75 to 100 "	0·000	0·000	0·000	0·000	0·000
50 to 75 "	0·000	0·000	0·000	0·000	0·000
35 to 50 "	0·000	0·000	0·000	0·000	0·000
25 to 35 "	0·000	0·000	0·000	0·000	0·000
0 to 25 "	0·000	0·000	0·000	0·000	1·000

⅜ Inch Tensor

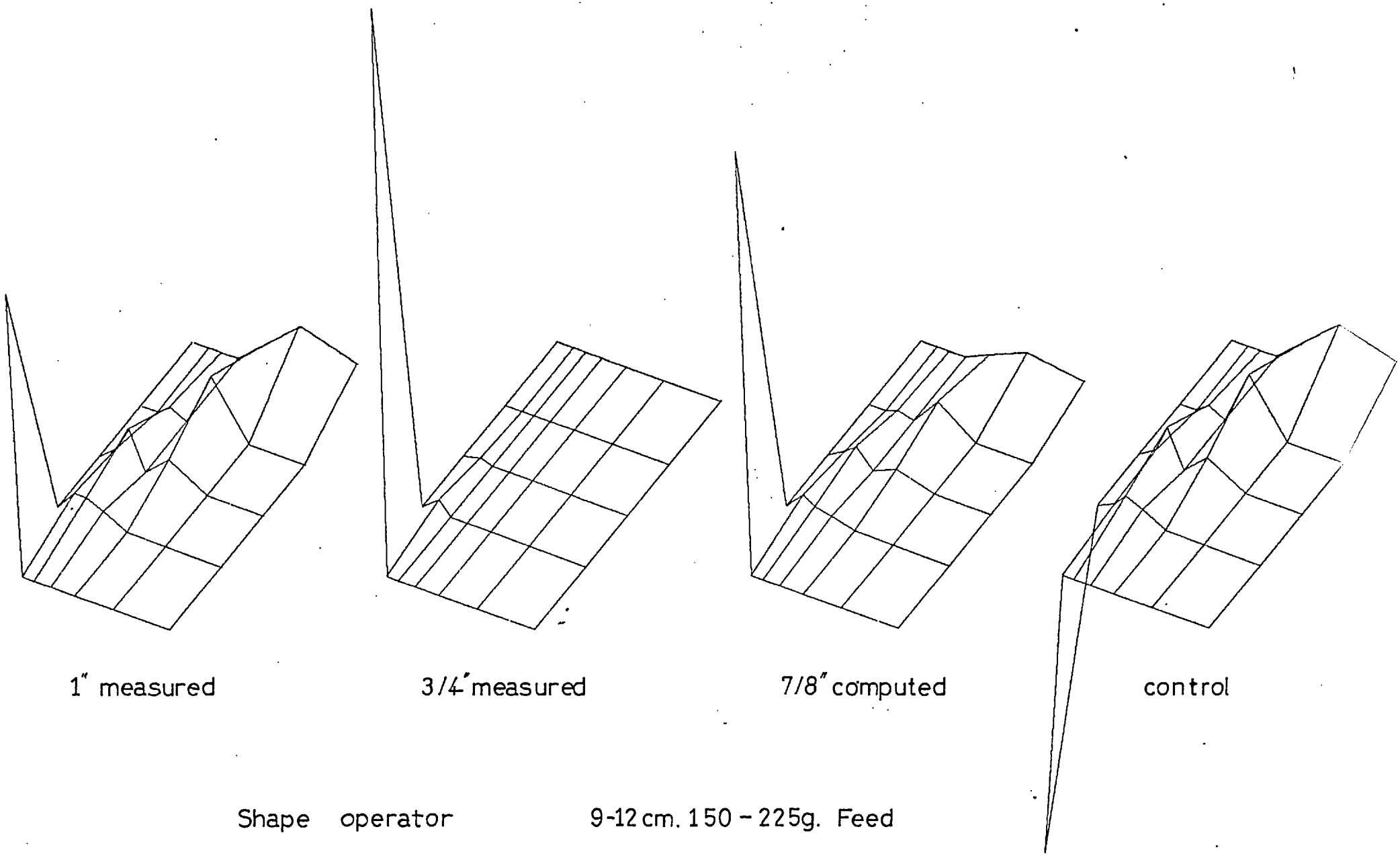
Lengths	12 To 9	9 To 7	7 To 5	5 To 3	3 To 0
Weights					
150 to 225 Grams	0·000	0·000	0·000	0·000	0·000
100 to 150 "	0·000	0·000	0·000	0·000	0·000
75 to 100 "	0·000	0·000	0·000	0·000	0·000
50 to 75 "	0·000	0·000	0·000	0·000	0·000
35 to 50 "	0·000	0·000	0·000	0·000	0·000
25 to 35 "	0·000	0·000	0·000	0·000	0·000
0 to 25 "	0·000	0·000	0·000	0·000	1·000

¾ Inch Tensor

Lengths	12 To 9	9 To 7	7 To 5	5 To 3	3 To 0
Weights					
150 to 225 Grams	0·000	0·000	0·000	0·000	0·000
100 to 150 "	0·000	0·000	0·000	0·000	0·000
75 to 100 "	0·000	0·000	0·000	0·000	0·000
50 to 75 "	0·000	0·000	0·000	0·000	0·000
35 to 50 "	0·000	0·000	0·000	0·000	0·000
25 to 35 "	0·000	0·000	0·000	0·000	0·000
0 to 25 "	0·000	0·000	0·000	0·000	1·000

Control Tensor

Lengths	12 To 9	9 To 7	7 To 5	5 To 3	3 To 0
Weights					
150 to 225 Grams	0·000	0·000	0.000	0.000	0·000
100 to 150 "	0·000	0·000	0·000	0·000	0·000
75 to 100 "	0·000	0·000	0·000	0·000	0·000
50 to 75 "	0·000	0·000	0·000	0·000	0·000
35 to 50 "	0·000	0·000	0·000	0·000	0·000
25 to 35 "	0·000	0·000	0·000	0·000	0·000
0 to 25 "	0·000	0·000	0·000	0·000	0·000



Shape operator 9-12 cm. 150 - 225g. Feed

figure 6/9

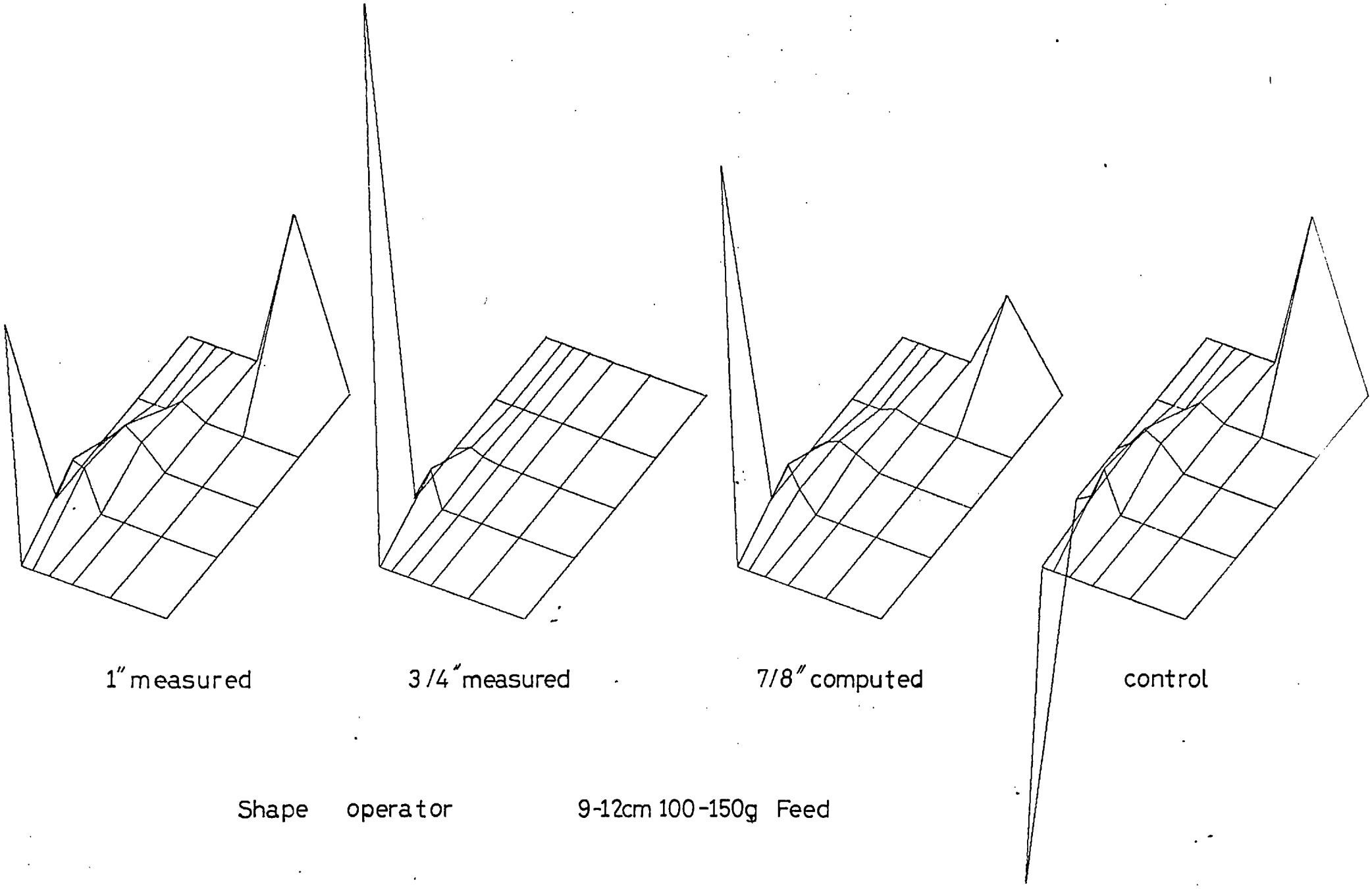
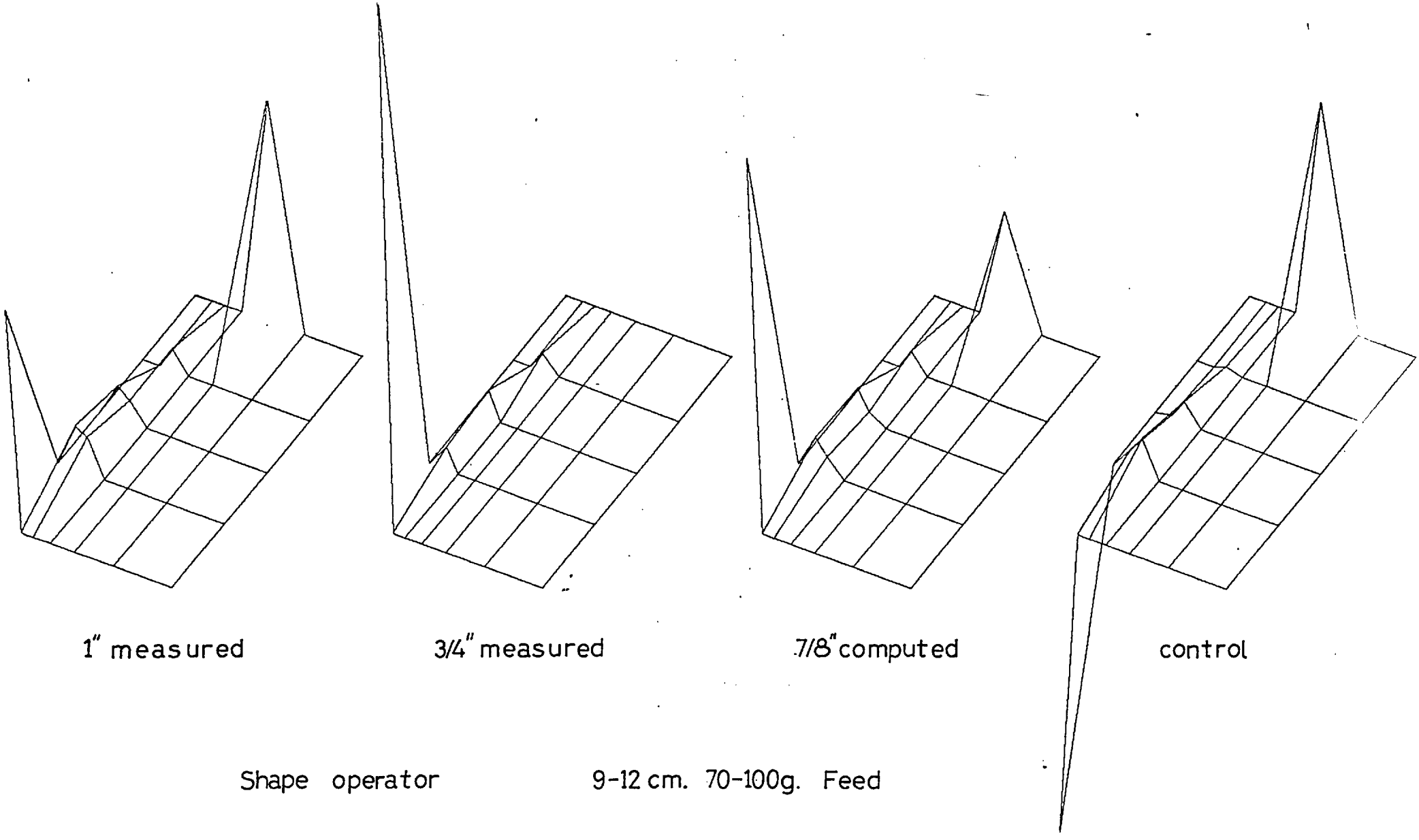
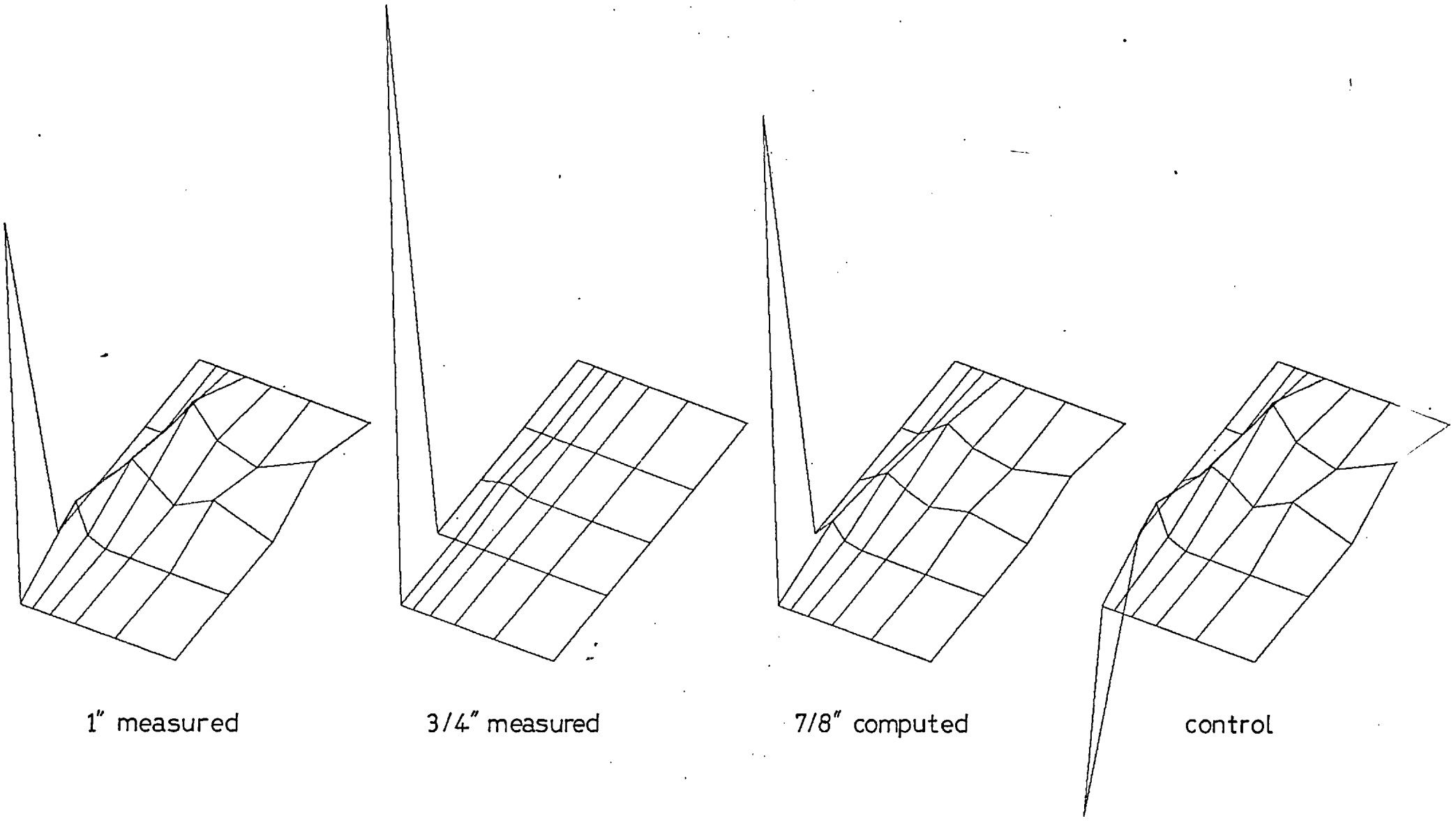

1" measured
3/4" measured
7/8" computed
control
Shape operator
9-12cm 100-150g Feed

figure 6/10



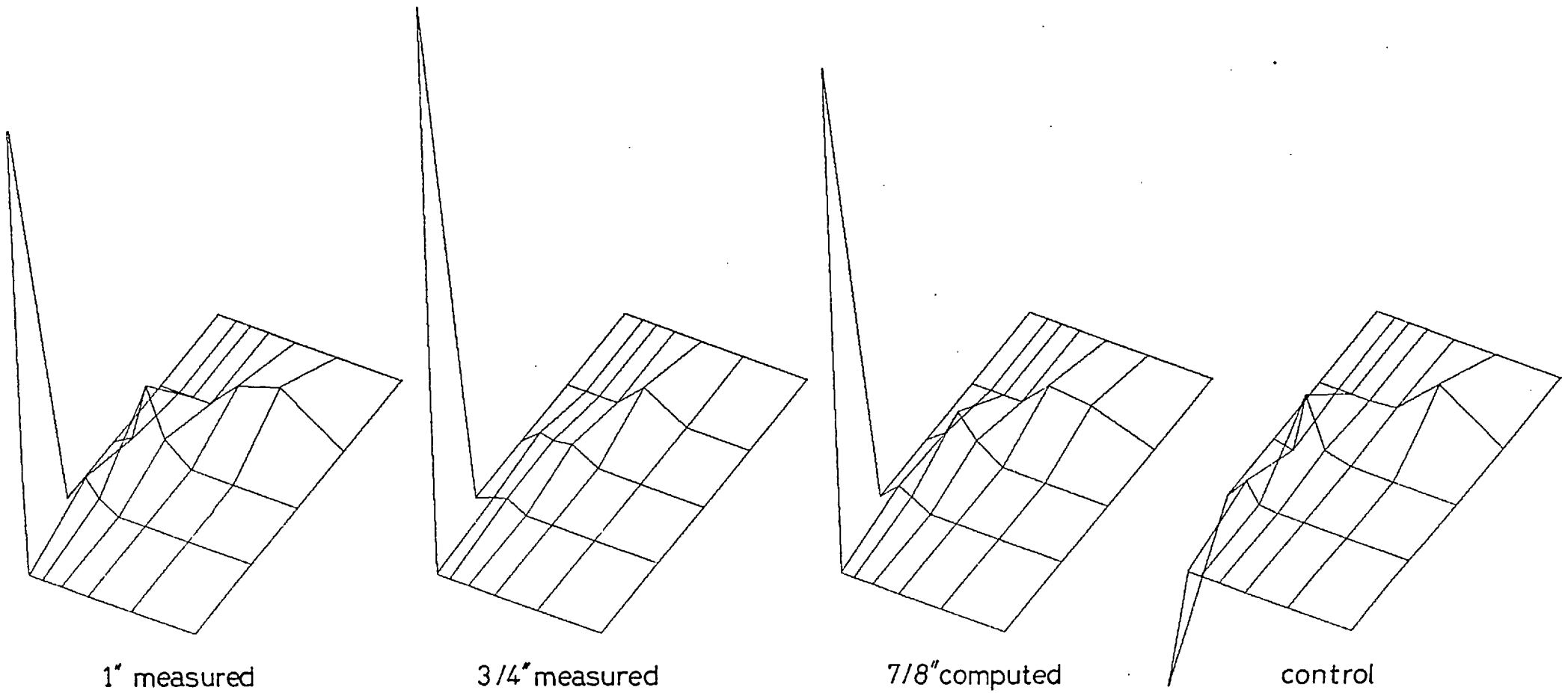
Shape operator 9-12 cm. 70-100g. Feed

figure 6/11



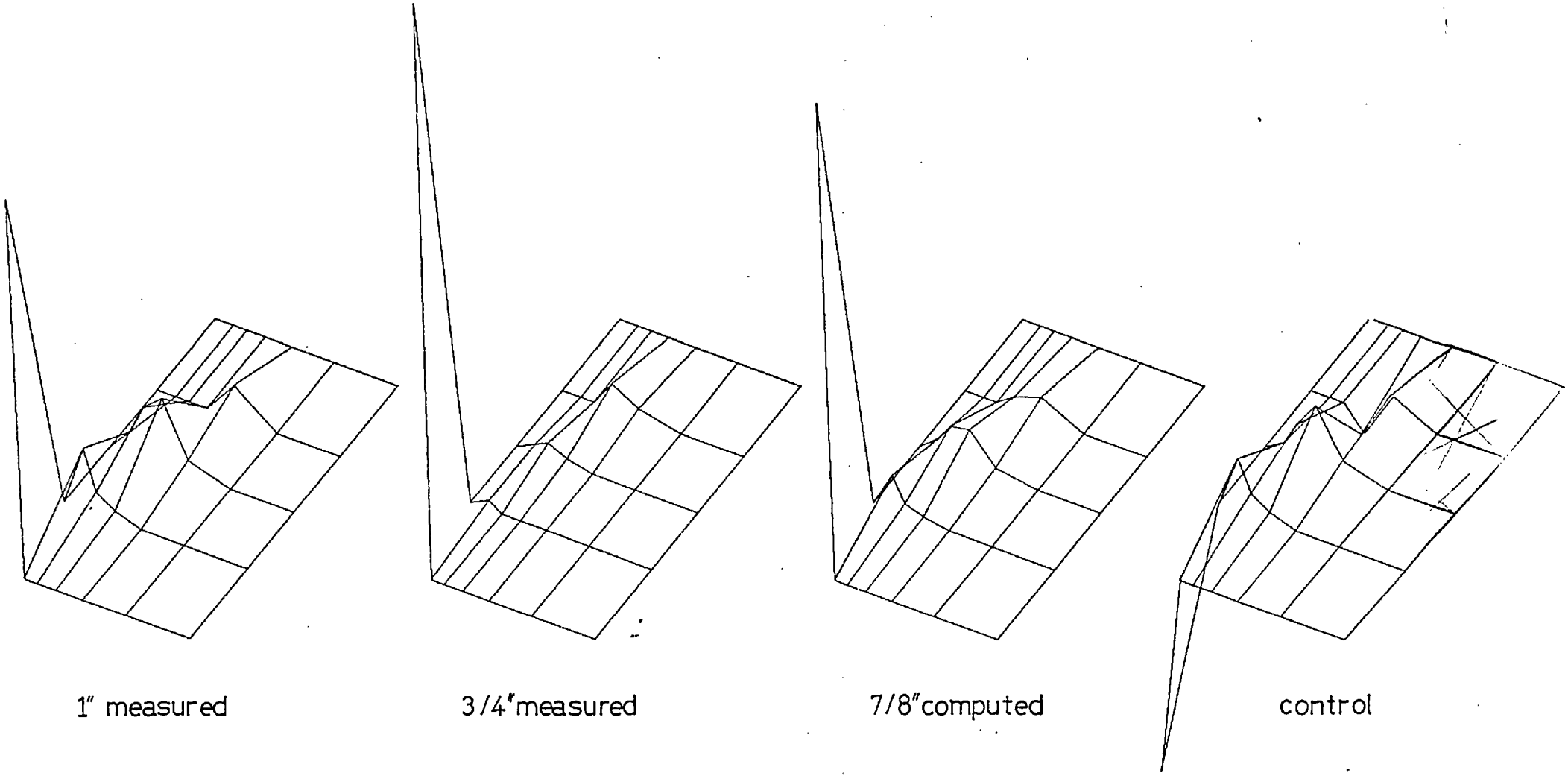
Shape operator 7-9cm. 150-225g. Feed

figure 6/12



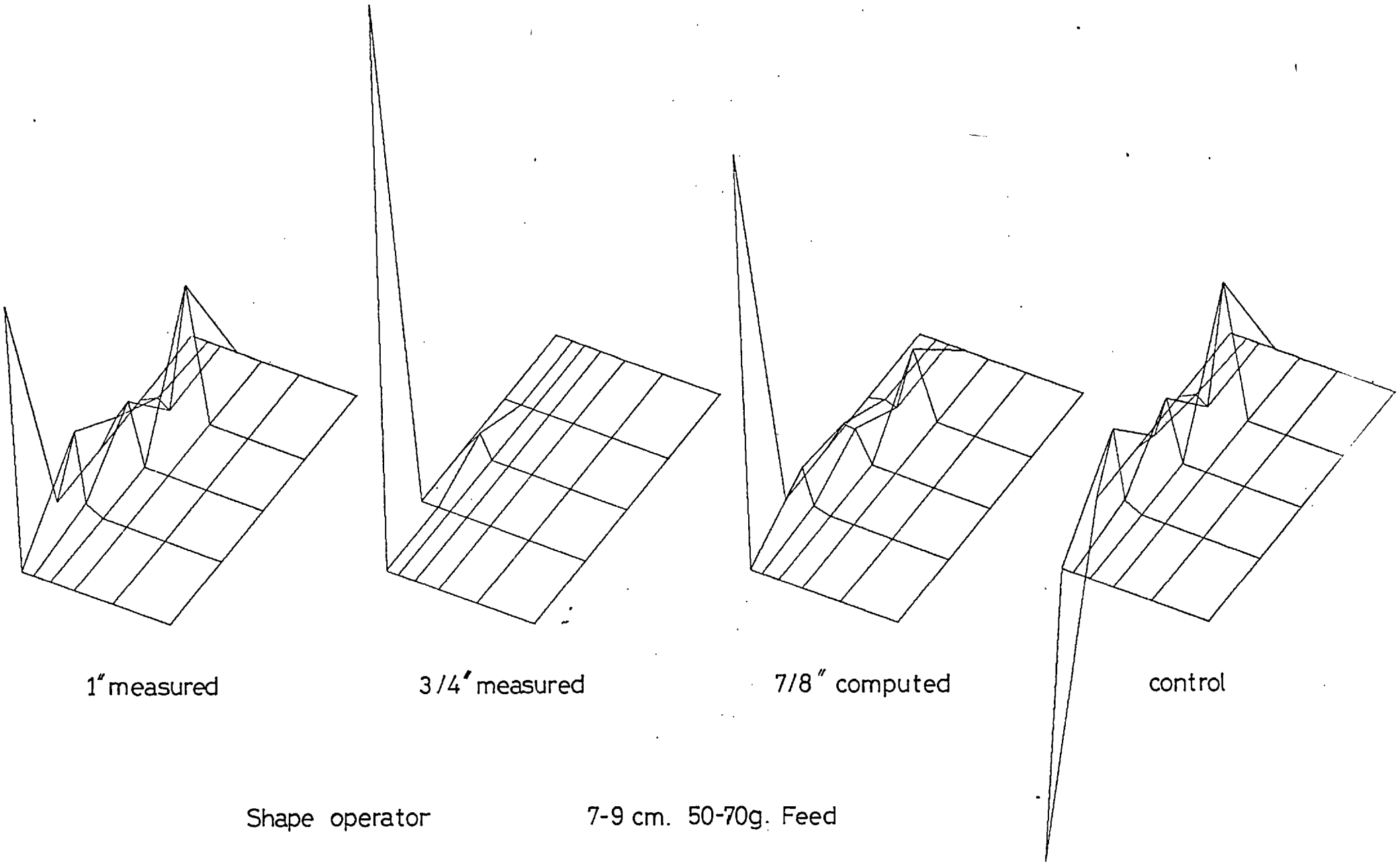
Shape operator 7-9 cm. 100-150g. Feed

figure 6/13



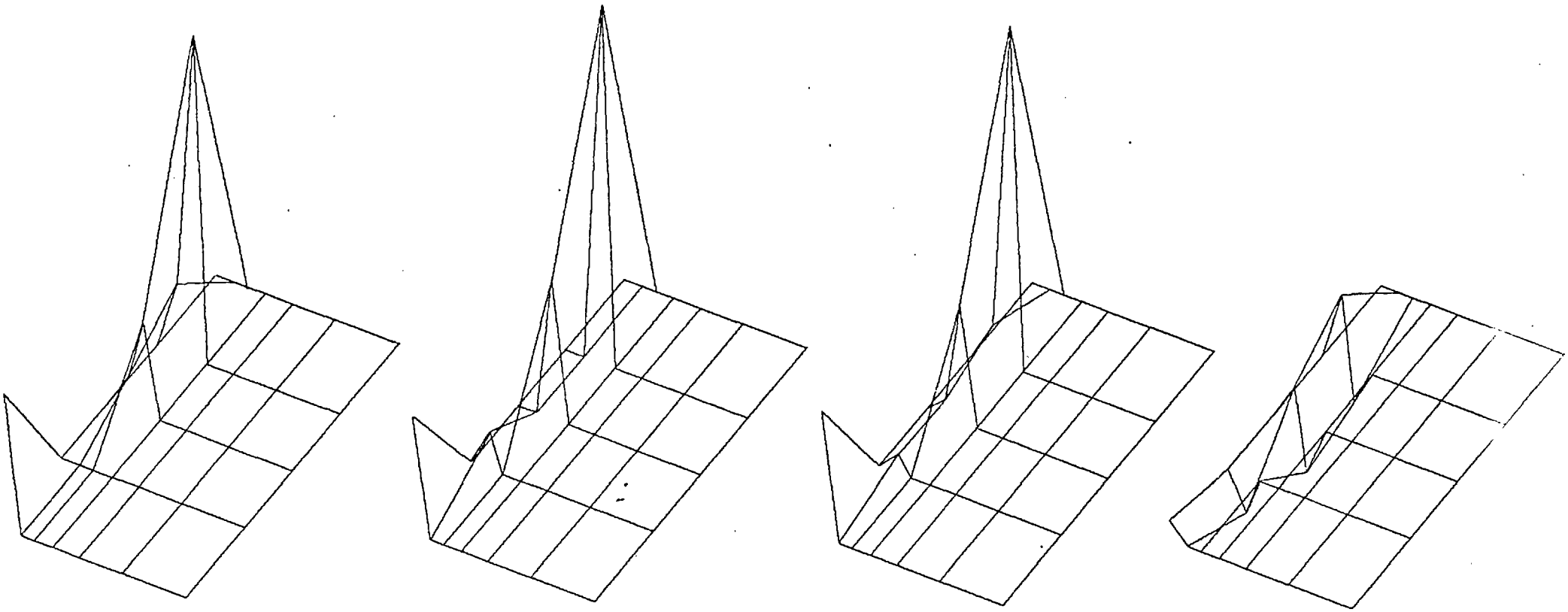
Shape operator 7-9 cm 70-100g Feed

figure 6/14



Shape operator 7-9 cm. 50-70g. Feed

figure 6/15



1" measured

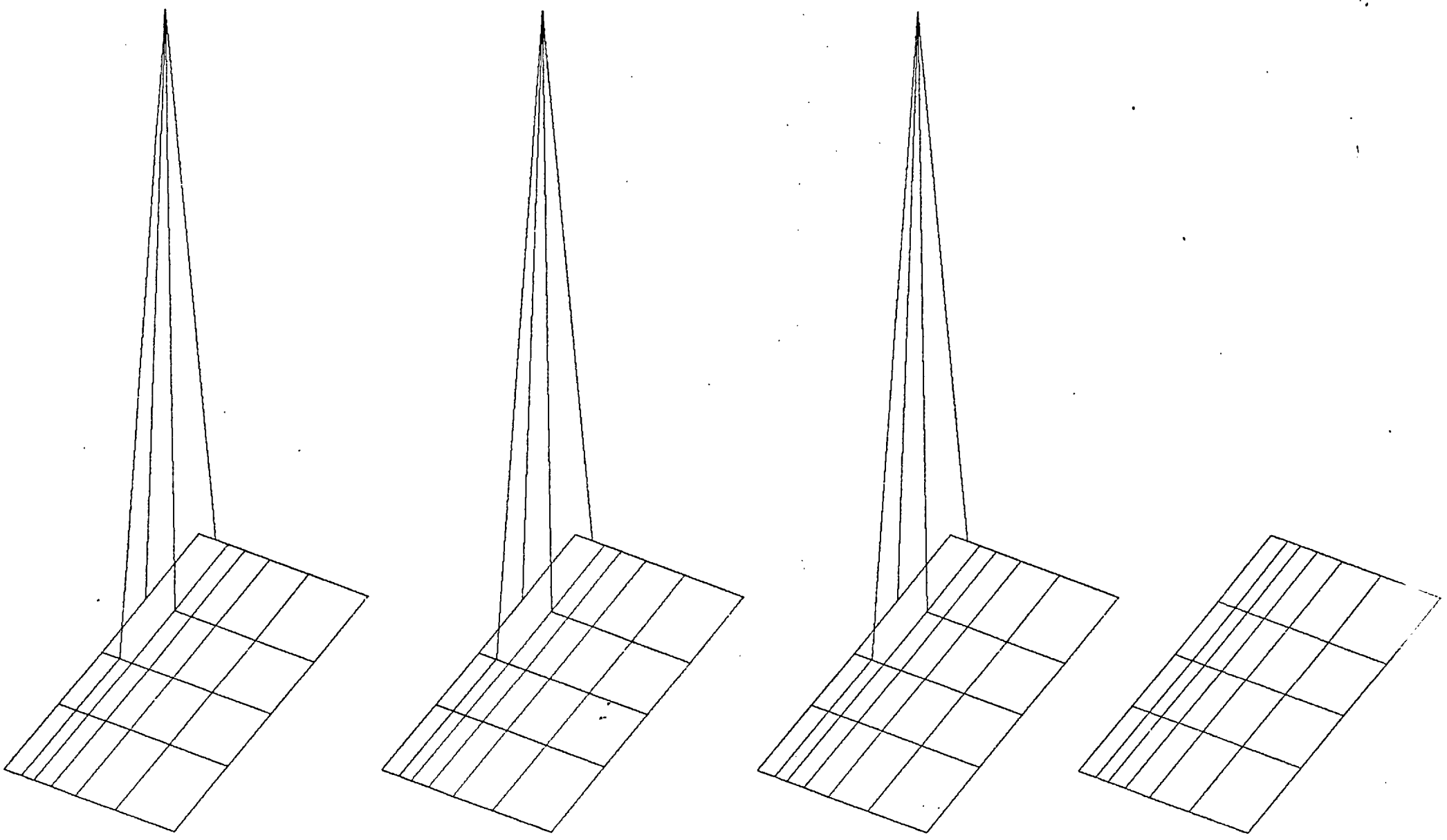
3/4" measured

7/8" computed

control

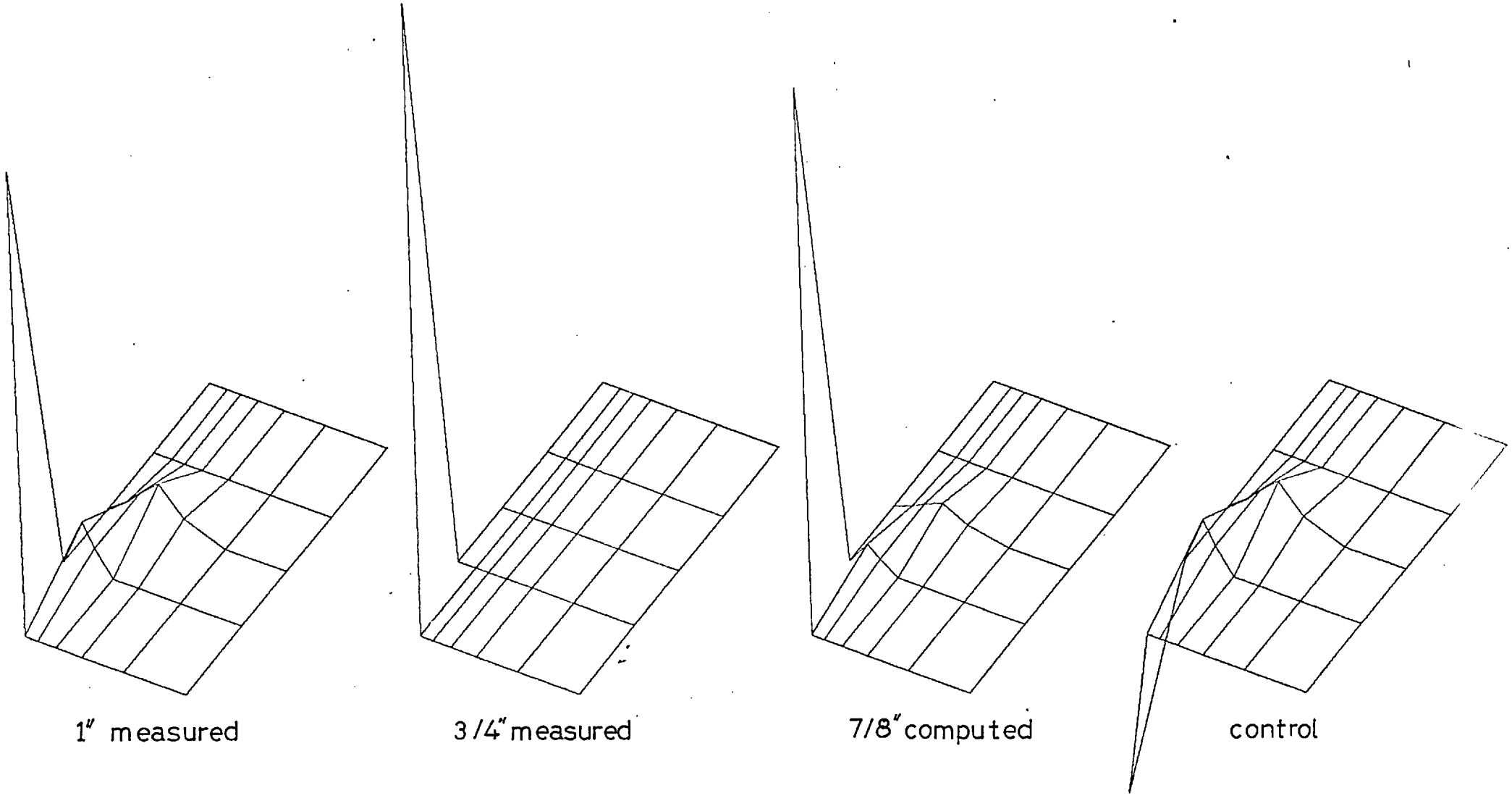
Shape operator 7-9cm. 35-50g. Feed

figure 6/16



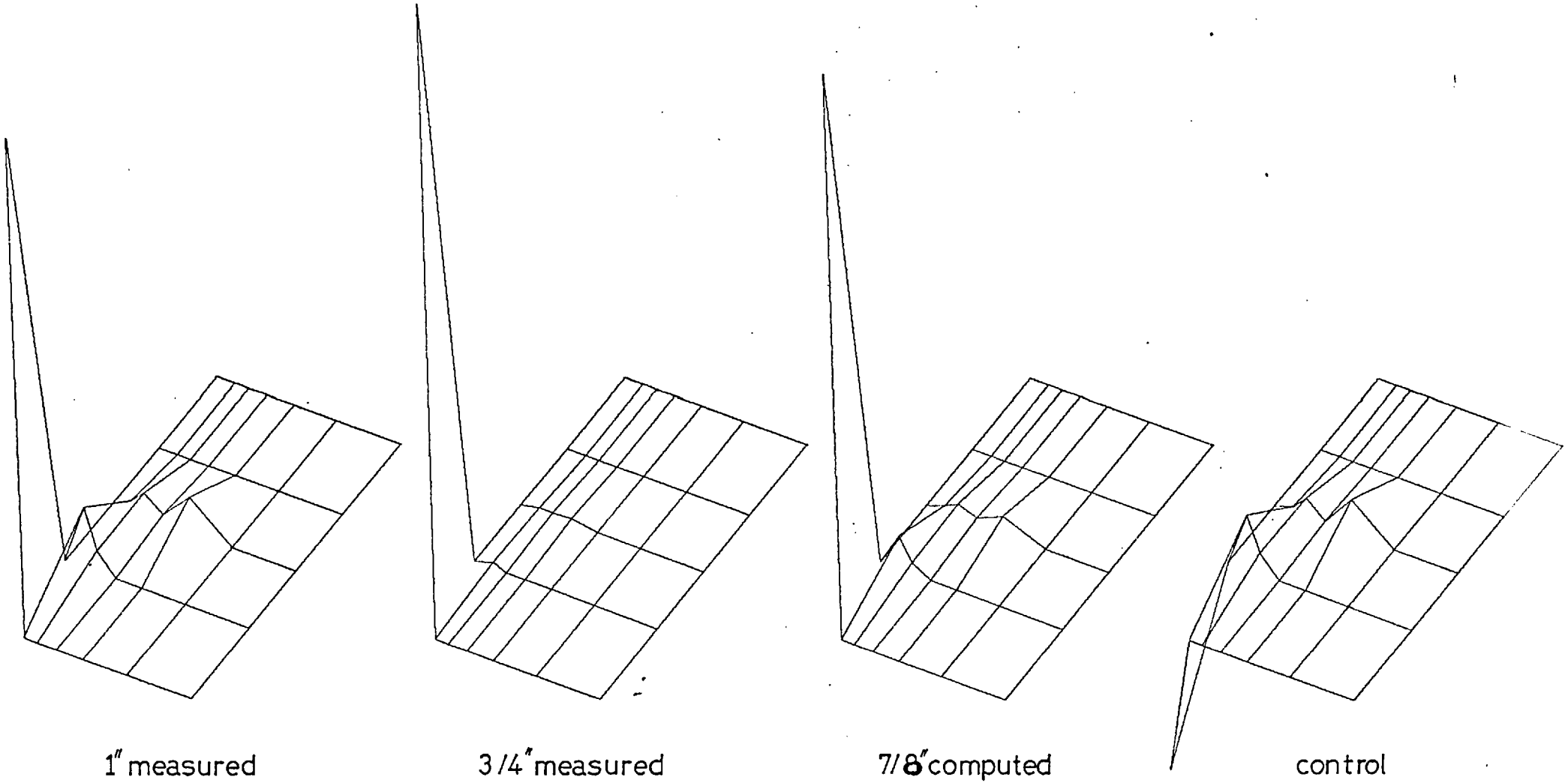
Shape operator 7-9cm. 25-35g. Feed

figure 6/17



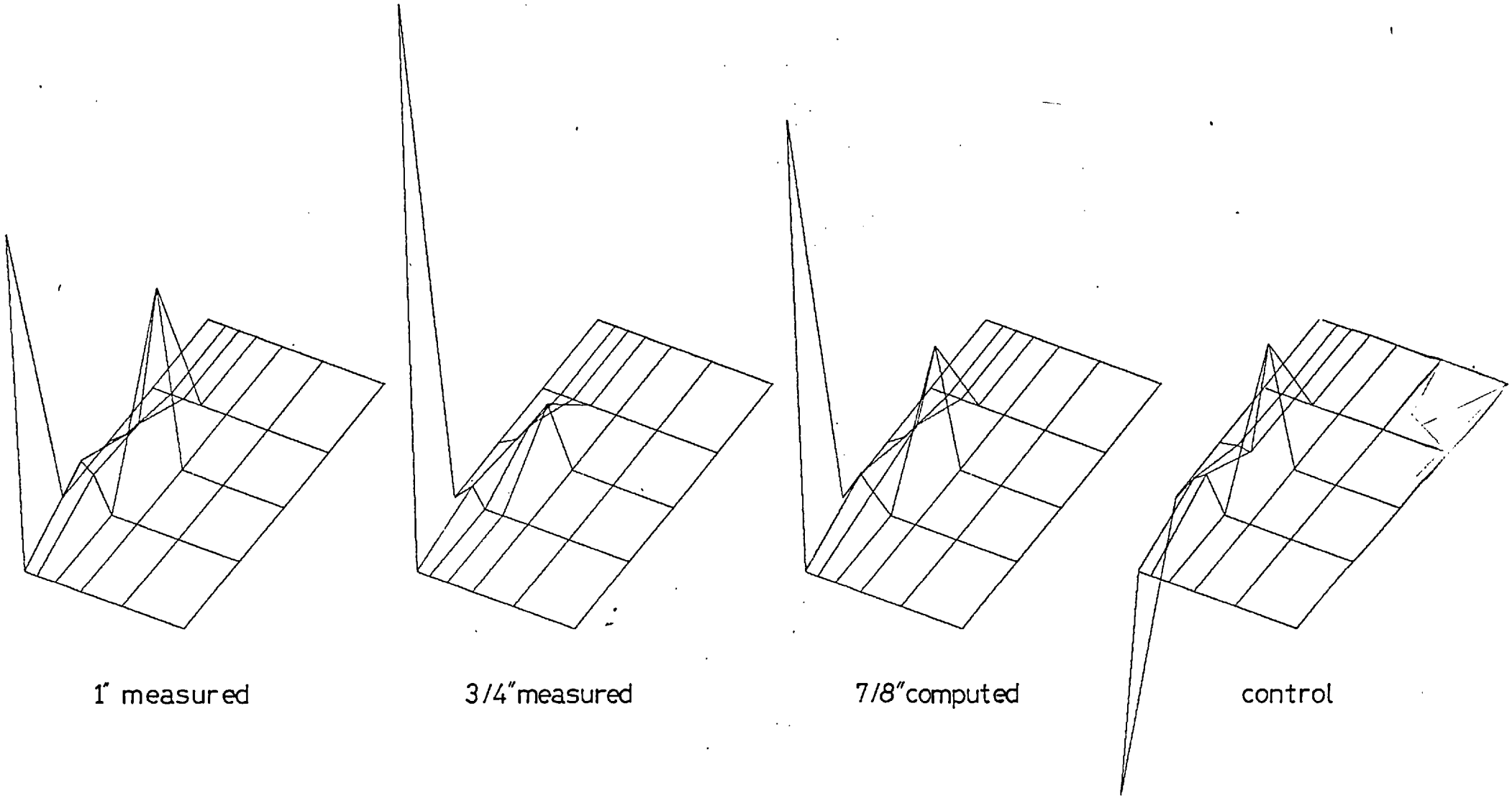
Shape operator 5-7cm. 100-150g. Feed

figure 6/18



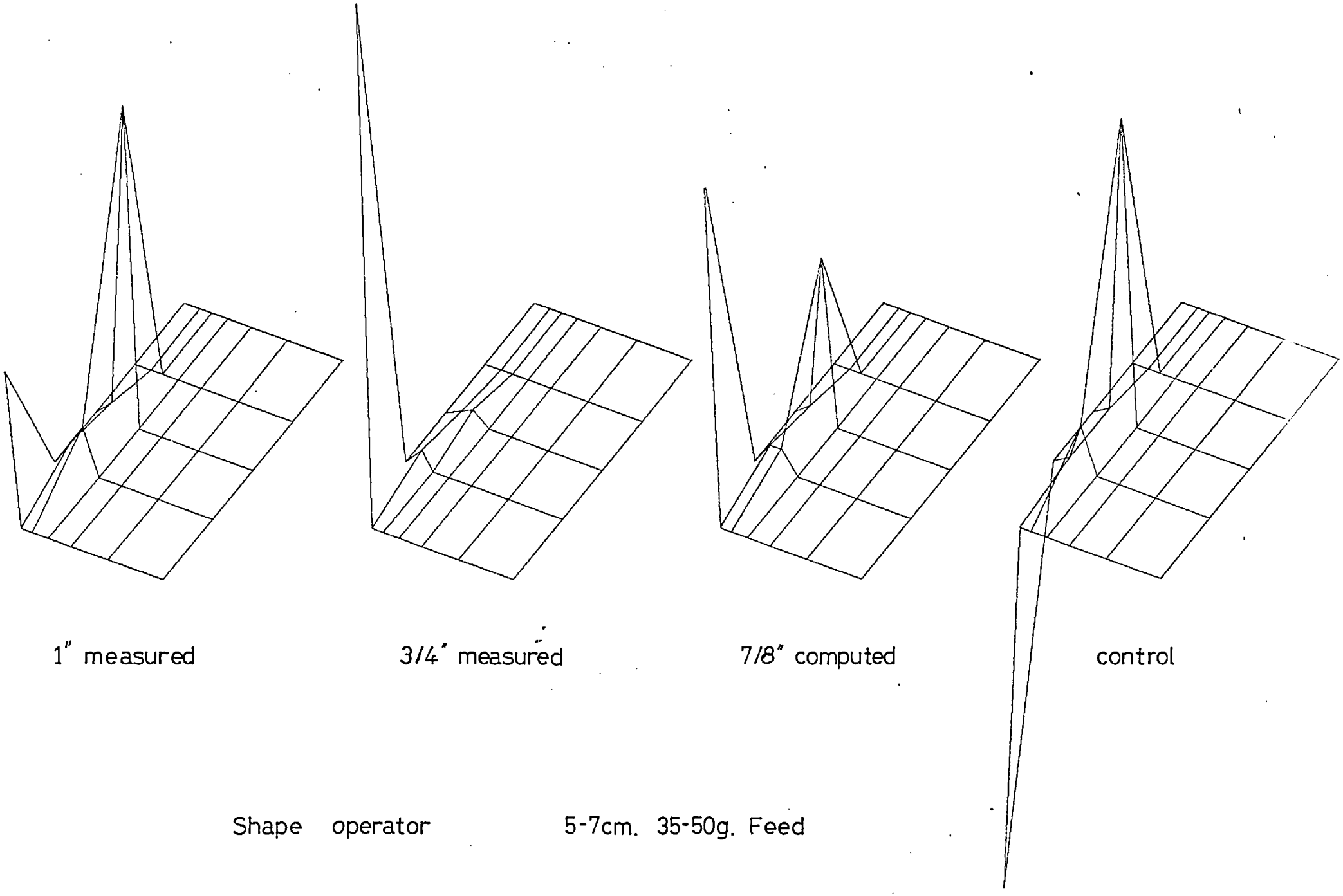
Shape operator 5-7cm. 70-100g. Feed

figure 6/19



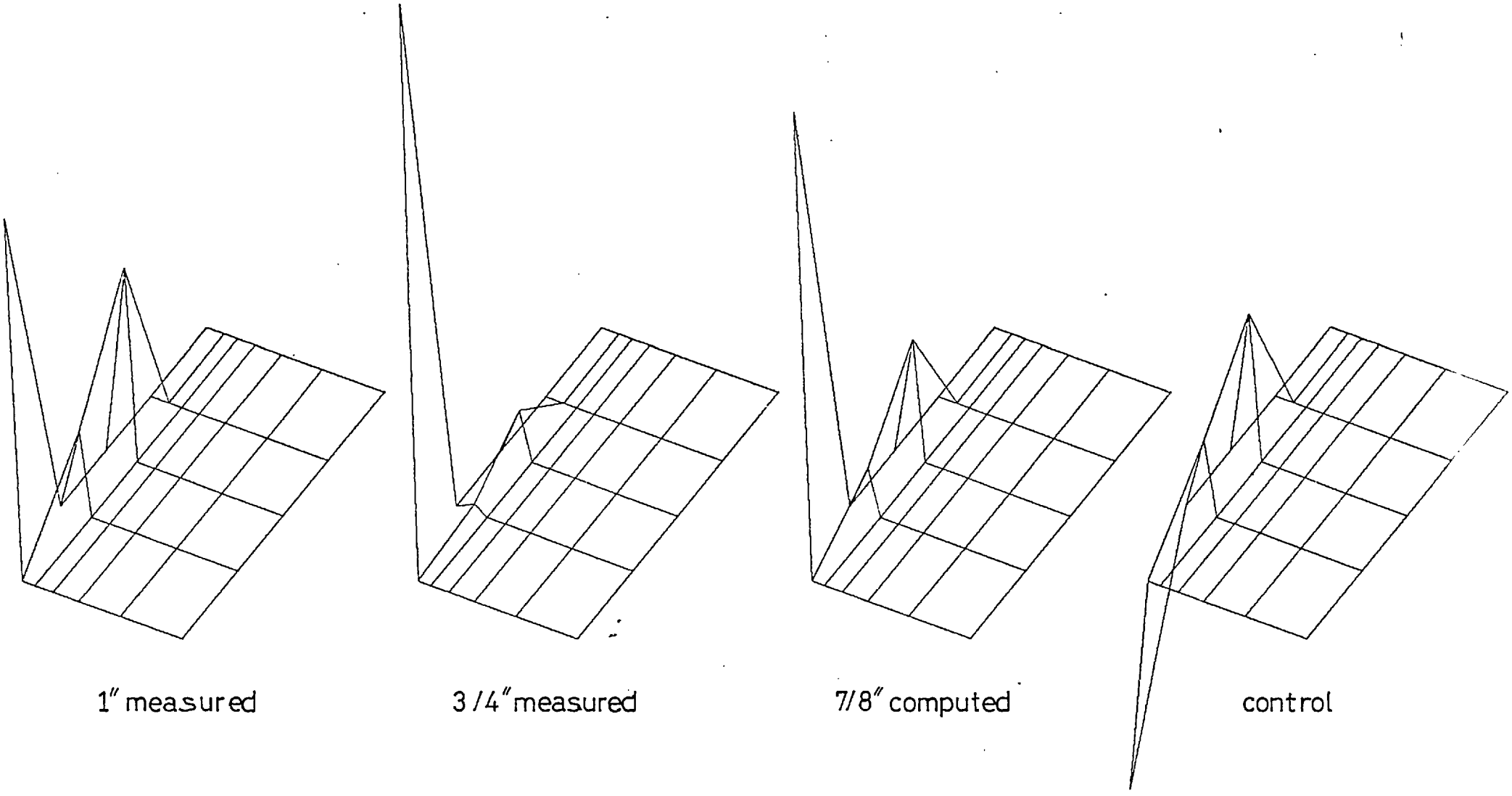
Shape operator 5-7cm. 50-70g. Feed

figure 6/20



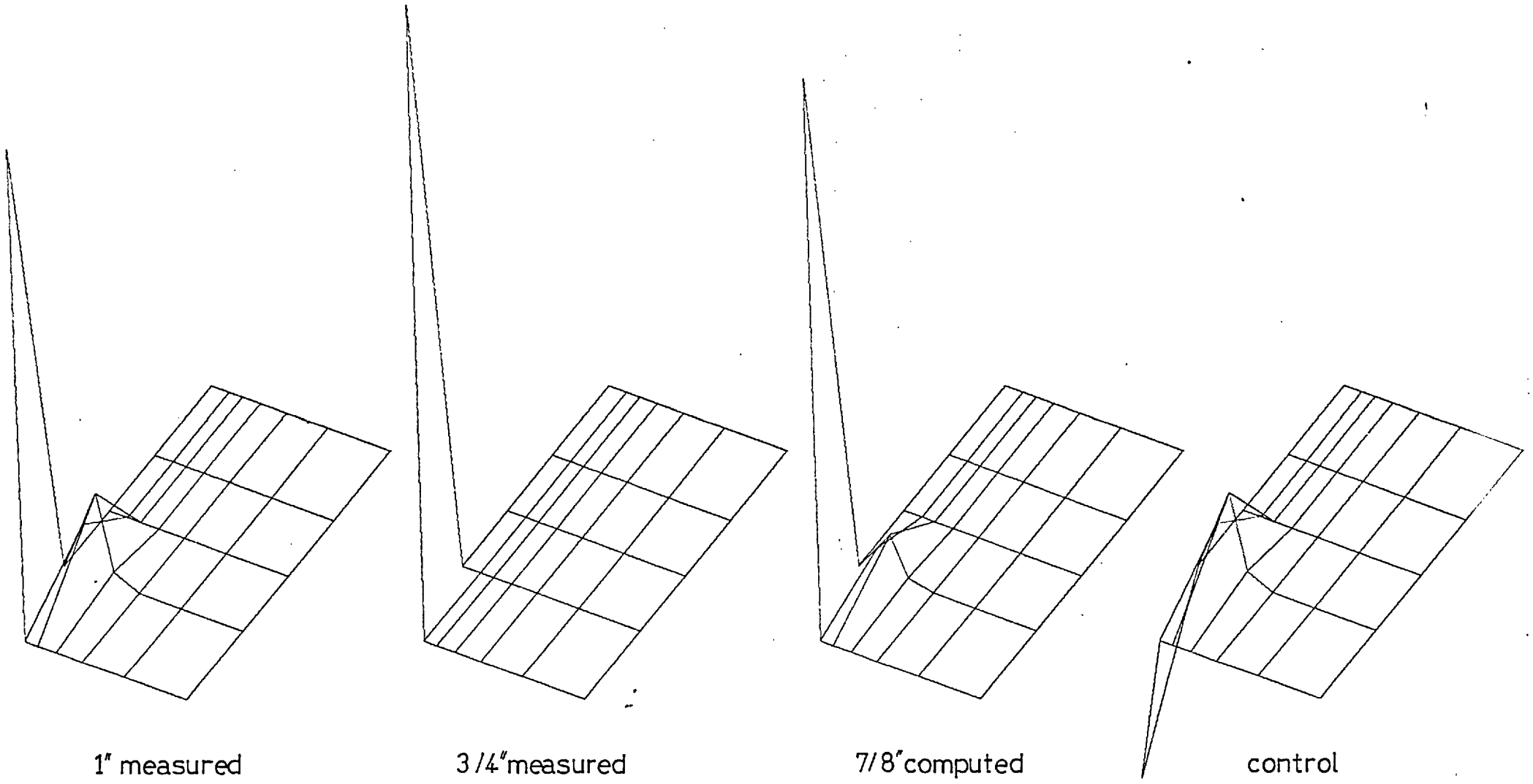
Shape operator 5-7cm. 35-50g. Feed

figure 6/21



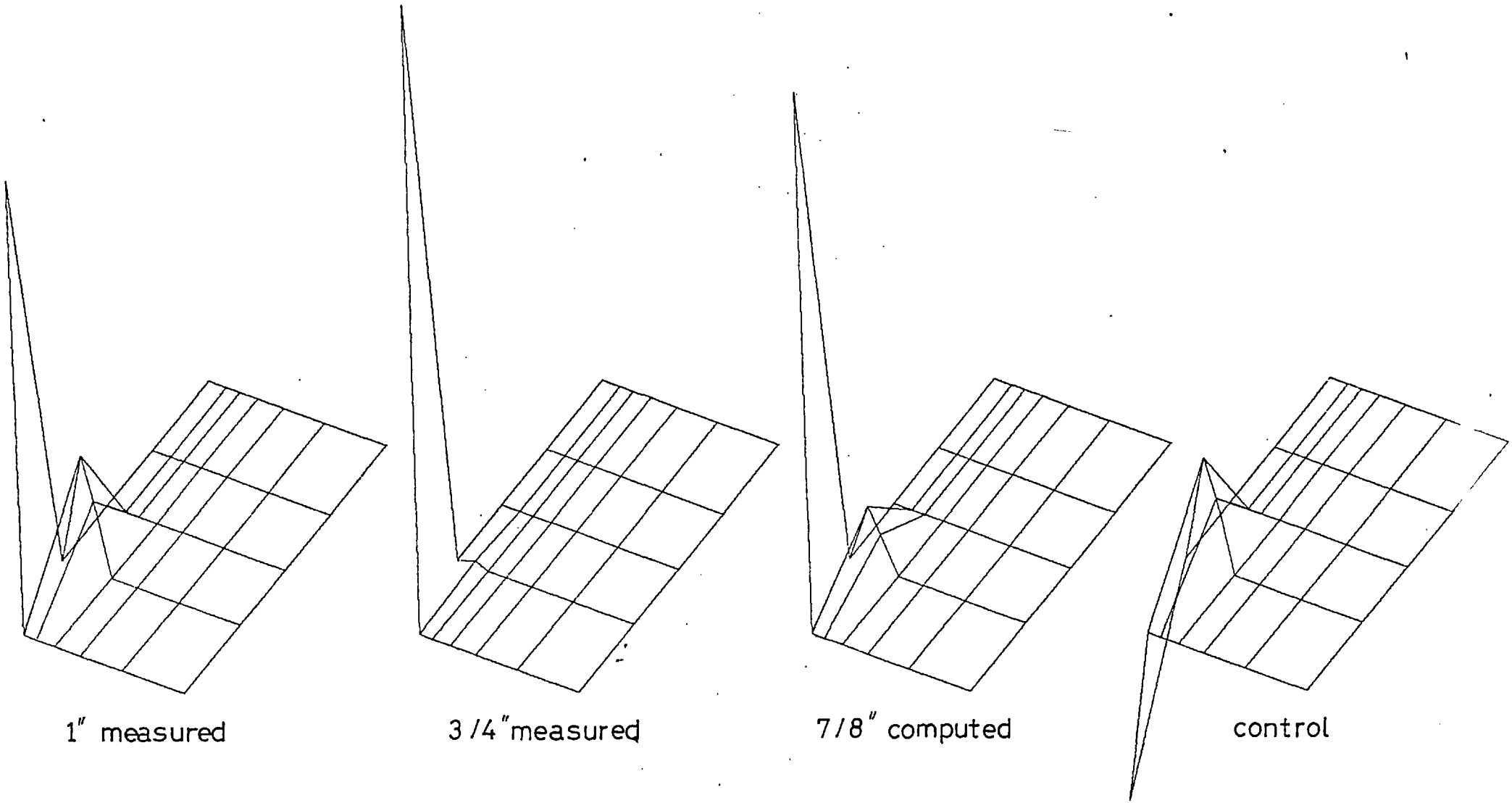
Shape operator 5-7cm. 25-35g. Feed

figure 6/22



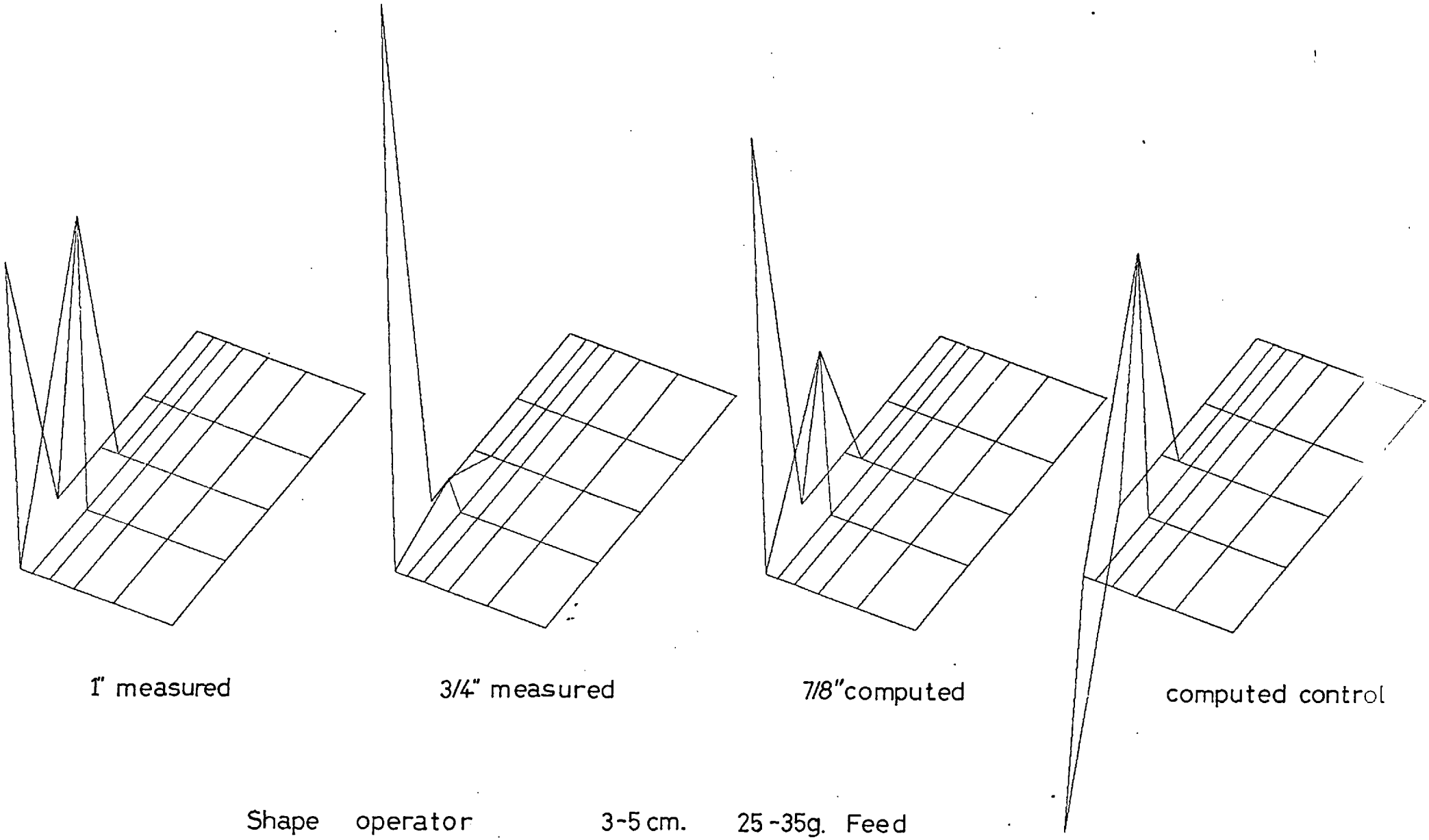
Shape operator 3-5cm. 50-70g. Feed

figure 6/23



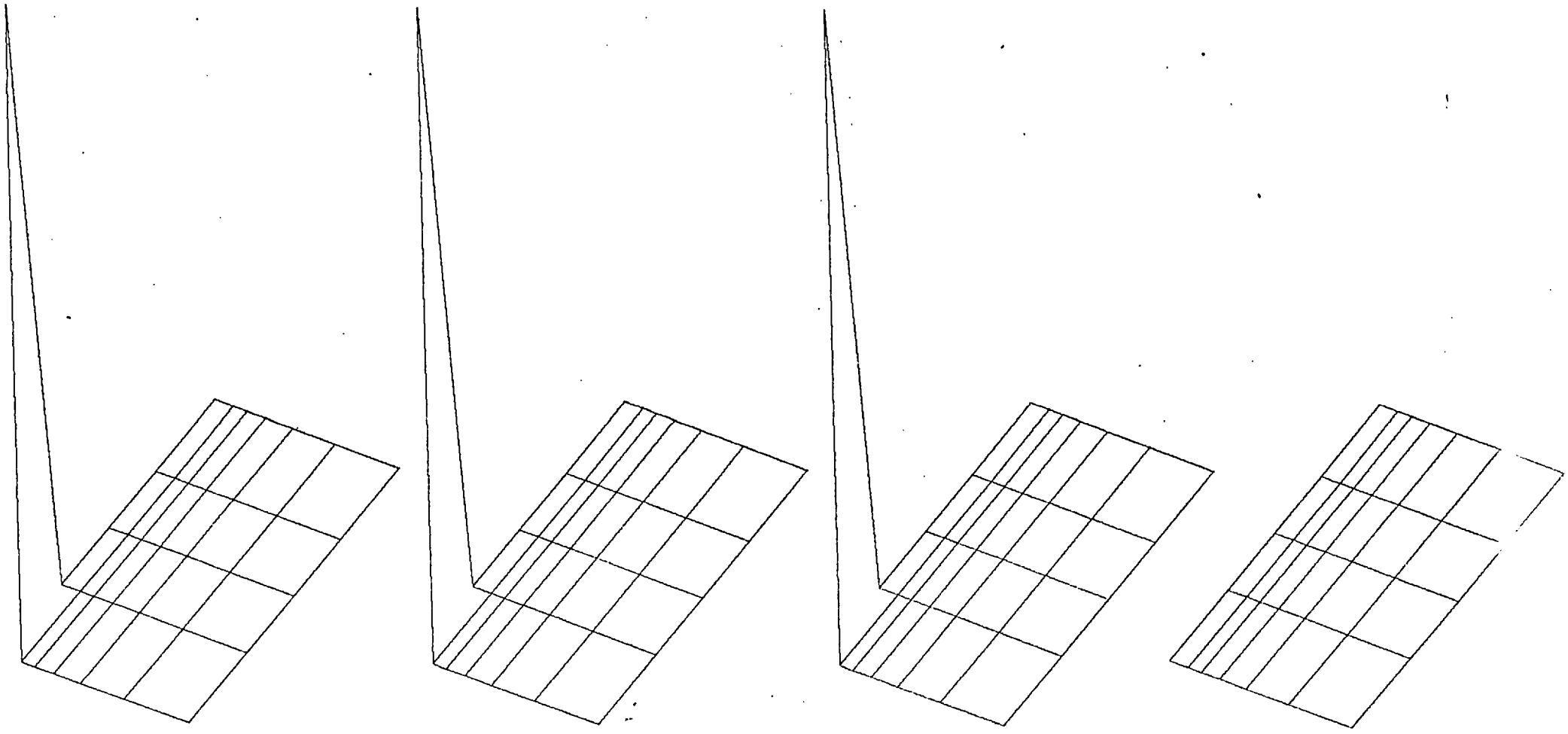
Shape operator 3-5cm. 35-50g. Feed

figure 6/24



Shape operator 3-5 cm. 25-35g. Feed

figure 6/25



Shape operator 0-3cm. 0-25g. Feed

figure 6/26

Let $\dagger$ be the particle size

let $\dagger_{Li}$ be the lower limit of size range i

let $\dagger_{ui}$ be the upper limit of size range i

Then if, and only if,

$$\dagger_{Li} < \dagger \leq \dagger_{ui}$$

the particle is said to belong to size range i.

It is convenient, in general, to consider systems in which:-

$$\dagger_{ui} \equiv \dagger_{L(i+1)}$$

$$\dagger_{L1} \equiv 0$$

$$\dagger_{un} = \infty \qquad \text{assuming n ranges}$$

That is to say, systems in which the ranges are tangent, non-overlapping and span the whole axis.

There is no requirement that the ranges should be spaced in any particular (e.g. linear) manner.

The size axis is called a primary axis.

Consider a collection of particles: this collection can be described by a set of elements W_i where W_i is the total mass of particles belonging to the ith range.

Consider the array W of elements W_i with i ranging from 1 to n. It is noted that, if A, B and C are such arrays having elements

(Continued .....)

a_i, b_i, c_i where i ranges from 1 to n and α, β and γ are scalar constants, then the following properties hold true:-

1. Addition exists and is closed

   $A + B = C$

   as $a_i + b_i = c_i$ exists and is valid for all i.

2. Addition commutes

   $B + A = A + B$

   as $a_i + b_i = b_i + a_i$ for all i.

3. Addition is associative

   $(A + B) + C = A + (B + C)$

   as $(a_i + b_i) + c_i = a_i + (b_i + c_i)$ for all i.

4. There exists a null such that

   $A + O = A$

   as $a_i + O = a_i$ for all i.

5. A negative exists such that

   $A + (-A) = O$

   as $a_i - a_i = O$ for all i.

6. Multiplication by a scalar exists and is closed

   αA exists and has form like A

   as αa_i exists for all i and αA has elements αa_i.

7. Scalar multiplication is distributive under addition of arrays

(Continued .....)

$$\alpha(A + B) = \alpha A + \alpha B$$

as $\alpha(a_i + b_i) = \alpha a_i + \alpha b_i$ for all i.

8. Scalar multiplication is distributive under addition of scalars

$$(\alpha + \beta)A = \alpha A + \beta A$$

as $(\alpha + \beta)a_i = \alpha a_i + \beta a_i$ for all i.

9. Scalar multiplication is associative under scalar multiplication

$$\alpha\beta(A) = \alpha(\beta A)$$

as $\alpha\beta(a_i) = \alpha(\beta a_i)$ for all i.

10. There exists a unit scalar such that

$$1.A = A$$

as $1.a_i = a_i$ for all i.

Thus as W, the description of the particle collection, has these ten properties, it is a vector.

Consider particle flow vectors with 4 ranges (4 range vectors are considered for convenience; no generality is lost).

If E_1, E_2, E_3, E_4 are 4 such vectors with the properties that the determinant (assuming the vectors to be row vectors)

$$\begin{vmatrix} E_1 \\ E_2 \\ E_3 \\ E_4 \end{vmatrix} \neq 0$$

(Continued .....)

then any particle flow vector W, defined as above, can be represented by the equation:

$$W = \alpha E_1 + \beta E_2 + \gamma E_3 + \theta E_4$$

Such a set of vectors E_1 is called a basis set.

Two common basis sets useful in mineral processing are:-

$E_1 = 1 \quad 0 \quad 0 \quad 0$

$E_2 = 0 \quad 1 \quad 0 \quad 0$ discrete size distribution

$E_3 = 0 \quad 0 \quad 1 \quad 0$

$E_4 = 0 \quad 0 \quad 0 \quad 1$

and

$E_1 = 1 \quad 1 \quad 1 \quad 1$

$E_2 = 1 \quad 1 \quad 1 \quad 0$ cumulative size distribution

$E_3 = 1 \quad 1 \quad 0 \quad 0$

$E_4 = 1 \quad 0 \quad 0 \quad 0$

The elements of W with respect to the first basis set are α, β, γ, θ and with respect to the second set $\alpha + \beta + \gamma + \theta$, $\alpha + \beta + \gamma$, $\alpha + \beta$, α.

Consider in more detail the properties of the first set. (It is possible to transform any vector defined, with respect to any other basis set, into a vector defined, with respect to this particular set, by means of a matrix multiplication.

It has been chosen to have the following properties:

(Continued .....)

1. It is canonical.

2. Its determinant is 1.

3. The vectors in it are orthogonal, i.e.

$E_j \, E_i = \delta_{ij}$, where δ_{ij} is the Kroenecker Delta

i.e. $\delta_{ij} = 0$ if $i \neq j$

$\delta_{ij} = 1$ if $i = j$

If the magnitude of a vector in the direction E_i is $\bar{E}_i$, a flow vector W described with respect to the first basis set (E_i) has the following elements:

$$W_j = \sum_{\text{all } i} \frac{\partial W_j}{\partial \bar{E}_i} E_i$$

as $W = \alpha E_1 + \beta E_2 + \gamma E_3 + \theta E_4$

and

$$\frac{\partial W_1}{\partial \bar{E}_1} = \alpha$$

$$\frac{\partial W_2}{\partial \bar{E}_2} = \beta$$

$$\frac{\partial W_3}{\partial \bar{E}_3} = \gamma$$

$$\frac{\partial W_4}{\partial \bar{E}_4} = \theta$$

and

$$\frac{\partial W_j}{\partial \bar{E}_i} = 0 \quad \text{for } i \neq j$$

(Continued .....)

It follows (by definition) that the vector W is contragredient with respect to the chosen basis vector set.

The basis set defines a space with axes having vector equations respectively

$\lambda \; E_1$

$\epsilon \; E_2$

$\psi \; E_3$

$\Omega \; E_4$

As the particle flow vector is a contragredient vector, with respect to the basis set of vectors, it is also a contravarient tensor in the space defined by that vector set.

If there were n ranges defined in the primary axis the particle collection is described by the tensor

$$T^n$$

in the space of the chosen basis set.

Now, in general, it is convenient mathematically to consider covarient tensors and it is possible to "Lower the index" by the use of an arbitrary covarient tensor G_{ik}

$T_i = G_{ik} T^k$ using the Einstein Convention, see Appendix 7 .

The choice of G_{ik} is arbitrary but of great significance. G_{ik} is known as the fundamental tensor and its correct choice can

(Continued .....)

greatly simplify the mathematical manipulation. It is usual for the fundamental tensor to be chosen as equal to the metric tensor, as tensor calculus is widely used in systems with metric properties. However, with the tensors being used here there is no meaningful metric property defined which leads to a simple form for G_{ik}, and so the choice of fundamental is one of convenience. For the purposes of mineral process analysis it will simplify manipulation if the pseudo-euclidean metric tensor is chosen for a fundamental tensor. This limits manipulation to linear change of bases. In fact this limitation is not serious as other changes of bases do not have any physical significance. Further, as an elementary orthogonal basis set has been chosen, the pseudo-Euclidean metric tensor is used in its canonical form, i.e.

The elements of G_{ik} of g_{ik} are

$$g_{ik} = \delta_{ik}, \text{ the Kroenecker Delta}$$

Further the converse operation G^{ik} is defined and has elements g^{ik} where

$$g^{ik} = \delta^{ik}$$

also

$$G^{ik} G_{ji} = \delta^{k}_{j}$$

The elements of Tn (a covarient tensor) are therefore identical to those of T^n the contravarient to which Tn corresponds.

To summarise:

T^n is a contravarient tensor in a pseudo-Euclidean space which

(Continued .....)

describes a particle collection. It can be changed to a covarient tensor by multiplying by G_{ik}, the fundamental tensor, which was chosen so that the elements of T_n are identical to those of T^n.

The pseudo-Euclidean space of T_n is called the secondary space.

Up to this point the method discussed has been restricted to describing particles only by their size: it will now be generalised to consider particles defined by as many variables as are necessary.

Let a particle be uniquely described by v variables. It can then be described by defining a point in a v dimensional primary space: each of the v properties defines a primary axis in the space. As before, it is not generally possible to define precisely every particle under consideration. Each primary axis is therefore divided into a set of a_i ranges. The v dimensional primary space is therefore divided into p hyper-rectangular apertures where:-

$$p = \prod_{i=1}^{v} a_i$$

Let the properties of a given particle be $\gamma_1 \ldots\ldots \gamma_v$ it is said to belong to aperture $Q_{abc} \ldots\ldots \ell$ if, and only if,

$$L_{ai} < \gamma_i \leqslant U_{ai}$$

$$L_{qi} < \gamma_i \leqslant U_{qi}$$

$$I_{\ell v} < \gamma_v \leqslant U_{ev}$$

(Continued .....)

Where L_{qi} is the lower bound of the qth range of the ith primary axis, and U_{qi} is the upper bound of the qth range of the ith primary axis.

In general, as before, systems will be considered in which:

$$L_{1n} \equiv 0$$

$$L_{gn} \equiv U_{(g-1)n}$$

$$L_{mn} \equiv \infty \qquad \text{if there are m ranges in the nth primary axis.}$$

That is to say, systems in which the apertures are such that each particle belongs to one and only one aperture.

Consider a collection of particles: they can be divided into p categories. The collection can then be described by an array: each element of the array is the total mass of the particles belonging to the respective aperture.

It can be shown that this array obeys the axioms used above to show that the size array was a vector. Furthermore, with respect to an appropriate vector set defined by

$$E_{ijk} \ldots\ldots v = \delta_{ijk} \ldots\ldots v,$$ where $\delta_{ijk} \ldots\ldots v$ is the generalised Kroenecka Delta,

this vector is contragredient.

It is therefore, by a similar process of reasoning to that above, a contravarient tensor in the space defined by the basis set. As before the pseudo-Euclidean metric tensor is chosen as fundamental tensor and the indices lowered.

(Continued .....)

For ease of illustration, a three dimensional primary space will be considered, although all the notation developed below is possible in more complex primary spaces. Having lowered the indices the particle collection tensor is

$$T_{ijk}$$

As, in general, flows of particles are of prime importance, T_{ijk} will normally refer to the flow of particles. This is also a tensor as the operation of conversion from a static collection to a flow of particles is simply a scalar multiplication.

6.7.1 Reduction of Primary Axes (or contraction)

It is often necessary to reduce the number of primary axes defining a flow. For example, a particle flow is described in a size-assay-hardness primary space and its size distribution is required.

The following notation will be used:

If T_{ijk} is the particle flow tensor and its elements are w_{pqr}, then

T_{ij*} is the tensor describing the flow in the ij primary space only and its elements are W_{pq*} where

$$W_{pq*} = \sum_{r=1}^{k} W_{pgr}$$

Similarly for T_{i*k} and T_{*jk}

(Continued .....)

T_{i**} is the tensor describing the flow in the i primary space only, and its elements are W_{p**} where

$$W_{p**} = \sum_{q=1}^{j} W_{pq*}$$

or alternatively

$$W_{p**} = \sum_{q=1}^{j} \sum_{r=1}^{k} W_{pqr}$$

Similarly for T_{*j*} and T_{**k}

Lastly the total mass flow W, or T_{***}

$$W = T_{***} = \sum_{p=1}^{i} W_{p**}$$

$$= \sum_{p=1}^{i} \sum_{q=1}^{j} W_{pq*}$$

$$= \sum_{p=1}^{i} \sum_{q=1}^{j} \sum_{r=1}^{k} W_{pqr}$$

6.7.2 The Process

Consider a process which has an input flow of particles and an output flow of particles. Let the process be at steady state and all the controls fixed at some set point.

Let F_{ijk} be the tensor describing the feed particle flow and P_{qrs} be the tensor describing the product particle flow.

Then as all other variables have been held constant:

$$P_{qrs} = f(F_{ijk})$$

(Continued .....)

Assume the process to be piecewise linear then:

$$P_{qrs} = E\, F_{ijk}$$

where E is a linear operator. Each term of P_{qrs} is a linear combination of all the terms in F_{ijk}. E therefore has qrsijk terms.

Consider the operator

$$E^{ijk}_{qrs}$$

defined such that for small changes in flow

$$P_{qrs} = E^{ijk}_{qrs}\, F_{ijk}$$

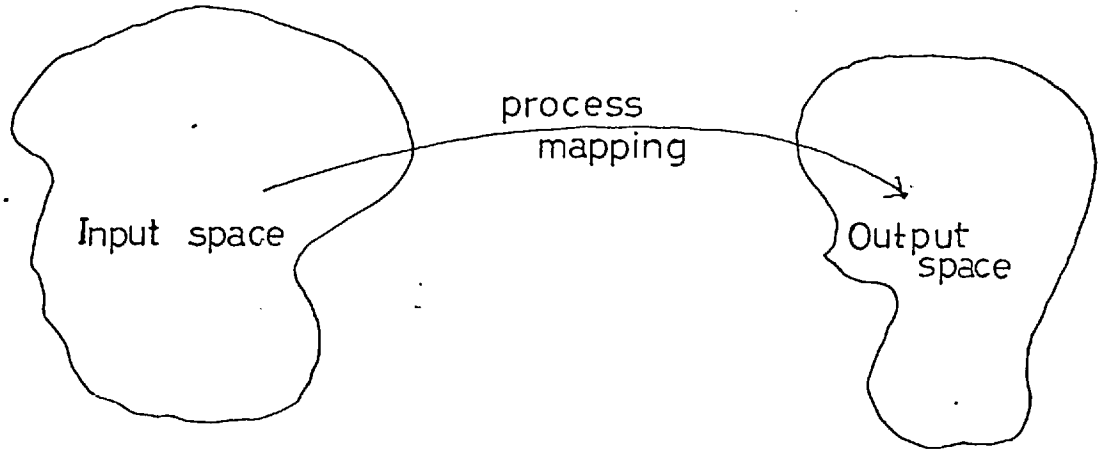
The operator has q r s i j k terms and it is linear. It follows from the quotient law of tensors that E^{ijk}_{qrs} is a tensor of covariance qrs and contravariance ijk. Therefore the process description becomes:

$$P_{qrs} = E^{ijk}_{qrs}\, F_{ijk}$$ (remembering the Einstein Convention).

The process tensor can be considered to be the mapping from a point in the input secondary space to a point in the output secondary space, see figure 6/27. The input and output spaces may be different as in Figure 6/27A, or can be the same space as in Figure 6/27B. In Figure 6/28 the relationship between particles spaces for a rod mill is shown.

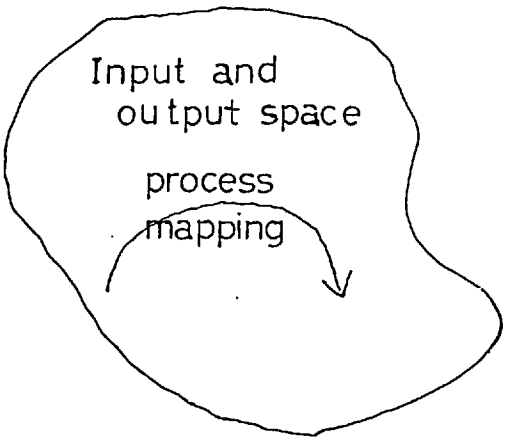
The mapping from input to output is a one-to-one mapping, but the reverse mapping from output to input can be a one-to-many

(Continued .....)



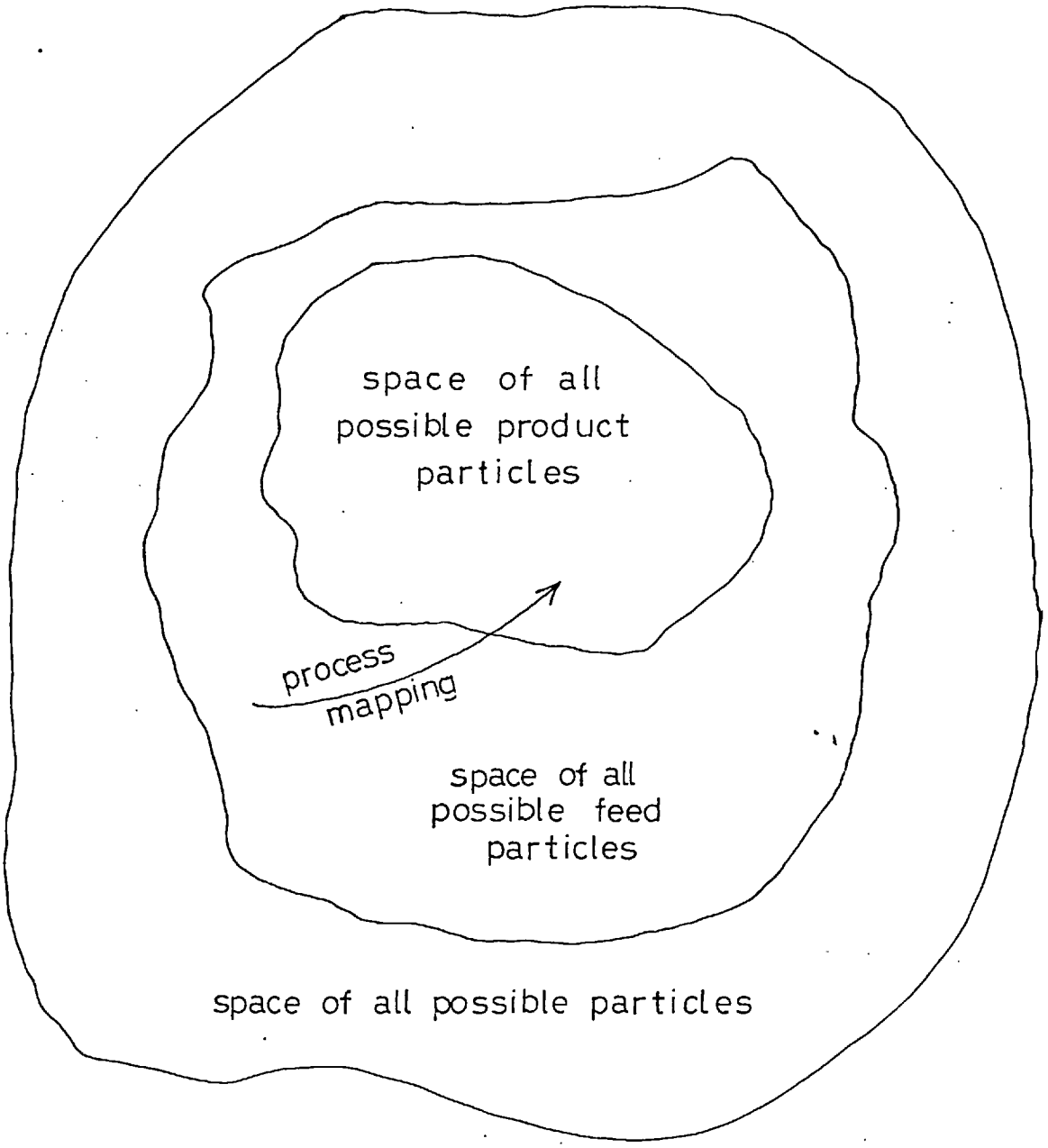
A) different input and output spaces

B) identical input and output spaces



Process Topology

figure 6/27



Topological diagram of a rod mill.

mapping, i.e. the process is not necessarily reciprocal, or, in mineral processing terms, the feed properties cannot necessarily be determined from the product properties.

6.7.3 Control

Now in general the process will have controls (motor speeds, flow rates, etc.). These can also be described by a tensor C^v. This has v elements which describe the current states of the v controls.

Now the process operator will change with control state and thus:

$$E^{ijk}_{qrs} = f(C^v)$$

Consider the elements of E^{ijk}_{qrs} which are e^{ijk}_{qrs}. If c^a are the elements of C^v then by applying a Taylor expansion:

$$e^{ijk}_{qrs} = h^{ijk}_{qrs} + \sum_{a=1}^{v} \frac{\partial e^{ijk}_{qrs}}{\partial c^a} \delta c^a + \ldots\ldots$$

Where h^{ijk}_{qrs} are the elements of the plant tensor at the control set point (i.e. $c^a = 0$ for $a = 1 \rightarrow v$) and δc^a are the excursions of the controls from their set points. Assuming linearity about the set point (arbitrarily shifted so that at the set point $C^v = 0$) then

$$E^{ijk}_{qrs} = H^{ijk}_{qrs} + X^{ijk}_{qrsv} C^v$$

(Continued .....)

From the quotient law X^{ijk}_{qrsv} is a tensor, and is contravarient in ijk and covarient in qrsv. It is covarient in v as it has elements of the form:

$$\frac{\partial e^{ijk}_{qrs}}{\partial C^a}$$

Therefore the piecewise linear plant description at steady state is:

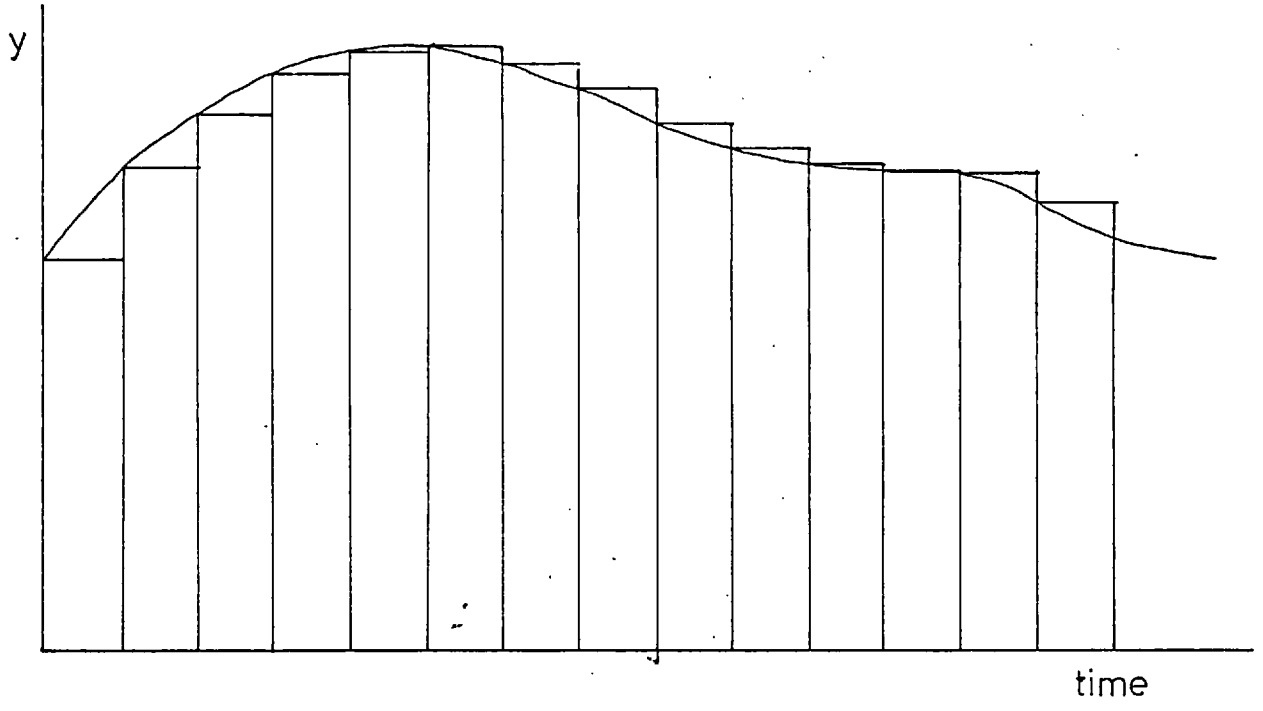
$$P_{qrs} = \left(H^{ijk}_{qrs} + X^{ijk}_{qrsv} C^v\right) F_{ijk}$$

6.7.4 Plant Dynamics

The real plant is rarely in steady state operation. As mining proceeds the feed F_{ijk} will vary in properties as geological structures are never uniform over the entire orebody. In order to optimise plant performance, the controls C^v will be changed to suit the changes in F_{ijk}. The dynamics of the plant will be critical in determining whether any proposed control algorithm will be stable. As the control and feed tensors interact to form the product tensor, the classical methods of phase space, frequency domain analysis or state vector analysis are inapplicable except in special cases. The interactive process dynamics can be described by a weighting function technique suitably modified. Before adding this concept to the tensor analysis the weighting function technique will be reviewed.

Any signal can be considered to be made up froma series of unit impulse functions suitably delayed - see Figure 6/29.

(Continued .....)



Signal as a sum of unit impulses

figure 6/29

If f(t) is the input signal and w(τ) is the unit impulse response of the process (which is assumed linear) and y(t) is the output of the process then:

$$y(t) = \int_{-\infty}^{t} f(t)\, w\,(t - \tau)\, \delta\tau$$

or, in summation form counting time increments Δt backwards in time from t

$$y(t) = \sum_{i=1}^{i=n} f(ti)\, w(t - t_i)\, \Delta t$$

where $N\Delta T$ is sufficiently large for $w(N\Delta T) \rightarrow 0$. This is a usual case in mineral processing as mass is conserved.

Using this method, for the tensor form, the following equation is obtained:

$$P_{qrs}\ (\text{time} = 0) = \left(H^{ijkt}_{qrs} + X^{ijkt}_{qrsvt}\, C^{vt}\right) F_{ijkt}$$

(remembering the Einstein Convention)

To describe the system at all points in time, a time-shift notation is used:

$X(t + \tau)$ = value of X at t shifted by τ increments back in time.

then

$$P_{qrs\tau} = \left(H^{ijkt}_{qrs} + X^{ijkt}_{qrsvt}\, C^{v(t+\tau)}\right) F_{ijk\,(t+\tau)}$$

and this equation describes the linearized plant completely.

(Continued .....)

6.7.5 Non-Linearity

Now it may occur that H and X are not independent of F, in which case further elements may be added to C which are functions of the elements of F, and then all continuous functions of F, despite non linearity, can be treated. As the control variables are, generally, incremental in form, it is considered that the linear relationship will suffice for the interaction of control and process provided that the relationship

$$E = f(C)$$

is analytic in the region under consideration.

The formal statement of notation is now complete. Some of the possible consequences and special cases will now be reviewed.

6.7.6 Constraint

Because the processes concerned are governed by physical laws the complexity of description can be reduced by imposing physical constraints: in tensor terms, the study of invariants. These constraints will be discussed for flow tensors using the simple basis set. The choice of basis set is important as the nature of the constraint is dependent upon the choice of fundamental tensor.

Mineral processes can be divided into two principle classes:

a) Sorting devices

b) Physical processing devices.

Any process which apparently has both these functions can be described by a combination of these elements.

(Continued .....)

Sorting Devices

These devices do not change the physical properties of the particles: they sort the input flow into two streams according to the particle properties.

Examples

Classifiers

Flotation Cells

Shaking Tables

Magnetic Separators

Electrostatic Separators

Dense Medium Separators

If X is the tensor describing the relationship between the input flow and one output flow, then I-X is the tensor describing the relationship between the input flow and the other output flow.

As no particles can change apertures the input and output spaces are identical and the transform tensor X is hyperdiagonal; that is, if x^i_j is an element of X, then

$x^i_j = a^i_j \delta_{ij}$, where δ_{ij} is the Kroenecka Delta

and a^i_j is a coefficient constant subject to the constraint

$$0 \geqslant a^i_j \geqslant 1$$

(Continued .....)

Physical Processing Devices

These devices change the physical properties of particles; they only have one output.

Examples

Crushers

Grinding Mills

Chemical Processes

Smelters

The universal constraint on these devices is the conservation of mass.

If x_{ijk}^{pqr} is an element of the process tensor describing the relation between input and output flows then

$$x_{***}^{pqr} \equiv 1 \quad \text{for all } p, q, r$$

using the convention defined earlier.

Also $x_{***}^{***} = m$

if the input space has m apertures.

In all plant steady state operators every element x_{ijk}^{pqr} must satisfy the relation

$$0 \leqslant x_{ijk}^{pqr} \leqslant 1$$

In certain processes more constraint is applied. For example, in crushers, particles never get larger, and thus if size is one of

(Continued .....)

the primary axes then the process tensor is hyper-triangular.

6.8 Addition of Flows

Addition, component by component, is only defined for tensors defined with respect to the same basis set. In general it will be possible to arrange for this to be true.

Occasionally it will be found that the space of one tensor is a sub space of the other, in which case the spaces can be made identical by the addition of rows of zeros in appropriate places.

Example

Flow one is defined in the following size apertures

0-1" 1-2" 2-3" 3-4" 4-5" 5-6"

It is fed to a crusher the product sized and all particles greater than 4" returned for recrushing. Flow two (the recirculating load) is therefore defined in apertures

4-5" 5-6"

It is therefore defined in a sub space of the space of flow 1 if flow 1 has tensor

(a b c d e f)

and flow two

(g h)

It is possible to add these; first expand flow two to

(0 0 0 0 g h)

and add component by component

(a b c d e+g f+h)

(Continued .....)

Great care must be taken when dealing with % flows, these must be returned to mass flows, or the answers will give incorrect results.

6.9 Simplification in the Time Domain

Often in considering process dynamics only changes in either control or feed properties are of interest, in which case the equations can be simplified.

Consider the system:

$$P_{qrs\tau} = \left(H^{ijkt}_{qrs} + X^{ijkt}_{qrsvt} C^{v(t+\tau)} \right) F_{ijk(t+\tau)}$$

If the control state is fixed for all time then the equation reduces to:

$$P_{qrs\tau} = E^{ijkt}_{qrs} F_{ijk(t+\tau)}$$

or if the feed tensor is fixed for all time the system reduces to:

$$P_{qrs\tau} = Y_{qrs\Psi} + Z_{qrsvt} C^{v(t+\tau)}$$

where $Y_{qrs\Psi}$ is constant over all Ψ

Note however that E is a function of C
and Y and Z are functions of F

With either of these simplifications the system can be described by various dynamic systems:

$$P_{qrs(jw)} = E^{ijk}_{qrs(jw)} F_{ijk(jw)} \qquad \text{(Fourier analysis)}$$

$$P_{qrs(p)} = E^{ijk}_{qrs(p)} F_{ijk(p)} \qquad \text{(Laplace transform)}$$

These operators may only be used in the cases C = constant or F = constant. When both C and F are allowed to vary simultaneously

(Continued .....)

the analysis is essentially non-linear. This is a major reason for the failure of classical set point control in mineral processing.

6.10 Primary and Secondary Spaces and the Basis Set

The primary space has axes, each of which describe the value of some parameter about a particle. A collection of particles could be represented by a probability density function in the primary space. However the mathematical description of such a probability function would be extremely complex. The tensor reduces a continuous probability density function to a set of discrete probabilities; each probability describing the quantity of matter to be found in a given area of the primary space. Each region of the primary space therefore gives rise to a separate axis of the secondary space. Every increase in descriptive accuracy gives rise to further axes in the secondary space.

The original derivation of the aperture concept divided the axes into ranges. This gave rise to hyper-rectangular apertures. Figure 6/30 shows an example in a two dimensional primary space. There is no mathematical necessity for ranges to be rectangular, any shape can be used, e.g. Figure 6/31. The only mathematical requirement imposed on a set of apertures is that it covers sufficient of the primary space that every particle considered belongs to an aperture. If a canonical basis set is desired then apertures may not overlap.

The simplest basis set below has been used so far:

(Continued .....)

$$\begin{pmatrix} 1 & 0 & 0 & 0 \\ 0 & 1 & 0 & 0 \\ 0 & 0 & 1 & 0 \\ 0 & 0 & 0 & 1 \end{pmatrix}$$

Equally the set

$$\begin{pmatrix} 1 & 1 & 1 & 1 \\ 1 & 1 & 1 & 0 \\ 1 & 1 & 0 & 0 \\ 1 & 0 & 0 & 0 \end{pmatrix}$$

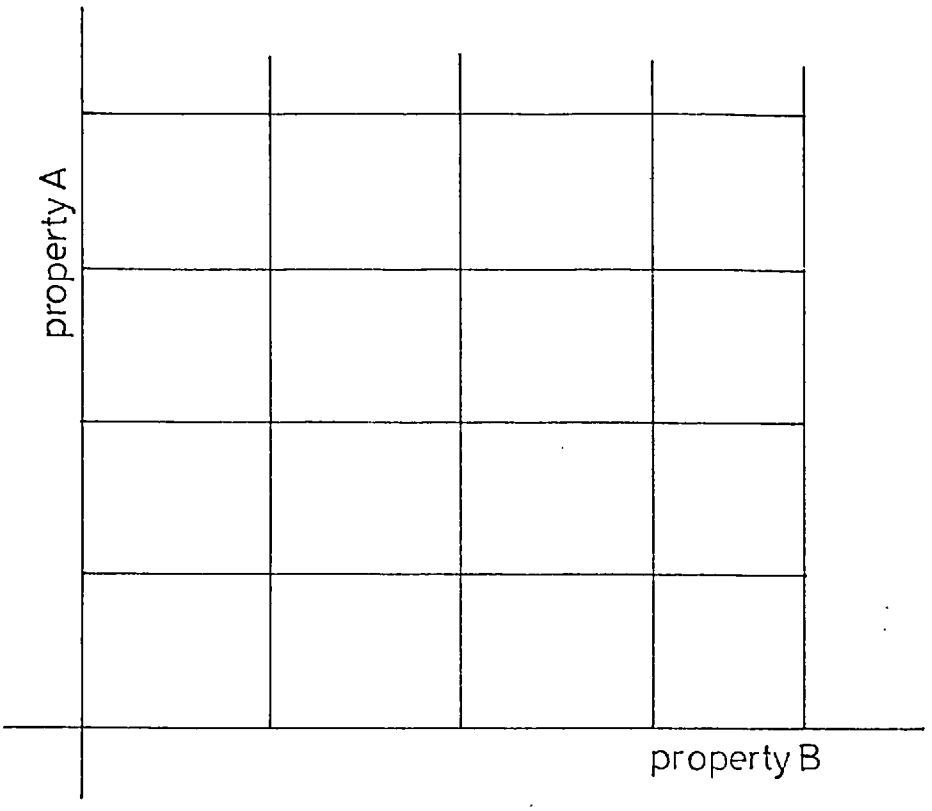
could have been chosen.

In order to convert from the second basis set to the first, the flow tensor is post-multiplied by a linear rotation tensor

$$\begin{pmatrix} 0 & 0 & 0 & 1 \\ 0 & 0 & 1 & -1 \\ 0 & 1 & -1 & 0 \\ 1 & -1 & 0 & 0 \end{pmatrix}$$

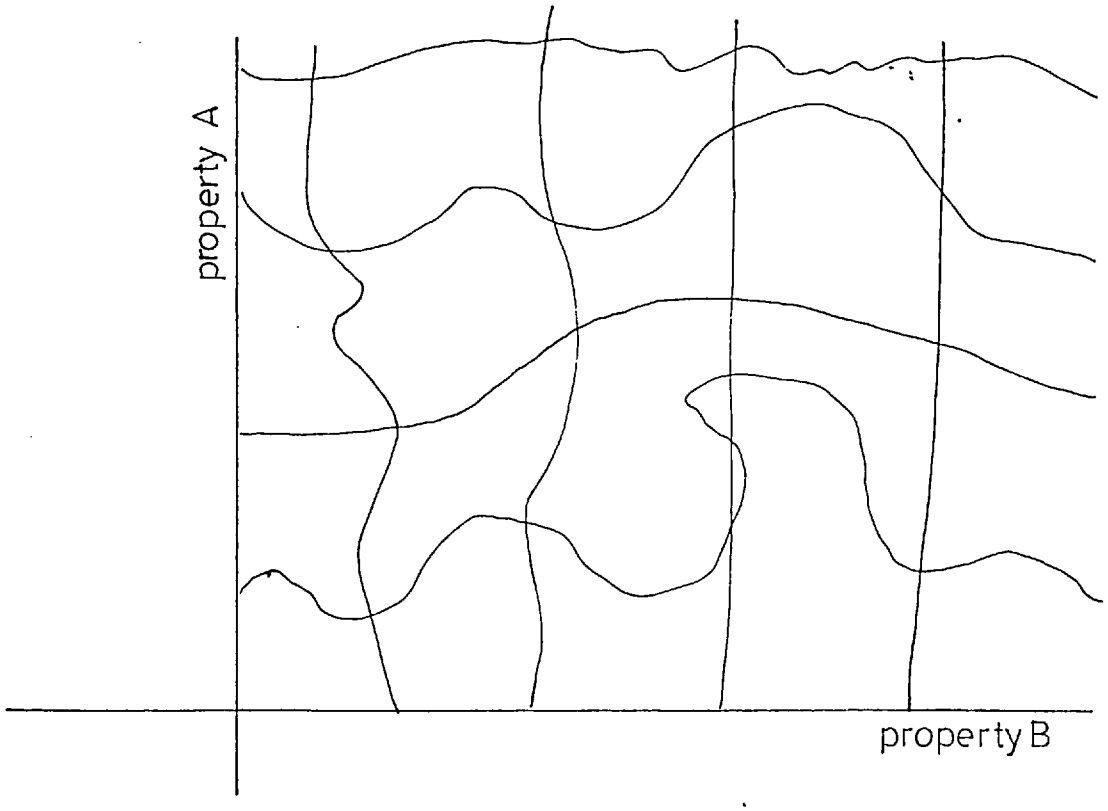
It is possible to convert any flow tensor, defined with respect to any basis set which can be described by a linear function of a second basis set, to a tensor defined with respect to a second basis set. However it is not possible to compute exact transforms for changing the apertures of a primary space in any way except to those aperture sets which have common boundaries with the original set. Approximate transforms can be made if, and only if, the distribution of particles within the apertures can be assumed, or is known.

(Continued .....)



Rectangular aperture set

figure 6/30



Irregular aperture set

figure 6/31

6.11 Control of the Incompletely Observed Process

Consider a particle flow whose properties are known to vary in a two dimensional primary space. Let only one of these primary axes be observable. The available knowledge is therefore:

$$F_{*r}$$

$$P_{*j}$$

$$C^{v}$$

By blender policy, the variations of F_{*r} in the $*$ axis are constrained to be slow.

By observing the variations of F_{*r}, perturbing C^{v}, and observing the effect on P_{*j}, it is possible to derive a real time model of the tensors:

$$\overset{*}{H}{}^{j}_{r} \quad \text{and} \quad \overset{*}{X}{}^{j}_{rs}$$

where $P_{*j} = \left(\overset{*}{H}{}^{j}_{r} + \overset{*}{X}{}^{j}_{rv}\, C^{v}\right) F_{*r}$

note $\overset{*}{H}{}^{j}_{r} \neq H^{*j}_{*r}$

$$\overset{*}{X}{}^{j}_{rv} \neq X^{*j}_{*rv}$$

If this is done at successive points in time it is possible to extrapolate and predict the approximate value of these tensors at the next point in time

i.e. $\overset{*}{X}{}^{j}_{rv}(n+1) = f\left(\overset{*}{X}{}^{j}_{rv}(n), \quad \overset{*}{X}{}^{j}_{rv}(n-1) \ldots\ldots\right)$

where f is a suitable extrapolation function.

(Continued .....)

Having derived predictions of the tensors, some control state is chosen to maximise the desired goal function, i.e. some C^v is chosen such that

$$\mathcal{Z}(C, X, F, H, P) \text{ is maximised}$$

where $\mathcal{Z}$ is a goal function.

This optimal control scheme is a short term feed-forward coupled with long term feed-back system.

It is short term feed-forward because control action is taken on the plant tensor predicted at the next time increment. It is long term feed-back because the prediction is gradually modified by feed-back from the plant.

6.12 A Tensor Approach to the Unit Process

The tensor method for describing the input-output analysis of both unit and multiple processes has been described. Whilst this method is very powerful for the design of systems, the mineral process engineer also needs analytical tools to design the actual processes themselves.

Design of plant involves two problems: firstly the design of the internal process itself, and secondly the design of the hardware needed to actuate the process. The latter is a straightforward matter of design and reliability engineering and can be accomplished using well-established techniques. The design of the internal process itself is more complex, and advanced design techniques

(Continued .....)

similar to those used for the straightforward engineering would be of great value to the designer.

There are two approaches available: firstly empirical or design by past experience, and secondly design from first principles. Two tensor techniques will be developed below, one for each type of design.

6.12.1 Design by Empirical Methods

Let the design criteria of a machine be defined by n variables.

Let D^n be a tensor whose elements are the values of the n variables.

The performance tensors M_p^f of earlier available designs are measured and values estimated for the tensor S_{pn}^f, defined such that

$$M_p^f = S_{pn}^f D^n$$

for all the available M_p^f.

This tensor S_{pn}^f describes the sensitivity of the machine performance to the design criteria.

The designer then chooses some goal function $\mathcal{Z}$ for M_p^f and calculates a value for D^n such that

$$\mathcal{Z}\left(M_p^f\right) \text{ is maximised}$$

The value of D^n forms the basis for the new machine design. This method is simply the tensor equivalent of a factorial experiment.

(Continued .....)

6.12.2 Design by First Principles

Consider a small volume $\delta x \ \delta y \ \delta z$ in a machine. This volume may be located by reference to the machine frame or by reference to some control volume in the particle flow. Let the particles in this volume be described by the tensor A(xyz) where x y z identify the particular volume under consideration.

Consider the function

$$\lim_{\delta x \ \delta y \ \delta z \to 0} \frac{A(xyz)}{\delta x \ \delta y \ \delta z} = T(xyz)$$

This is also a tensor and T(xyz) describes the particle probability density throughout the range of x, y, z, of the machine.

Consider the particle probability tensor Tabc at a fixed point in the flow or the machine.

It is noted that:

$$\frac{d\ Tabc}{dt} = f(Tabc) + g(Txyz),$$

that is to say, that the change of particle probability tensor at a fixed point with time depends on the rate of change of particle properties at that point by processing (comminution agglomeration, etc), and on the flow of particles to and from that fixed point.

For a real problem the functions f and g can be defined. For example, in a dense medium separation plant the function f will be zero as particles do not change properties, and the function g will be

(Continued .....)

a tensor whose elements will depend on the values of density throughout the machine. The density can be calculated at any point from the values of Txyz and the definition of the ranges of Txyz. The whole process can then be simulated and the performance of a particular design evaluated.

6.13 Examples

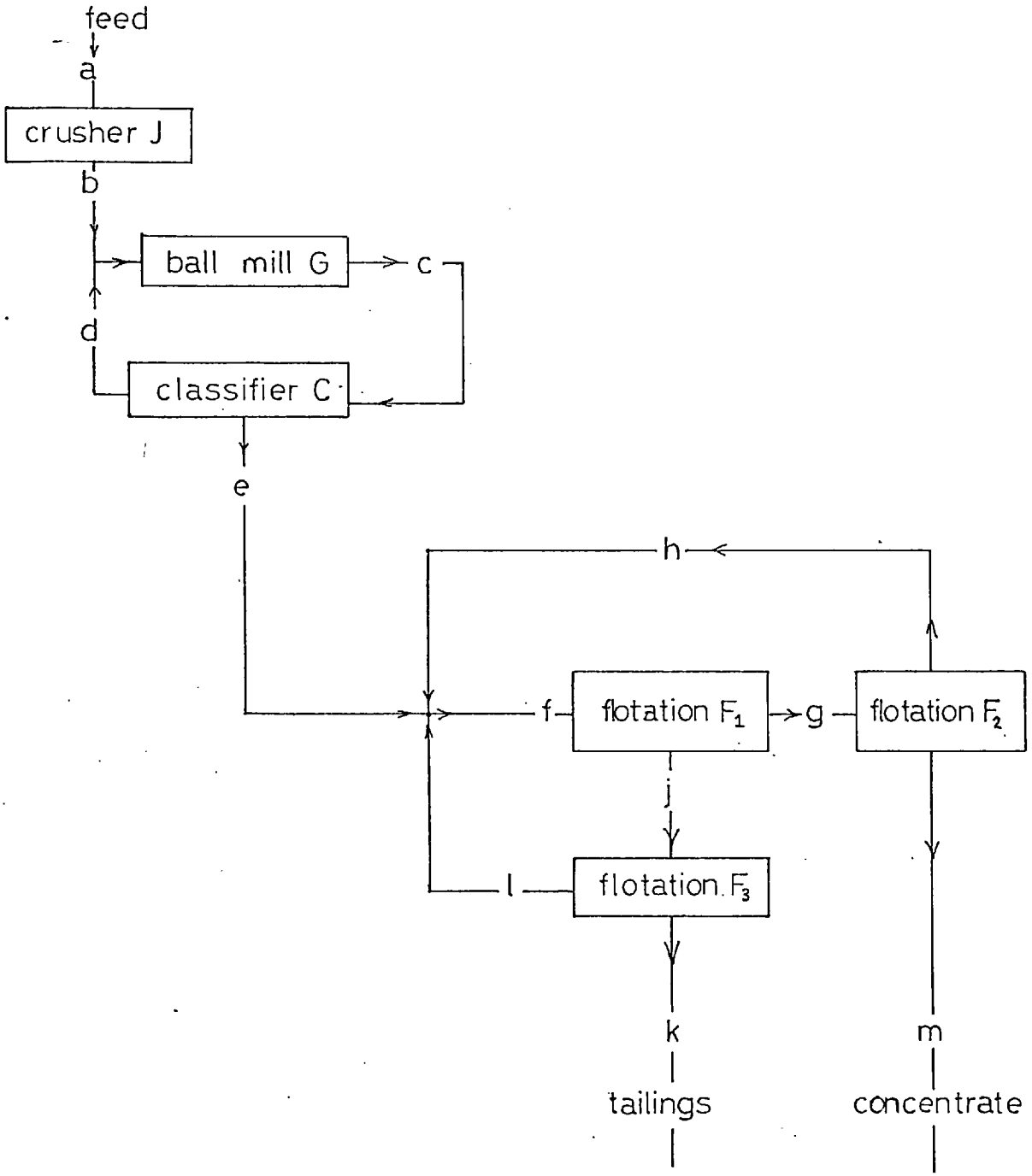
Some further examples of the technique and its use will be given.

6.13.1 Complete Plant Analysis

Consider the plant with flow sheet as in Figure 6/32. A size assay primary space is assumed, all controls are fixed, and the plant is at steady state. Sub and superscripts are dropped for ease. The following equations are written: lower case letters refer to particle flow tensors, upper case to process tensors.

1.	b	=	Ja	crushing
2.	c	=	G(b + d)	grinding
3.	d	=	Cc	classifier
4.	e	=	c-d	classifier
5.	g	=	$F_1 f$	flotation cell 1
6.	j	=	f-g	flotation cell 1
7.	m	=	$F_2 g$	flotation cell 2
8.	h	=	g-m	flotation cell 2
9.	l	=	$F_3 j$	flotation cell 3
10.	k	=	j-l	flotation cell 3

(Continued .....)



Plant flow sheet

11. $f = e + l + h$, middlings return

from 1 and 2

12. $c = GJa + Gd$

from 3 and 12

$c = GJa + GCc$

13. Therefore

$c = (I - GC)^{-1}GJa$

from 3 and 4

$e = c - Cc$

14. $e = (I - C)c$

from 13 and 14

15. $e = (I - C)(I - GC)^{-1}GJa$

let $(I - C)(I - GC)^{-1}G = B$

16. $e = Ba$

from 6, 9 and 10 eliminate j

17. $l = F_3 f - F_3 g$

18. $k = f - g - l$

from 5, 7, 8, 17 and 18 eliminate g

19. $m = F_2 F_1 f$

20. $h = F_1 f - m$

21. $l = F_3 f - F_3 F_1 f$

22. $k = f - F_1 f - l$

from 19 and 20 eliminate m

23. $h = F_1 f - F_2 F_1 f$

from 11, 21 and 22 eliminate l

24. $f = e + h + F_3 (I - F_1)f$

25. $k = (I - F_1)f - F_3 (I - F_1)f$

from 23 and 24 eliminate h

(Continued .....)

$$f = e + F_3 (I - F_1)f + F_1 f - F_2 F_1 f$$

$$f = e + (F_3 - F_3 F_1 + F_1 - F_2 F_1)f$$

26. $$f = (I - F_3 + F_3 F_1 - F_1 + F_2 F_1)^{-1} e$$

from 25

$$k = (I - F_1 - F_3 + F_3 F_1)f$$

hence

27. $$k = (I - F_1 - F_3 + F_3 F_1)(I - F_3 + F_3 F_1 - F_1 + F_2 F_1)^{-1} e$$

put $$A = (I - F_1 - F_3 - F_3 F_1)$$

$$k = A(A + F_2 F_1)^{-1} e$$

but $$e = BA$$

therefore

$$k = A(A + F_2 F_1)^{-1} Ba$$

where $$A = I - F_1 - F_3 + F_3 F_1$$

and $$B = (I - C)(I - GC)^{-1} G$$

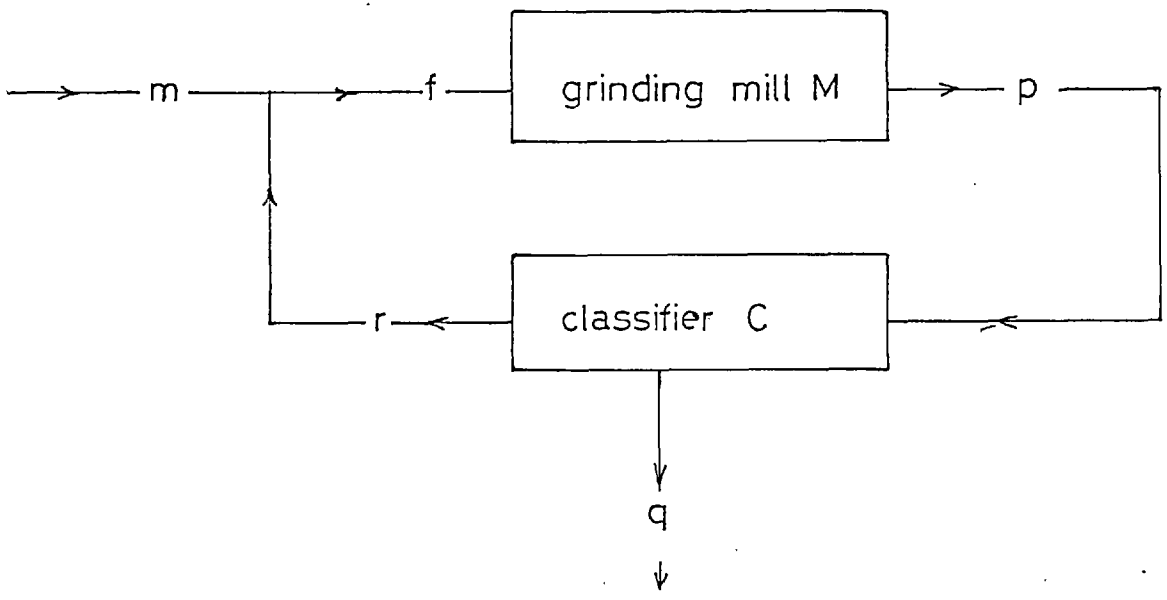
and thus the concentrate flow can be calculated from a knowledge of the process tensors and the feed tensor. If the tensors are defined in the size-array primary space the recoveries and size distributions can be calculated.

It should be noted that if the tensor $(I - GC)$ is singular the grinding circuit will be unstable. Similarly if the tensor $(A + F_2 F_1)$ is singular the flotation circuit is unstable.

6.13.2 Dynamics of Grinding

Consider the system of Figure 6/33. The following tensor equations hold:-

(Continued .....)



Grinding circuit

figure 6/33

1) $f = m + r$

2) $p = Mf$

3) $r = Cp$

4) $q = (I-C)p$

from 1 and 2

5) $p = M(m + r)$

from 5 and 3

$$p = M(m + Cp)$$

$$(I - MC)p = Mm$$

6) $p = (I - MC)^{-1}Mm$

from 4 and 6

$$q = (I - C)(I - MC)^{-1}Mm$$

It is assumed that controls are held constant. A simplified dynamic solution can be used.

It is postulated that the elements of M are of the form:-

$$\frac{m_{ij}}{1 + t_{ij}D}$$

where D is the differential operator $^{d}/_{dt}$. That is to say that the mill is a first order time-constant process.

The equations were solved numerically by computer. Mill and classifier tensors were derived from Callcott's paper and their values given in table 6/4 and 6/5. The time constants t_{ij} were all assumed identical. The results were plotted in terms of the time constant. Nine size ranges were used and Figures 6/34 - 6/42 show the effects of step changes in a single size fraction of the feed. Graph 6/43 shows the effects of a step change in feed rate for a feed of size distribution given by Callcott- Table 6/6.

(Continued .....)

Table 6/4

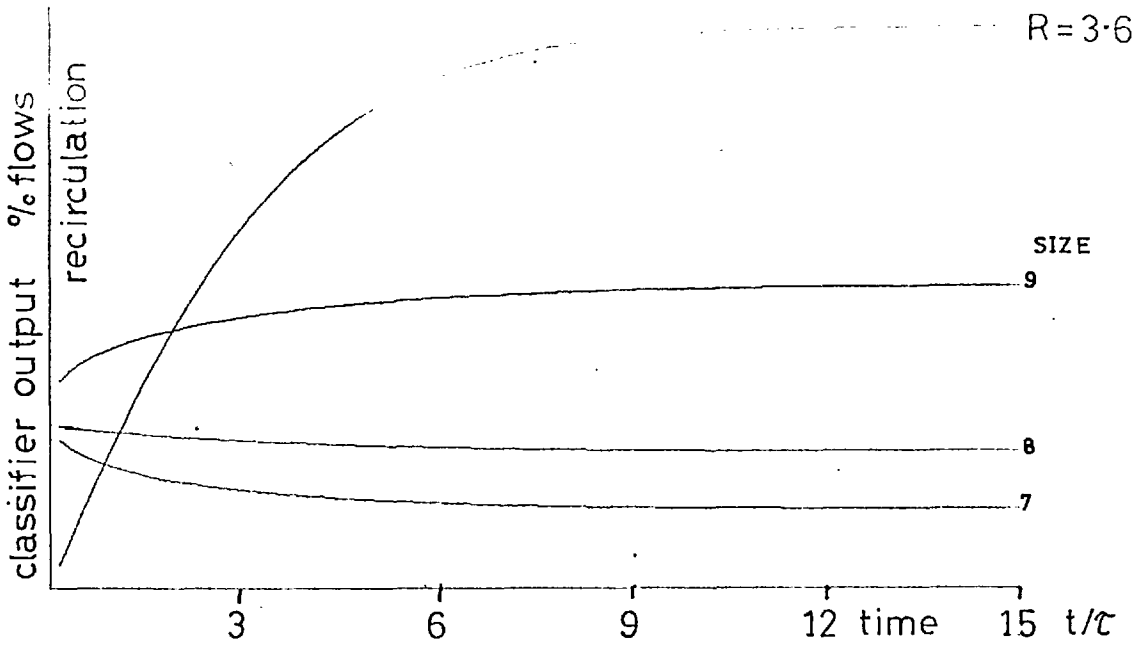
Mill Performance Tensor

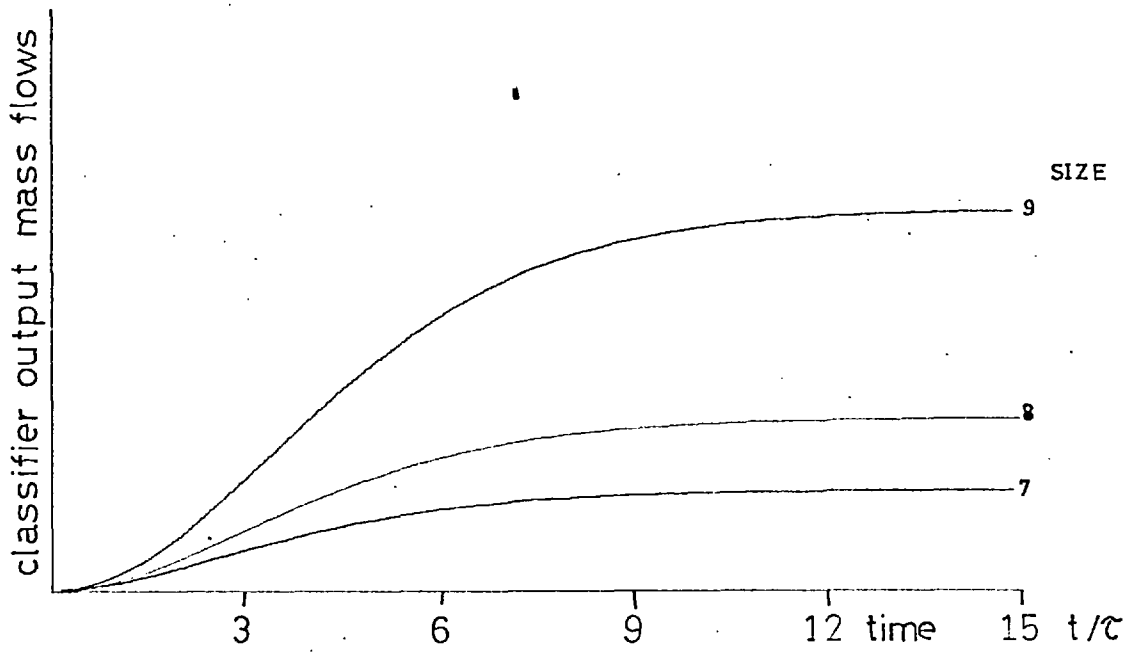
Row \ Column	1	2	3	4	5	6	7	8	9
1	.20	0	0	0	0	0	0	0	0
2	.33	.20	0	0	0	0	0	0	0
3	.21	.33	.20	0	0	0	0	0	0
4	.12	.21	.33	.20	0	0	0	0	0
5	.07	.12	.21	.33	.20	0	0	0	0
6	.03	.07	.12	.21	.33	.20	0	0	0
7	.02	.03	.07	.12	.21	.33	.20	0	0
8	.01	.02	.03	.07	.12	.21	.33	.20	0
9	.01	.02	.04	.07	.14	.26	.47	.80	1.00

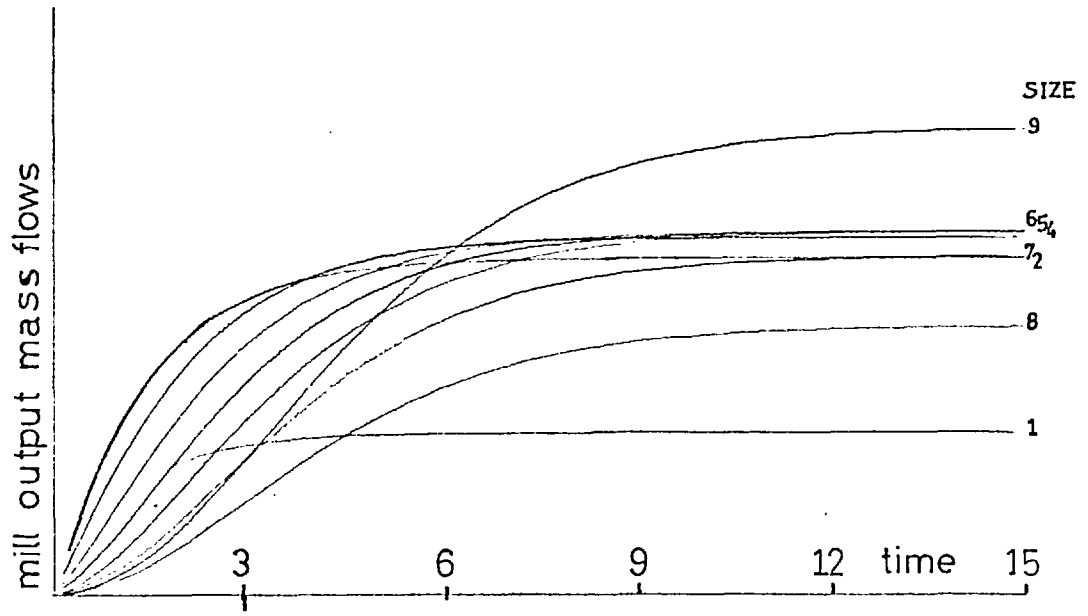
Table 6/5

Classifier Performance Tensor

Row \ Column	1	2	3	4	5	6	7	8	9
Value	1	1	1	1	1	1	.7	.35	.175

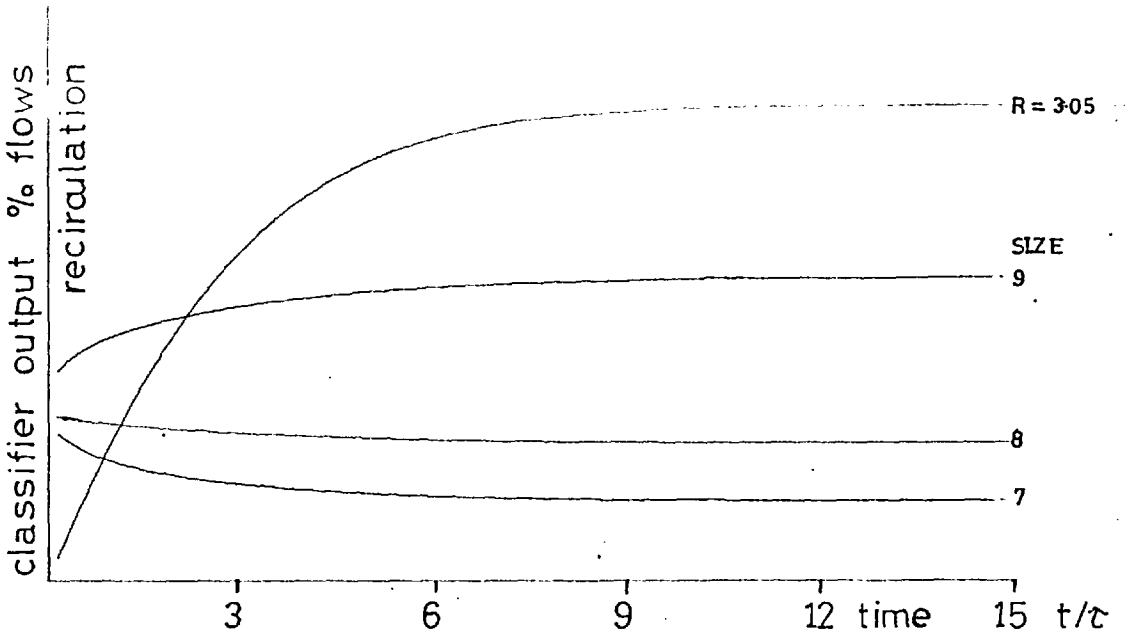


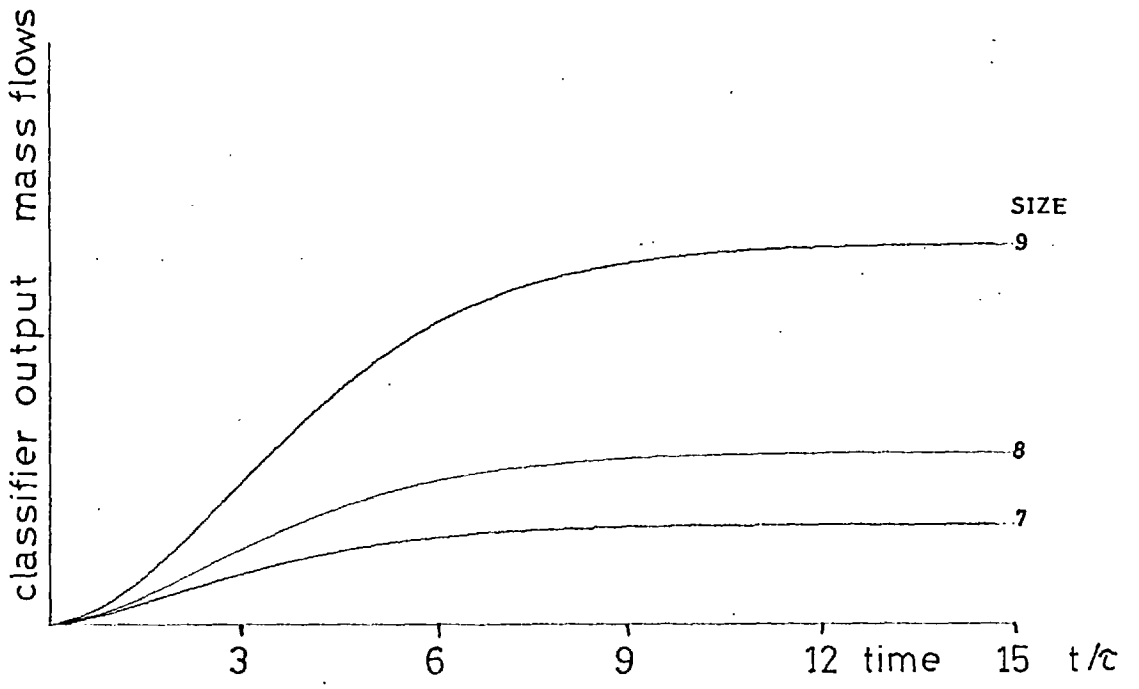


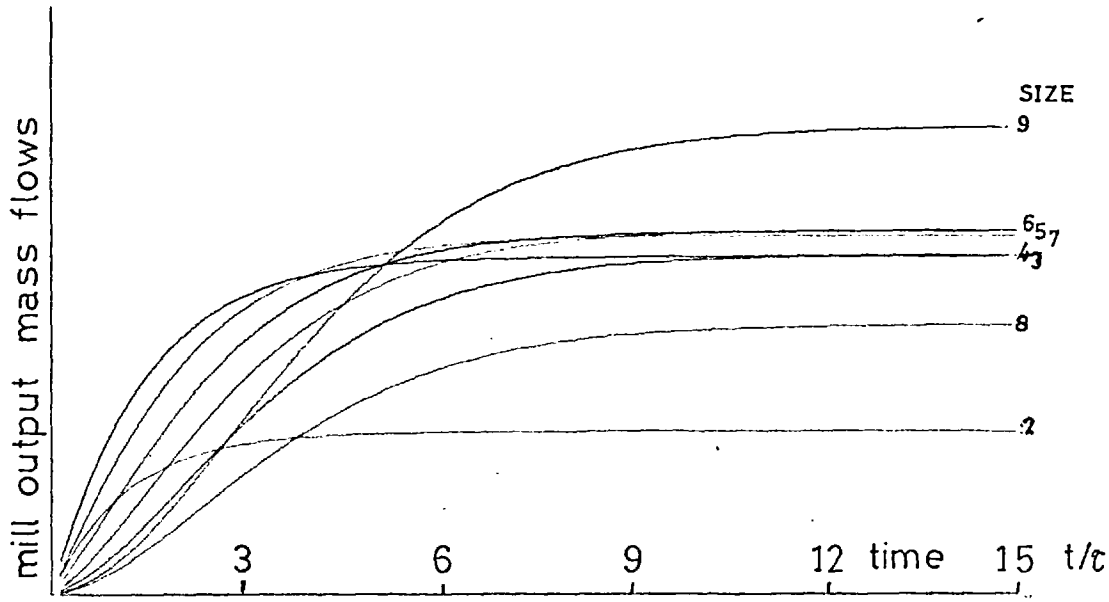


Effect of a step of feed in size 1

figure 6/34

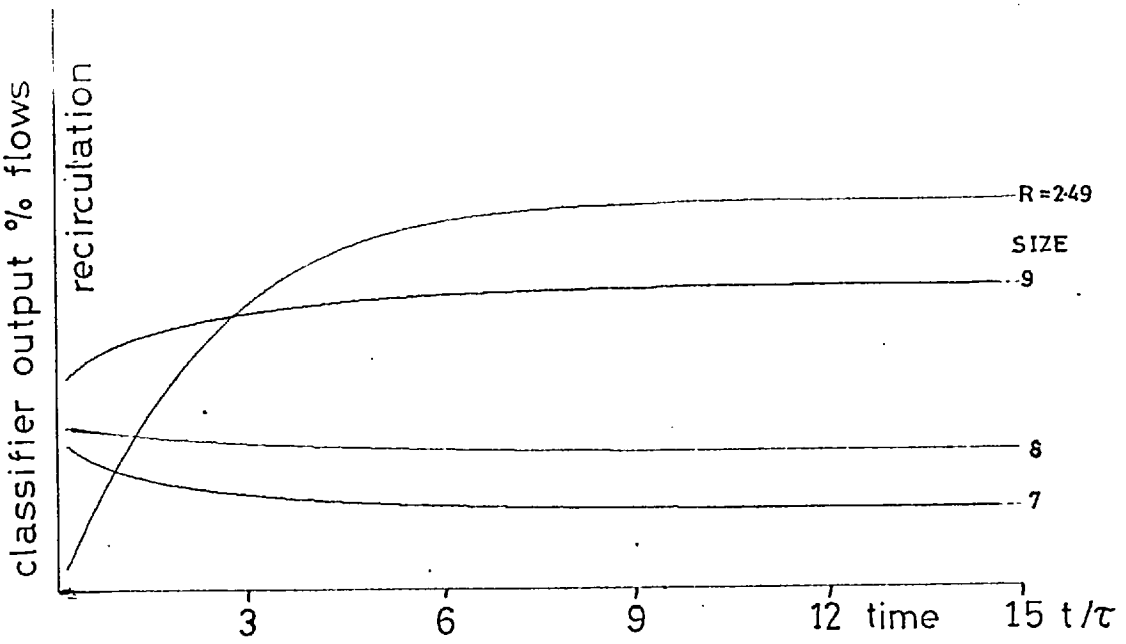


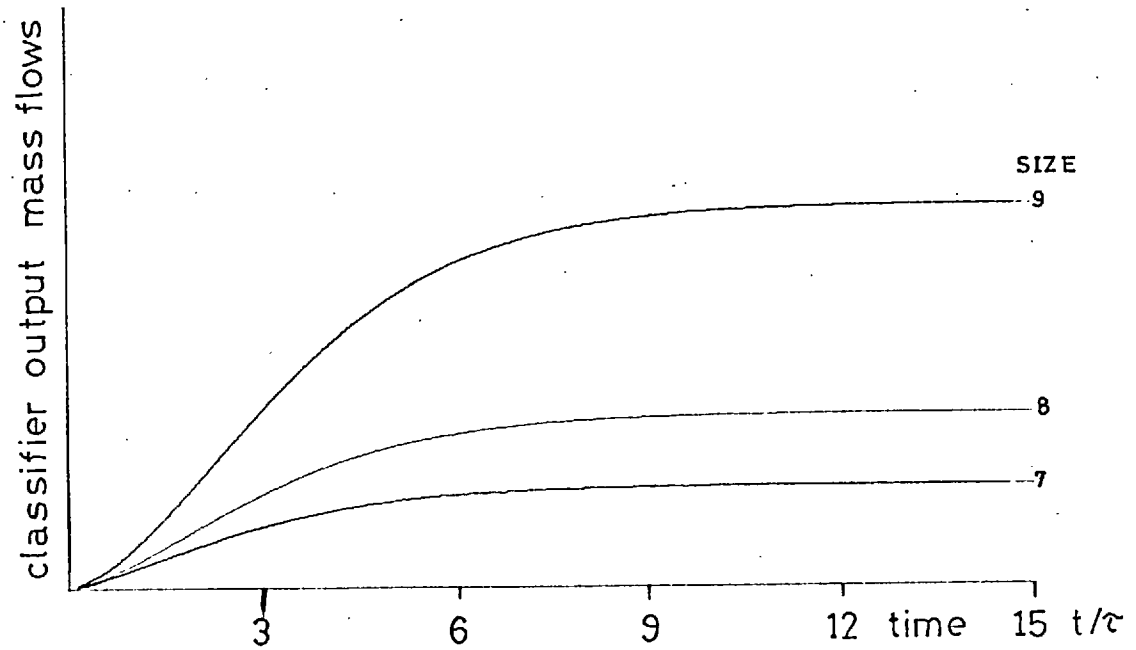


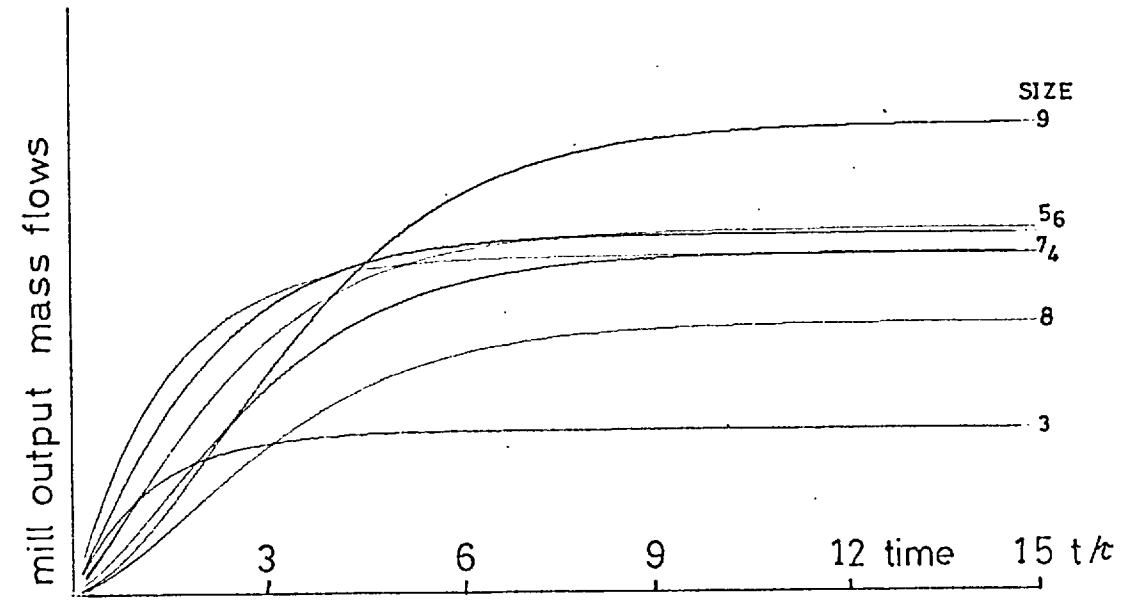


Effect of a step of feed in size 2

figure 6/35

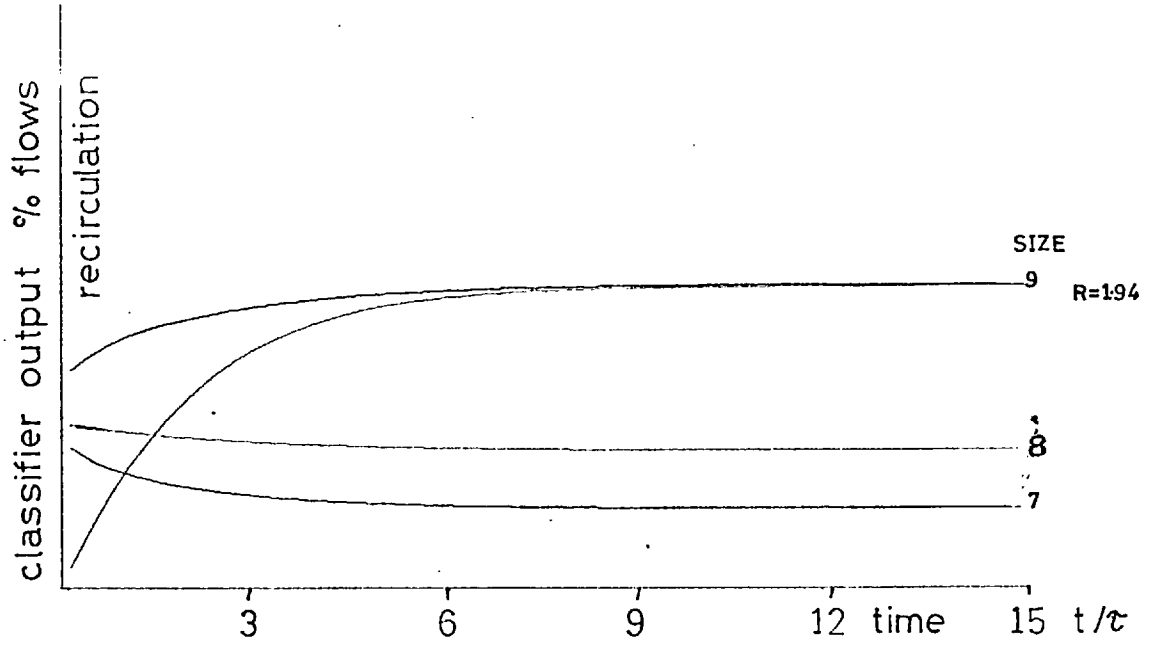


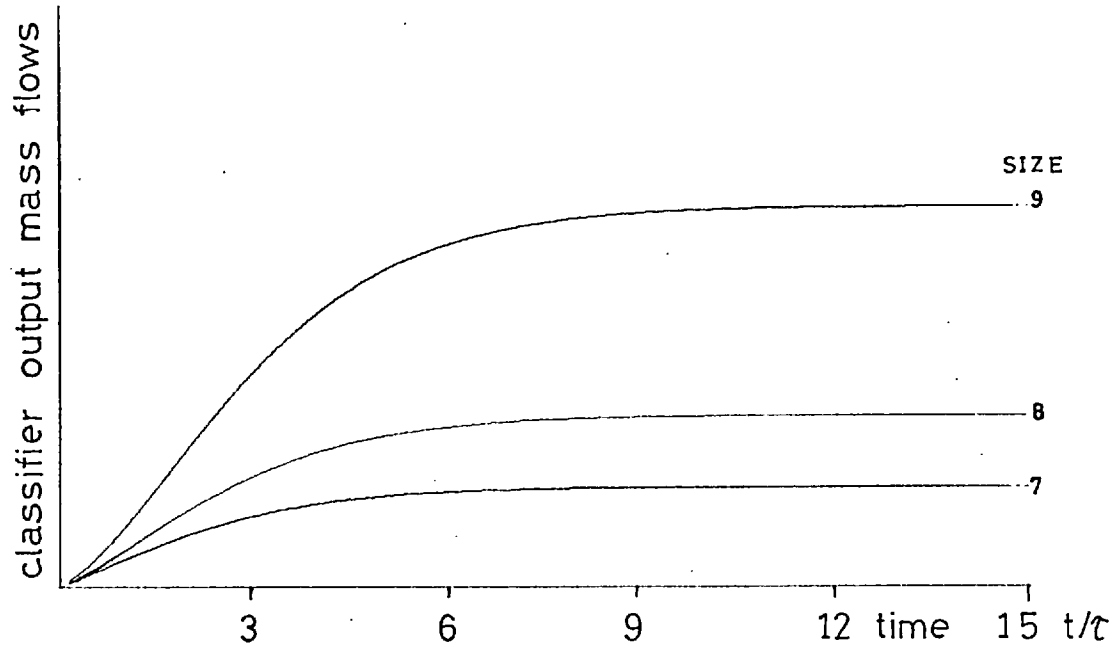


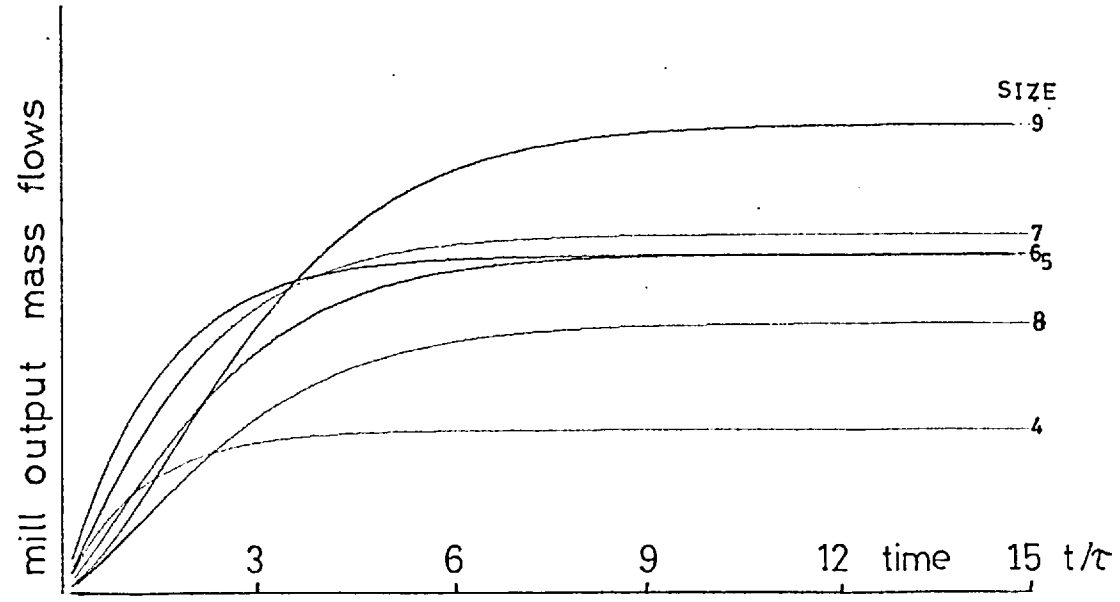


Effect of a ste of feed in size 3

figure 6/36

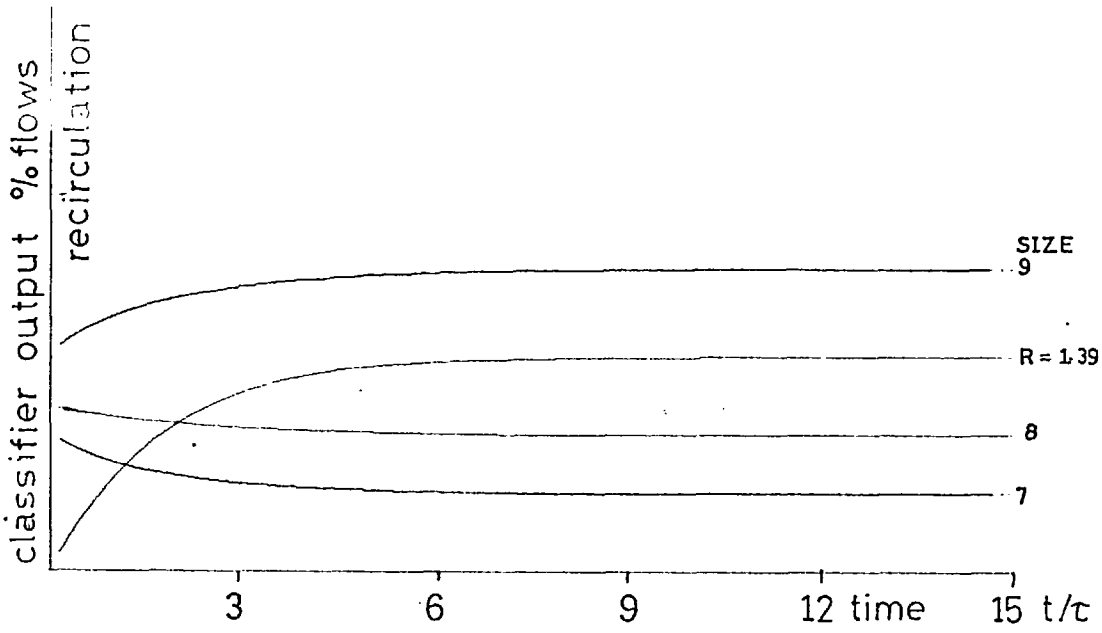


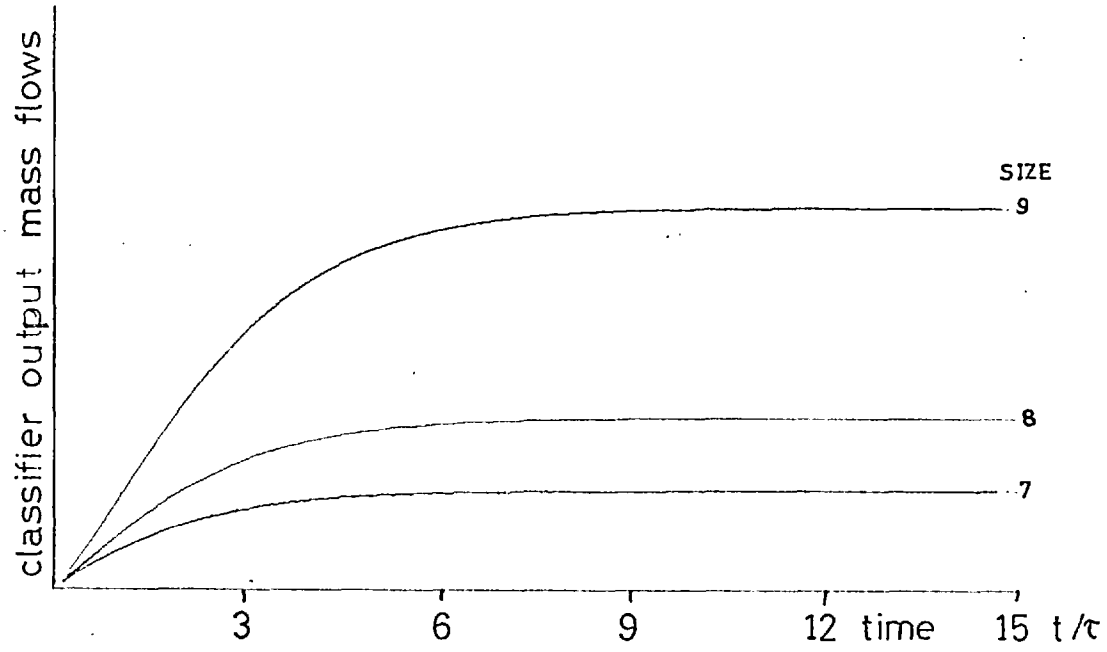


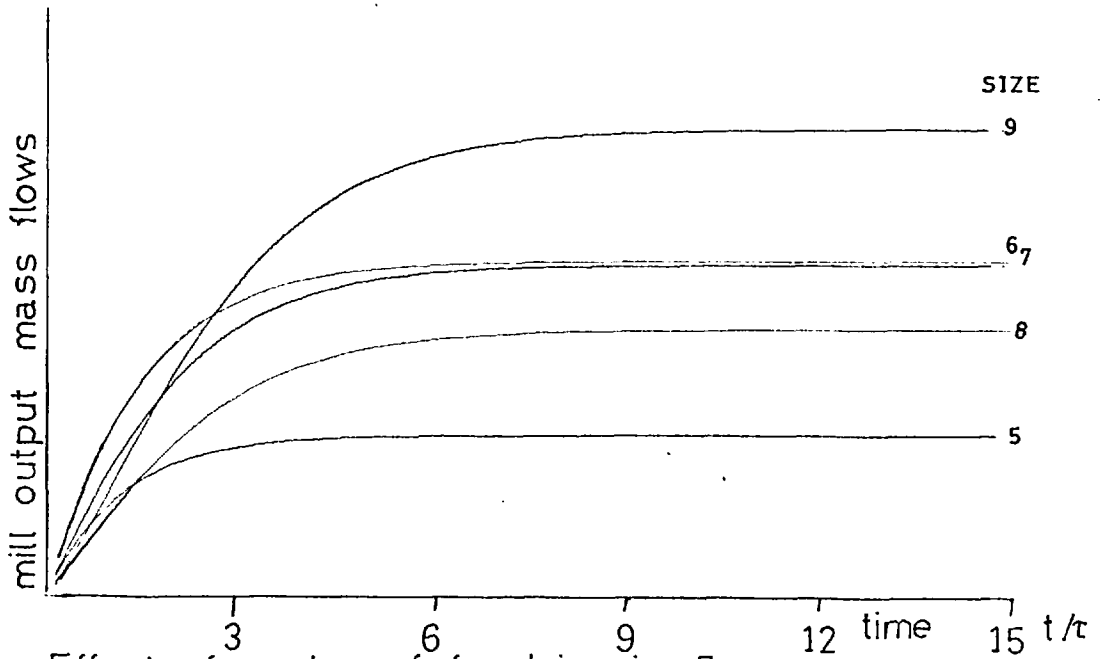


Effect of a step of feed in size 4

figure 6/37

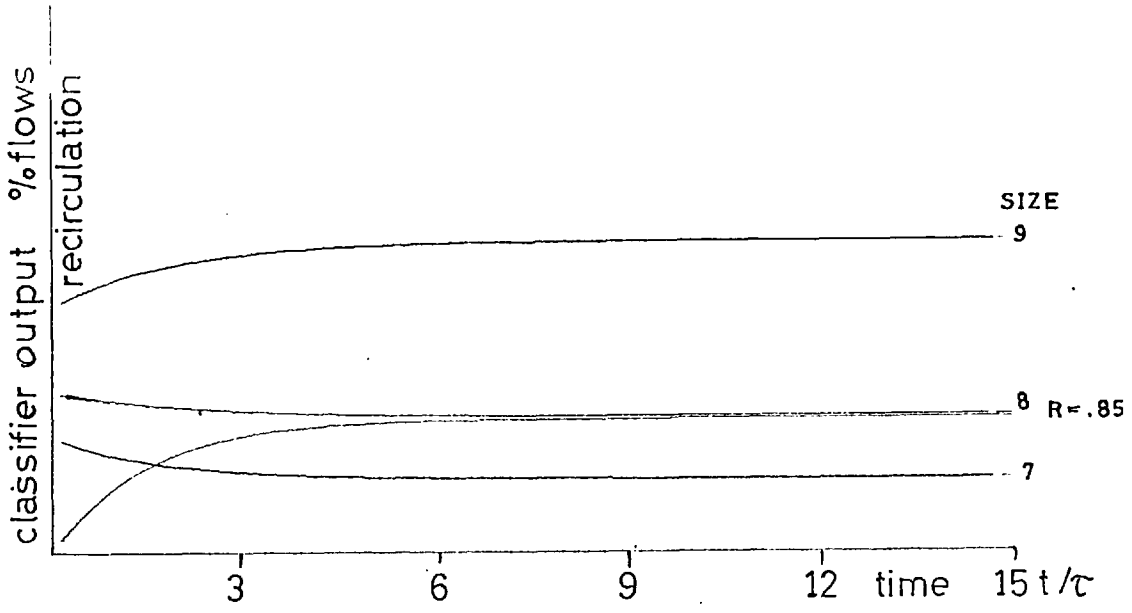


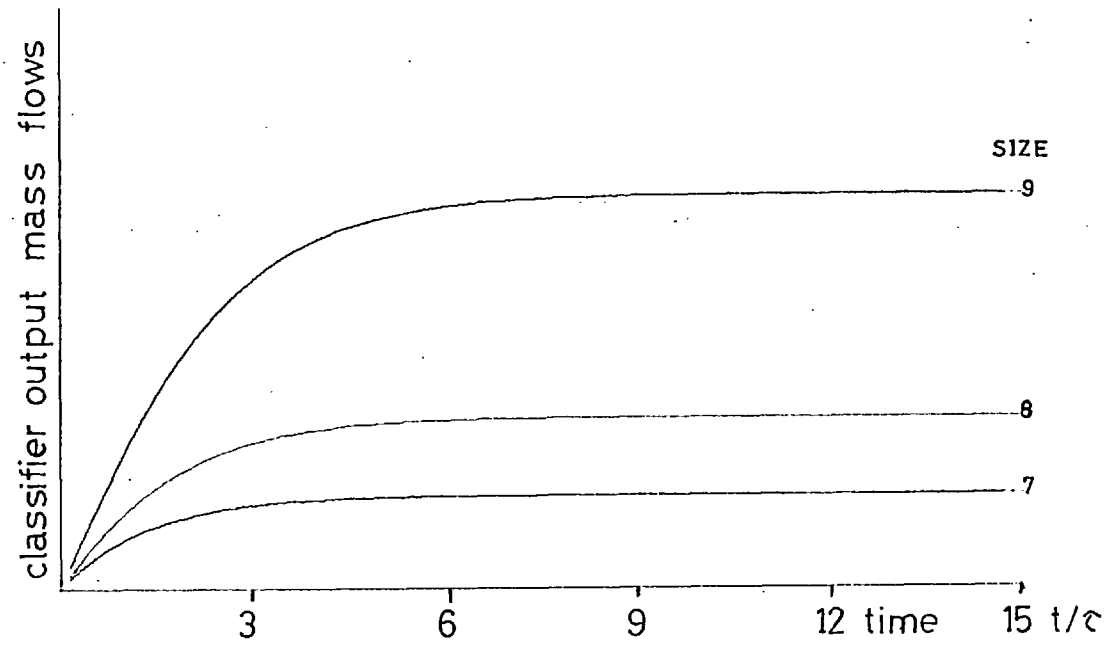


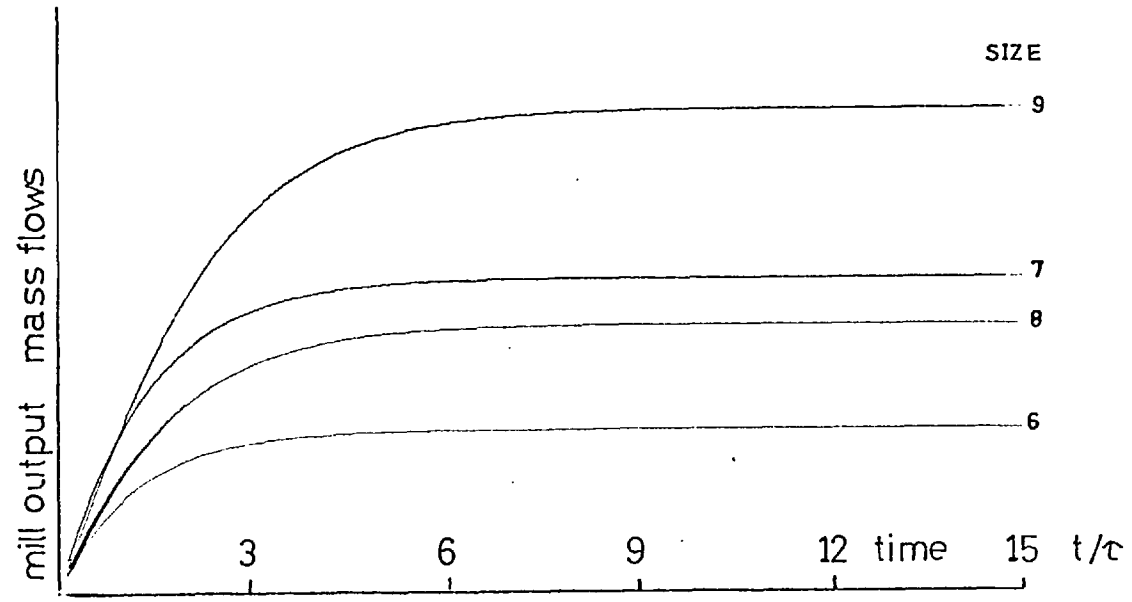


Effect of a step of feed in size 5

figure 6/38

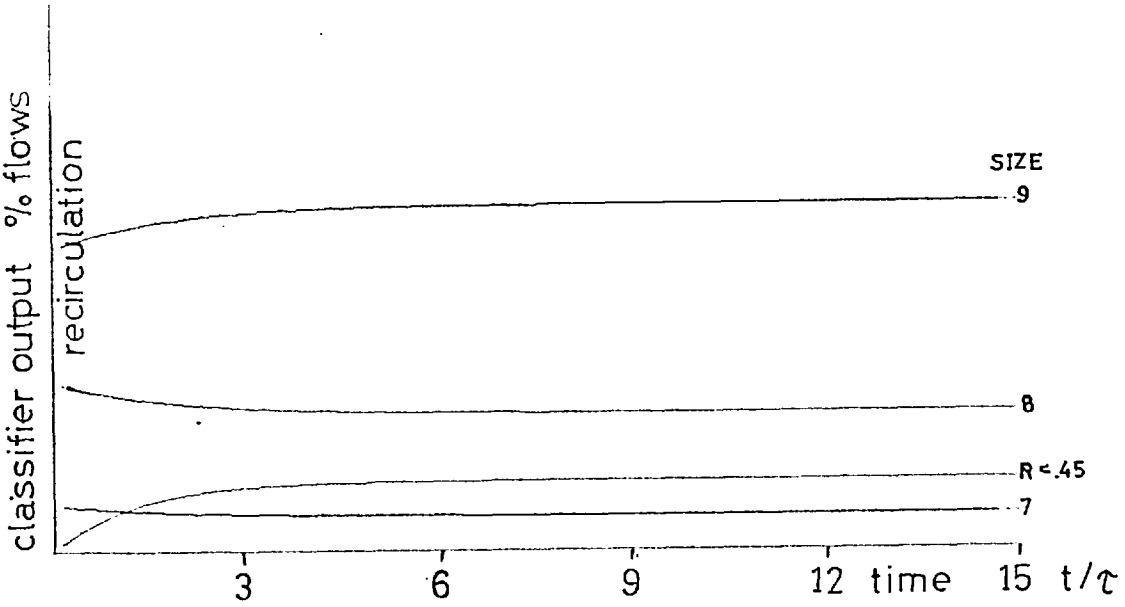


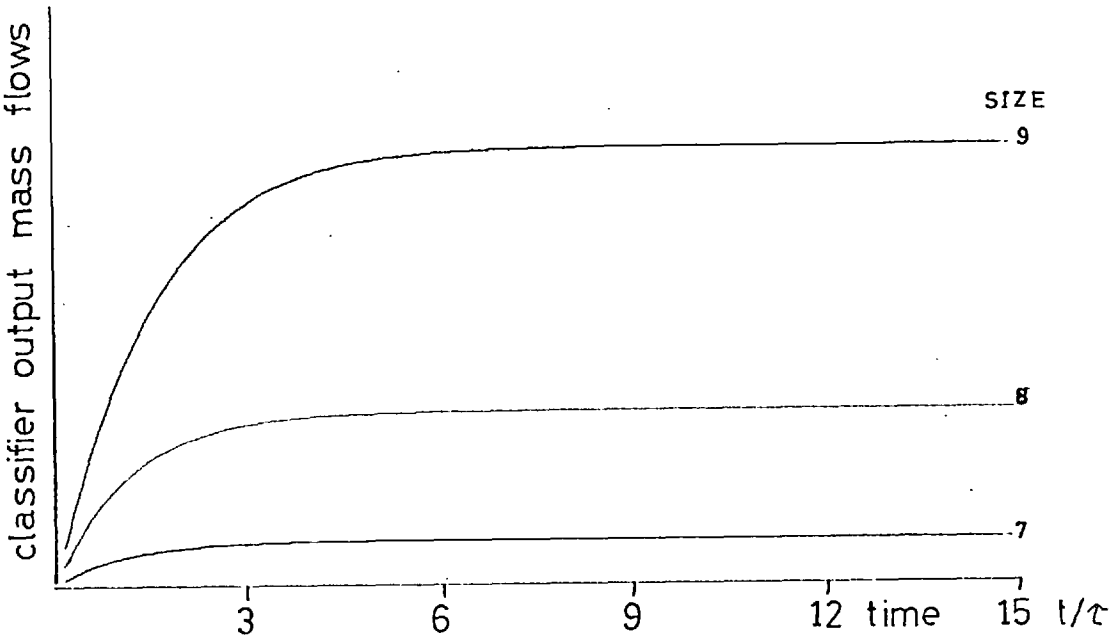


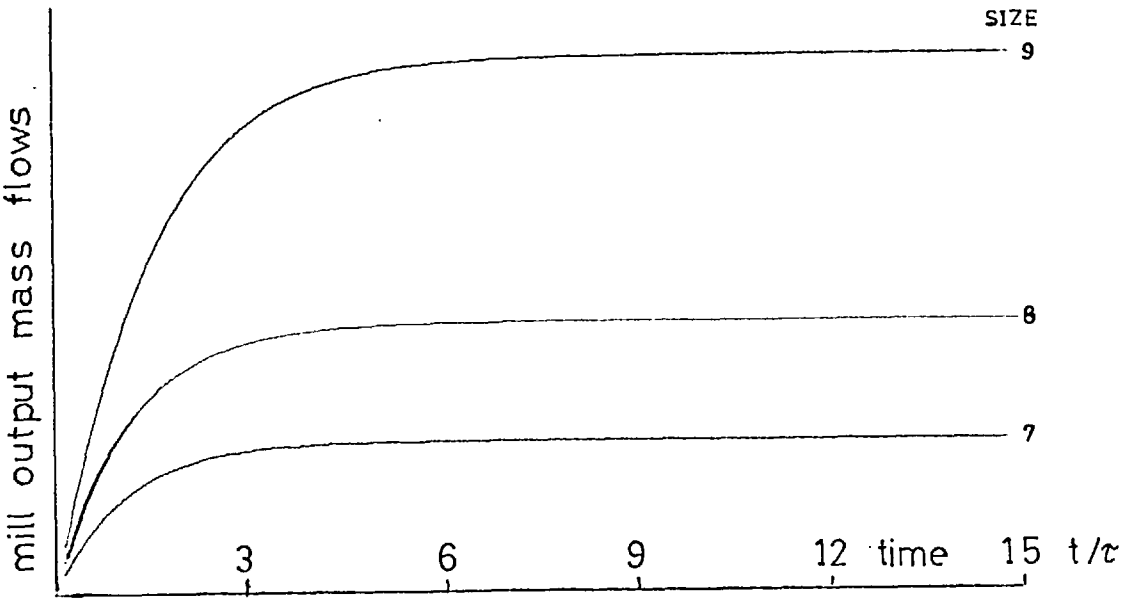


Effect of a step of feed in size 6

figure 6/39

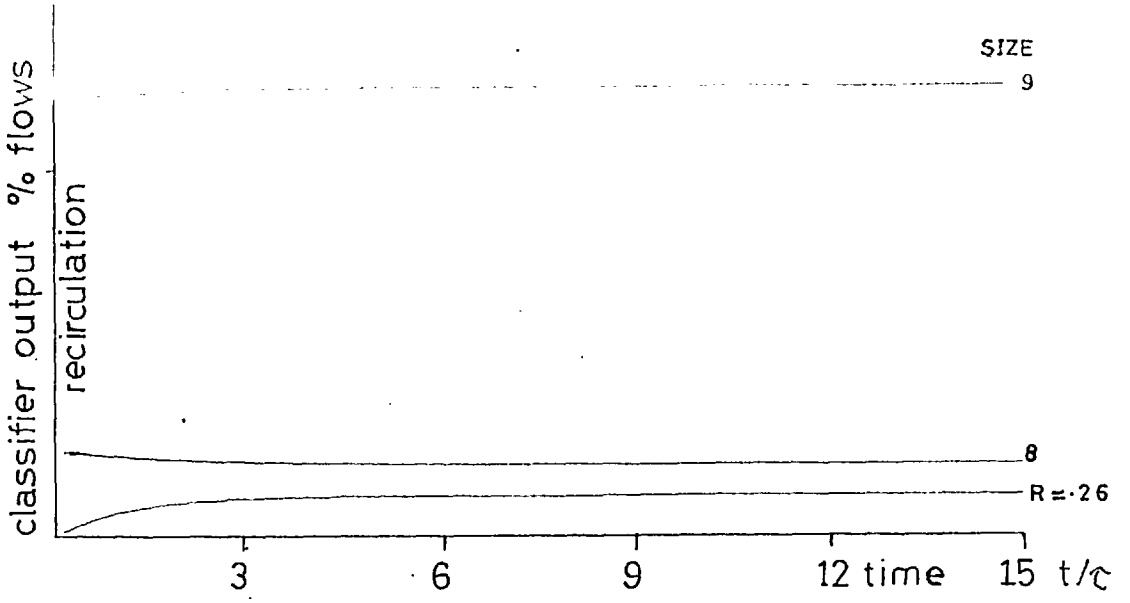


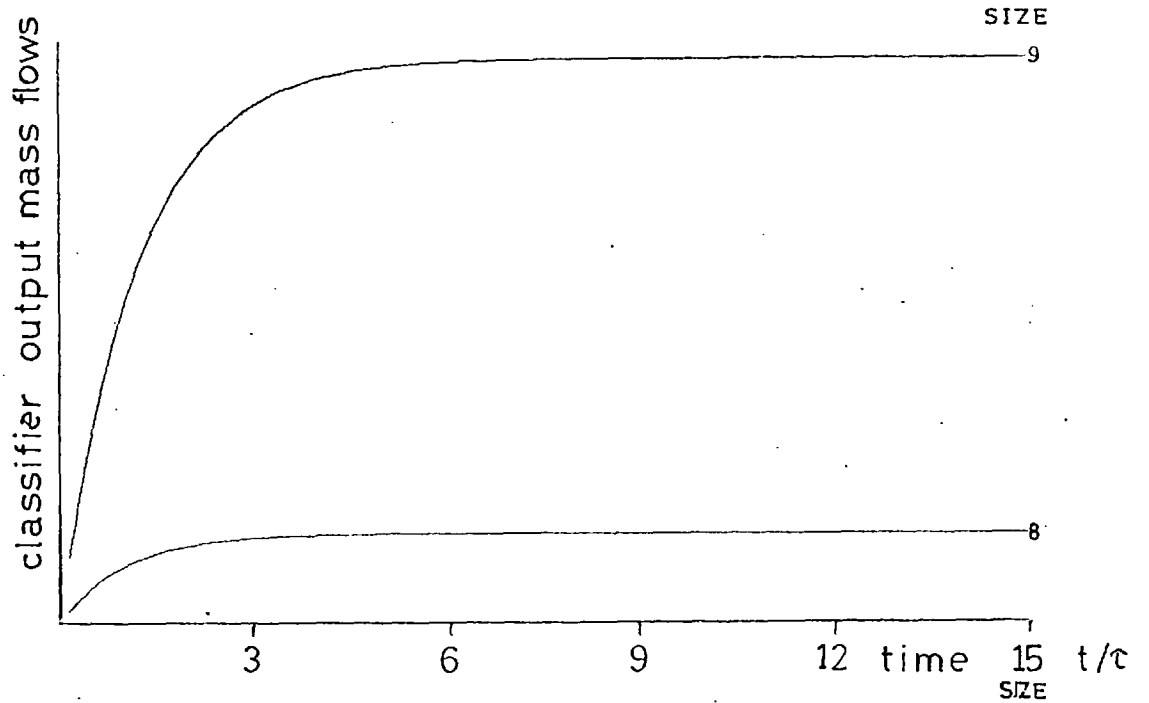


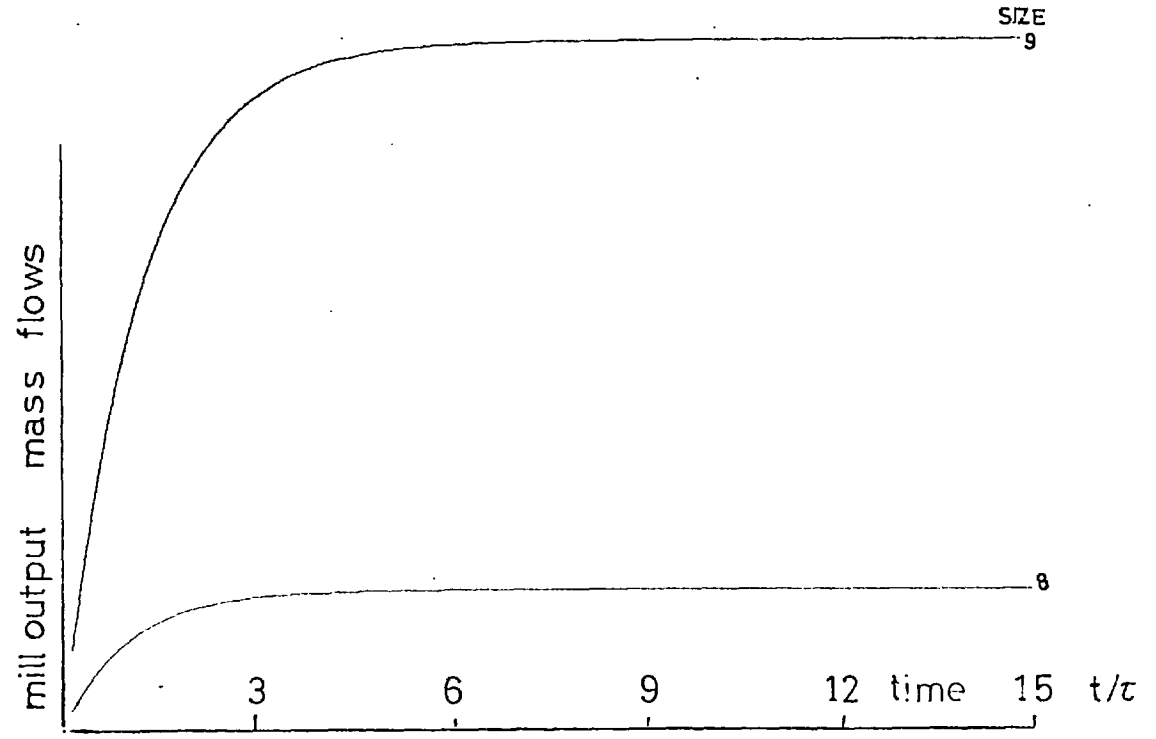


Effect of a step of feed in size 7

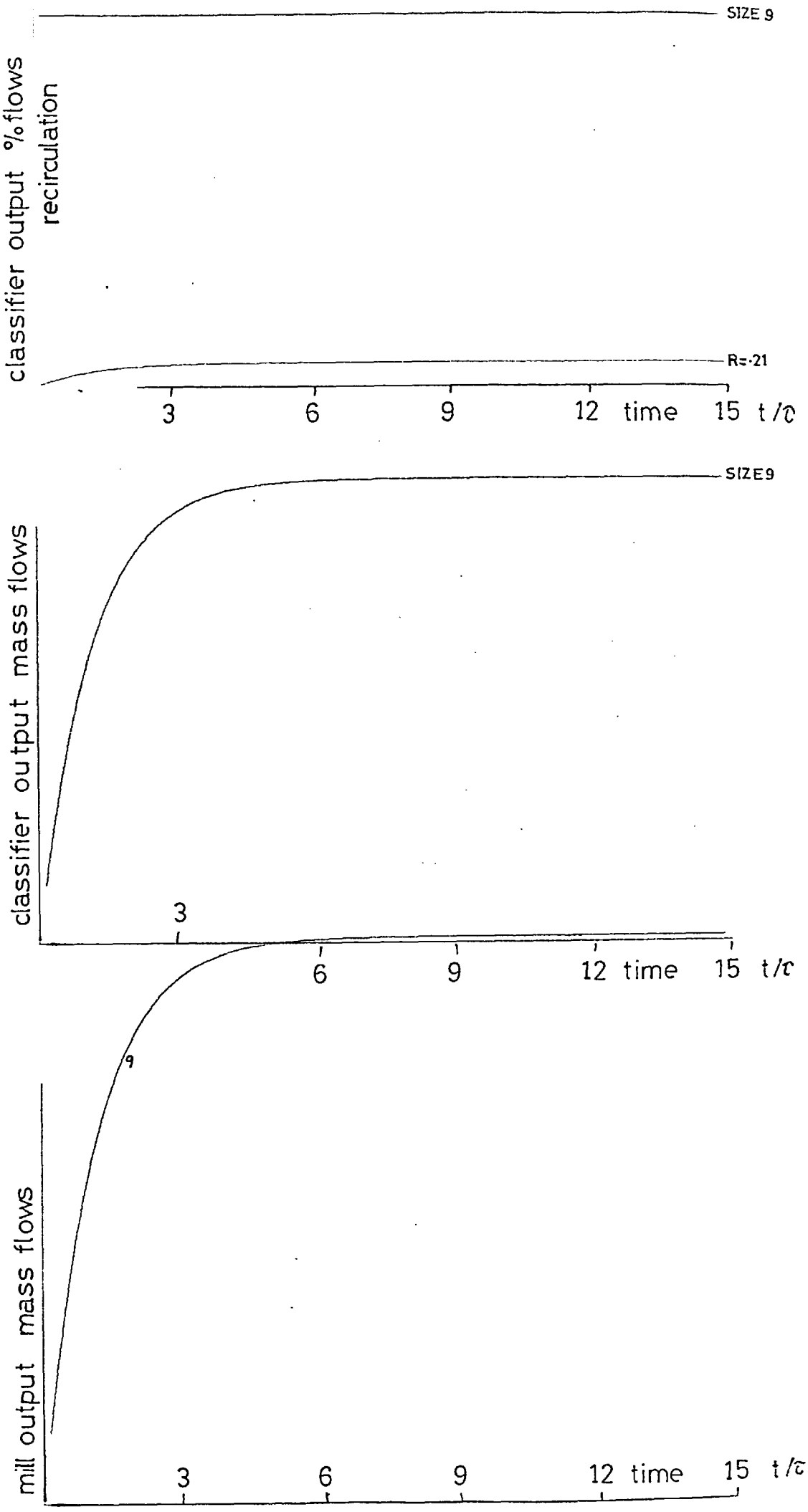
figure 6/40





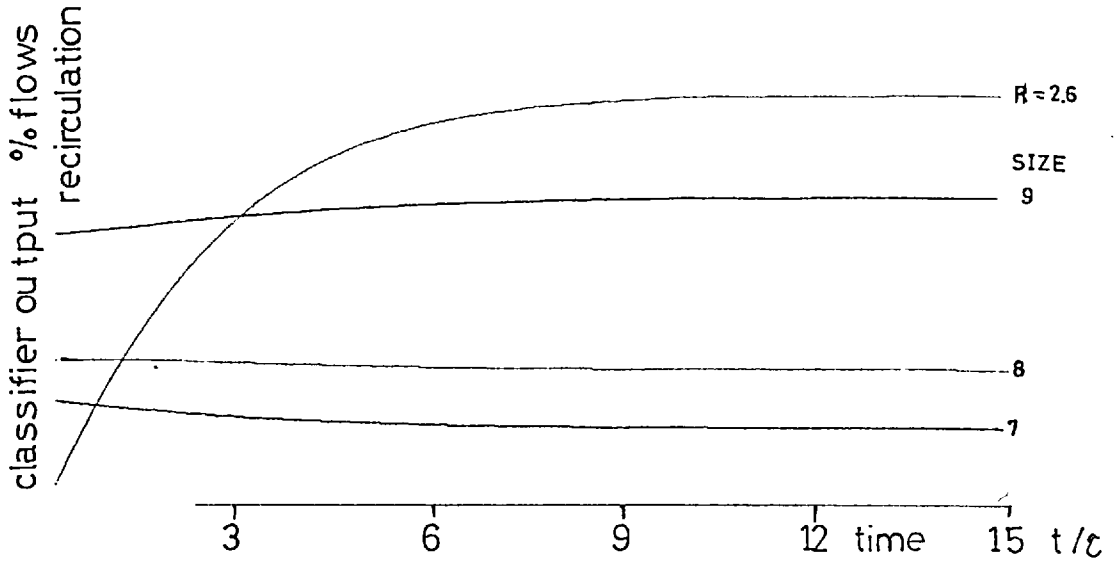


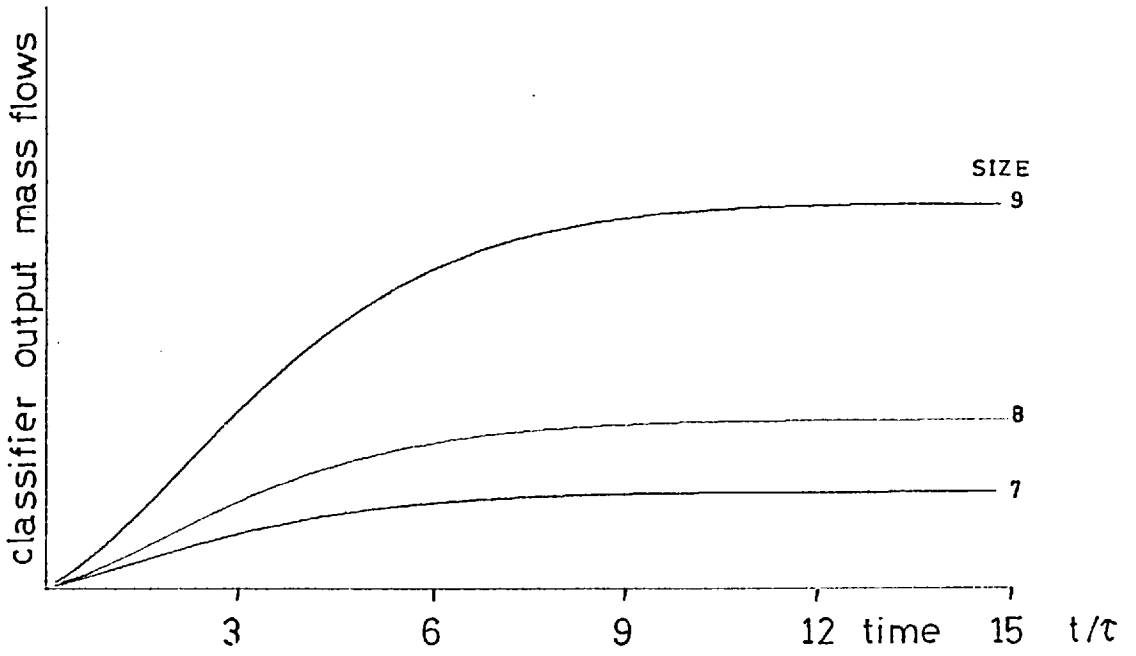
Effect of a step of feed in size 8 figure 6/41

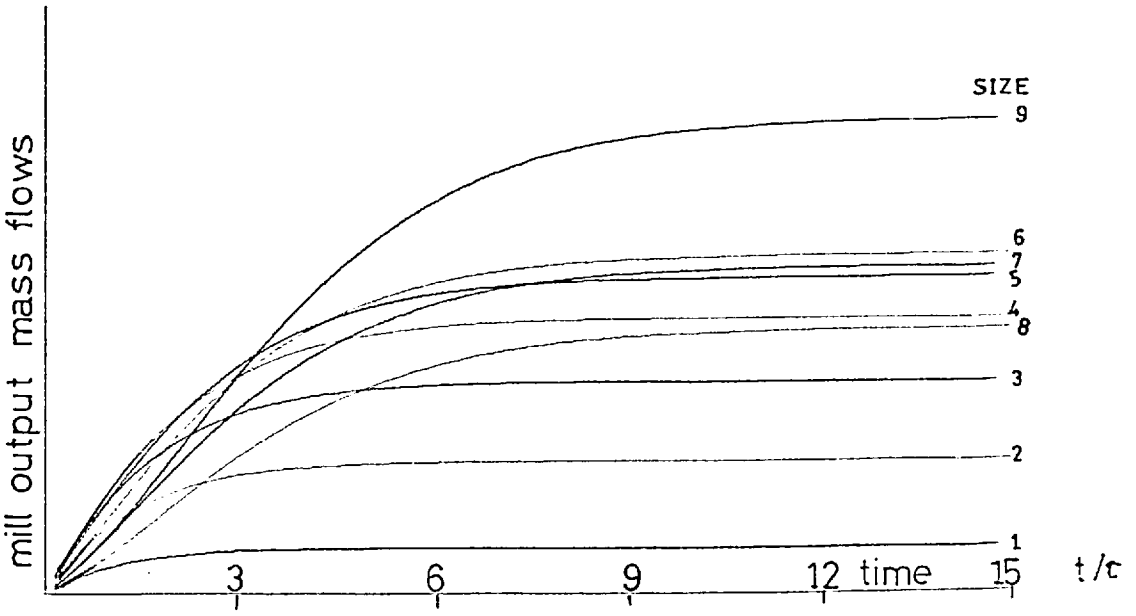


Effect of a step of feed in size 9

figure 6/42







Effect of a step of feed with distribution of table 6/6 figure 6/43

The system settling time was very much larger than would be expected from a consideration of the mill time constant although it is noted that the percentage size distributions appear to settle much faster than the true mass flows.

6.13.3 Dynamics of a Change of Grindability

In the previous example the particle flow tensor only described flow in terms of size. This can, of course, be generalised and so the example was repeated with a primary space of grindability - size. The grindability axis was divided into two ranges: hard-to-grind and easy-to-grind. Figures 6/44 - 6/52 show the effect of a change of grindability on the particle flows with a single size feed, beginning with easy-to-grind and then changing to hard-to-grind. The tensor for the hard-to-grind mill fraction had elements as in Table 6/7; that for the easy-to-grind had elements as in Table 6/4; and the classifier as in Table .

The tensors were also derived from Callcott's paper. The graphs show, as before, very long settling times, and although the feed rate was held constant an overshoot was observed. This is because the rate of decay of easy-to-grind material is initially greater than the rate of increase of hard-to-grind in the recirculating load.

Table 6/6

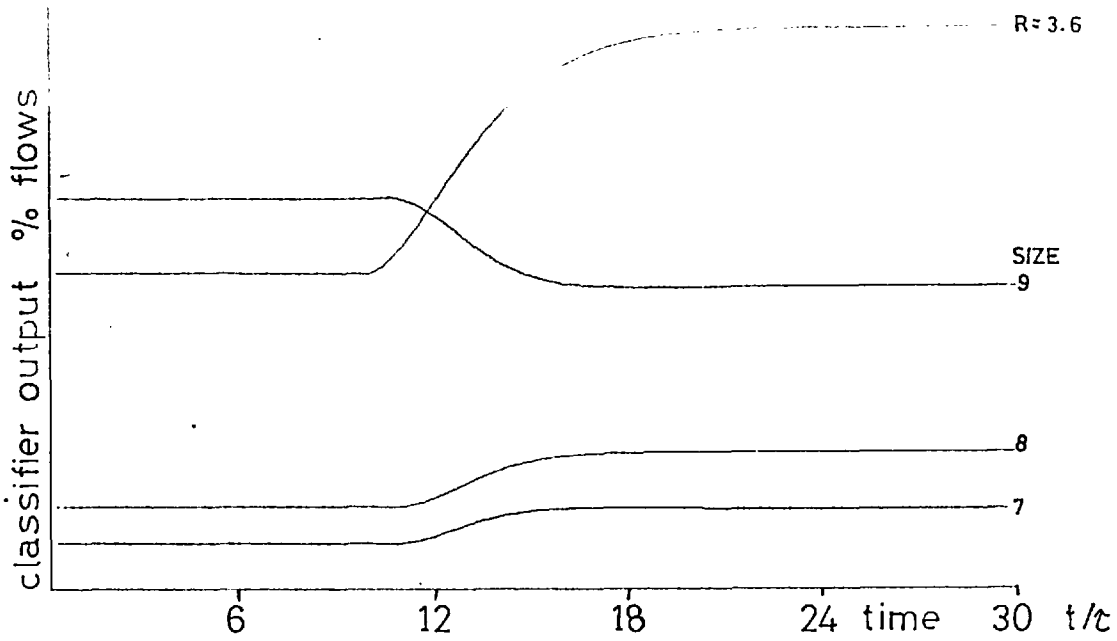
Input Size Distribution for Calcott's Coal A

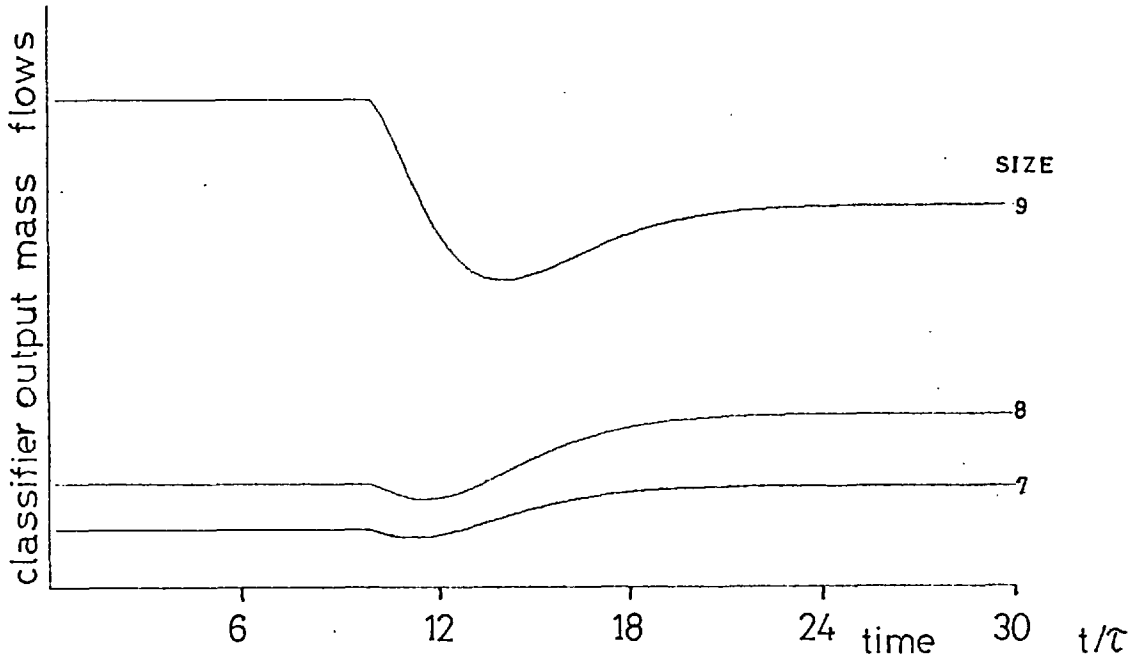
Size	1	2	3	4	5	6	7	8	9
Feed Mass Flow	0.280	0.230	0.210	0.130	0.074	0.036	0.020	0.010	0.010

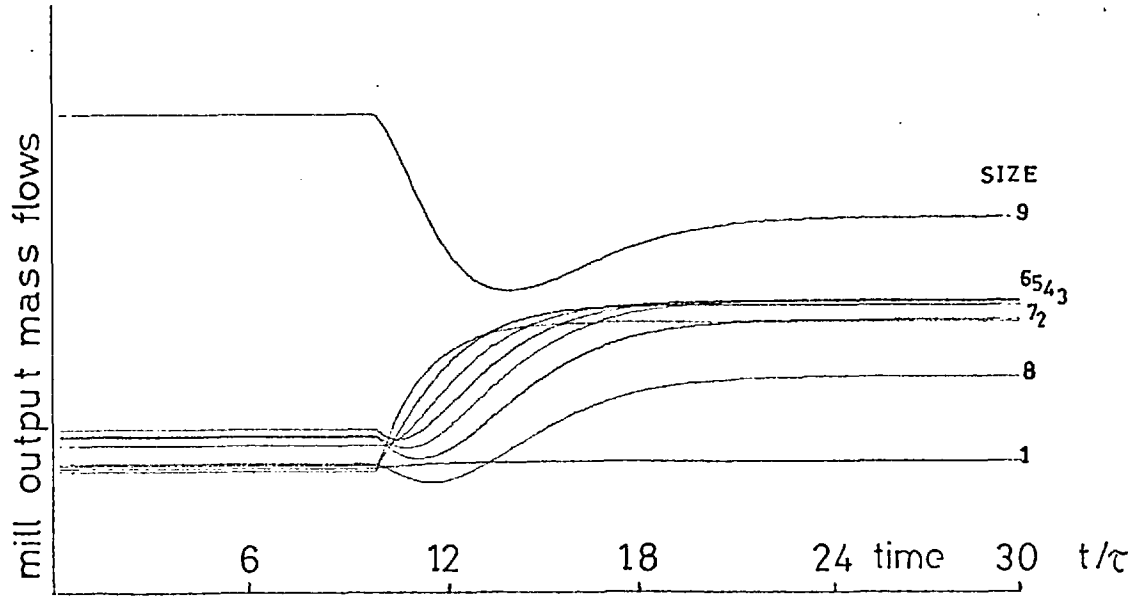
Table 6/7

Mill Performance Tensor (Easy to Grind)

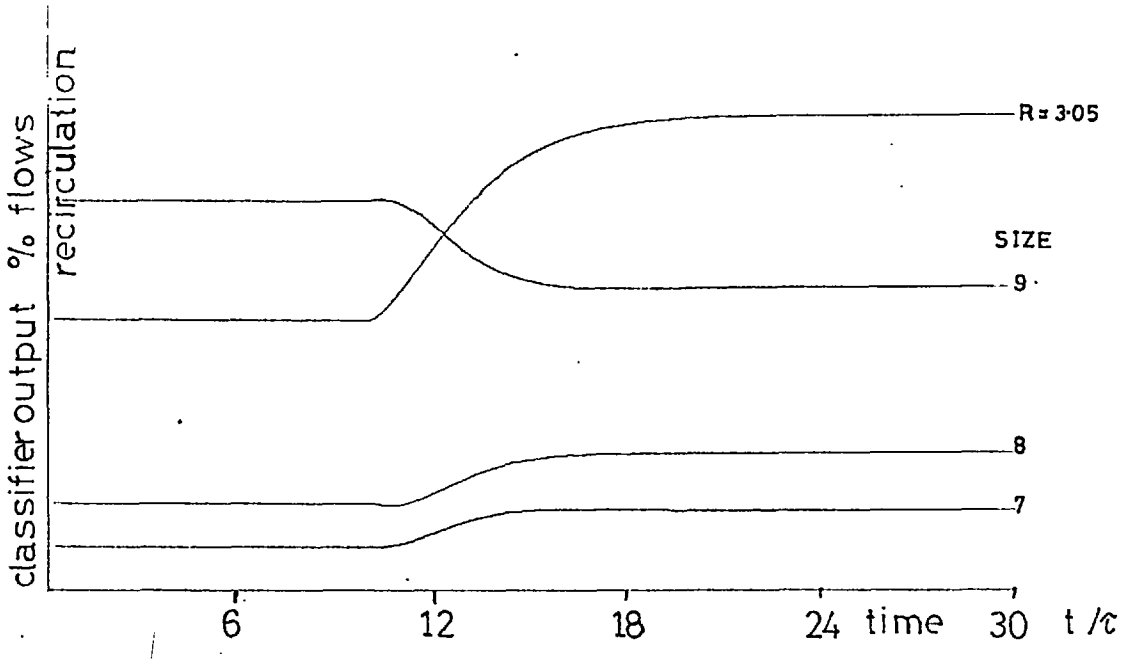
Row \ Column	1	2	3	4	5	6	7	8	9
1	.19								
2	.15	.19							
3	.13	.15	.19						
4	.13	.13	.15	.19					
5	.12	.13	.13	.15	.19				
6	.08	.12	.13	.13	.15	.19			
7	.07	.08	.12	.13	.13	.15	.19		
8	.04	.07	.08	.12	.13	.13	.15	.19	
9	.09	.13	.20	.28	.40	.53	.66	.81	1.0

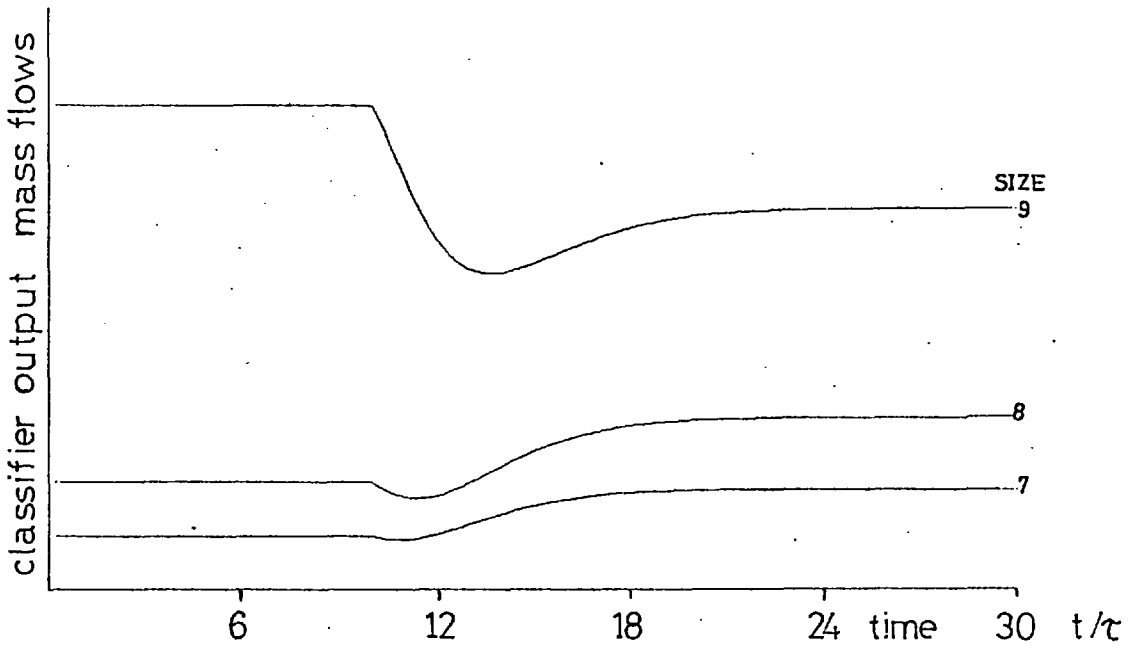


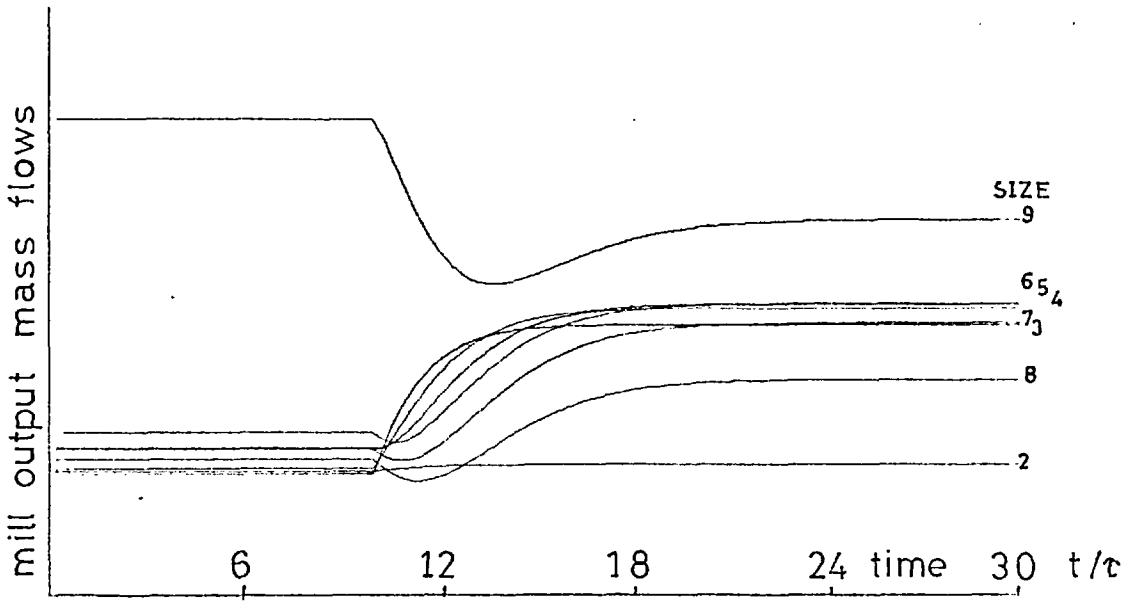




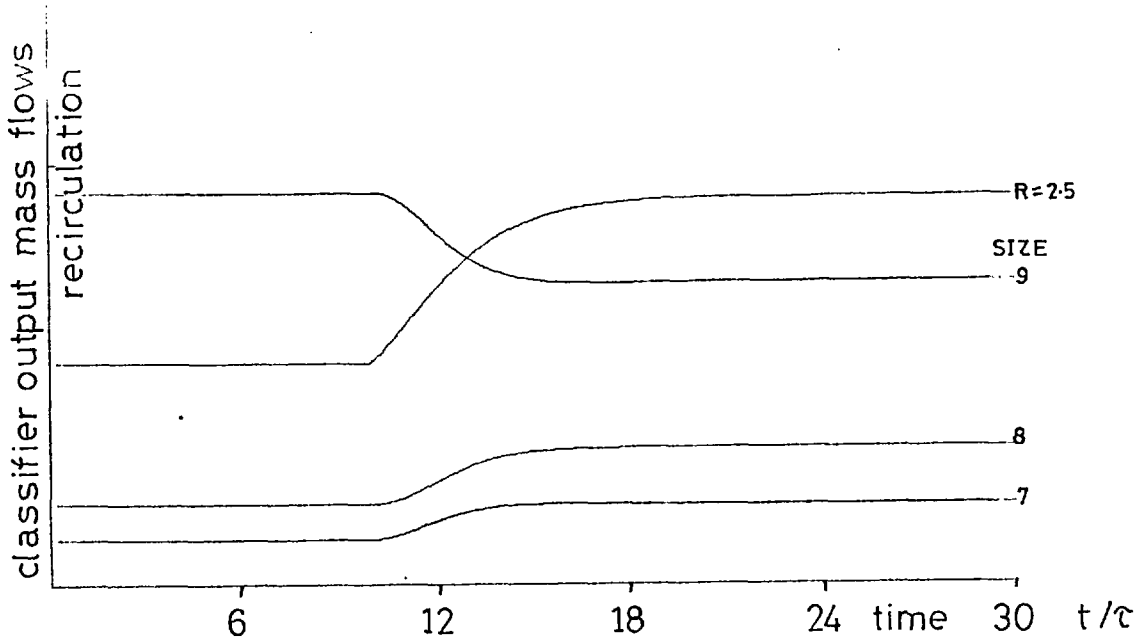
Effect of changing the grindability of size 1 figure 6/44

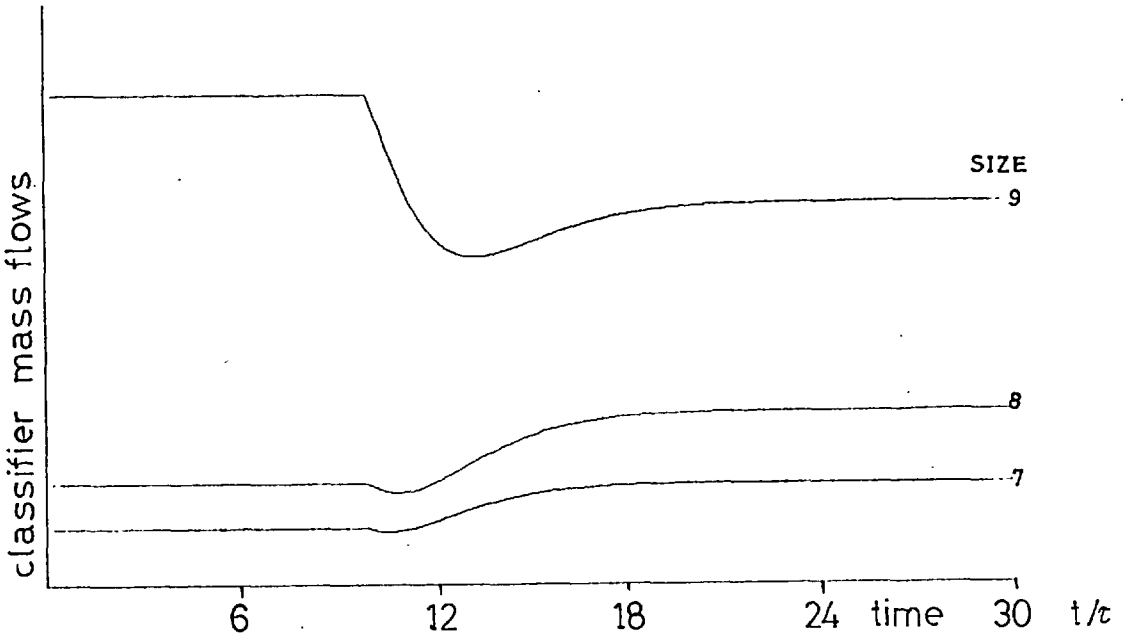


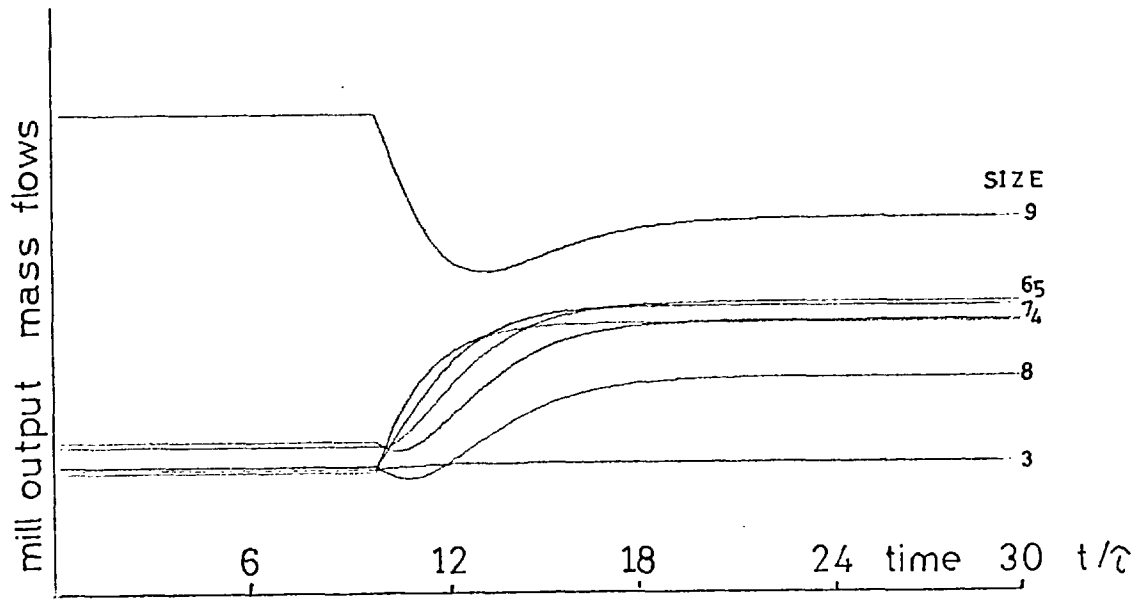




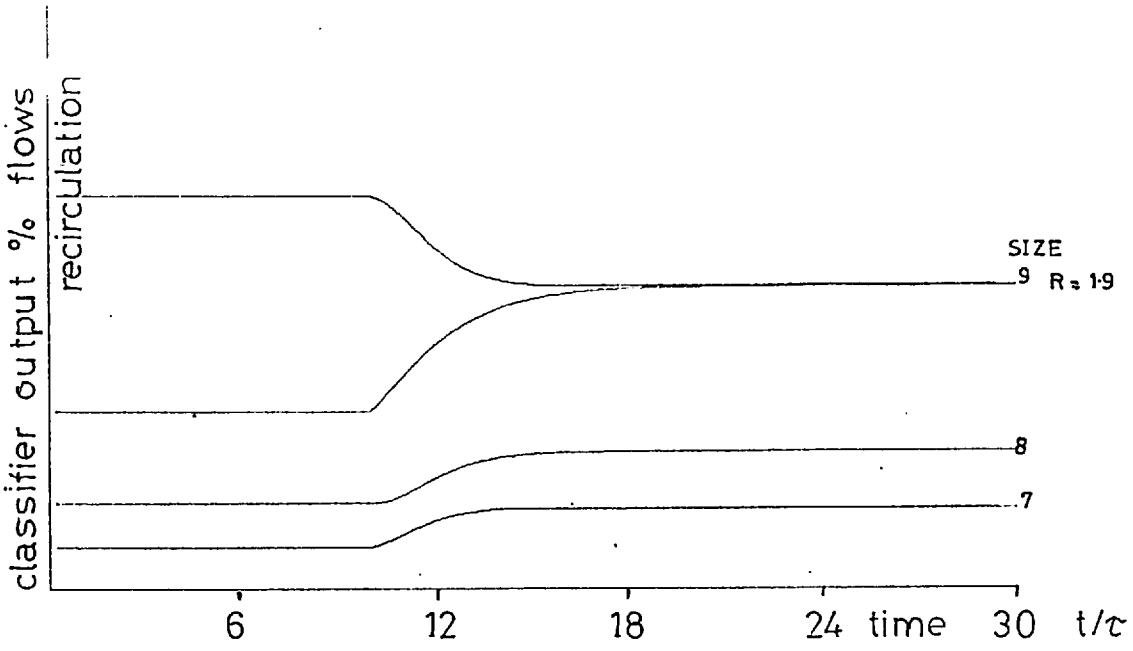
Effect of changing the grindability of size 2 figure 6/45

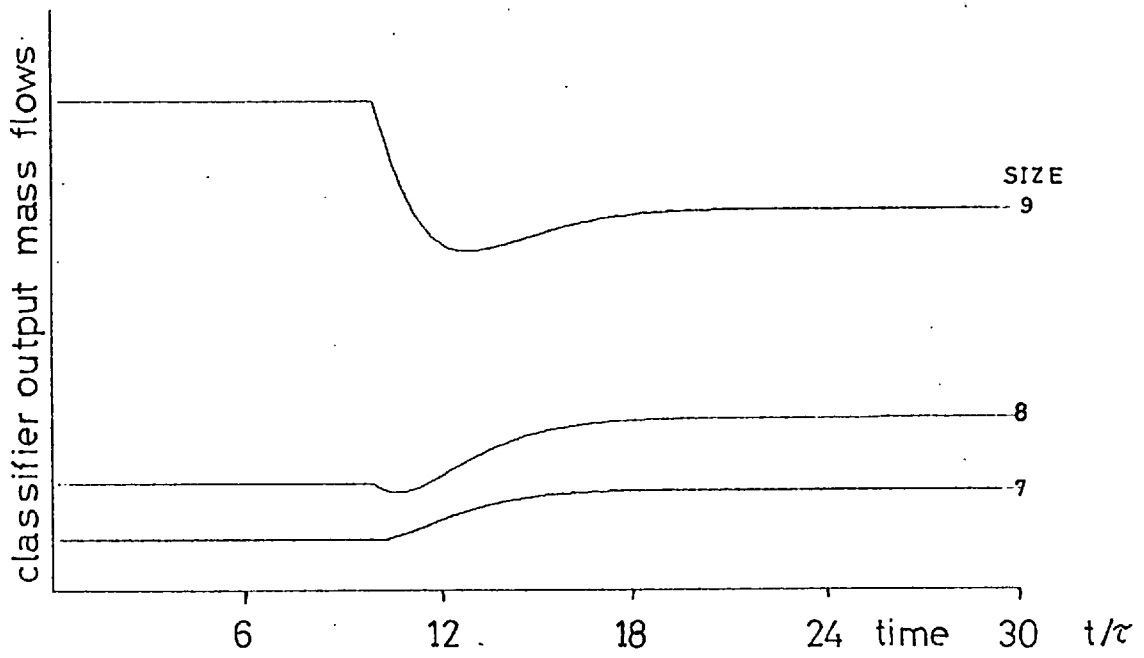


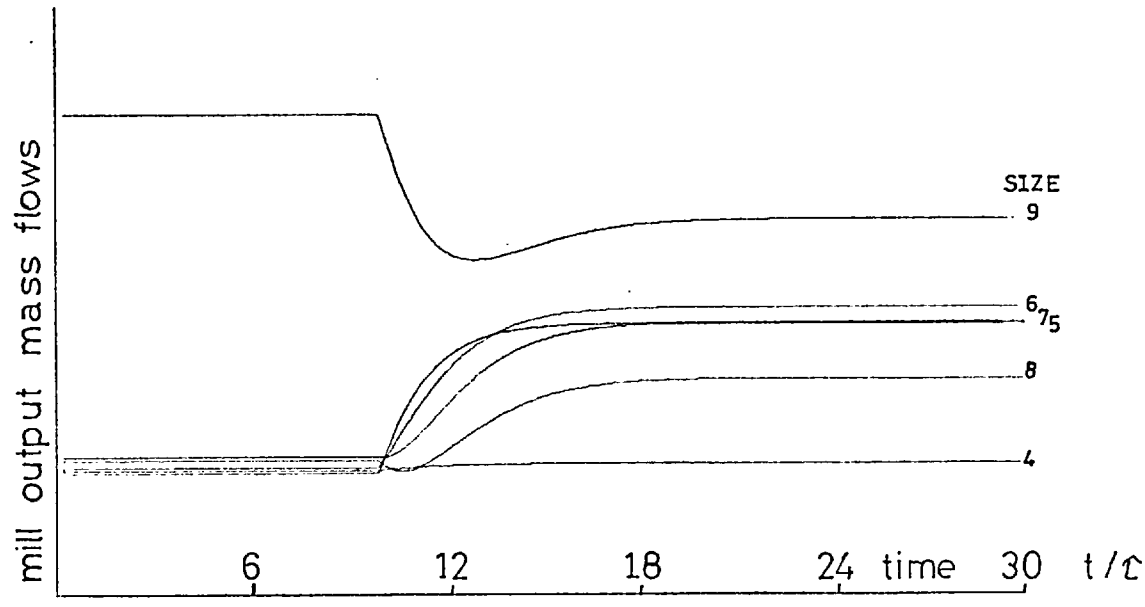




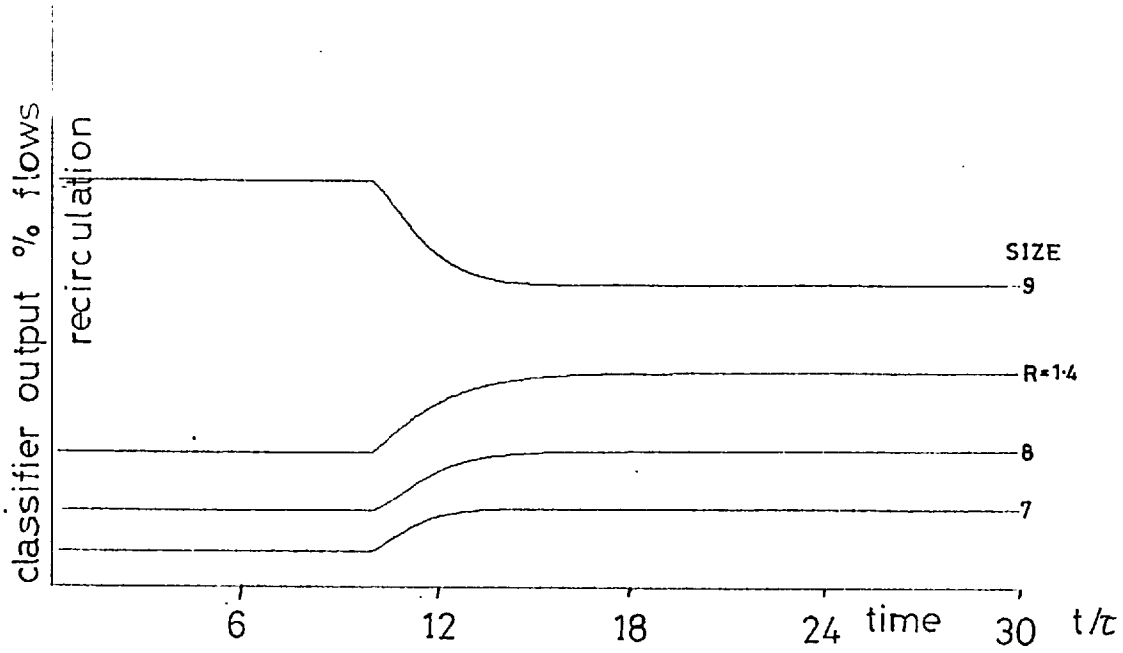
Effect of chan in the grindability of size 3 figure 6/46

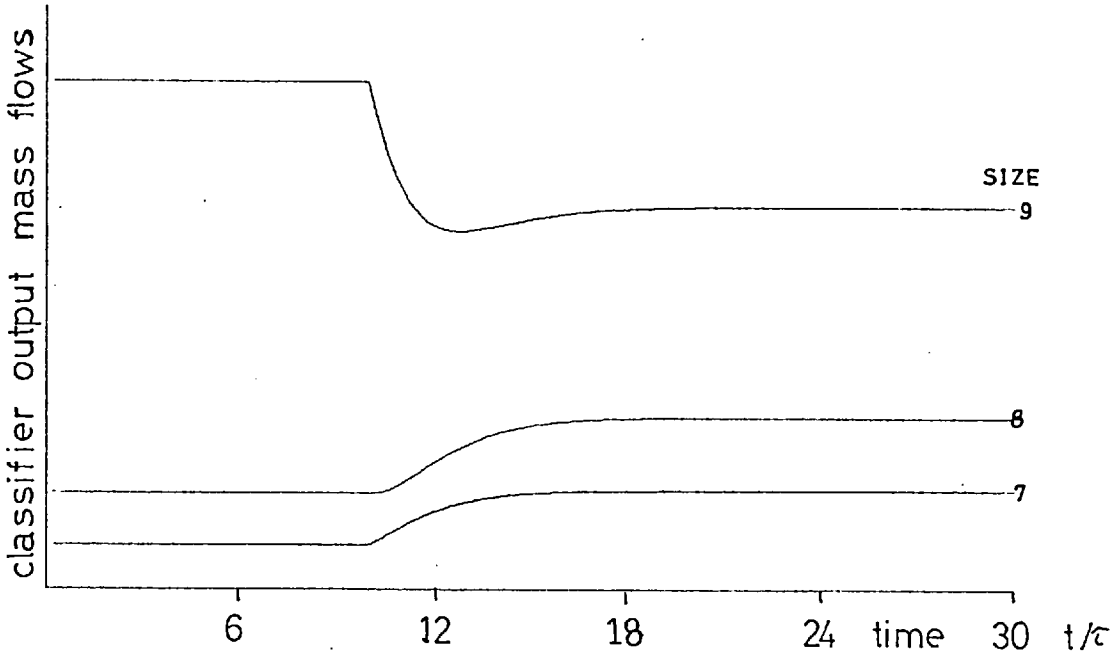


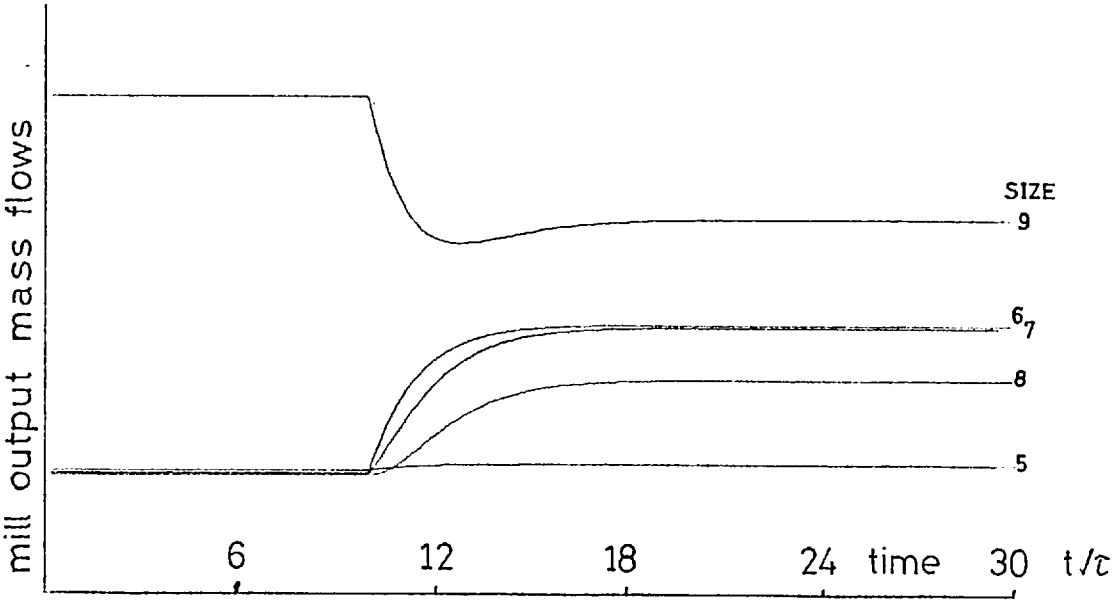




Effect of changing the grindability of size 4 figure 6/47

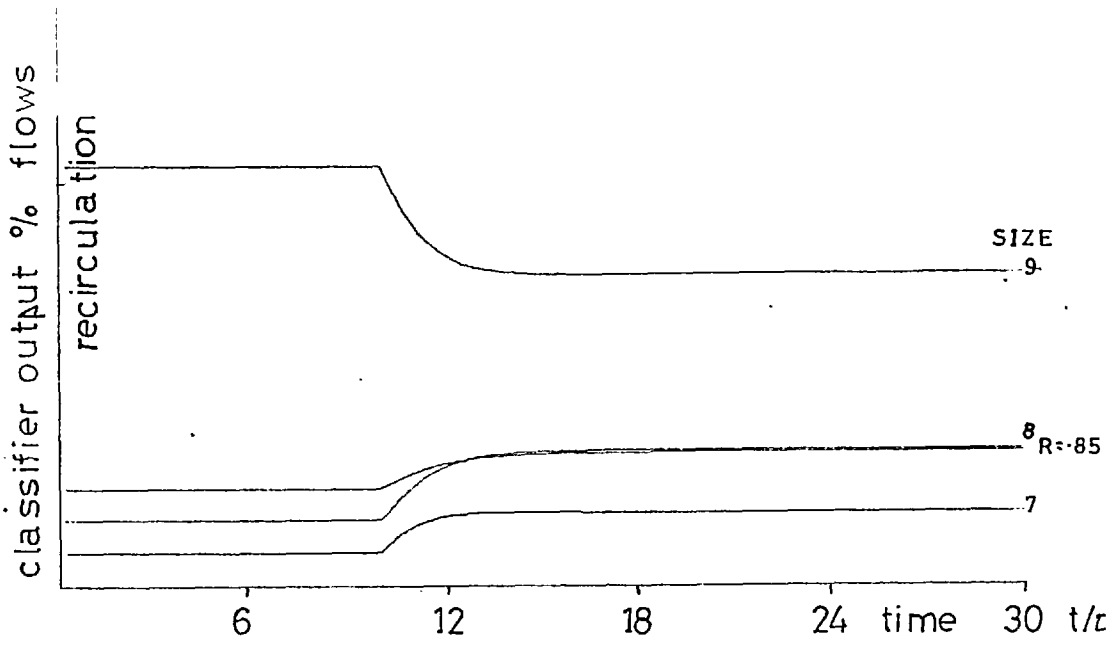


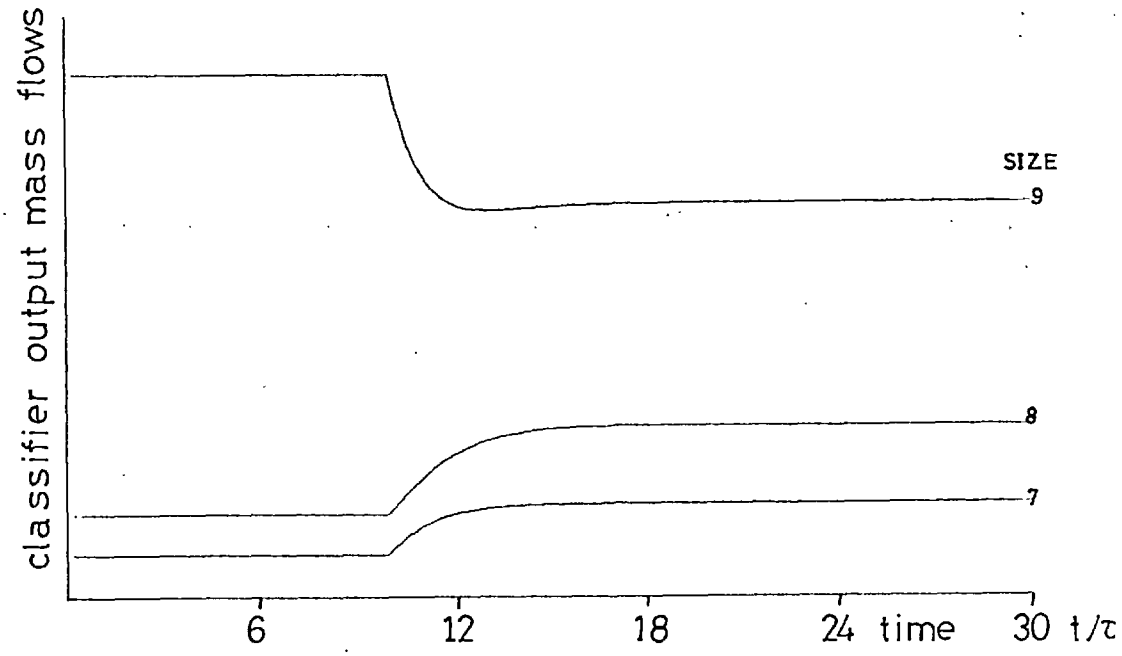


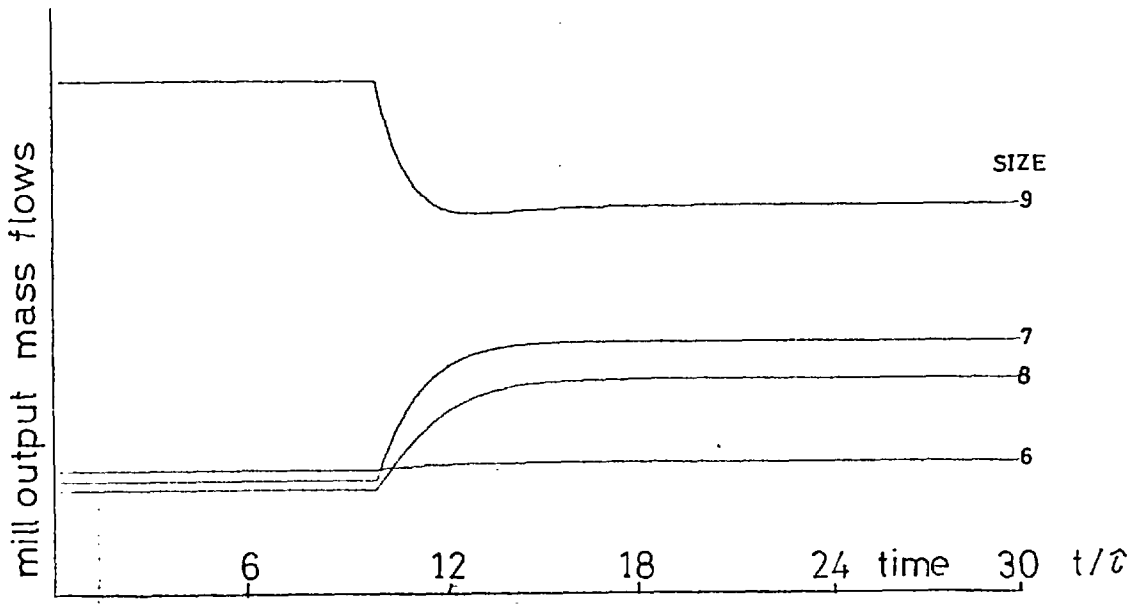


Effect of changing the grindability of size 5

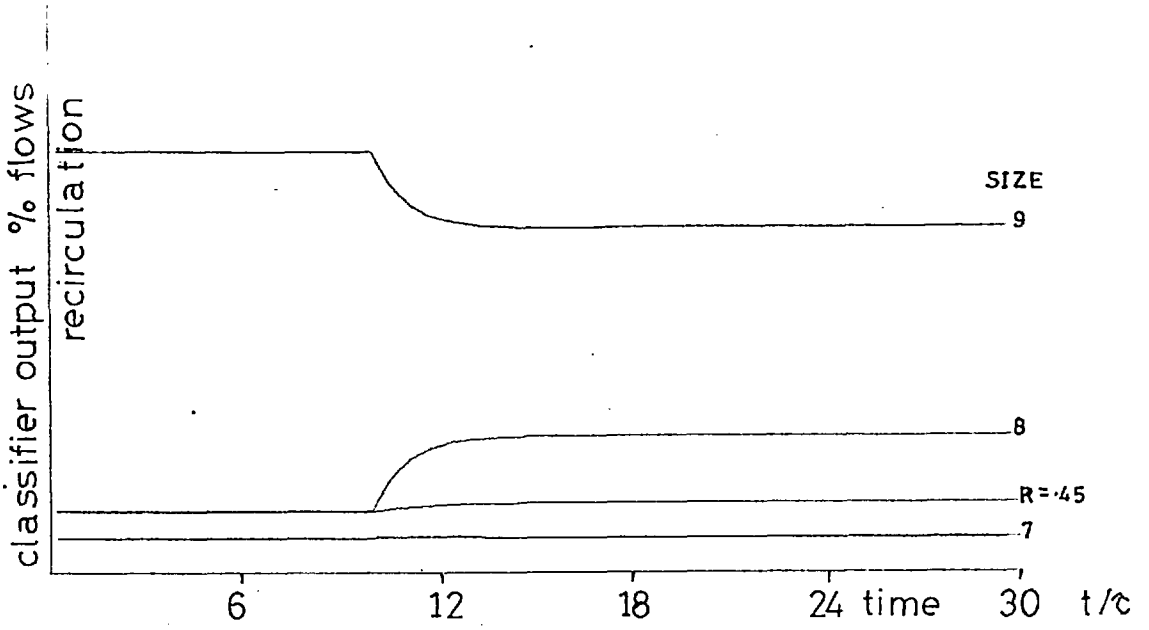
figure 6/48

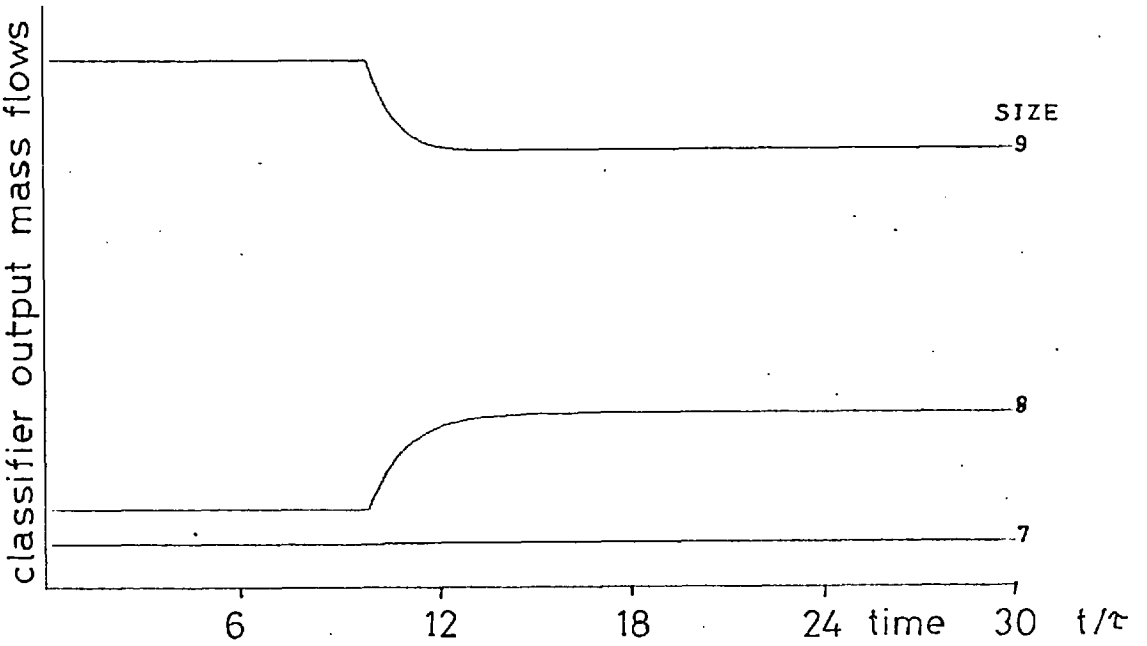


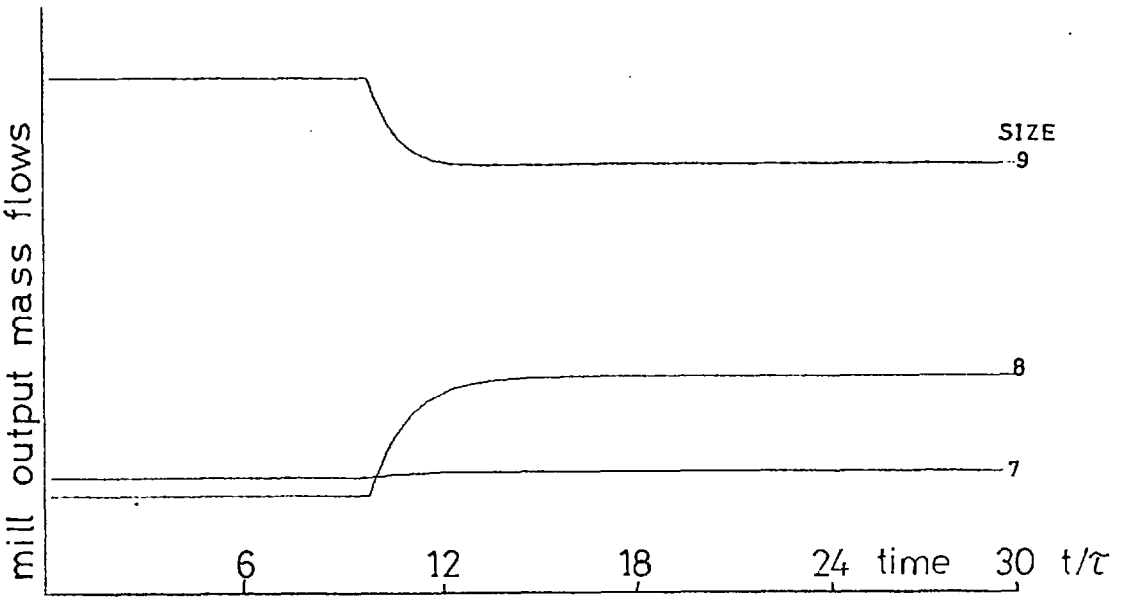




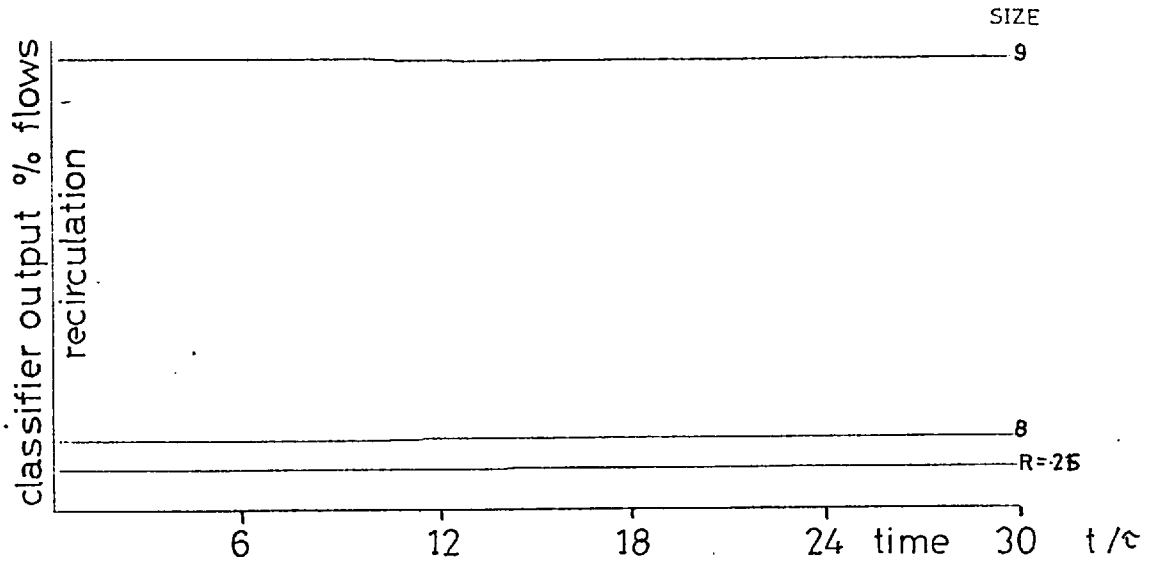
Effect of changing the grindability of size 6 figure 6/49

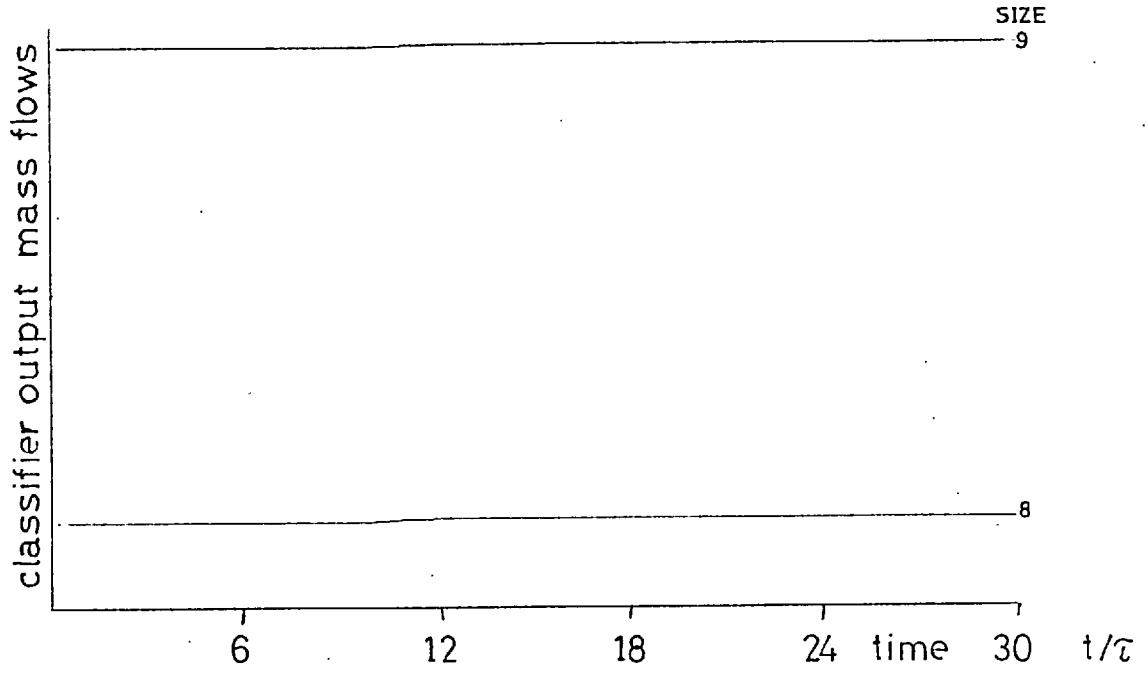


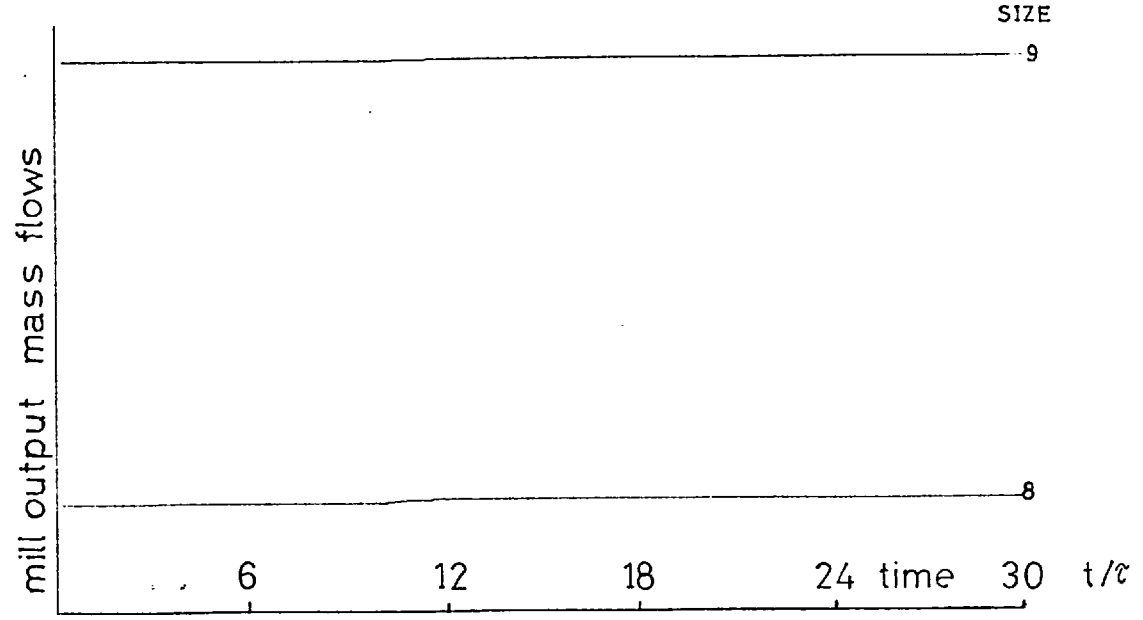




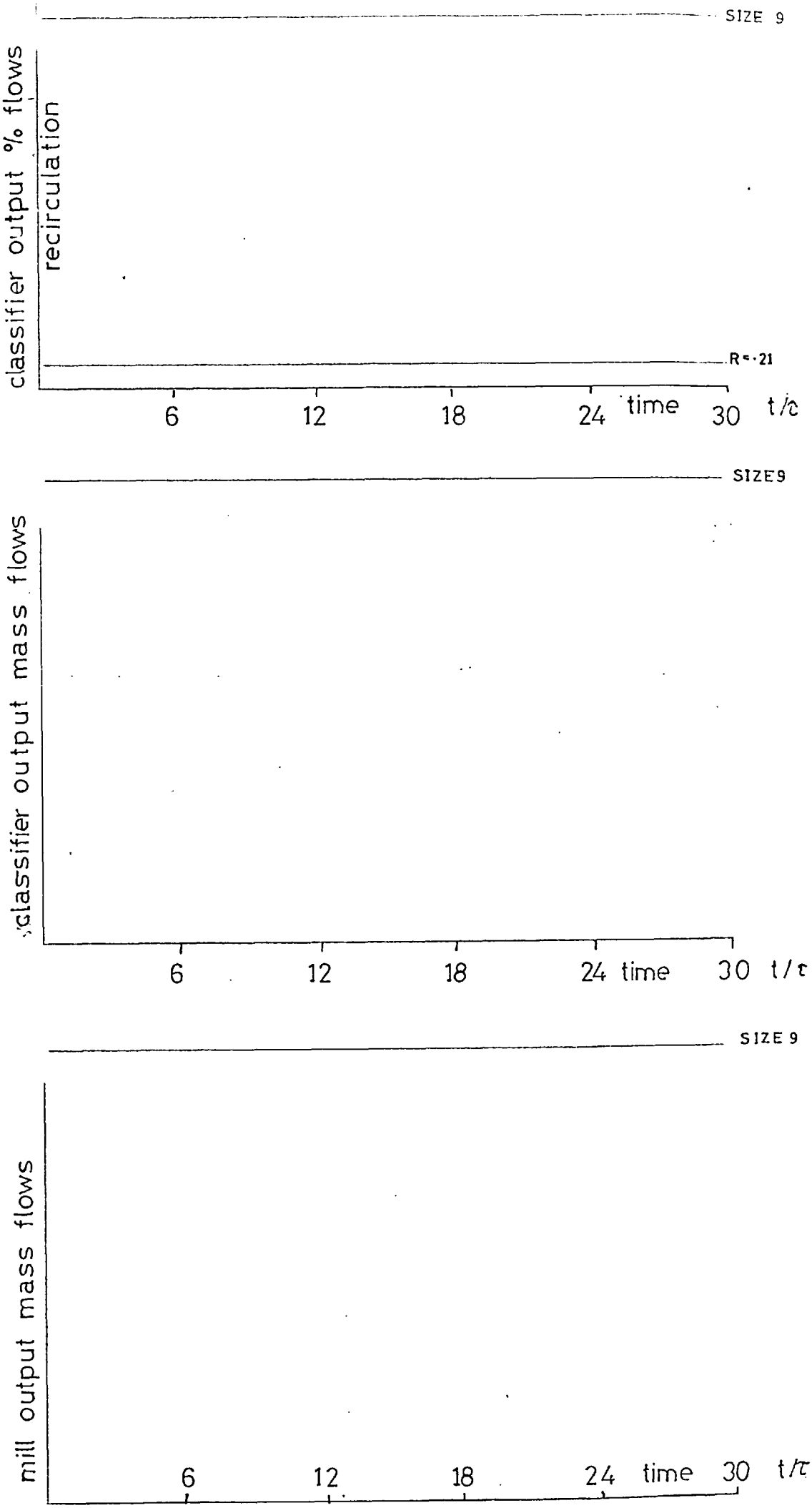
Effect of changing the grindability of size 7 figure 6/50







Effect of changing the grindability of size 8 figure 6/51



Effect of changing the grindability of size 9

figure 6.52

Part 7 - Suggestions for Further Work

7.1 Breakdown of Water

a) Measure time-lags for a range of electrode shapes and sizes with varying conductivity water. Test the theoretical work against these results.

b) Develop a theoretical method to account for the scatter of breakdown time-lags. This could be done by a Monte-Carlo analysis of variations in densities and spark initiation points.

c) Measure time-lags on surfaces and test theory against the results.

d) Test the numerical technique and theory to see if it fits data for other fluids; in particular long air sparks, compressed sulfahexaflouride, and liquid ammonia.

7.2 Discharge Processes

a) Develop a method of theoretically predicting spark pressures on rock surfaces.

b) Develop better pressure measurement techniques, possibly manganin wire gauges, or piezo electric gauges with feedback.

7.3 Stress Analysis

Develop methods of predicting crack paths in dynamic stress

(Continued .....)

conditions. Develop methods of modelling stresses in non-linear materials.

7.4 Comminution

Conduct more crushing experiments and find correlation functions between rock properties and crushing energy. Calculate an energy balance for the whole process.

7.5 Mineral Process Modelling

Measure process tensors for ball mills, flotation cells, etc. Model from fundamental laws a simple process, e.g. dense media separation. Develop control algorithms using the tensor analysis. Study the technique in the Finsler space of metric

$$\delta s = \sum_{\text{all } i} \delta x_i$$

Appendix 1

Apparatus for Measuring Breakdown Time Lags

The apparatus for measuring breakdown times is essentially in four parts:

The charging control unit

The high voltage circuit

The electrodes

The measurement equipment

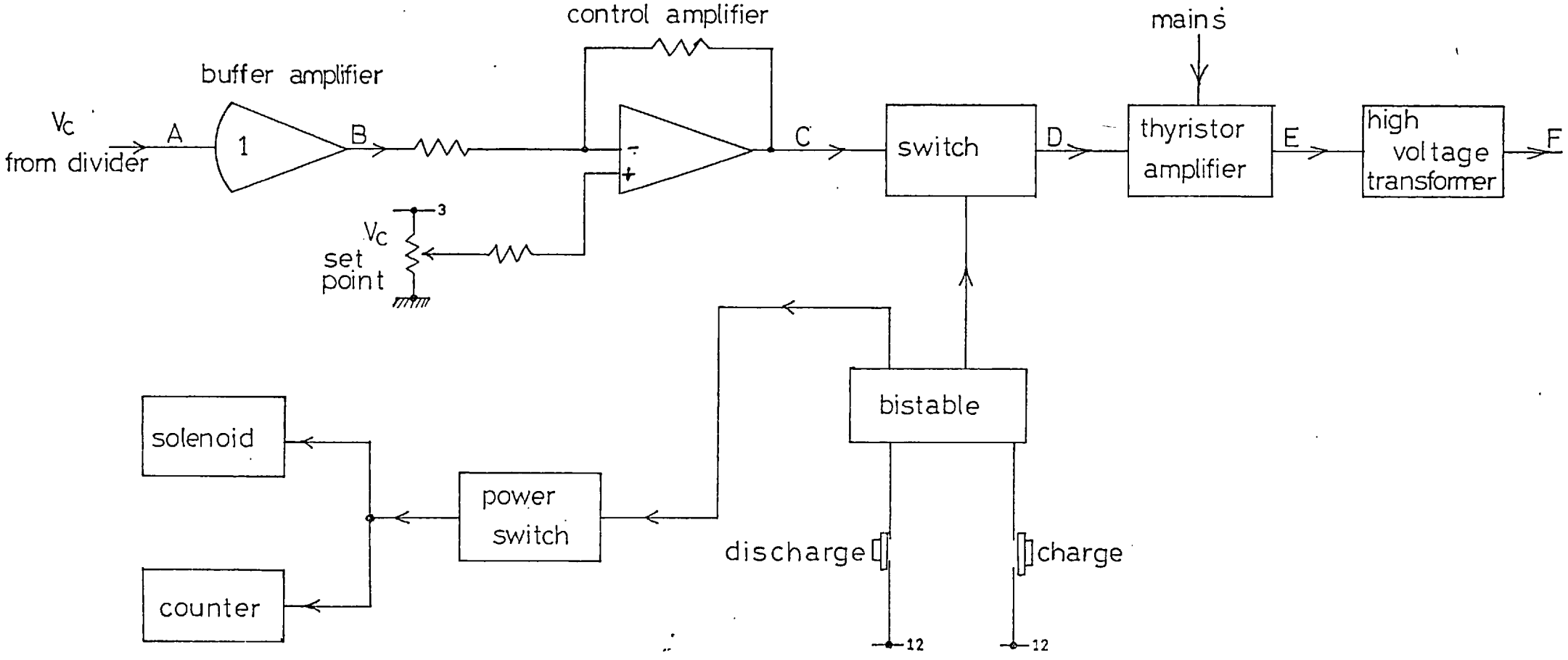
Each of these will be considered in turn.

The Charging Control Unit

The charging control unit is shown diagramatically in Figure A1/1.

When the charge button is pressed the bistable changes state and the switch closes. The thyristor controller is turned hard on and the transformer rectifier begins charging the capacitor. Vc rises and so the output of the buffer amplifier rises. This causes the output of the error amplifier to decrease, and this reduces the signal to the thyristor controller. When Vc has reached its set value the thyristor controller is shut off. The loop ABCDEF forms a feedback loop around the capacitor keeping its voltage accurately at the set point. The maximum fluctuation observed from the set point was 50 Volts which in comparison with the set point of 40 KV is negligible (.12%). The bistable state change also causes the solenoid of the auxiliary gap to rise and the counter to count one.

(Continued .....)



Block diagram of charging control unit

figure A1/1

When the discharge button is pressed the thyristor is switched off and the charging stops. The solenoid closes and fires the gap.

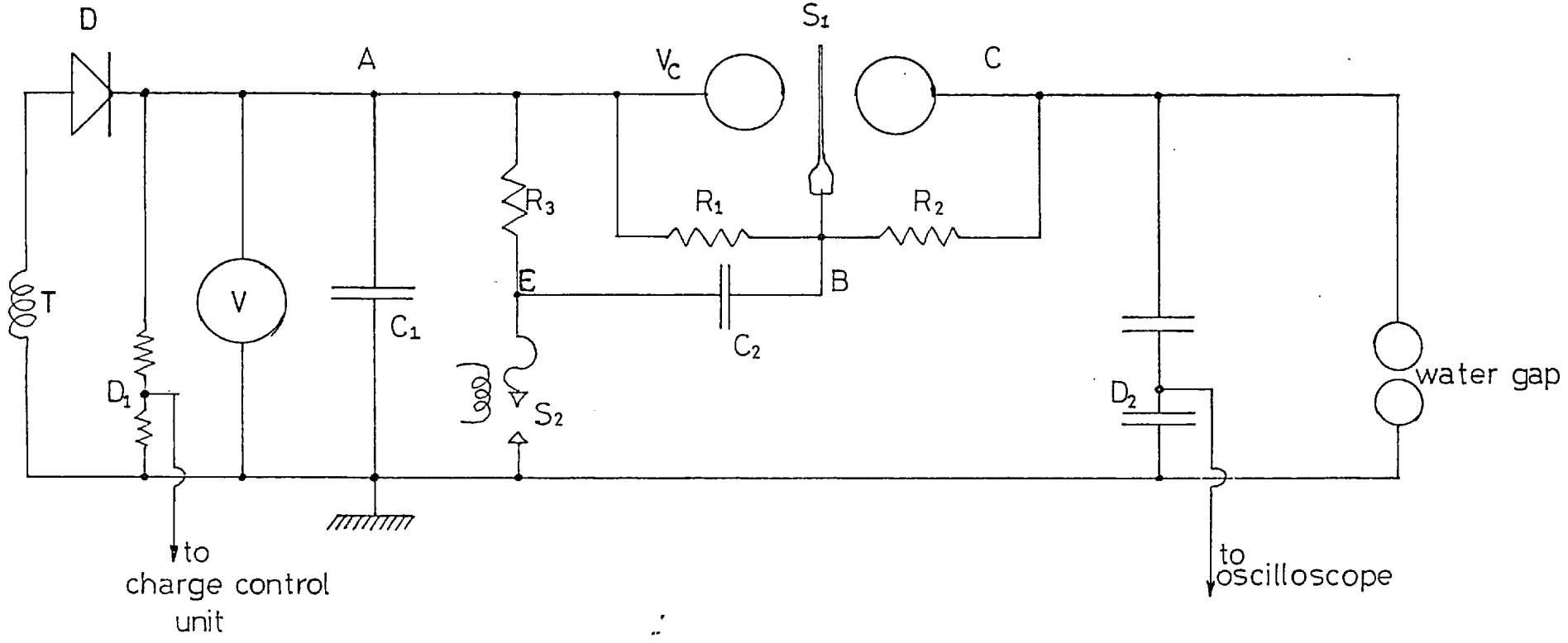
The High Voltage Circuit

The high voltage circuit is shown in Figure A1/2. The capacitor C_1 is charged by the transformer rectifier set T D, the input to the transformer coming from the thyristor output stage of the charge control unit. The current is limited by the output impedance of the transformer. The capacitor voltage is reduced by divider D_1 and fed back to the charging control unit. The discharge gap S_1 is a field distortion gap consisting of two spheres with a spike centrally placed on an equipotential line. The spike voltage is held to the value of its equipotential ($\frac{1}{2}V_c$) by the divider R_1 R_2. The other end of the pulse capacitor C_2 is charged to V_c by resistor R_3. When the discharge button is pressed a solenoid drops, giving the auxiliary gap S_2, and a pulse of magnitude $-V_c$ is passed to the spike via capacitor C_2. The potential between sphere and spike changes from $\frac{1}{2}V_c$ to $1\frac{1}{2}V_c$ and the sphere-spike gap is ignited. The spike potential rapidly rises to V_c and the second part of the gap is also ignited. The potential at point C then rises to V_c rapidly, sending a pulse to the measurement system via divider D_2, and supplying the full voltage to the water gap electrodes. The water gap, after a time lag, breaks down and capacitor C_1 is discharged.

The Electrode System

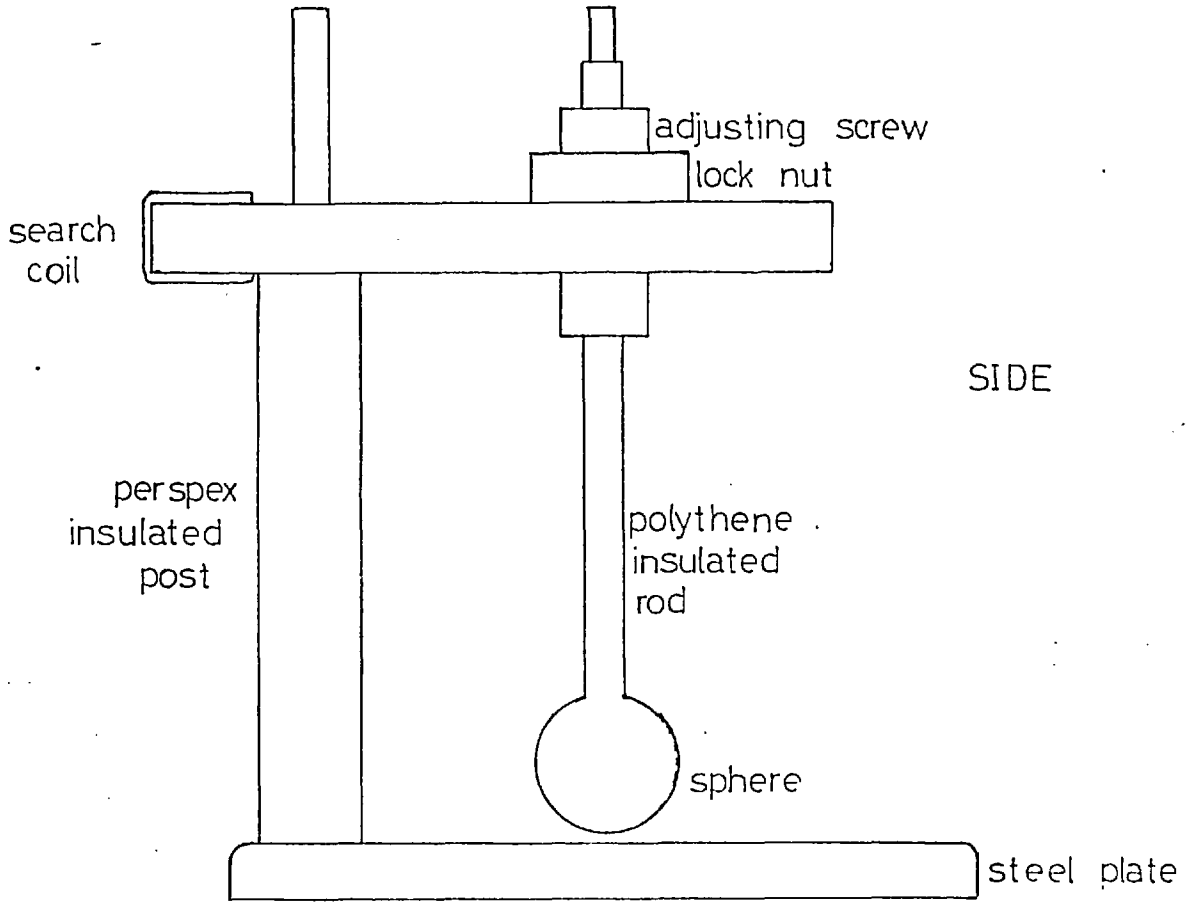
The electrodes are shown in Figure A1/3. They consist of a mild steel sphere and a mild steel plate. Near to the return conductor is a three turn search coil which is used to time the

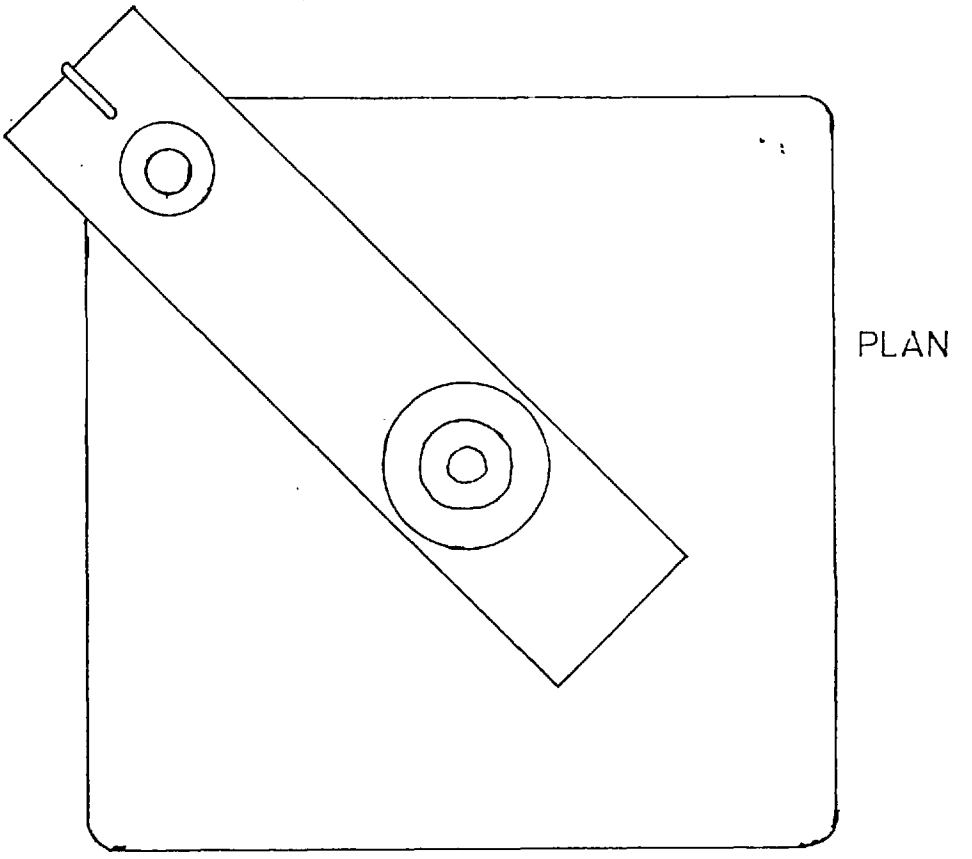
(Continued .....)



High voltage circuit

figure A1/2





Sphere plane electrode system

figure A1/3

discharge.

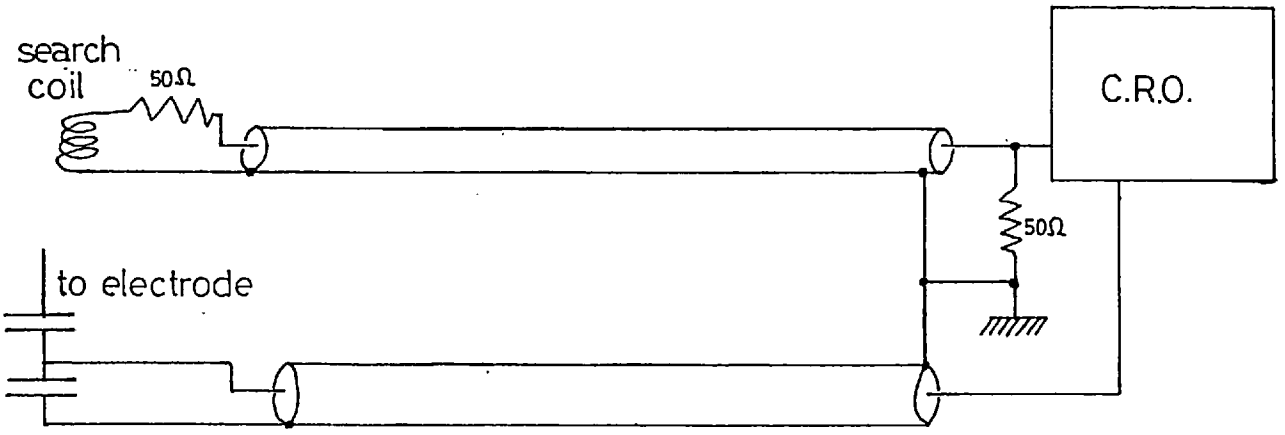
The Measurement System

a) Voltage

The capacitor voltage is measured by a Miles High volt divider and an AVO Digital Voltmeter; the overall accuracy is = ·1%.

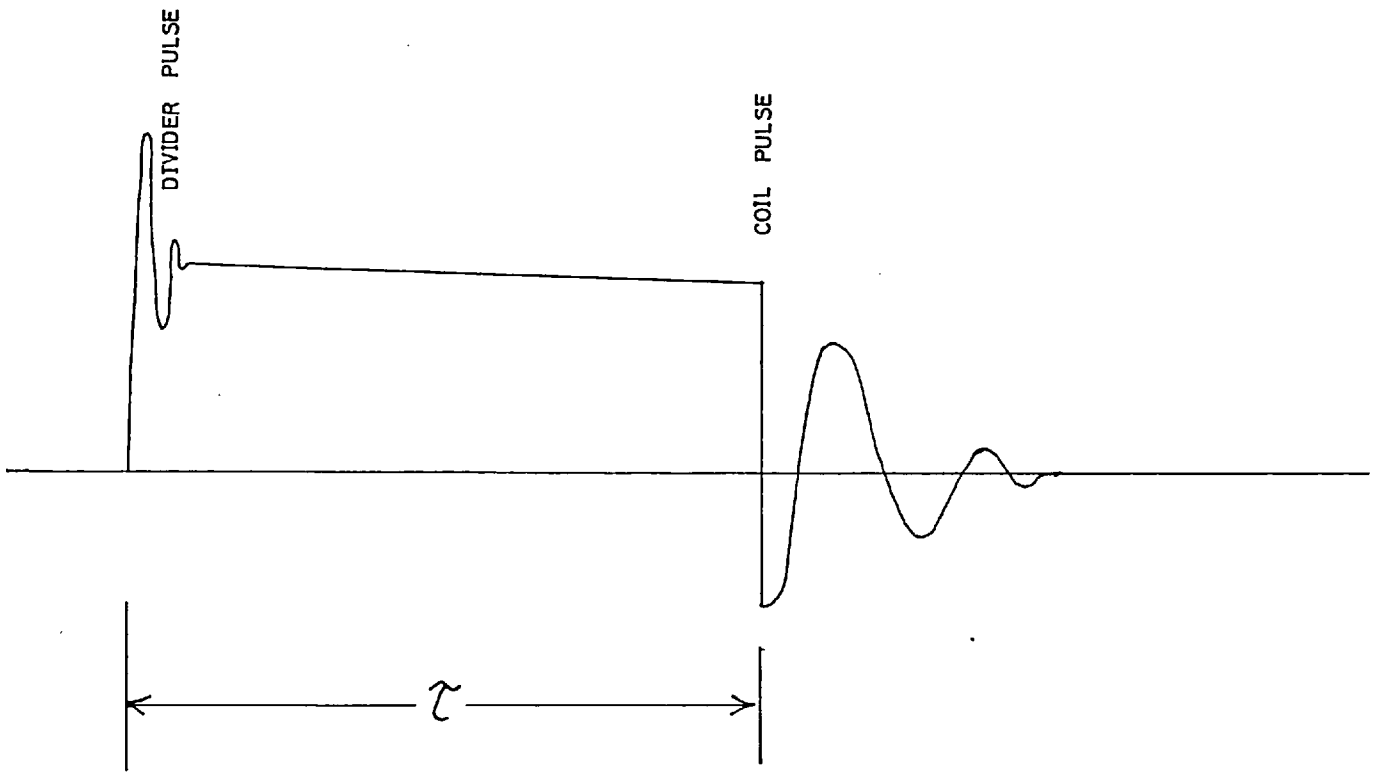
b) Breakdown Time

The output of the pulse divider (D_2 in Figure A1/2) and the output of the search coil (see Figure A1/3) are fed into a Tectronix type CA plug-in, summed and displayed on a Tectronic type 549 storage oscilloscope. The measurement circuit is shown in Figure A1/4. The resistors are used to match the search coil to the cable thus eliminating cable ringing. A typical oscillogram is sketched in Figure A1/5 showing the pulse from the divider and the search coil pulse.



Measuring circuit

figure A1/4



Typical oscillogram

figure A1/5

Appendix 2

A Model for the Breakdown Time-Lags in Water

1. Introduction

This appendix discusses a physical model for the breakdown of water. The mathematical method used to calculate the breakdown time is described and the discrepancy between predicted and experimental values evaluated statistically.

2. Physical Assumptions

a) It is assumed that water consists of positive and negative ions moving in an environment of water molecules. The ions will move under the action of the field.

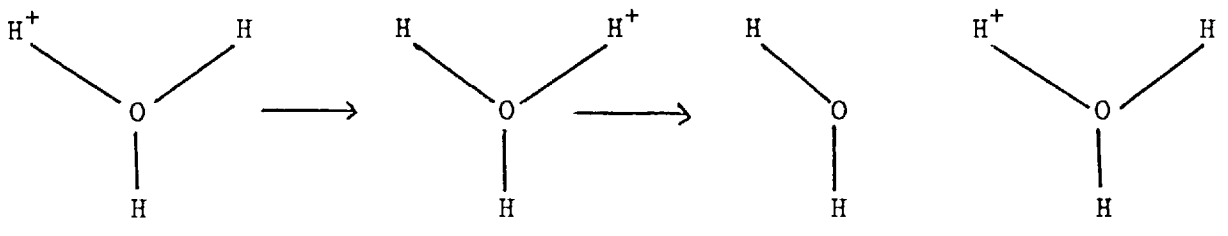
$$v_+ = \mu_+ E \qquad v_- = \mu_- E$$

v = velocity of ion

μ = mobility of ion

E = field

As the ion species are not known values for μ_+ and μ_- were taken as the observed values for H^+ and OH^- (reference 155). These values are much lower than those theoretically calculated and it is speculated that the H^+ ion mass as an H_3O^+ or $H_9O_4^+$



(Continued .....)

the charge "hopping" from molecule to molecule. Similar mechanisms are postulated for the negative ion.

It was assumed that all positive ion species have the observed H^+ mobility and that all negative ion species have the observed OH^- mobility.

b) It is assumed that the electric potential in the water is everywhere determined by Poissons Equation

$$\nabla^2 V = \frac{-\rho}{t_o t_r}$$

V = voltage

ρ = unbalanced charge density

t_o = permettivity of free space

t_r = dielectric constant of water

∇^2 = Laplacian Operator

This implies that the current is low; a good assumption until breakdown occurs.

c) The initial ion densities are calculated from the equations:

$$\sigma = (\rho^+ \mu_+ + \rho^- \mu_-)e$$

(equation of conductivity)

and $\rho^+ = \rho^-$

(space charge neutrality)

ρ^+ = density positive ions

ρ^- = density negative ions

σ = initial water conductivity

e = electronic charge

(Continued .....)

d) It is assumed that when an ion reaches a boundary it forms part of the streamer. The streamer is assumed to be perfectly conducting i.e. that the streamer has the same potential as the electrode. The streamer is assumed to be of constant ion density throughout the process, i.e. that each ion that joins the streamer adds a constant volume to the streamer. The number of ions per unit volume at the positive electrode was assumed to be twice the number per unit volume at the negative electrode so that in a uniform field the positive streamer moves twice as fast as the negative. It was found that the assumptions about the streamers had little effect on the results.

e) As the ions move in the water they will collide with water molecules. It is assumed that some of these collisions will cause further ionisation. It is also assumed that the number of new ions generated is given by the equation:

$$n^+ = n^- = \beta \frac{W}{W_i}$$

n^+ = no. of new +ve ions

n^- = no. of new -ve ions

W = energy dissipated in collisions

W_i = energy needed to break a water molecule

β = constant

The assumption that n is proportional to W is valid as W determines the total number of collisions. The assumption that β is constant however is not strictly valid as the proportion of collisions which generate new ions will depend on the field, and the proportions of various ion species. However to generate a more accurate function

(Continued .....)

requires data which is not available. This assumption is the major cause of the error in fitting between predicted and experimental results. The value of β was determined by a best-fit method.

3. Mathematical Method

The programme main flow sheet is shown in Figure A2/1. Each of the subroutines will be discussed. The full programme is given at the end of this appendix with a table of variables - table A2/1.

a) Main Programme

This part of the programme controls the sequence of operations. First it sets up a voltage to be tested, then it initializes all the variables. It then simulates the process until breakdown occurs when it stores the breakdown time. It then tests a new value for the voltage. When all the voltages have been tested a table of time-lags is printed.

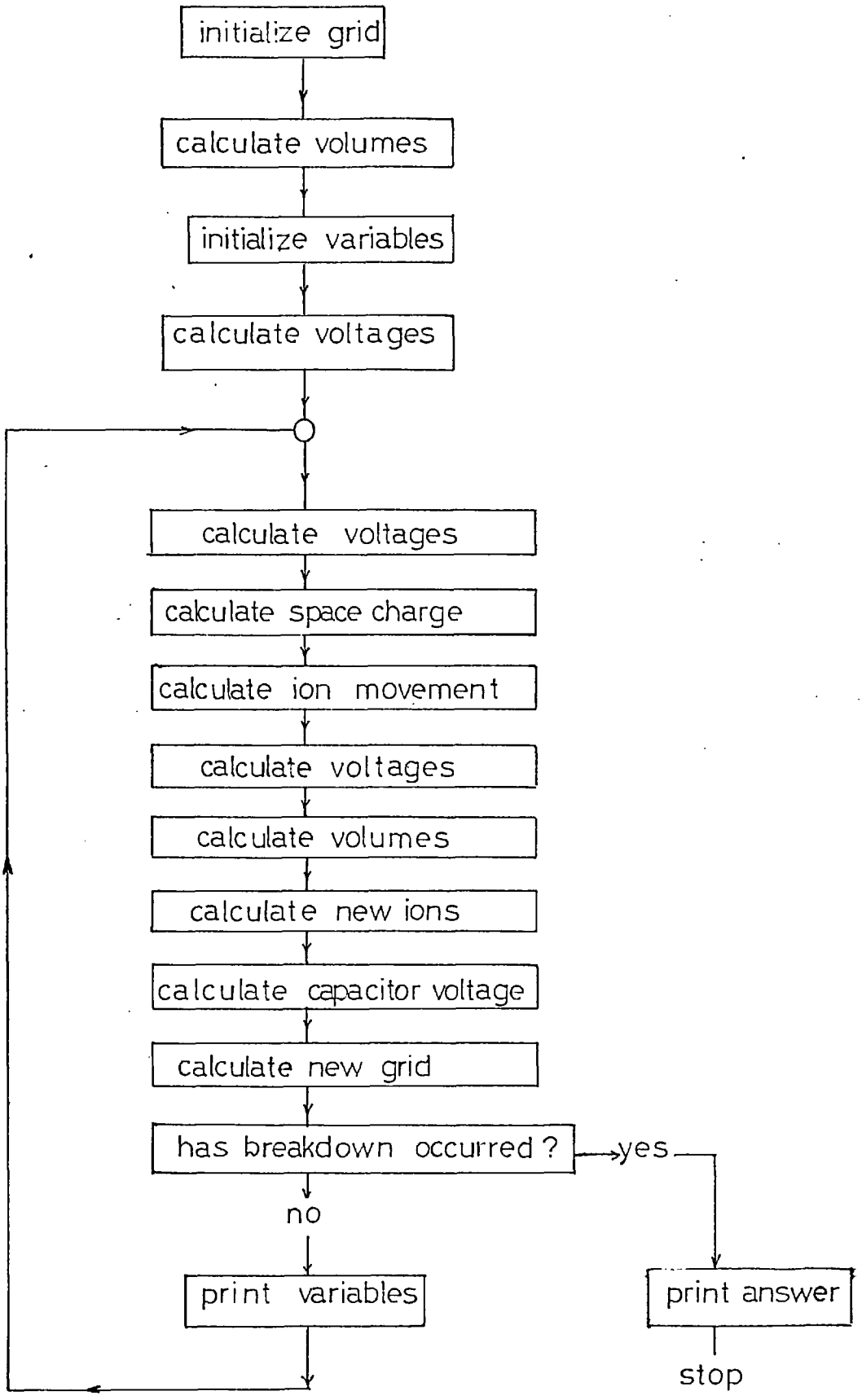
b) Subroutine Gnit

This subroutine sets up the initial grid, the upper electrode is spherical. The axial grid lines are at constant interval; M = 1, corresponding to the axis of symmetry. The axial grid lines are divided into equal parts giving the grid shown in Figure A2/2A.

c) Subroutine Init

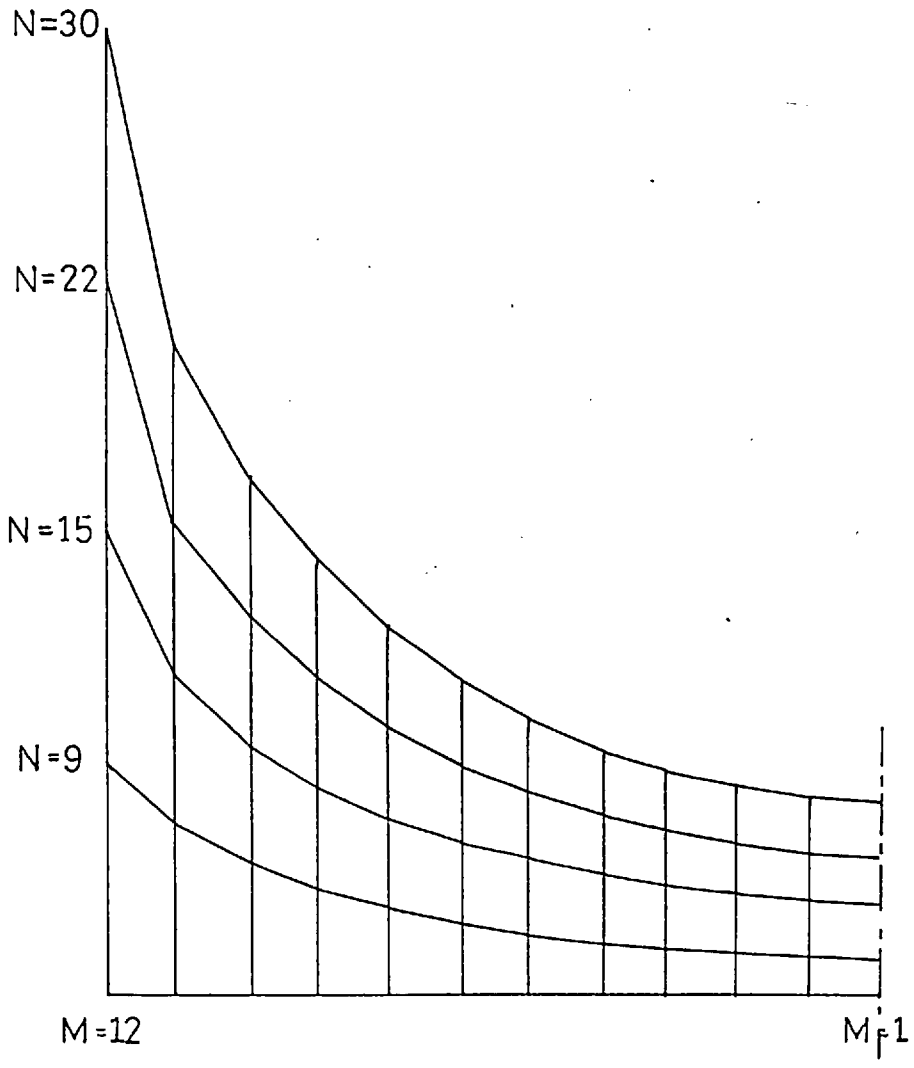
This routine initializes all the variables, gives values for

(Continued .....)



Water programme flow chart

figure A2/1



Grid for water program (not all N lines are shown)

figure A2/2A

constants and makes a first guess for the voltages.

d) Subroutine Volt

This routine calculates the voltages; it uses the following iterative technique.

As the field is defined in circular cylindrical coordinates Poisson's Equation becomes

$$\frac{\rho}{t_o t_r} = \frac{\partial^2 V}{\partial r^2} + \frac{1}{r}\frac{\partial v}{\partial r} + \frac{1}{r^2}\frac{\partial^2 \phi}{\partial \psi^2} + \frac{\partial^2 \phi}{\partial z^2}$$

$$\frac{\partial^2 \phi}{\partial \psi^2} = 0 \quad \text{as the field is symmetrical}$$

Consider the grid in figure A2/2B

$$\frac{\partial^2 V}{\partial r^2} \simeq \frac{\dfrac{V(M+1,N) - V(M,N)}{XUP(M+1) - XUP(M)} - \dfrac{V(M,N) - V(M-1,N)}{XUP(M+1) - XUP(M)}}{(XUP(M+1) - XUP(M-1))/2}$$

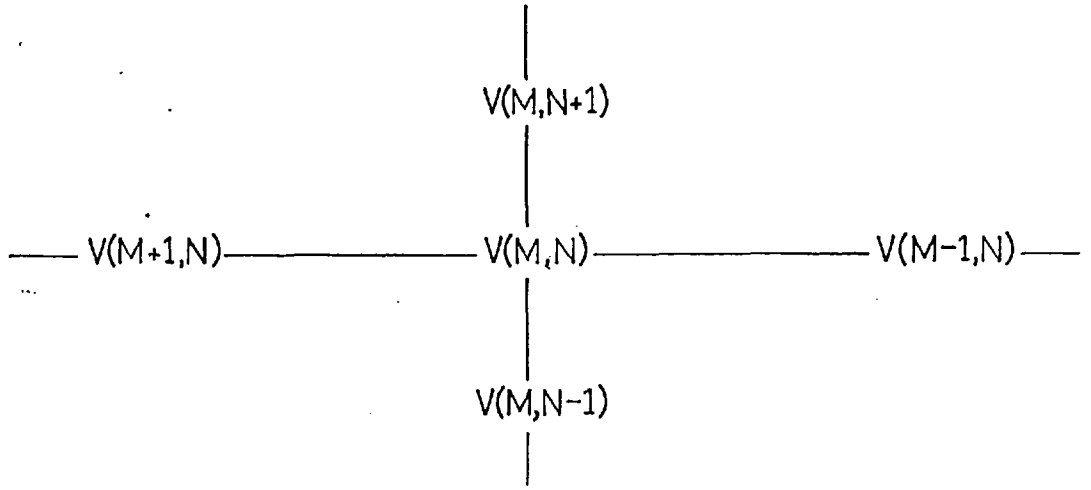
$$\frac{1}{r}\frac{\partial v}{\partial r} = \frac{1}{XUP(M)}\left(\frac{V(M+1) - V(M-1,N)}{XUP(M+1) - XUP(M-1)}\right)$$

$$\frac{\partial^2 \phi}{\partial z^2} = \frac{\dfrac{V(M,N+1) - V(M,N)}{Y(M,N+1) - Y(M,N)} - \dfrac{V(M,N) - V(M,N-1)}{Y(M,N) - Y(M,N-1)}}{(Y(M,N+1) - Y(M,N-1))/2}$$

$$\frac{\rho}{t_o t_r} = \frac{PN(M,N) - PP(M,N)}{VOL(M,N) * EATA * CAPPA} = P(M,N)$$

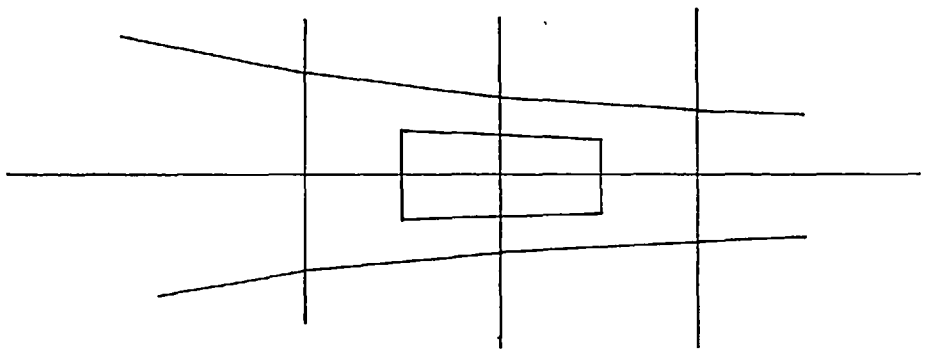
Poissons equation can then be expressed in the form

(Continued .....)



Section of grid

figure A2/2B



Area of grid element

figure A2/3

$$V(M,N) = \alpha P(M,N) + \beta\ V(M+1,N) + \gamma\ V(M-1,N) + \delta\ V(M,N+1) + \eta\ V(M,N-1)$$

This forms the basis for an iteration.

The iteration is speeded up by using updated values for V(M + 1,N) etc., and is also over-relaxed by:

$$V(M,N) = 1{\cdot}5\ (\alpha P(M,N) + \ldots\ldots\ \eta\ V(M,N-1)\ ) - {\cdot}5_{*}\ V(M,N)$$

This was found to give very rapid convergence.

The iteration is stopped when the change in V(1,2) and V(1,29) is small. These two voltages are the ones which change the most as calculation proceeds.

e) Subroutine Space

As the positive and negative charge mobilities are different a space charge must appear at one electrode to maintain external current balance. It is assumed that this space charge causes a voltage which must be added to the electrode voltage. The space charge voltage is adjusted by an iteration using the method of regula falsi until the external currents are balanced.

f) Subroutine Move

This subroutine calculates the charge movement. It does so by comparing voltages at adjacent grid points. Let V_a and V_b be voltages of adjacent points, then if

(Continued .....)

$V_a > V_b$ +ve charge flows from b to a; and

-ve charge flows from a to b.

and if

$V_b < V_a$ +ve charge flows from a to b; and

-ve charge flows from b to a.

g) Subroutine Volu

This subroutine calculates the element volume. The element volume is assumed to be of area shown in Figure A2/3 and be at radius XUP(M). It also calculates the conversion factor for the unbalanced charge.

h) Subroutine Hot

This routine calculates the new ions generated. As the ion generation rate is high the routine calculates in 10 steps of 1/10 TDEL for greater accuracy.

First the element conductivity is calculated, then the lost energy is calculated from:

$$\frac{\sigma E^2 \tau}{A}$$

σ = conductivity E = field

A = area τ = time

This energy is converted to ions and the loop repeated.

i) Subroutine Cap

This routine calculates the new capacitor voltage by reducing its charge by the current taken by the gap multiplied by the time

(Continued .....)

increment.

j) Subroutine Gnew

This routine generates the new grid. First the streamer displacement is calculated by adding on the volume of the ions which have joined each annulus of the streamer. Then the grid is adjusted to fit the new space. It is assumed that this grid movement (which is small) does not effect the ion densities at the grid point. This is unlikely to cause large errors as the ion densities are nearly constant throughout the volume except near the boundaries.

k) Subroutine Tripa

This routine prints values of various quantities at each iteration.

Stability

The programme was found to be stable and gave the same results over a wide range of grid sizes and time increments provided that the time increment was small in comparison with the breakdown time.

Unknown Values

Apart from the usual physical constants the programme requires two values to be given:-

(Continued .....)

1) The volume occupied by an ion in a streamer. This is an effective volume as the ion will also pull in water molecules. A value of

DEX = 2.5×10^{16} ions/cc was chosen.

This assumes either

The streamer consists only of the ions joining it and the streamer temperature is 3×10^{5} ^{o}k and atmospheric pressure

or the streamer value consists of 1/1,000 part of ions and the rest ions from water molecules at S.T.P.

or any intermediate step.

The value assumed has little effect on the computation accuracy. If it is chosen low then β is also low, if high then β is high.

2) The proportion (β) of energy lost which causes new ions. The value for β was found by a least squares method to be .0000409 at DEX = 2.5×10^{16}. (Reference 155)

Statistical Evaluation of the Results

The following are known:

A set of 4 voltages x_i

A set of 4 predictions y_{ci}

A set of n_i readings at each x_i; y_{oin}

Let $\bar{z}$ be the mean of z

V(z) be the variance of z

(Continued .....)

E(z) be the expected value of z

It is postulated that there are a set of true experimental values y_{ei}

$$y_{ei} = y_{oin} + \text{errors}$$

It is assumed that errors consist of two components:

1) A normally distributed random error

2) A biased error proportional to y_{oin}

Therefore $\bar{y}_{oi} = y_{ei} + \text{mean error}$

$$= y_{ei} + \text{mean random error} + \text{mean bias error}$$

$$= y_{ei} + 0 + \alpha_i \bar{y}_{oi}$$

$$y_{ei} = (1 - \alpha_i) \bar{y}_{oi}$$

The hypothesis is made that

$$y_{ei} = y_{ci} \qquad \text{for each } x_i$$

put $Y_i = y_{ei} - y_{ci}$

Therefore the hypothesis is

$$E(Y_1) = 0$$

$$V(Y_i) = V(y_{ei} - y_{ci})$$

$$= V((1 - \alpha_1) \bar{y}_{oi} - y_{ci})$$

The variance of a sum = sum of the variances and $V(y_{ci}) = 0$

(Continued .....)

$$= \frac{(1 - \alpha_1)^2}{n_i} V(\bar{y}_{oi})$$

$$S = \frac{(1 - \alpha_i)}{\sqrt{n_i}} \sqrt{V(y_{oi})}$$

Form $\chi_i = \frac{Y_i}{S}$ for x_i

$$= \frac{Y_{ei} - Y_{ci}}{(1 - \alpha_1) \frac{1}{\sqrt{n_i}} \sqrt{V(y_{oin})}}$$

$$= \frac{(1 - \alpha_1)\bar{y}_{oi} - y_{ci}}{(1 - \alpha_1) \frac{1}{\sqrt{n_i}} \sqrt{V(y_{oi})}}$$

This statistic has mean 0 and standard deviation 1. It has the properties of the χ^2 distribution.

Therefore compute $\chi^2 = \sum_{i = 1 \to 4} \chi_i^2$

This has 3 degrees of freedom

Values obtained

for an unbiased measurement $\alpha_i = 0$

and $\chi^2 = \cdot 286$

and thus the result has a probability of less than 5% of occurring by chance.

Now the breakdown time-lags at 25kv were measured on a different oscilloscope range and there is a possibility of a calibration difference. If this difference is 5%, $(1 - \alpha) = \cdot 95$

(Continued .....)

and

$$\chi^2 = .18745$$

and the result has a probability of less than 2·5% of occurring by chance.

The predictions are therefore statistically significant at a chance level of 1 in 20 and thus the hypothesis is valid.

Table A2/1

Names Used in the Programme

Name	Type	Where Used	Description
A	real variable	WATER, INIT, VOLT, SPACE, CAP	Capacitor voltage
AAB	real variable	VOLT	Intermediate result
ABAL	real variable	GNEW	Increase in negative streamer length
AH	real variable	HOT	Intermediate result
ALFA	real variable	GNEW	Increase in positive streamer length
ARH	real variable	HOT	Intermediate result
ASET	(4x1) real array	WATER	Voltages to be tested
AXA	real variable	VOLT	Intermediate result
AXB	real variable	VOLT	Intermediate result
BALL	real variable	GNIT	Sphere radius squared
BH	real variable	HOT	Intermediate result
BONK	real variable	HOT, VOLU	Intermediate result
BRH	real variable	HOT	Intermediate result
BURP	real variable	HOT, WATER	Proportion of collisions that cause ionization
CAP	subroutine name	WATER, CAP	Calculates capacitor voltage
CAPPA	real variable	GNIT	Dielectric constant of water
CENT	real variable	SPACE	Normalized error of charge movements across to streamers
CHAR	real variable	INIT, CAP	Charge on capacitor
COD	real variable	INIT, CAP	Capacitance
CON	(30x12) real array	INIT, MOVE, VOLU	Converts unbalanced charge density to effective potential

(Continued .....)

Name	Type	Where Used	Description
COND	real variable	HOT	Conductivity
CUR	real variable	INIT, SPACE, CAP, TRIPA	Current
DELA	real variable	GNEW	Intermediate result
DELB	real variable	GNEW	Intermediate result
DENS	real variable	INIT	Initial ion density
DEX	real variable	GNEW	Plasma number density in positive streamer
DEY	real variable	GNEW, WATER	Plasma number density in negative streamer
DN	(30x12) real array	MOVE	change in -ve ion numbers
DNI	12x1 real array	SPACE, GNEW	Charge joining +ve streamer
DNNN	real variable	SPACE	Total charge joining +ve streamer
DP	(30x12) real array	MOVE	Change in +ve ion numbers
DPI	(12x1) real array	SPACE, GNEW	Charge joining -ve streamer
DPPP	real variable	SPACE	Total charge joining -ve streamer
EATA	real variable	GNIT	Permitivity of free space
EHYD	(12x1) real array	GNEW	Number of positive ions in streamer
ELECT	real variable	GNIT, INIT, SPACE, HOT	Electronic charge
EMOB	real variable	INIT, SPACE, HOT	Negative ion mobility
EOXY	(12x1) real array	GNEW	Number of negative ions in streamer
ERR	real variable	SPACE	ERR in external current balance

(Continued .....)

Name	Type	Where Used	Description
GNEW	Subroutine name	WATER, GNEW	Generates new grid
GNIT	Subroutine name	WATER, GNIT	Generates initial grid
HEAT	real variable	HOT	Number of new ions
HOT	Subroutine name	WATER, HOT	Calculates number of new ions
ICALC	4x1 integer array	WATER	Calculated breakdown time
INIT	Subroutine name	WATER, INIT	Initializes variables
J	Integer	SPACE	Flag that notes if excess charge is positive or negative
JUMBO	Integer	WATER, GNEW	Flag that notes if breakdown has occurred
M	Integer	All subroutines	Radial coordinate
MOVE	Subroutine name	WATER, MOVE	Calculates charge movement
N	Integer	All subroutines	Axial coordinate
NTRIAL	Integer	WATER	Number of test
P	(12x30) real array	INIT, VOLT, MOVE	Effective non neutralized charge
PIE	real variable	GNIT, VOLU	π
PMOB	real variable	INIT, SPACE, HOT	Positive ion mobility
PN	30x12 real array	INIT, SPACE, MOVE, HOT	Number of negative ions
PNAB	real variable	SPACE	Intermediate result
PNN	real variable	SPACE	Intermediate result
PP	30x12 real array	INIT, SPACE, MOVE, HOT	Number of positive ions
PPAB	real variable	SPACE	Intermediate result
PPP	real variable	SPACE	Intermediate result

(Continued .....)

Name	Type	Where Used	Description
PQAB	real variable	SPACE	Intermediate result
PQAN	real variable	SPACE	Intermediate result
SIGMA	real variable	INIT	Water conductivity
SPACE	Subroutine name	WATER, SPACE	Calculates boundary charge movements
SPACN	real variable	SPACE	Space charge voltage on negative electrode
SPACP	real variable	SPACE	Positive streamer space charge voltage
SURO	(12x1) real array	INIT, GNEW	Surface area
TDEL	real variable	All subroutines	Time increment
TESTA	real variable	VOLT	Error in voltage iteration
TEST B	real variable	VOLT	Error in voltage iteration
TOM	real variable	TRIPA, WATER	Total elapsed time
TREND	real variable	SPACE	Intermediate result
TRIPA	Subroutine name	WATER, TRIPA	Controls intermediate printing
UN	real variable	SPACE, MOVE	Intermediate result
UP	real variable	SPACE, MOVE	Intermediate result
V	(12x30) real array	VOLT, INIT, SPACE, MOVE, HOT, TRIPA	Voltage
VAM	real variable	VOLT	Intermediate result
VC	real variable	CAP, INIT	Capacitor voltage
UDEL	real variable	SPACE	Intermediate result
VIM	real variable	VOLT	Intermediate result
VOL	30x12 array	INIT, VOLU, HOT	Element volume
VOLU	Subroutine name	WATER, VOLU	Calculates element volumes

(Continued .....)

Name	Type	Where Used	Description
VOLT	Subroutine name	WATER, VOLT	Calculates voltages
WATER	Programme Name	WATER	Title of programme
XA	real variable	VOLT, MOVE	Intermediate result
XB	real variable	VOLT, MOVE	Intermediate result
XC	real variable	VOLT	Intermediate result
XUP	12x1 array	GNIT, INIT, VOLT, MOVE, VOLU, HOT	Radial grid
Y	30x12 array	GNIT, INIT, VOLT, MOVE, VOLU, HOT, SPACE, GNEW	Axial grid
YA	real variable	VOLT, MOVE	Intermediate result
YB	real variable	VOLT, MOVE	Intermediate result
YO	(12x1) array	GNIT, GNEW	Lower electrode
YC	real variable	VOLT	Intermediate result
YU	(12x1) array	GNIT, GNEW	Upper electrode
ZETA	real variable	GNIT, VOLU	Intermediate result
ZING	real variable	HOT	Intermediate result
ZOB	(30x12) array	VOLT	Weighting factors
ZXA	(30x12) array	VOLT	Weighting factors
ZXB	(30x12) array	VOLT	Weighting factors
ZYA	(30x12) array	VOLT	Weighting factors
ZYB	(30x12) array	VOLT	Weighting factors

```
JOB(U%CK012,J12,CM20000,T300)                    HASKELL          WATER
FUN(S,,,,,,11610)
LGO.
,
      PROGRAMWATER(INPUT,OUTPUT,TAPE5=INPUT,TAPE6=OUTPUT)
      COMMONY(12,30),VOL(12,30),CON(12,30),YO(12),YU(12),PMOB,EMOB,
     1TDEL,A,V(12,30),P(12,30),PP(12,30),PN(12,30),DPPP,DNNN,CUR,CHAR,
     2COD,BURP     ,ELECT,VC,    EATA,CAPPA,PIE,DPI(12),DNI(12),XUP(12),
     3SPACP,SPACN,SURO(12),EHYD(12),EOXY(12),ITIM,JUMBO,       UN,UP,
     4ZETA,ZXA(12),ZXB(12),ZYA(12,30),ZYB(12,30),ZOB(12,30),TOM
      DIMENSION ASET(4),ICALC(4)
C
C     THIS PROGRAM IS DESIGNED TO COMPUTE THE BREAKDOWN PROPERTIES OF
C        WATER
C
C
C
      DO 2005 NTRIAL=1,4
      A=NTRIAL*5000.+20000.
      ASET(NTRIAL)=A
      WRITE(6,1101)
      TOM=0.
      JUMBO=0
      CALL GNIT
      CALL VOLU
      CALL INIT
      CALL VOLT
      CALL TRIPA
      TOM=0.
 2002 CONTINUE
      CALL VOLT
      CALL SPACE
      CALL MOVE
      CALL VOLT
      CALL VOLU
      CALL HOT
      CALL CAP
      CALL GNEW
      IF(JUMBO.EQ.1)GOTO 2004
      CALL TRIPA
      GOTO2002
 2004 CONTINUE
      ICALC(NTRIAL)=ITIM
 2005 CONTINUE
      WRITE(6,2006)DEY,BURP
      DO 2007 NTRIAL=1,4
      WRITE(6,2008)ASET(NTRIAL),ICALC(NTRIAL)
 2007 CONTINUE
 1101 FORMAT(6X,4HTIME,6X,11HSPACE VOLTS,5X,7HCURRENT,5X,
     113HDISPLACEMENTS,10X,8HVOLTAGES)
 2006 FORMAT(//////,25X,4HDEY=,E10.6,10X,5HBURP=,E10.6)
 2008 FORMAT(//,25X,2HA=,F10.4,10X,5HTIME=,I8)
      STOP
      END
```

```
      SUBROUTINE GNIT
      COMMONY(12,30),VOL(12,30),CON(12,30),YO(12),YU(12),PMOB,EMOB,
     1TDEL,A,V(12,30),P(12,30),PP(12,30),PN(12,30),DPPP,DNNN,CUR,CHAR,
     2COD,BURP     ,ELECT,VC,    EATA,CAPPA,PIE,DPI(12),DNI(12),XUP(12),
     3SPACP,SPACN,SURO(12),EHYD(12),EOXY(12),ITIM,JUMBO,       UN,UP,
     4ZETA,ZXA(12),ZXB(12),ZYA(12,30),ZYB(12,30),ZOB(12,30),TOM
C
C      THIS ROUTINE CALCULATES THE STARTING POINTS FOR THE GRID
C       1 INCH DIAMETER SPHERE
C
       BALL=1.27*1.27
      PIE=3.14159
      EATA=8.8546E-10
      CAPPA=80
      ELECT=1.6021E-19
      ZETA=EATA*CAPPA/ELECT
      DO 301 M=1,12
      XUP(M)=(M-1)*.1152
      YO(M)=0.
      YU(M)=1.582-SQRT(BALL-XUP(M)*XUP(M))
      YP=(YU(M)-YO(M))/29.
      DO 301 N=1,30
      Y(M,N)=((N-1)*YP)+YO(M)
  301 CONTINUE
      RETURN
      END
```

```
      SUBROUTINE INIT
      COMMONY(12,30),VOL(12,30),CON(12,30),YO(12),YU(12),PMOB,EMOB,
     1TDEL,A,V(12,30),P(12,30),PP(12,30),PN(12,30),DPPP,DNNN,CUR,CHAR,
     2COD,BURP     ,ELECT,VC,    EATA,CAPPA,PIE,DPI(12),DNI(12),XUP(12),
     3SPACP,SPACN,SURO(12),EHYD(12),EOXY(12),ITIM,JUMBO,       UN,UP,
     4ZETA,ZXA(12),ZXB(12),ZYA(12,30),ZYB(12,30),ZOB(12,30),TOM
C
C     THIS ROUTINE INITIALISES ALL THE VALUES
C
      PMOB=.00362
      EMOB=.00198
      SIGMA=.000012
      DENS=SIGMA/(ELECT*(PMOB+EMOB))
      DPPP=0.
      DNNN=0.
      TDEL=1.0E-7
      COD=.0000005
      CHAR=COD*A
      CUR=0.
      VC=A
      DO 325 M=1,12
      DO 325 N=1,30
      V(M,N)=14000.*N
  325 CONTINUE
      DO 326 N=2,29
      DO 326 M=1,12
      PN(M,N)=-DENS*VOL(M,N)
      PP(M,N)=DENS*VOL(M,N)
      P(M,N)=(PP(M,N)+PN(M,N))/CON(M,N)
  326 CONTINUE
      DO 327 M=1,12
      SURO(M)=(XUP(M)+XUP(M+1))*PIE*(XUP(M+1)-XUP(M))
      EHYD(M)=0.
      EOXY(M)=0.
      PP(M,1)=0.
      PN(M,1)=0.
      P(M,1)=0.
      P(M,30)=0.
      PP(M,30)=0.
      PN(M,30)=0.
  327 CONTINUE
      RETURN
      END
```

```
      SUBROUTINE VOLT
      COMMONY(12,30),VOL(12,30),CON(12,30),YO(12),YU(12),PMOB,EMOB,
     1TDEL,A,V(12,30),P(12,30),PP(12,30),PN(12,30),DPPP,DNNN,CUR,CHAR,
     2COD,BURP     ,ELECT,VC,    EATA,CAPPA,PIE,DPI(12),DNI(12),XUP(12),
     3SPACP,SPACN,SURO(12),EHYD(12),EOXY(12),ITIM,JUMBO,       UN,UP,
     4ZETA,ZXA(12),ZXB(12),ZYA(12,30),ZYB(12,30),ZOB(12,30),TOM
C
C     THIS ROUTINE CALCULATES ALL THE VOLTAGES
C
      DO207 M=2,11
      XA=XUP(M)-XUP(M-1)
      XB=XUP(M+1)-XUP(M)
      XC=(XA+XB)/2.
      AAB=.5/(XUP(M)*XC)
      AXA=1./(XA*XC)
      AXB=1./(XB*XC)
      ZXA(M)=AXA-AAB
      ZXB(M)=AXB+AAB
      DO207N=2,29
      YA=Y(M,N)-Y(M,N-1)
      YB=Y(M,N+1)-Y(M,N)
      YC=(YA+YB)/2.
      ZYA(M,N)=1./(YA*YC)
      ZYB(M,N)=1./(YB*YC)
      ZOB(M,N)=1.5/(AXA+AXB+ZYA(M,N)+ZYB(M,N))
  207 CONTINUE
      XB=XUP(2)-XUP(1)
      ZXB(1)=1./XB
      DO208N=2,29
      YA=Y(1,N)-Y(1,N-1)
      YB=Y(1,N+1)-Y(1,N)
      ZYA(1,N)=1./YA
      ZYB(1,N)=1./YB
      ZOB(1,N)=1.5/(ZXB(1)+ZXB(1)+ZYA(1,N)+ZYB(1,N))
  208 CONTINUE
      VAM=0.
      VIM=0.
      DO 202 M=1,12
      V(M,1)=0.
      V(M,30)=A
  202 CONTINUE
  200 CONTINUE
      DO201M=2,11
      DO201 N=2,29
      V(M,N)=ZOB(M,N)*(ZXA(M)*V(M-1,N)+ZXB(M)*V(M+1,N)+ZYA(M,N)*V(M,N-1
     1+ZYB(M,N)*V(M,N+1)+P(M,N))-.5*V(M,N)
  201 CONTINUE
      DO205N=2,29
      V(1,N)=ZOB(1,N)*(ZXB(1)*(V(2,N)+V(2,N))+ZYA(1,N)*V(1,N-1)+ZYB(1,N
R     1*V(1,N+1)+P(1,N))-V(1,N)*.5
  205 CONTINUE
      DO 206 N=2,29
      V(12,N)=V(11,N)+V(11,N)-V(10,N)
  206 CONTINUE
       TESTA=ABS(V(1,2)-VAM)
      TESTB=ABS(V(1,29)-VIM)
      VIM=V(1,29)
      VAM=V(1,2)
      IF(TESTA.GT.0.01)GOTO200
```

```
      SUBROUTINE SPACE
      COMMONY(12,30),VOL(12,30),CON(12,30),YO(12),YU(12),PMOB,EMOB,
     1TDEL,A,V(12,30),P(12,30),PP(12,30),PN(12,30),DPPP,DNNN,CUR,CHAR,
     2COD,BURP     ,ELECT,VC,    EATA,CAPPA,PIE,DPI(12),DNI(12),XUP(12),
     3SPACP,SPACN,SURO(12),EHYD(12),EOXY(12),ITIM,JUMBO,       UN,UP,
     4ZETA,ZXA(12),ZXB(12),ZYA(12,30),ZYB(12,30),ZOB(12,30),TOM
C
C     THIS ROUTINE CALCULATES THE CHARGE CROSSING THE BOUNDARY AND THE
C     SPACE CHARGE VOLTAGES
C
      UN=EMOB*TDEL
       UP=PMOB*TDEL
      J=0
  458 CONTINUE
      DO452M=1,12
      DNI(M)=0.
      DPI(M)=0.
  452 CONTINUE
      DO 451 M=1,12
      IF(V(M,29).GT.V(M,30)) GOTO 450
      DNI(M)=UN*PN(M,29)*(V(M,30)-V(M,29))/(Y(M,30)-Y(M,29))
  450 CONTINUE
      IF(V(M,1).GT.V(M,2)) GOTO 453
      DPI(M)=UP*PP(M,2)*(V(M,2)-V(M,1))/(Y(M,2)-Y(M,1))
  453 CONTINUE
  451 CONTINUE
      PPP=0.
      PNN=0.
      DO 454 M=1,12
      PPP=PPP+DPI(M)
      PNN=PNN+DNI(M)
  454 CONTINUE
      PPAB=ABS(PPP)
      PNAB=ABS(PNN)
      IF(J.EQ.1) GOTO 456
      IF(J.EQ.2) GOTO 460
      IF(PNAB.GT.PPAB) GOTO 455
      PQAB=PPAB
      VDEL=.5*V(1,2)
      DO 457 M=1,12
      V(M,1)=VDEL+V(M,1)
  457 CONTINUE
      J=1
      GOTO 458
  455 CONTINUE
      PQAN=PNAB
      VDEL=.5*(V(1,30)-V(1,29))
      DO 459 M=1,12
      V(M,30)=V(M,30)-VDEL
  459 CONTINUE
      J=2
      GOTO 458
  456 CONTINUE
      CENT=ABS((PPAB-PNAB)/PNAB)
      IF(CENT.LT.0.01)GOTO 461
      TREND=(PPAB-PQAB)/VDEL
      ERR=PNAB-PPAB
      VDEL=ERR/TREND
      DO 462 M=1,12
```

```
      V(M,1)=V(M,1)+VDEL
  462 CONTINUE
      POAB=PPAB
      GOTO 458
  460 CONTINUE
      CENT=ABS((PPAB-PNAB)/PPAB)
      IF(CENT.LT.0.01) GOTO 461
      TREND=(PNAB-PQAN)/VDEL
      ERR=PPAB-PNAB
      VDEL=ERR/TREND
      DO 463 M=1,12
      V(M,30)=V(M,30)+VDEL
  463 CONTINUE
      POAN=PNAB
      GOTO 458
  461 CONTINUE
      SPACP=V(M,1)
      SPACN=V(1,30)-A
      DPPP=PPAB+DPPP
      DNNN=DNNN+PNAB
      CUR=PPAB*ELECT/TDEL
      RETURN
      END
```

```
      SUBROUTINE MOVE
      COMMONY(12,30),VOL(12,30),CON(12,30),YO(12),YU(12),PMOB,EMOB,
     1TDEL,A,V(12,30),P(12,30),PP(12,30),PN(12,30),DPPP,DNNN,CUR,CHAR,
     2COD,BURP     ,ELECT,VC,    EATA,CAPPA,PIE,DPI(12),DNI(12),XUP(12),
     3SPACP,SPACN,SURO(12),EHYD(12),EOXY(12),ITIM,JUMBO,       UN,UP,
     4ZETA,ZXA(12),ZXB(12),ZYA(12,30),ZYB(12,30),ZOB(12,30),TOM
      DIMENSION DP(12,30),DN(12,30)
C
C     THIS ROUTINE CALCULATES THE CHARGE MOVEMENT
C
      DO400M=1,12
      DO400N=1,30
      DP(M,N)=0.
      DN(M,N)=0.
  400 CONTINUE
      DO 401 M=1,11
      IF(M.EQ.1)GOTO5000
      XA=XUP(M)-XUP(M-1)
 5000 CONTINUE
      XB=XUP(M+1)-XUP(M)
      DO401 N=2,29
      YA=Y(M,N)-Y(M,N-1)
      YB=Y(M,N+1)-Y(M,N)
      IF(V(M,N-1).GT.V(M,N))GOTO 430
      DN(M,N)=UN*PN(M,N-1)*(V(M,N)-V(M,N-1))     /YA
      DP(M,N)=-UP*PP(M,N)*(V(M,N)-V(M,N-1))      /YA
      GOTO434
  430 DN(M,N)=-UN*PN(M,N)*(V(M,N-1)-V(M,N))      /YA
      DP(M,N)=UP*PP(M,N-1)*(V(M,N-1)-V(M,N))     /YA
  434 IF(V(M,N+1).GT.V(M,N))GOTO432
      DN(M,N)=(UN*PN(M,N+1)*(V(M,N)-V(M,N+1)))/YB+DN(M,N)
      DP(M,N)=(-UP*PP(M,N)*(V(M,N)-V(M,N+1)))/YB+DP(M,N)
      GOTO 436
  432 DN(M,N)=(-UN*PN(M,N)*(V(M,N+1)-V(M,N)))/YB+DN(M,N)
      DP(M,N)=(UP*(PP(M,N+1)*(V(M,N+1)-V(M,N))))/YB+DP(M,N)
  436 IF(M.EQ.1) GOTO 438
  437 IF(V(M-1,N).GT.V(M,N))GOTO435
      DN(M,N)=(UN*PN(M-1,N)*(V(M-1,N)-V(M,N)))/XA+DN(M,N)
      DP(M,N)=(-UP*PP(M,N)*(V(M-1,N)-V(M,N)))/XA+DP(M,N)
      GOTO 438
  435 DN(M,N)=(-UN*PN(M,N)*(V(M-1,N)-V(M,N)))/XA+DN(M,N)
      DP(M,N)=(UP*PP(M-1,N)*(V(M-1,N)-V(M,N)))/XA+DP(M,N)
  438 IF(V(M+1,N).GT.V(M,N))GOTO439
      DN(M,N)=(UN*PN(M+1,N)*(V(M,N)-V(M+1,N)))/XB+DN(M,N)
      DP(M,N)=(-UP*PP(M,N)*(V(M,N)-V(M+1,N)))/XB+DP(M,N)
      GOTO441
  439 DN(M,N)=(-UN*PN(M,N)*(V(M+1,N)-V(M,N)))/XB+DN(M,N)
      DP(M,N)=(UP*PP(M+1,N)*(V(M+1,N)-V(M,N)))/XB+DP(M,N)
  441 CONTINUE
  401 CONTINUE
      DO403M=1,11
      DO403N=2,29
      PP(M,N)=PP(M,N)+DP(M,N)
      PN(M,N)=PN(M,N)+DN(M,N)
      P(M,N)=(PP(M,N)+PN(M,N))/CON(M,N)
  403 CONTINUE
      RETURN
      END
```

```
      SUBROUTINE VOLU
      COMMONY(12,30),VOL(12,30),CON(12,30),YO(12),YU(12),PMOB,EMOB,
     1TDEL,A,V(12,30),P(12,30),PP(12,30),PN(12,30),DPPP,DNNN,CUR,CHAR,
     2COD,BURP     ,ELECT,VC,    EATA,CAPPA,PIE,DPI(12),DNI(12),XUP(12),
     3SPACP,SPACN,SURO(12),EHYD(12),EOXY(12),ITIM,JUMBO,       UN,UP,
     4ZETA,ZXA(12),ZXB(12),ZYA(12,30),ZYB(12,30),ZOB(12,30),TOM
C
C     THIS ROUTINE CALCULATES THE VOLUMES OF EACH OF THE ELEMENTS
C
      DO 351 M=2,11
      BONK=(XUP(M+1)-XUP(M))*XUP(M)
      DO 351 N=2,29
      VOL(M,N)=BONK*(Y(M,N+1)-Y(M,N))*PIE/2.
  351 CONTINUE
      DO 352 N=2,29
      VOL(1,N)=PIE*XUP(2)*XUP(2)*(Y(1,N+1)-Y(1,N-1))/8.
  352 CONTINUE
      BONK=(XUP(12)-XUP(11))*XUP(12)*PIE
      DO 353 N=2,29
      VOL(12,N)=BONK*(Y(12,N+1)-Y(12,N-1))
  353 CONTINUE
      DO 354 M=1,12
      DO 354 N=2,29
      CON(M,N)=VOL(M,N)*ZETA
  354 CONTINUE
      RETURN
      END
```

```
      SUBROUTINE HOT
      COMMONY(12,30),VOL(12,30),CON(12,30),YO(12),YU(12),PMOB,EMOB,
     1TDEL,A,V(12,30),P(12,30),PP(12,30),PN(12,30),DPPP,DNNN,CUR,CHAR,
     2COD,BURP     ,ELECT,VC,    EATA,CAPPA,PIE,DPI(12),DNI(12),XUP(12),
     3SPACP,SPACN,SURO(12),EHYD(12),EOXY(12),ITIM,JUMRO,       UN,UP,
     4ZETA,ZXA(12),ZXB(12),ZYA(12,30),ZYB(12,30),ZOB(12,30),TOM
C
C     THIS ROUTINE CALCULATES THE NUMBER OF NEW IONS GENERATED
C
      BURP=.0000409
      ZING=.1*TDEL*BURP/8.0E-20
      DO552 L=1,10
      DO 550 M=2,11
      BONK=XUP(M+1)-XUP(M-1)
      DO 550 N=2,29
      COND=((PP(M,N)*PMOB)-(PN(M,N)*EMOB))*ELECT/VOL(M,N)
      AH=(V(M,N-1)-V(M,N+1))/(Y(M,N-1)-Y(M,N+1))
      BH=(V(M-1,N)-V(M+1,N))/BONK
      BRH=2.*VOL(M,N)/BONK
      ARH=2.*VOL(M,N)/(Y(M,N+1)-Y(M,N-1))
      HEAT=((AH*AH*ARH)+(BH*BH*BRH))*COND*ZING
      PP(M,N)=PP(M,N)+HEAT
      PN(M,N)=PN(M,N)-HEAT
  550 CONTINUE
      BONK=XUP(2)-XUP(1)
      DO 551 N=2,29
      COND=((PP(1,N)*PMOB)-(PN(1,N)*EMOB))*ELECT/VOL(1,N)
      AH=(V(1,N-1)-V(1,N+1))/(Y(1,N-1)-Y(1,N+1))
      BH=(V(1,N)-V(2,N))/BONK
      ARH=2.*VOL(1,N)/(Y(1,N+1)-Y(1,N-1)   )
      BRH=2.*VOL(1,N)/BONK
      HEAT=((AH*AH*ARH)+(BH*BH*BRH))*COND*ZING
      PP(1,N)=PP(1,N)+HEAT
      PN(1  ,N)=PN(1,N)-HEAT
  551 CONTINUE
  552 CONTINUE
      RETURN
      END
```

```
      SUBROUTINE CAP
      COMMONY(12,30),VOL(12,30),CON(12,30),YO(12),YU(12),PMOB,EMOB,
     1TDEL,A,V(12,30),P(12,30),PP(12,30),PN(12,30),DRPP,DNNN,CUR,CHAR,
     2COD,DURP     ,ELECT,VC,    EATA,CAPPA,PIE,DPI(12),DNI(12),XUP(12),
     3SPACP,SPACN,SURO(12),EHYD(12),EOXY(12),ITIM,JUMBO,        UN,UP,
     4ZETA,ZXA(12),ZXB(12),ZYA(12,30),ZYB(12,30),ZOB(12,30),TOM
C
C       THIS ROUTINE CALCULATES THE CAPACITOR VOLTAGE
C
      CHAR=CHAR-(CUR*TDEL)
      VC=CHAR/COD
      A=VC
      RETURN
      END
```

```
      SUBROUTINE GNEW
      COMMONY(12,30),VOL(12,30),CON(12,30),YO(12),YU(12),PMOB,EMOB,
     1TDEL,A,V(12,30),P(12,30),PP(12,30),PN(12,30),DPPP,DNNN,CUR,CHAR,
     2COD,BURP     ,ELECT,VC,    EATA,CAPPA,PIE,DPI(12),DNI(12),XUP(12),
     3SPACP,SPACN,SURO(12),EHYD(12),EOXY(12),ITIM,JUMBO,       UN,UP,
     4ZETA,ZXA(12),ZXB(12),ZYA(12,30),ZYB(12,30),ZOB(12,30),TOM
C
C     THIS ROUTINE CALCULATES THE NEW GRID COORDINATES AND THE
C     STREAMER MOVEMENTS
C
      DEY=1.25E16
      DEX=2.*DEY
      DO 701 M=1,12
      ALFA=ABS(DPI(M)/(SURO(M)*DEX))
      ABAL=ABS(DNI(M)/(SURO(M)*DEY))
      EHYD(M)=EHYD(M)+ALFA
      EOXY(M)=EOXY(M)+ABAL
      Y(M,30)=YU(M)-EHYD(M)
      Y(M,1)=YO(M)+EOXY(M)
      IF(Y(M,30).LT.Y(M,1))GOTO704
      DELB=ABAL/29.
      DELA=ALFA/29.
      DO 701 N=2,29
      Y(M,N)=Y(M,N)-DELA*(N-1)+DELB*(30-N)
  701 CONTINUE
      GOTO 705
  704 CONTINUE
      WRITE(6,1701)ITIM
      JUMBO=1
 1701 FORMAT(////,5X,24HBREAKDOWN OCCURRED AFTER     ,I15,2X,
     111HNANOSECONDS.    )
  705 CONTINUE
      RETURN
      END
```

```
      SUBROUTINE TRIPA
      COMMONY(12,30),VOL(12,30),CON(12,30),YO(12),YU(12),PMOB,EMOB,
     1TDEL,A,V(12,30),P(12,30),PP(12,30),PN(12,30),DPPP,DNNN,CUR,CHAR,
     2COD,BURP     ,ELECT,VC,    EATA,CAPPA,PIE,DPI(12),DNI(12),XUP(12),
     3SPACP,SPACN,SURO(12),EHYD(12),EOXY(12),ITIM,JUMBO,       UN,UP,
     4ZETA,ZXA(12),ZXB(12),ZYA(12,30),ZYB(12,30),ZCB(12,30),TOM
C
C       THIS ROUTINE PRINTS INTERMEDIATE RESULTS
C
      TOM=TOM+TDEL
      ITIM=TOM*1.E9
      WRITE(6,1100)ITIM,SPACP,SPACN,CUR,EHYD(1),EOXY(1),V(1,1),V(1,2),
     1V(1,29),V(1,30)
 1100 FORMAT(5X,I6,9E10.4)
      RETURN
      END
```

Appendix 3 - Dynamic Relaxation

Introduction

This appendix describes the method of writing programmes for dynamic stress analysis by the method of dynamic relaxation.

Dynamic relaxation was originally developed as an iterative process for the solution of static stress patterns. The method solves the static case by using the dynamic solution with critical damping. If the damping term is reduced, then the iteration steps give the dynamic stress state.

Description of the Technique

The technique will be described for the example of a square with a two dimensional stress state (i.e. plane strain or plane stress). The technique is equally applicable for three dimensional problems but the description will be more clear if restricted to the two dimensional case.

Step by Step Derivation of the Fortran

1. Draw an Interlaced Mesh

The interlaced mesh is the basis of the technique. It consists of two meshes; firstly a mesh of displacements and secondly, interlaced between the displacement points, a mesh of stresses. It is

(Continued .....)

important to note that horizontal and vertical displacements are not defined at the same point. The mesh used in the example is shown in Figure A3/1.

2. Write down Hooke's Law

This step permits the calculation of the vertical, shear and horizontal stresses from the displacements.

$$\sigma x = A \frac{\partial \bar{u}}{\partial x} + B \frac{\partial \bar{v}}{\partial y}$$

$$\sigma y = B \frac{\partial \bar{u}}{\partial x} + A \frac{\partial \bar{v}}{\partial y}$$

$$\tau xy = C \left(\frac{\partial \bar{u}}{\partial y} + \frac{\partial \bar{v}}{\partial x}\right)$$

Using the grid these equations become in Fortran:

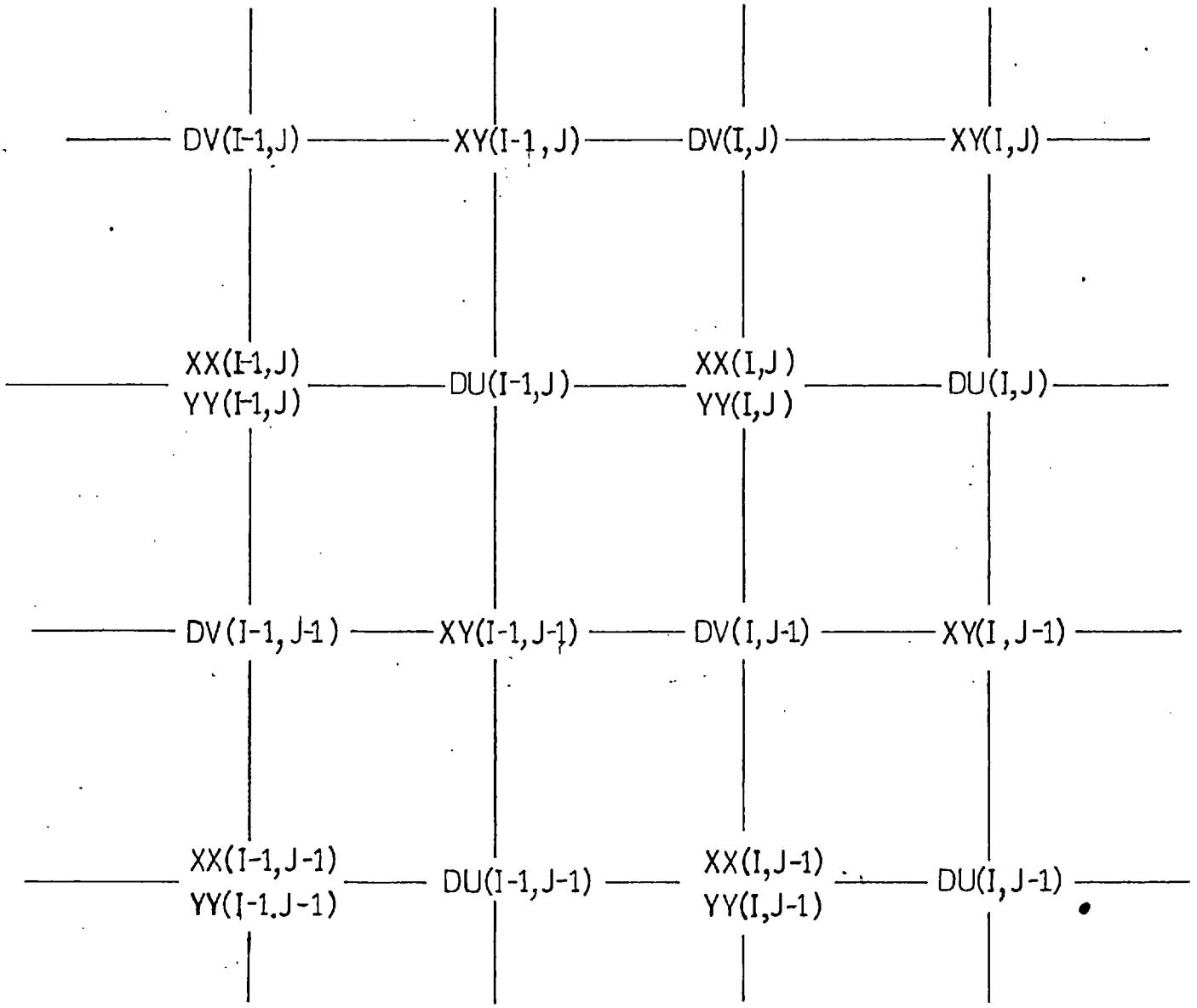
```
XX(I,J) = A*(DU(I,J) - DU(I-1,J))/XDEL
        + B*(DV(I,J) - DV(I,J-1))/YDEL

YY(I,J) =A*(DV(I,J) - DV(I,J-1))/YDEL
        + B*(DU(I,J) - DU(I-1,J))/XDEL

XY(I,J) = C*(DV(I+1,J) - DV(I,J))/XDEL
        + C*(DU(I,J+1) - DU(I,J))/YDEL
```

The range over which I and J are evaluated will be decided later.

(Continued .....)



Interlaced mesh

figure A3/1

3) Write down the differential equations for the acceleration

$$\rho \frac{\partial^2 \bar{v}}{\partial t^2} = \frac{\partial \sigma_x}{\partial x} + \frac{\partial \tau_{xy}}{\partial y}$$

$$\rho \frac{\partial^2 \bar{v}}{\partial t^2} = \frac{\partial \tau_{xy}}{\partial x} + \frac{\partial \sigma_y}{\partial y}$$

This leads to the Fortran statements:

```
AX(I,J) = (XX(I+1,J) - XX(I,J))/RHO*XDEL
        + (XY(I,J) - XY(I,J-1))/RHO*YDEL

AY(I,J) = (YY(I,J+1) - YY(I,J))/RHO*YDEL
        + (XY(I,J) - XY(I,J))/RHO*XDEL
```

4) Write down the integration formulae for velocity

$$u = \int \frac{du}{dt}\, dt \qquad u = o \quad t = o$$

$$v = \int \frac{dv}{dt}\, dt \qquad v = o \quad t = o$$

gives using a simple numerical integrator

```
U(I,J) = U(I,J) + AX(I,J)*TDEL
V(I,J) = V(I,J) + AY(I,J)*TDEL
```

5) Write down the integration formulae for displacements

$$\bar{u} = \int u dt \qquad \bar{u} = o \quad t = o$$

$$\bar{v} = \int v dt \qquad \bar{v} = o \quad t = o$$

using a simple integrator

(Continued .....)

DU(I,J) = DU(I,J) + U(I,J)*TDEL

DV(I,J) = DV(I,J) + V(I,J)*TDEL

again the choice of ranges over which I and J will be considered later.

6) Choose the boundaries

This is an important step as it determines the ranges of I and J in the previous steps.

The boundary is assumed to be free as rock is acoustically mismatched to water and the ratio

$$\frac{\text{acoustic impedance of rock}}{\text{acoustic impedance of water}}$$

is large.

The conditions at the boundary are therefore

$$\sigma_n = o$$

$$\tau_{xy} = o$$

The boundary line is chosen to go through the XY(I,J) points along the lines

I = 1

I = 11

J = I

J = 11

this gives the following Fortran statements

```
      DO1 I = 1,11
      XY(I,1) = 0.0
      XY(I,11) = 0.0
1     CONTINUE
```

(Continued .....)

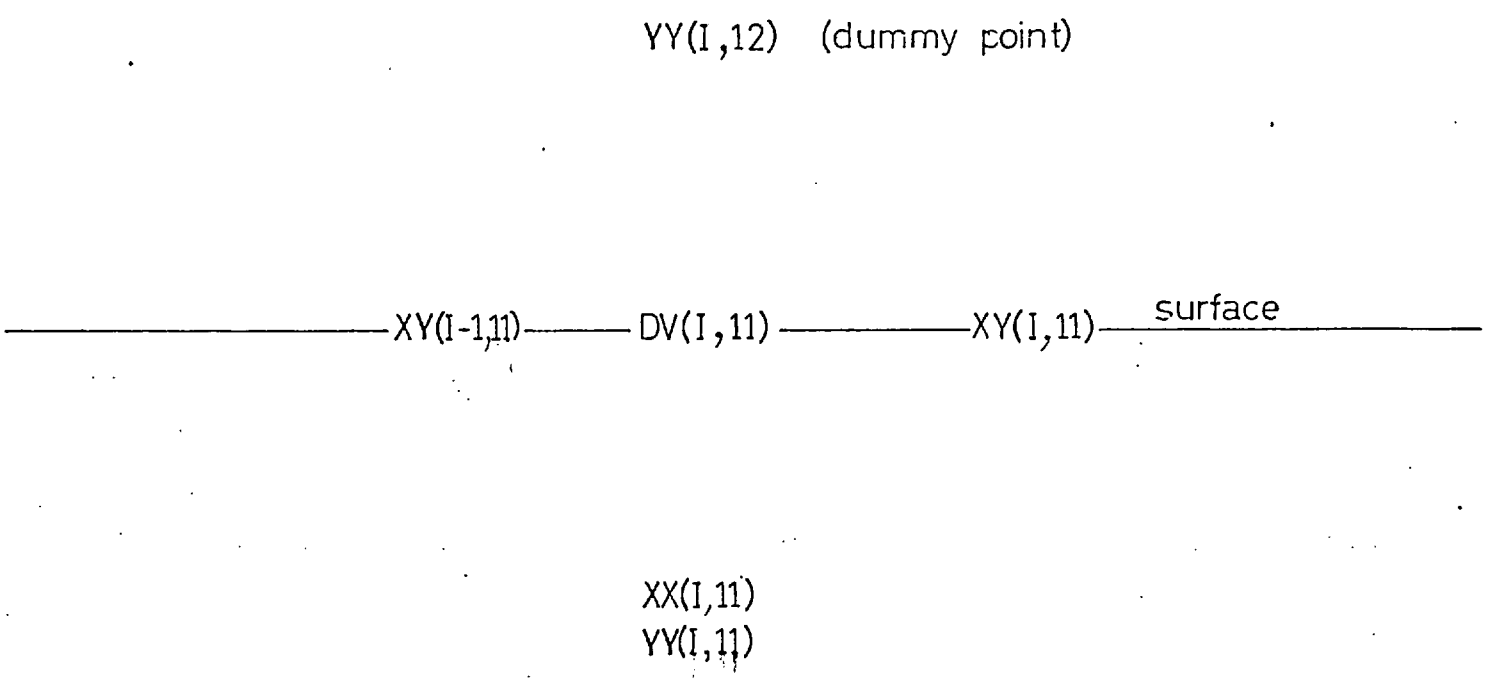

YY(I,12) (dummy point)
XY(I-1,11)
DV(I,11)
XY(I,11)
surface
XX(I,11)
YY(I,11)
boundary of mesh

figure A3/2

It follows that XX and YY must be evaluated over the range

I = 2→11

J = 2→11

This leads to the Fortran statements:

```
      DO6 J = 2,11
      DO6 I = 2,11
      XX(I,J) = F*(DU(I,J) - DU(I-1,J)) + G*(DV(I,J) - DV(I,J-1))
      YY(I,J) = H*(DV(I,J) - DV(I,J-1)) + P*(DU(I,J) - DU(I-1,J))
6     CONTINUE
```

From consideration of the grid

AX, U and DU are defined over the range

J = 2,11

I = 1,11

and consequently eliminating AX to save storage

```
      DO7 J = 2,11
      DO7 I = 1,11
      U(I,J) = CEX(XX(I+1,J) - XX(I,J)) + CEY*(XY(I,J) - XY(I,J-1))
                                                          + U(I,J)
      DU(I,J) = DU(I,J) + U(I,J)*TDEL
7     CONTINUE
```

Similarly

```
      DO8 J = 1,11
      DO8 I = 2,11
      V(I,J) = CEY*(YY(I,J+1) - YY(I,J)) + CEX*(XY(I,J) - XY(I-1,J))
                                                          + V(I,J)
      DV(I,J) = DV(I,J) + V(I,J)*TDEL
8     CONTINUE
```

(Continued .....)

```
      DO2 J = 1,11
      XY(1,J) = 0.0
      XY(11,J) = 0.0
2     CONTINUE
```

The shear stresses are calculated inside these limits thus

```
      DO3 I = 2,10
      DO3 J = 2,10
      XY(I,J) = D*(DV(I+1,J) - DV(I,J)) + D*(DU(I,J+1) - DU(I,J))
3     CONTINUE
```

In order to compute DV(I,11) Y(I,12) is required. As σn at the point DV(I,11) must be 0 a dummy set of points YY(I,12) are introduced - see Figure A3/2

and YY(I,12) = -YY(I,11)

as $\sigma n = \frac{YY(I,12) + YY(I,11)}{2} \doteq 0$

By this method the normal stress conditions are obtained

```
      DO4 J = 2,11
      XX(1,J) = -XX(2,J)
      XX(12,J) = -XX(11,J)
4     CONTINUE

      DO5 J = 2,11
      YY(I,1) = -YY(I,2)
      YY(I,12) = -YY(I,11)
5     CONTINUE
```

(Continued .....)

Next all the statements are checked for consistency. No statement may use a value which is not defined. If the equations are not self-consistent then one of three possibilities arise:

a) The grid is incorrectly designed.

b) The equations are incorrect.

c) The boundaries are incorrectly defined.

If the equations are consistent then the next step is to derive the load equations.

This is done by using the dummy points. In setting the boundary stress to zero we used the equation, see Figure A3/2 ,

$$\frac{XX(1,J) + XX(2,J)}{2} = \sigma_n$$

to apply a normal load at points 6 and 7 we use the Fortran

```
XX(1,7)  =  PULSE - XX(2,7)
XX(1,6)  =  PULSE - XX(2,6)
```

where PULSE has a value of twice the applied stress.

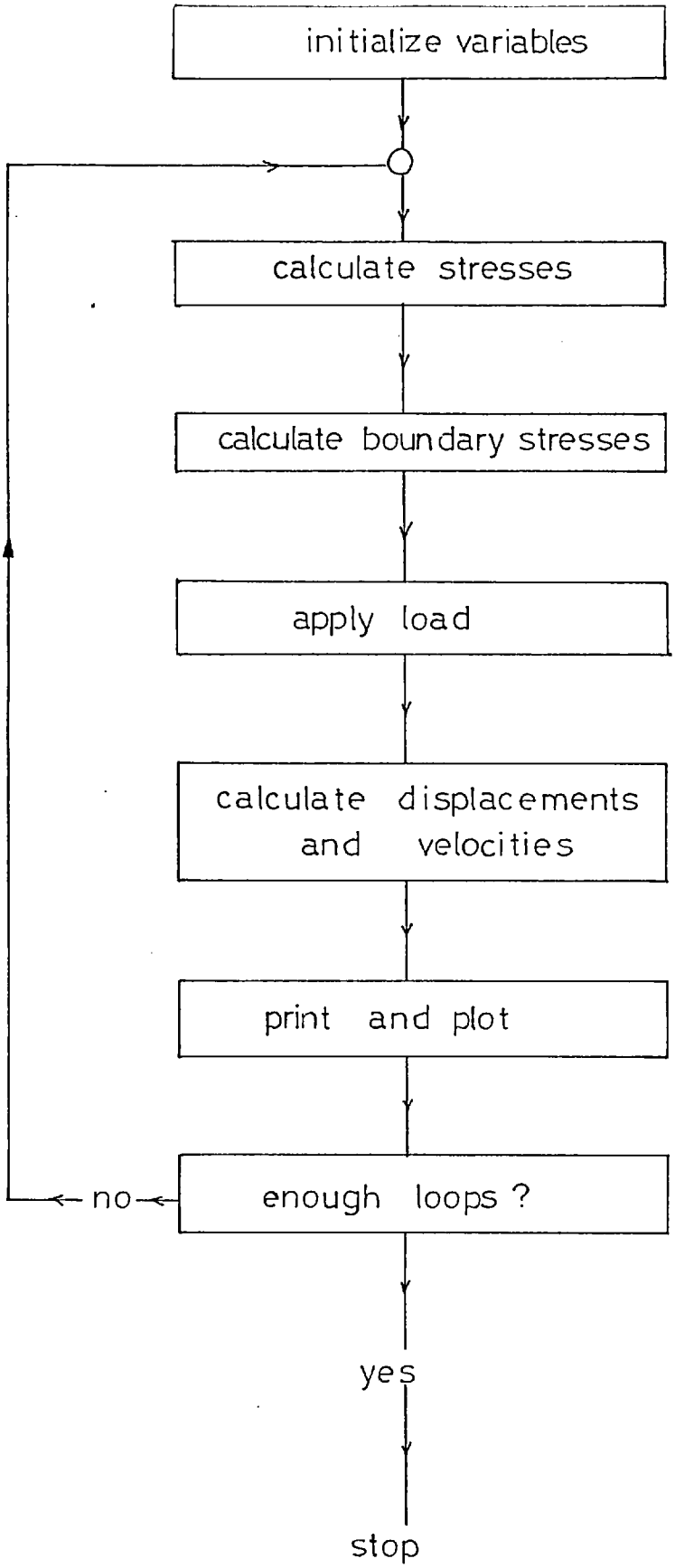
The programme is arranged according to the flow sheet in Figure A3/3 and the listing for the example case is given at the end of this section.

Stability

It can be shown by experiment that the calculation is stable provided

$$TDEL < \frac{XDEL}{Vs}$$

(Continued .....)



Flow chart for stress analysis programmes

figure A3/3

or more simply that the time increment must be less than the time required for the stress wave to cross the grid. Experiments were carried out to test this criterion and it was found that a wide range of TDEL give the same resulting stresses at fixed times in the programme.

One consequence of the time increment size is that a small stress is computed ahead of the wave form, see Figure A3/4. However the error involved is insignificant.

Graphical Output

A large amount of data is generated by dynamic stress analysis programmes and in general it is very difficult to comprehend when presented in tabulated form. In order to present the results in an easily assimulated form several graphical techniques were developed.

At each grid point the following variables can be computed:

$\sigma_x, \sigma_y, \tau_{xy}$, u, v, $\bar{u}$, $\bar{v}$, σ_1, σ_3, τ

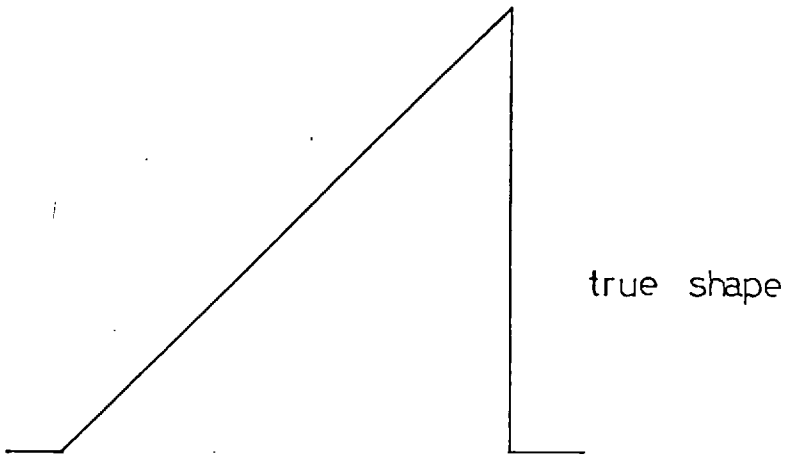
Any simple representation of the total stress state on a single graph is consequently not possible.

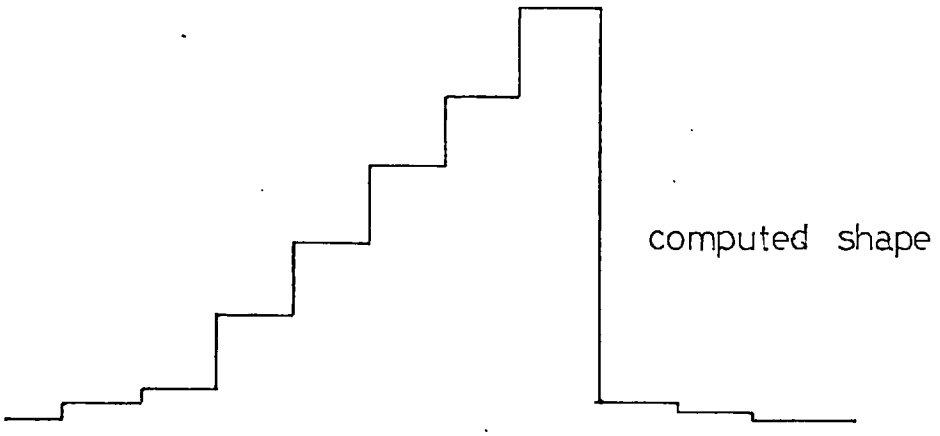
Several techniques were therefore developed each showing different facets of the behaviour of the material under load.

a) Distortion Grid

A square block is drawn with a square grid plotted on it. The

(Continued .....)





Effect of numerical method on pulse shape

figure A 3/4

displacements of the points of the grid, greatly scaled up, are added to the grid coordinates; the resulting grid is plotted at each time increment. The example shown in Figures 4/3 to 4/18 is for the following case:

A square block of rock with properties

P wave velocity = 3.5×10^3 metres/sec

Poisson's ratio = .2

Specific gravity = 2·6

Constant transverse stress

Size 5 cms x 5 cms

Pulse Exponential with decay time of 400 nS

Time scale 1 μ sec per picture

b) Trajectory Map

The displacements of each point form a locus, with time as a parameter. The locus for each grid point during the first 100 μSecs was plotted - Figure 4/19 - the origin of each locus is at its respective rest position of the grid. It should be noted that the final point of the locus is above starting position as the block has been given momentum upwards by the load. The particular case data is as above.

c) Stress Isometric

At each point in time the stresses are functions of the space coordinates. The stress can therefore be plotted as a pseudo

(Continued .....)

isometric having x and y as independent axes and stress as vertical axis. At each point in time three such pictures are drawn showing, respectively, the principal major stress, the principal minor stress and the shear stress. See Figures 4/20 - 4/39. The example shown was for the following case:

A square block of rock with properties

P wave velocity = $3{\cdot}5 \times 10^3$ m/sec

Poisson's ratio = ·2

Specific gravity = 2·6

Block size = 12·5 x 12·5 cms

Pulse exponential with time constant of 400 nS

Time scale 1 second per set of pictures

Extension of the Technique

The examples given have all assumed a two dimensional, linear elastic, homogeneous, isotropic rock. The technique can be extended to the general case but time and data were not available to the author and consequently it was not attempted.

List of Symbols

Original Equations	Meaning	Fortran
x)	coordinate directions	I
y)		J
$\bar{u}$	x displacement	DU(I,J)
$\bar{v}$	y displacement	DV(I,J)
u	x velocity	U(I,J)
v	y velocity	V(I,J)
	x acceleration	AX(I,J)
	y acceleration	AY(I,J)
	X increment	XDEL
	Y increment	YDEL
	time increment	TDEL
σ_x	x stress	XX(I,J)
σ_y	y stress	YY(I,J)
τ_{xy}	x-y shear stress	XY(I,J)
σ_n	normal stress	
σ_1	principal major stress	
σ_2	principal minor stress	
τ	shear stress	
	applied stress	PULSE

(Continued .....)

Original Equations	Meaning	Fortran
ρ	Density	RHO
	Elastic constants	A, BC FGHP
V_s	P wave velocity	
	Intermediate constants	CEX, CEY

```
JOB(UMCK012,J9,CM40000,T100,D1)                    HASKELL          WOBL.
REQUEST(TAPE27,HI,X)ICCALCOMPTAPEWRITEPERMIT.
FUN(S,,,,,,11610)
LGO.
'
      PROGRAMWOBL(INPUT,OUTPUT,TAPE5=INPUT,TAPE6=OUTPUT,TAPE27,TAPE25)
      COMMONA(12,12),B(12,12)
      DIMENSIONXX(12,12),YY(12,12),XY(12,12),U(12,12),V(12,12)
     1,DU(12,12),DV(12,12)
      PULSE=100.
      CALL START
      CALL PLOT(5.0,3.0,-3)
      L=0
      LIM=0
      LAM=0
      DO11I=1,12
      DO11J=1,12
      XX(I,J)=0.
      YY(I,J)=0.
      XY(I,J)=0.
      DU(I,J)=0.
      DV(I,J)=0.
      V(I,J)=0.
      U(I,J)=0.
      A(I,J)=0.
      B(I,J)=0.
   11 CONTINUE
      READ(5,51)TDEL,XDEL,YDEL
   51 FORMAT(3E10.4)
      READ(5,52)ELAST,POISS,RHO
   52 FORMAT(3E10.4)
      A=ELAST/(1.-POISS*POISS)
      B=ELAST/(2.*(1.+POISS))
      C=A*POISS
      F=A/XDEL
      G=C/YDEL
      H=A/YDEL
      P=C/XDEL
      DXM=B/XDEL
      DYM=B/YDEL
      CEX=TDEL/(XDEL*RHO)
      CEY=TDEL/(YDEL*RHO)
      CD=1.
      N=0
   10 N=N+1
      DO1J=2,11
      DO1I=2,11
      XX(I,J)=F*(DU(I,J)-DU(I-1,J))+G*(DV(I,J)-DV(I,J-1))
    1 YY(I,J)=H*(DV(I,J)-DV(I,J-1))+P*(DU(I,J)-DU(I-1,J))
      DO2J=2,10
      DO2I=2,10
    2 XY(I,J)=DXM*(DV(I+1,J)-DV(I,J))+DYM*(DU(I,J+1)-DU(I,J))
      DO3J=2,11
      XX(1,J)=-XX(2,J)
    3 XX(12,J)=-XX(11,J)
      XX(1,6)=2.*PULSE-XX(2,6)
      XX(1,7)=2.*PULSE-XX(2,7)
      PULSE=PULSE*.75
      DO4I=2,11
```

```
      YY(I,1)=-YY(I,2)
    4 YY(I,12)=-YY(I,I1)
      DO5I=1,11
      XY(I,1)=0.0
    5 XY(I,11)=0.0
      DO6J=1,11
      XY(1,J)=0.0
    6 XY(11,J)=0.0
      DO7J=2,11
      DO7I=1,11
      U(I,J)=CEX*(XX(I+1,J)-XX(I,J))+CEY*(XY(I,J)-XY(I,J-1))+CD*U(I,J)
    7 DU(I,J)=DU(I,J)+U(I,J)*TDEL
      DO8J=1,11
      DO8I=2,11
      V(I,J)=CEY*(YY(I,J+1)-YY(I,J))+CEX*(XY(I,J)-XY(I-1,J))+CD*V(I,J)
    8 DV(I,J)=DV(I,J)+V(I,J)*TDEL
      L=L+1
      IF(L.EQ.10)GOTO91
      GOTO92
   91 CONTINUE
      L=0
      LIM=LIM+1
      WRITE(6,65)N
   65 FORMAT(I5)
      DO95 J=2,11
      DO95I=2,11
      A(I,J)=I*.2-2.E9*(DU(I,J)+DU(I-1,J))
      B(I,J)=J*.2-2.E9*(DV(I,J)+DV(I,J-1))
   95 CONTINUE
      WRITE(6,71)
   71 FORMAT(/10X,23HHORIZONTAL DISPLACEMENT/)
      DO22J=2,11
      WRITE(6,67)( A(I,J),I=2,11)
   22 CONTINUE
   67 FORMAT(5X,10E12.4)
      WRITE(6,72)
   72 FORMAT(/10X,21HVERTICAL DISPLACEMENT/)
      DO23J=2,11
      WRITE(6,67)( B(I,J),I=2,11)
   23 CONTINUE
      CALL DROR
      IF(LIM.EQ.4)GOTO200
      GOTO201
  200 CONTINUE
      LIM=0
      LAM=LAM+1
      IF(LAM.EQ.2)GOTO202
      CALL PLOT(0.0,5.0,-3)
      GOTO203
  201 CONTINUE
      CALL PLOT(0 .0,2.5,-3)
      GOTO203
  202 CONTINUE
      LAM=0
      CALL PLOT (10.0,-20.0,-3)
  203 CONTINUE
   92 CONTINUE
      IF(N.LT.642)GOTO10
      CALL ENPLOT(2.)
      STOP
      END
```

```
      SUBROUTINE DROR
      COMMONA(12,12),B(12,12)
      DO100I=1,5
      N=2*I
      X=-B(2,N)
      Y=A(2,N)
      CALL PLOT(X,Y,3)
      DO101M=2,11
      X=-B(M,N)
      Y=A(M,N)
      CALL PLOT(X,Y,2)
  101 CONTINUE
      N=2*I+1
      X=-B(11,N)
      Y=A(11,N)
      CALL PLOT(X,Y,3)
      DO100J=2,11
      M=13-J
      X=-B(M,N)
      Y=A(M,N)
      CALL PLOT(X,Y,2)
  100 CONTINUE
      DO102J=1,5
      M=2*J
      X=-B(M,2)
      Y=A(M,2)
      CALL PLOT(X,Y,3)
      DO103N=2,11
      X=-B(M,N)
      Y=A(M,N)
      CALL PLOT(X,Y,2)
  103 CONTINUE
      M=2*J+1
      X=-B(M,11)
      Y=A(M,11)
      CALL PLOT(X,Y,3)
      DO102I=2,11
      N=13-I
      X=-B(M,N)
      Y=A(M,N)
      CALL PLOT(X,Y,2)
  102 CONTINUE
      RETURN
      END
```

Appendix 4 - The Charging of Capacitors

In section 5·2 the efficiency of an electrohydraulic crusher was shown to be

$$\eta = \eta_c \ \eta_a \ \eta_f$$

η = overall efficiency

η_c = capacitor charging efficiency

η_a = efficiency of converting electrical energy to acoustic energy

η_f = efficiency of converting acoustic energy to fractures

The capacitor charging efficiency is therefore of considerable economic importance. This appendix considers various methods of capacitor charging.

1. Charging from Constant Voltage Sources

Efficient constant voltage sources are readily available. They are cheap and can be made, by using a 3 to 12 phase transformer, to present a low harmonic resistive load to the supply. The two simple methods of charging from a constant voltage source are:

resistive charging and inductive charging.

Resistive Charging

Assume at $t = 0 \quad V_c = 0$

$$I = \frac{E}{R} \ e^{\frac{-t}{RC}}$$

(Continued .....)

Power from source

$$P_s = E \int_0^{t_c} I\,dt$$

Power dissipated in R

$$P_R = R \int_0^{t_c} I^2\,dt$$

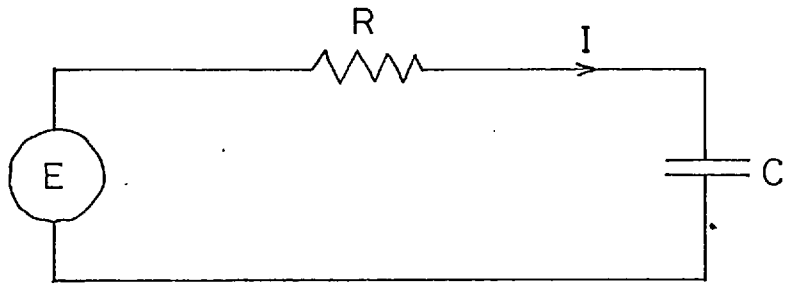
Efficiency =

$$1 - \frac{R \int_0^{t_c} I^2\,dt}{E \int_0^{t_c} I\,dt}$$

$$= 1 - \frac{R \int_0^{t_c} \frac{E^2}{R^2} e^{\frac{-2t}{RC}}\,dt}{E \int_0^{t_c} \frac{E}{R} e^{\frac{-t}{RC}}\,dt}$$

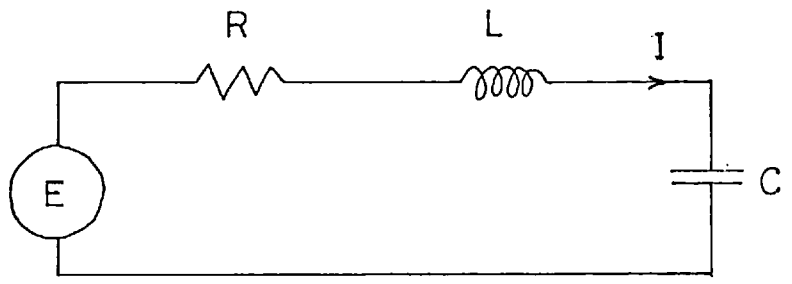
$$= 1 - \frac{\int_0^{t_c} e^{\frac{-2t}{RC}}\,dt}{\int_0^{t_c} e^{\frac{-t}{RC}}\,dt}$$

(Continued .....)



Resistive charging

figure A4/1



Inductive charging

figure A4/2

$$= 1 - \frac{\left[\frac{RC}{2} e^{\frac{-2t}{RC}}\right]_o^{t_c}}{\left[RC\ e^{\frac{-t}{RC}}\right]_o^{t_c}}$$

$$= 1 - \frac{1 - e^{\frac{-2t_c}{RC}}}{2\left[1 - e^{\frac{-t_c}{RC}}\right]}$$

$$= 1 - \tfrac{1}{2}\left(1 + e^{\frac{-t_c}{RC}}\right) = \tfrac{1}{2}\left(1 - e^{\frac{-t_c}{RC}}\right)$$

Thus the maximum possible efficiency in resistive charging is 50%.

Inductive Charging

$$q = CE\left(1 - \frac{e^{-\xi_1 \frac{t}{T}} \cos(wt - \phi)}{1 - \xi_1^2}\right)$$

where

$$\xi_1 = \frac{R}{2}\sqrt{\frac{C}{L}}$$

$$T = \sqrt{LC}$$

$$w = \frac{1}{T}\sqrt{1 - \xi_1^2}$$

$$\text{Tan } \phi = \frac{\xi_1}{1 - \xi_1^2}$$

$$i = \frac{dq}{dt} = \frac{CE}{T} e^{-\xi_1 \frac{t}{T}} \sin wt$$

When i = 0, charging stops as the supply will have a diode in it.

$$t = \frac{T\ \pi}{\sqrt{1 - \xi_1^2}}$$

(Continued .....)

$$Q = C E \left(1 + e^{\frac{-\pi\xi}{\sqrt{1-\xi^2}}}\right) \text{ where } Q = \text{charge}$$

$$\text{Total energy use} = \int_0^Q E\, dq = EQ$$

$$\text{Energy in capacitor} = \frac{1}{2}\frac{Q^2}{C}$$

$$\text{Therefore efficiency} = \frac{1}{2}\frac{Q^2}{C}\frac{1}{EQ} = \frac{Q}{2CE}$$

$$= \frac{1}{2}\left(1 + e^{\frac{-\pi\xi}{\sqrt{1-\ \ ^2}}}\right)$$

Let $\overline{Q}$ = circuit 'Q'

$$= \frac{woL}{R}$$

$$= \frac{1}{\sqrt{LC}}\frac{L}{R} = \sqrt{\frac{L}{CR^2}}$$

$$\eta = \frac{1}{2}\left(1 + e^{\frac{-\pi}{\sqrt{4Q^2 - 1}}}\right)$$

η max = 100%

Take some typical values

$C = \cdot 1 \mu F$

$RC \quad 10^{-3}$ secs

$R = 10^4$

To make $\xi^2 = \cdot 1 \quad \frac{R^2C}{4L} = \cdot 1 \quad$ (i.e. $\overline{Q} = 20$)

$$L = \frac{10^8 \times 10^{-7}}{4 \times \cdot 1} = 25 \text{ Henries}$$

(Continued .....)

$$\eta \simeq \frac{1}{2}\left(1 + e^{-\frac{\cdot 3 \times \pi}{\sqrt{\cdot 9}}}\right) = 70\%$$

$$\text{Charging time} = \frac{\sqrt{LC} \times \pi}{\sqrt{\cdot 9}} \simeq \pi \times \sqrt{25 \times 10^{-7}}$$

$$\simeq 5 \text{ m Secs}$$

If $E = 40\text{kv}$

$$i = 40 \times 10^{3} \sqrt{\frac{10^{-7}}{25}} \simeq 2{\cdot}5 \text{ amps}$$

A 25 Henry inducter of Q = 20 capable of carrying 3 amps and insulated to 60kv is a bulky and expensive device. A possibility is to use a transformer rectifier supply and allow the transformer leakage reactance and resistance to provide L and R.

Constant Current Charging

A charge generating device would offer 100% efficiency without difficulty. The development of electrostatic generators is progressing rapidly and within the next decade suitable devices should be commercially available. The only losses would be in the bearings of the machine giving overall efficiencies of charging of about 99%. It is the author's opinion that, in the long term, electrostatic generators will be the most suitable capacitor charging devices (reference 126, 127).

Appendix 5 - Switching Techniques

Introduction

Because the leakage currents in water are high it is necessary to place a switch between the capacitor and the water gap. This appendix considers various switch types and shows that spark gaps are the only switches feasible at present.

The required properties of a switch for an electrohydraulic crusher are:-

a) It must not close until the capacitor is charged, i.e. it must hold off many kilovolts.

b) It must be capable of opening and closing rapidly. For a reasonable throughput it must operate many times per second.

c) It must allow a current of many kiloamperes to flow when closed.

d) It must have low inductance when closed.

e) It must have low resistance when closed.

f) It would be advantageous to time the spark precisely.

Possible switches include:-

a) Thyratrons

b) Ignitrons

c) Thyristors

d) Two-electrode spark gaps

e) Rotary spark gaps

f) Three-electrode spark gaps

(Continued .....)

Each of these will be considered in turn.

a) Thyratrons

Suitable thyratrons have excellent high voltage hold off (100 KV), can operate at high pulse repetition frequencies (1 kHz), and can be precisely timed (250 nS). They are unable to carry sufficient current.

b) Ignitrons

Capacitor discharge ignitrons (e.g. BK 178) are ideal for single shot experiments. Typical performance is:

Hold-off voltage	25 KV
Peak Anode Current	100 KA
Arc Voltage drop	60 V

The maximum pulse repetition frequency is only about 1 pulse per 5 seconds.

c) Thyristors

In order to obtain the necessary hold-off voltage and peak currents, a series-parallel combination of many thyristors would be needed. This arrangement would inevitably be highly inductive.

d) Two-electrode spark gaps

Air spark gaps are convenient switches in that they can hold off large voltages and carry large currents. With air blasting the

(Continued .....)

pulse repetition rate can be high, and with coaxial geometry the inductance is low.

The resistance of a simple gap is (reference 111):-

$$R = \frac{k\,l}{Q}$$

R = resistance ohms

k = constant $= .8 \times 10^{-4}$

l = length of gap in centimetres

Q = charge transmitted by the gap

A simple example will show the resistance:-

Assume capacity C = $\cdot 2\,\mu f$ (i.e. a 1KJ supply)

voltage V = 100 KV

$$Q = CV = 10^{5} \times \cdot 2 \times 10^{-6} = 2 \times 10^{-2}$$

$$Rf = \frac{kl}{Q}$$

Assume air pressure p = 10 atmospheres (150 psig)

Hold off voltage is proportional to $p\ell$: at p = 1 atmosphere a 1 cm uniform field air gap will hold off about 30 KV. Therefore at 10 atmospheres 1/3 cm is needed to hold off 100 KV.

Therefore $\ell = 1/3$

$$Rf = \frac{\cdot 8 \times 10^{-4}}{3 \times 2 \times 10^{-2}}$$

$$= 1 \cdot 33 \times 10^{-3}$$

which is small in comparison with the water gap resistance. However the firing voltage of the gap is also dependant on the content of dirt and moisture in the air. Precise timing is not possible.

(Continued .....)

e) Rotary Air Gaps

Rotary air gaps were developed for radar use and achieve good timing at pulse repetition frequencies of up to 5 KHz. They have similar properties to two electrode gaps but are more inductive.

f) Three-Electrode Spark Gaps

Three electrode spark gaps originally developed for fusion experiments (references 2, 93, 111, 121) offer all the advantages of two electrode gaps but have much lower resistance and inductance. They can be fired over a wide range of voltages and offer precise ($\pm$ 50 nS) timing. They do, however, require triggering pulses.

Conclusion

It is the author's opinion that the three-electrode spark gap is the best choice. The trigger pulses could be easily generated by a rotating spark gap driven by a stepper motor. This combination would offer precise control of spark rate and timing with the lowest inductance and resistance.

Appendix 6 - Electrohydraulic Crushing Technique

This appendix describes the apparatus and technique used in measuring the power consumption in electrohydraulic comminution.

The electrohydraulic crusher (Figure A6/1), originally constructed by Yigit, reference 136, was connected to the high voltage supply (Figure A6/2). The voltage was measured with a calibrated voltage divider and oscilloscope.

Approximately 2 kg of each feed size was prepared. Feed sizes used in the experiment were:

¼" - ⅜"

⅜" - ½"

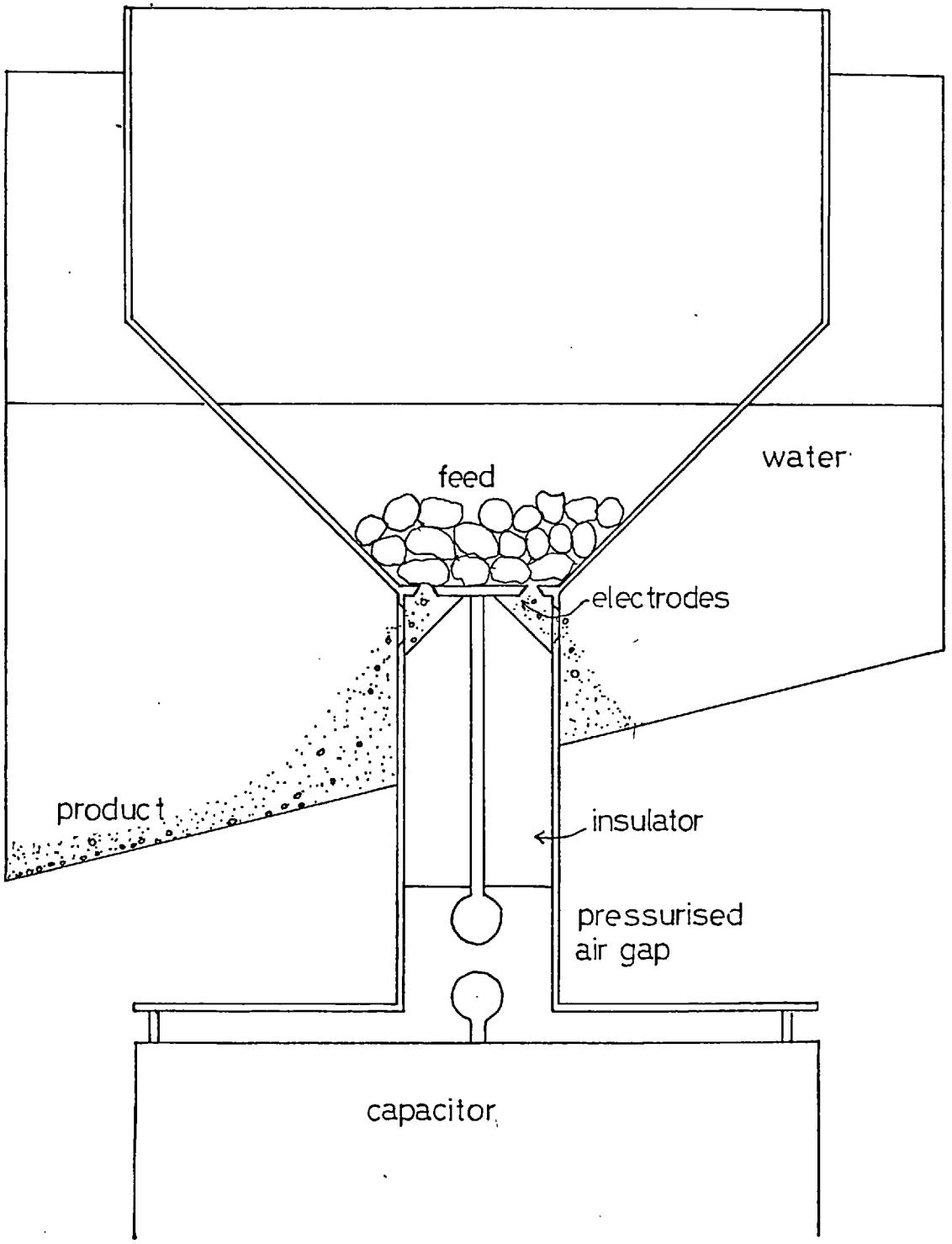
½" - ¾"

Each batch of feed was loaded into the crusher. The crusher was then filled with fresh, clean, demineralized water of conductivity approximately 12 μmhos/cm, and crusher was operated for 30 minutes. The voltage V was measured. The spark repetition frequency p was measured by stop watch and the energy consumed E was calculated from

$$E = \tfrac{1}{2}.C.V^2.p. \quad 1800 \text{ Joules, where } C = \cdot 1 \times 10^{-6} \text{ Farads}$$

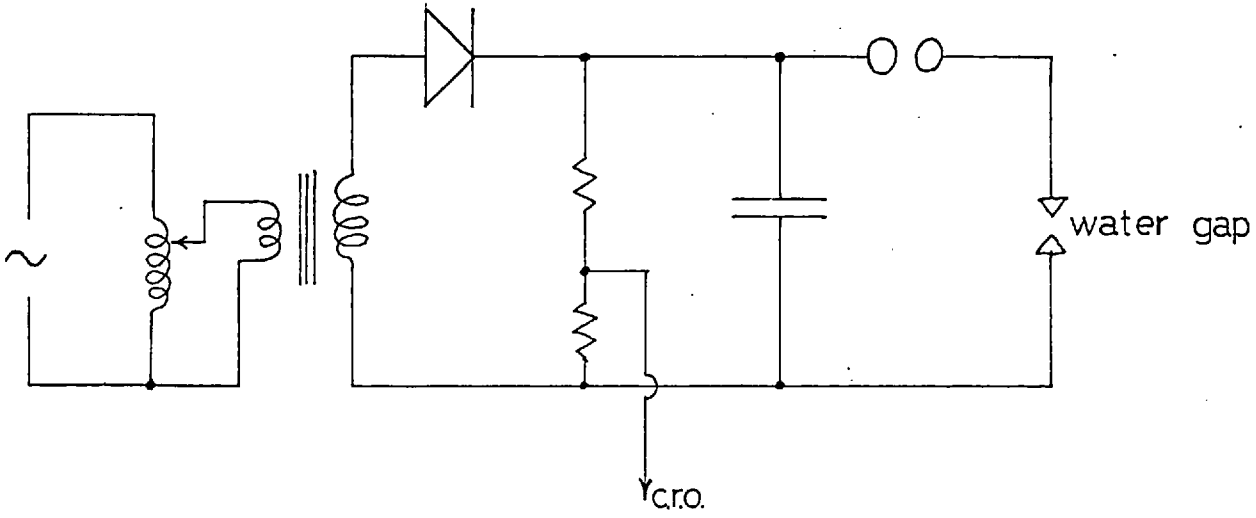
The product was then dried, sieved and weighed. Particles of the original feed size were discarded as uncrushed. Bond's Index and Kick's Constant were calculated from:-

(Continued .....)



Electrohydraulic crusher

figure A6/1



Crusher circuit diagram

figure A6/2

$$B.I. = \frac{E}{M} \cdot \frac{\sqrt{R}}{\sqrt{R} - 1} \sqrt{\frac{P}{100}}$$

$$K = \frac{E}{M \log r}$$

where

E = energy consumed

B.I. = Bond's Index

K = Kick's Constant

P = product size microns

F = feed size microns

R = F/P = reduction ratio

M = mass crushed

Strictly in the Bond's Index relationship the 80% passing size should be used. However, as scalped feeds were used, average sizes were used throughout.

Appendix 7 - The Einstein Convention

The Einstein Convention is used to expedite the operations of multiplying and contracting tensors. Its use will be restricted to contraction and the multiplication of covarient and contravarient tensors only when Latin sub and superscripts are used. When Greek sub and superscripts are used the outer product is implied thus:

$$T_i = G_{ik}\, T^k$$

implies

$$t_r = \sum_{S=1}^{k} g_{rs}\, t^s$$

where t_r is an element of T_i

where g_{rs} is an element of G_{ik}

where t^s is an element of T^k

but

$$T_{i\psi}^{\psi} = G_{i\psi}\, T^{\psi}$$

implies

$$t_{rv}^{s} = g_{rv}\, t^s$$

where t_{rv}^{s} is an element of $T_{i\psi}^{\psi}$

where g_{rv} is an element of $G_{i\psi}$

where t^s is an element of T^{ψ}

Appendix 8 - Bibliography

Introduction

This bibliography was compiled by the author during work on electrohydraulic comminution. The significance rating refers only to the importance of the reference to the project. The classification system was chosen for convenience. When there is doubt as to the correct classification the paper is classified under all possible headings. The source libraries are included for the convenience of those who wish to consult the papers. The references are in no particular order.

Classification Key

A Underwater

B Oceanography

C Instruments

D Bioscience

E Lasers

F Nuclear devices

G Rapid Excavation Methods

H Materials Handling

I High Pressures

J Stress Analysis

K Acoustics

L Fractures

M Rock

N Erosion

O Metal Forming

P Crushers

Q High Voltage Systems

R Magnetics

S Circuits

T Fields

U Capacitors

V Switches

W Breakdown

X Sparks

Y Exploding Wires

Z Electrohydraulics

(Continued .....)

! Patents

* Process Modelling - control

? Explosives

Significance Index

Very Important	***
Important	**
Interesting	*

Source Library Index

E	Electrical Engineering Library I.C.
P	P. E. Haskell
NLL	National Lending Library, Boston Spa
R.S.M.	Mining Library I.C.
Me	Mechanical Engineering Library I.C.
LP	Lyon Playfair Library I.C.

During the compilation of this bibliography the following have been thoroughly searched.

Journal of Applied Physics, Volumes (J.A.P.)	34
	35
	36
	37
	38
Transactions of the IEEE, Volumes	PAS 85
	PAS 86
	EI 1
	EI 2
	EI 3
International Journal of Rock Mechanics, Volumes	1
	2
	3
	5
Journal of the Acoustic Society of America, Volumes	39
	40
	42
	43
Proceedings of the IEE, Volumes	113
	114
	115

(Continued .....)

Japanese Journal of Applied Physics, Volumes	5
(Japanese J.A.P.)	6
	7
British Journal of Applied Physics Series 2 Volume	1

Significance Level	No.	Reference	Class	Source
	1	J.P. Barach Spectrographic measurements on an arc discharge. J.A.P. Vol.38 No.1 Jan.67	X	E
**	2	A.E. Bishop & G.D. Edwards Low inductance 100kv switch (spark gap) for starting, diverting and clamping, capacitor discharges. Proc I.E.E. Vol.113 No.9 Sep.66	V W X	E P
*	3	R.A. Graham & F.W. Nielson & W.B. Benedick Piezoelectric current from shock loaded quartz - a sub-microsecond stress gauge J.A.P. Vol.36 No.5 May 65 p.1775	C I	E
	4	R.L. Jameson & S.J. Lukasik & B.J. Permick Electrical resistivity measurements in detonating composition B and P Pentolite J.A.P. Vol.35 No.3 March 64	C I	E
	5	J.R. Hearst & L.B. Geesaman & D.V. Power Piezoelectric sensitivity and reproducability of Z cut tourmaline to 7 kbar J.A.P. Vol.35 No. 7 July 64	I C	E

(Continued .....)

Significance Level	No.	Reference	Class	Source
*	6	Proceedings of the international symposium on wave preparation and dynamic properties of earth materials A.M.Soc.Civ.Eng. Aug.23 1967	C I J K L M	NLL
*	7	E.O. Brigham & H.W. Smith & F.X. Bostick, Jr. & W.C. Duesterhoeft Jr. An iterative technique for determining inverse filters I.E.E.E. Trans on geoscience electronics Vol.GE-6 No.2 May 68	C	E
*	8	D.F. Binns & T.J. Randall Improved spark gap voltmeter Proc.I.E.E. Vol.113 No.9 Sep.66	X C	E P
	9	O.M. Stuetzer Impulse response measurement technique for piezoelectric transducer arrangements I.E.E.E. Trans on Sonics and Ultrasonics Vol.Su.15 No.1 Jan.68	C	E
*	10	W. Claussnitzer A generating voltmeter with calculable voltage current ratio for precise high voltage measurements I.E.E.E. Trans on Instruments and Measurement Vol.IM17 No.4 Dec.68	C Q	E

(Continued .....)

Significance Level	No.	Reference	Class	Source
	11	E.C. Cassidy, H.N. Cones, D.G. Wungch, S.R. Brooker Calibration of a Kerr Cell system for high voltage pulse measurements I.E.E.E. Trans on Instruments and measurement Vol.IM17 No.4 Dec.68	C Q	E
*	12	W.A. Riley & W.R. Klein Piezo Optic Coefficients of Liquids J.A.S.A. Vol.42 No.6 1967 p.1258	A I J K	E
	13	R.Vedam & G.Holton Specific volumes of water at high pressures, obtained from ultra sonic propagation measurements J.A.S.A. Vol.43 No.1 1968 p.108	A I K	E
*	14	I.W. Farmer & P.B. Attewell Experiments with water as a dynamic pressure medium Mine and Quarry Engineering Dec.63	A Z I K N	R.S.M.
	15	M.P. Hagelburg, G. Holton, S. Kao Calculation of B/A for water from measurements of ultrasonic velocity versus temperature and pressure 1 - 10,000 kg/cm^2 J.A.S.A. Vol.41 No.3 1967 p.564	I K	E

(Continued .....)

Significance Level	No.	Reference	Class	Source
	16	J.W. Robinson Measurements of plasma energy density and conductivity from 3 to 120 k bars J.A.P. Vol.38 No.1 Jan.1967	Y ? Z I	E
	17	M.E. Backman Form for the relation between stress and finite elastic and plastic strains under impulsive loading J.A.P. Vol.35 No.8 Aug.1964	I J	E
	18	T.J. Ahrens High pressure electrical behaviour and eq'n of state of magnesium oxide from shock wave measurements J.A.P. Vol.37 No.7 1966	I	E
	19	L.M. Barker, C.D. Lundergan and W. Herrmann Dynamic response of aluminum J.A.P. Vol.35 No.4 April 1964	I	E
	20	D.V. Keller and J.G. Trulio Mechansim of spall in Lucite J.A.P. Vol.34 No.1 Jan.1963 p.172	I	E

(Continued .....)

Significance Level	No.	Reference	Class	Source
	21	O.E. Jones and J.R. Holland Baushinger effect in explosively loaded mild steel J.A.P. Vol.35 No.13 1966	I	E
	22	T.J. Ahrens and M.H. Ruderman Imersed foil method for measuring shock wave profiles in solids J.A.P. Vol.37 No.13 1966	I	E
	23	B.M. Butcher and C.H. Karnes Strain rate effects in metals J.A.P. Vol.37 No.1 1966	I	E
	24	R.K. Linde and D.N. Schmidt Shock propagation in non-reactive porous solids J.A.P. Vol.37 No.8 July 1966	I	E
	25	R.K. Linde, W.J. Murri and D.G. Doran Shock induced electrical polarization of Alkali Halides J.A.P. Vol.37 No.7 1966	I	E
	26	L.M. Barker, B.M. Butcher and C.H. Karnes Yield point phenomena in impact loaded 1060 aluminum J.A.P. Vol.37 No.5 1966	I	E

(Continued .....)

Significance Level	No.	Reference	Class	Source
	27	B.R. Breed, C.L. Mader and D. Venable Technique for the determination of dynamic tensile strength characteristics J.A.P. Vol.38 No.8 July 1967	M I	E
	28	J.O. Erkman and A.B. Christensen Atenuation of shock waves in aluminium J.A.P. Vol.38 No.13 Dec.1967	I	E
	29	W. Zagieboylo Initial shock front interaction with solid models J.A.P. Vol.38 No.10 Sept.1967	I	E
	30	R.Bullough and J.J. Gilman Elastic explosions in solids caused by radiation J.A.P. Vol.37 No.6 1966	I	E
	31	B.W. Vanzart and R.C. DeHart Effect of hydrostatic pressure on shock waves from underwater explosions J.A.P. Vol.36 No.10 Oct.1965 p.3116	I	E

(Continued .....)

Significance Level	No.	Reference	Class	Source
	32	G.R. Fowles and W.M. Isbell A method for Hugoniot eq'n of state measurements at extreme pressures J.A.P. Vol.36 No.4 April 64 p.1377	I	E
	33	A.L. Ruoff Linear shock velocity - particle velocity relationship J.A.P. Vol.38 No.13 Dec.1967	I	E
	34	C.L. Dargan and A.E.D. Heyten Uniform field sparking voltages of gases in crossed magnetic fields Proc.I.E.E. Vol.115 No.7 July 1968	X W R	E P
*	35	E.F. Carome, C.E. Moeller and N.A. Clark Intense ruby laser induced acoustic pulses in liquids J.A.S.A. Vol.40 No.6 1966 p.1462	A E Z W X	E
***	36	K.W. Carley - Macauly, J.W. Hitchon and N.G. Maroudas Energy consumption in electrohydraulic crushing A.E.R.E. R 5054 1965	Z M P	P

(Continued .....)

Significance Level	No.	Reference	Class	Source
***	37	N.G. Maroudas and R.F. Taylor Processing in limited geometry Pt.IX Interim report on the electrohydraulic crushing of refractory materials A.E.R.E. M 1261 1963	Z M P	P
**	38	L.A. Yutkin The Electrohydraulic effect Mashgiz Moscow Translated as A.D. 267,722 1955	Z	P
***	39	A.E. Martin Ph.D Thesis on the underwater spark discharge Ann Arbour Michigan	Z Y	P
**	40	D.P. Frolov and N.A. Roi The electroacoustic efficiency of a spark discharge in water Soviet physics Doklady (Vol.3 No.1 1958 translation) Vol.118 Nos.1-6 original)	Z A	P
**	41	N.G. Maroudas, H.A. Johnston and E. Yigit The mechanism of electro-hydraulic crushing Dept. Mining and Mineral Technology RSM	Z M P	P

(Continued .....)

Significance Level	No.	Reference	Class	Source
	42	M. Allen Disinfecting with 'underwater lightning' New Scientist Vol.39 No.611 Aug.22 1968	A D Z	RSM P
	43	L. Edebo and I. Selin The effect of the pressure shock wave and some electrical quantities in the microbicidal effect of transient electric arcs in Aqueous systems. J. Gen. Microbiology Vol.50 p.253-259 1968	A D Z	P
**	44	K.W. Carley-Macauly, J.W. Hitchon and N.G. Maroudas Energy consumption in electrohydraulic crushing Trans. Inst. Chem. Eng. Vol.44 No.10 Dec.1966	A Z M P	P
	45	Materials handling research Hydraulic transportation of coarse solids U.S. Bureau of Mines No.RI 7283	G H	RSM
	46	Panel reports of the committee on rapid excavation Div.Eng.Nat.Res.Council, Nat. Acad.Sc., Nat.Acad.Eng., U.S. Bureau of Mines Sept. 1968	G	RSM

(Continued .....)

Significance Level	No.	Reference	Class	Source
	47	Symposium on R + D in Rapid Excavation Proceedings School of Engineering Sacremento State College California Oct.28-29 1968	?	RSM
	48	L.L. Felts, G.B. Clarck and J.J. Yancik A laboratory method of determining the thermodynamic efficiency of high explosives Mining Engineering March 1956	?	RSM
	49	J.P. Slifko Approximate methods of estimating energy spectra of line charges fired underwater J.A.S.A. Vol.41 No.1 1967 p.182	? A	E
	50	C.J. Haas and J.S. Rinehart Coupling between unconfined cylindrical explosive charges and rock Int J. Rock Mech. Vol.2 No.1 1965 p.13	? J M	RSM
	51	R.H. Cole Underwater explosions Dover N.Y. 1965	? A K .	P

(Continued .....)

Significance Level	No.	Reference	Class	Source
	52	D.F. Coates and M. Aslam The equations of state up to 250 kb of a magnetite and a quartzite Int J. Rock Mech Vol.5 p.495	I J M	RSM
	53	M. Young and M. Hercher Dynamics of laser induced breakdown in gases J.A.P. Vol.38 No.11 Oct.1967	E W	E
	54	W.T. Starr and L.J. Hague Effects of conditioning on life and reliability of capacitors I.E.E.E. Trans on Electrical Insulation Vol.E.I.2 No.2 Aug.1967	U Q	E
	55	B.R. Hayworth The behaviour of Polyester film energy storage capacitors I.E.E.E. Trans on Electrical Insulation Vol.E.I.3 No.2 May 1968	U Q	E
	56	Symposium on shaft sinking and tunnelling 1959 Inst. Mining Engineers	G	RSM
	57	F.C. Bond Mathematics of crushing and grinding in:- Recent developments in Mineral Dressing	P	RSM

(Continued .....)

Significance Level	No.	Reference	Class	Source
	58	F.C. Bond Work Indices Tabulated Mining Engineering Vol.5 March 1953	P	RSM
**	59	P.J.A. Fuller and J.H. Price Electrical conductivity of Manganin and Iron at high pressures Nature 193 p.262 Jan.20 1962	C I	E
**	60	D. Bernstein and D.D. Keough Piezoresistivity of manganin J.A.P. Vol.35 No.5 May 1964	C I	E
	61	L.O. Heflinger, R.F. Wuerkev and R.E. Brooks Holographic Interferometry J.A.P. Vol.37 No.2 1966	E	E
	62	D.F. Coates Rock mechanics principles Dept. of Energy, Mines and Resources, Canada Mines Branch Monograph 874	J M	RSM
*	63	Otter, Cassell and Hobbs Dynamic Relaxation Proc.I.Civ.Eng.Vol.35 pp 633-656 Dec.1966	J	P

(Continued .....)

Significance Level	No.	Reference	Class	Source
	64	I. Ito, M. Terada and T. Sakurai Stress waves in rocks and their effect on breakage Memoirs of the faculty of Engineering Kyoto University Vol. XXII Pt.1 1960	J L M	P NLL
	65	B.W. Holman and St. J.R.C. Shepherd Dielectric Mineral Separation. Notes on laboratory work Trans.I.M.M. p.343 Vol.33 1924	?	RSM
	66	B.R. Lazarenko Electrospark machining of metals Consultants Bureau 1964	X Q O	NLL
	67	J.R. Hearst, G.B. Irani and L.B. Geesaman Piezoelectric response of Z cut tourmaline to shocks of up to 21 kbars J.A.P. Vol.36 No.11 Nov.1965 p.3440	C I	E
	68	R.D. Medford and M. Pelovitz The analysis of transients in pulsed L C R Circuits with appreciable skin impedance Brit. J.A.P. (J. Phys D) Series 2 Vol.1 July 1968 p.901	Q R S	E

(Continued .....)

Significance Level	No.	Reference	Class	Source
	69	E.C. Cnare Magnetic flux compression by magnetically imploded metallic foils J.A.P. Vol.37 No.10 1966	? R	E
	70	Parkinson and Mulihall The generation of high magnetic fields Int. Cryogenics monograph series Heywood London 1967	? R S T U	NLL
	71	W.M. Albers Underwater acoustics Plenum Press N.Y. 1967	A B K	NLL
	72	G.E.G. Sargeant Review of acoustic equipments for studying submarine sediments TRANS IMM Sec.B Vol.75 1966 p.113	A B K	RSM
	73	H. Wakeshima and K. Nishigaka Mechanism of the inception of hydraulic cavitation. Japanese J.A.P. Vol.6 No.2 Feb.1967 p.263	A K	E
	74	R.A. Millar Hydrosonde, a marine seismic profiler Electronics and Communications (Canada) Vol.13 No.11 Nov.1965 p.29	A B K Z	NLL

(Continued .....)

Significance Level	No.	Reference	Class	Source
*	75	D.D. Caulfield Predicting sonic pulse shapes of underwater spark discharges A D 276 553 Woods Hole March 1962	A K Z	NLL P
**	76	Sheldon Gardner Electro Acoustic properties of the underwater spark discharge A D 259 947 Edo Corp 1 June 1961	K Z	NLL P
	77	R. Simon Transfer of the stress wave energy in the drill steel of a percussive drill to the rock Int J. Rock Mechanics Vol.1 p.397-411 May 1964	J K L M	RSM
	78	P.B. Attewell and D. Brentnall Internal friction: some considerations of the frequency response of rocks and other metallic and non metallic materials Int J. Rock Mechanics Vol.1 p.231-254 March 1964	K M	RSM
	79	N.G.W. Cook The application of seismic techniques to problems in rock mechanics Int J. Rock Mechanics Vol.1 p.169 March 1964	K M	RSM

(Continued .....)

Significance Level	No.	Reference	Class	Source
	80	W.G. Mayer Reflection and refraction of mechanical waves at solid liquid boundaries Pt I J.A.P. Vol.34 No.4 April 1963 Pt II J.A.P. Vol.34 No.11 Nov. 1963	I J	E
	81	J.L. Hill Torsional wave propagation from a rigid sphere semienbedded in an elastic half space J.A.S.A. Vol.40 No.2 1966	J K	E
**	82	A.G. Bagdoev Spatial non stationery motions of solid medium with shock waves Akad Sci Armenian SSR Erevan 1961 U.S. Trans as A.E.C. tr - 5400 Physics	K	P (Harwell)
*	83	G.L. Gooberman Ultrasonics theory and application E.U.P. London 1968	K	P
	84	F.J. Hiorns and J. Venables Propagation of fractures in brittle solids B.C.U.R.A. Vol.XXV No.10 pt.2 Oct.1961	L	RSM

(Continued .....)

Significance Level	No.	Reference	Class	Source
	85	G.M.C. Fisher The Auerbach Range in the Hertzian fracture of glass J.A.P. Vol.38 No.4 March 1967	L	E
**	86	W.G. Chase and H.K. Moore Exploding wires Vols 1, 2, 3, 4 Plenum Press N.Y. 1959	Y	RSM (Vol.1) NLL (rest)
*	87	J.R. Mcgrath Scaling underwater exploding wires J.A.P. Vol.37 No.12 1966	Y	E
	88	A. Hobson and C.K. Manka Premelt variation of current, temperature and resistance in exploding wires J.A.P. Vol.37 No.4 1966	Y	E
	89	H.D. Edelson and T. Korneff A comparative study of exploding wires in air and water J.A.P. Vol.37 No.5 1966	Y	E
	90	A.E. Vlastós Current pause in exploding wire discharges J.A.P. Vol.38 No.13 Dec.1966	Y	E

(Continued .....)

Significance Level	No.	Reference	Class	Source
*	91	W.G. Chase and C.V. Fish Charges in conductor shape during "Wire Explosion" J.A.P. Vol.38 No.10 Sept.1967	Y	E
	92	A.V. Hippel Dielectric materials and applications Technology Press MIT Wiley 1961	S Q	L P
	93	Y. Nakano, K. Hirano, H. Nishiyama and E. Yabe A study of the nanosecond triggering air gap Japanese J.A.P. Vol.6 No.7 July 1967	V W X	E
*	94	Z.T. Bieniawski The phenomena of terminal fracture velocity in rock Felsmechanik U Ingenieurgeol 6 113 - 125 1968	J L M	P
*	95	M.H. Miller The effect of stress wave duration on brittle fracture Int.J. Rock Mechanics Vol.3 No.3 p.191-203 1966	Z J L M	P

(Continued .....)

Significance Level	No.	Reference	Class	Source
***	96	H. Kolsky Stress waves in solids Clarendon Press 1953	I J K L ?	RSM
*	97	B.H. Bergstrom The electrohydraulic crusher Engineering and Mining Journal February 1961	A Z P	RSM
*	98	R.L. Kegg A study of energy requirements for electric discharge forming Trans A.S.M.E. Section B Vol. 86 No.2 p.127 May 1964	A Z O	Me
**	99	Y. Nakao and S. Sakamoto Research on underwater spark discharge Electrical Engineering in Japan Vol.87 No.5 p.83 1967	A Z W K	NLL P
	100	P. Felsenthal Nanosecond breakdown in liquid dielectrics J.A.P. Vol.37 No.10 Sept.1966	Z W A	E
	101	I.E. Lindstrom Plane shock initiation of an RDX plastic bonded explosive J.A.P. Vol.37 No.13 1966	I	E

(Continued .....)

Significance Level	No.	Reference	Class	Source
	102	H.D. Mallory Evidence of turbulence in the reaction zone of detonating liquid explosives J.A.P. Vol.37 No.13 1966	I	E
	103	V.G. Gregson Jr. Optical lever observation of hypervelocity impact shock waves J.A.P. Vol.38 No.4 March 1967	I	E
	104	D.B. Larson A shock induced phase transformation in Bismuth J.A.P. Vol.38 No.4 March 1967	I	E
	105	A.Jones, W.M. Isbell and C.J. Maiden Measurement of the very high pressure properties of materials using a light gas gun J.A.P. Vol.37 No.9 1966	I	E
	106	L.C. Burkhardt et al Pinch Effect J.A.P. Vol.28 No.5 May 1957	X T R	E P
	107	J.E. Harry and A.E. Guile Constricted or diffuse arcs rotating in high pressure fields in air at atmospheric pressure Proc.I.E.E. Vol.115 No.7 July 1968	X T R	E P

(Continued .....)

Significance Level	No.	Reference	Class	Source
	108	R.H. Galloway, H.McL. Ryan and M.F. Scott Calculation of electric fields by digital computer Proc.I.E.E. Vol.114 No.6 June 1967	T	E P
**	109	L.L. Alston High voltage technology Harwell P.G. Series O.U.P. 1968	C Q R S T U V W X	E P
	110	W.Y. Chen and J.F. Kulikowski Approximate calculation of a complex 2 dimensional electric field Proc.I.E.E. Vol.113 No.6 June 1966	T	E P
***	111	F.B.A. Frungel High speed pulse technology Vol. 1 Academic Press Inc. N.Y. 1965	A Z Q R S T U V W X Y I K N O D	P
	112	S. Seely Introduction to electro-magnetic fields McGraw Hill London 1958	T Q R	E P
	113	A. Cermat and P. Silvester Solutions of 2 dimensional field problems by boundary relaxation Proc.I.E.E. Sept.1968 Vol. 115 No.9	T	E P

(Continued .....)

Significance Level	No.	Reference	Class	Source
	114	H.McL. Ryan Prediction of alternating sparking voltages Proc.I.E.E. Vol.114 No.11 Nov. 1967	T W X	E P
	115	O. Farish and D.J. Tedford Temporal development of spark breakdown in nitrogen and air Proc.I.E.E. Vol.114 Feb.1967	T W	E P
	116	D.T.A. Blair Distribution of ionization in discharge gaps irradiated with radioactive material Proc.I.E.E. Vol.113 No.12 Dec. 1966	T W	E P
	117	H.McL. Ryan and C.A. Walley Sparking voltage of a conductor passing through an earthed plate Proc.I.E.E. Vol.114 No.1 Jan. 1967	T W	E P
	118	F.D.A. Boylett and B.G. Williams Influence of space change on corona growth in a positive point-plane gap in air subjected to a voltage impulse Proc.I.E.E. Vol.115 No.7 July 1968	T W	E P

Significance Level	No.	Reference	Class	Source
	119	A.E. Guile and K.A. Naylor Further correlation of experimental data for electric arcs in transverse magnetic fields Proc.I.E.E. Vol.115 No.9 Sept.1968	T W R	E P
	120	N.L. Allen and K.A. Bunting Breakdown of gases in crossed electric and magnetic fields with loss mechanisms Proc.I.E.E. Vol.114 No.8 Aug.1967	R T W	E P
	121	P. Felsenthal Nanosecond pulse microwave breakdown in air J.A.P. Vol.37 No.12 1966	T W	E P
	122	E. Kuffel and M. Abdullah Corona and breakdown-voltage characteristics in sphere-plane and rod-rod gaps under impulse voltages of various wavefront durations Proc.I.E.E. Vol.113 No.6 June 1966	T W	E P
*	123	Annual report on electrical insulation 1956-1968 Nat.Acad.Sci.	Q T U W	NLL

(Continued .....)

Significance Level	No.	Reference	Class	Source
**	124	C.C. Hsiao, S.R. Moghe, C.K. Soong and W.L. Yin Internal fracture caused by focusing of explosive waves J.A.P. Vol.37 No.6 1966	I J K L	E
	125	P. Silvester Network analogy solution of skin and proximity effect problems I.E.E.E. Trans on Power Apparatus and Systems Vol.PAS 86 No.2 Feb.1967	R S	E
	126	N.W. Snyder Energy conversion for space power. Progress in astronautics and rocketry Vol.3 Acad. Press 1961	Q	NLL
	127	La Physique des forces electrostatiques C.N.R.S. 1960	Q	LP
***	128	N.P. Mel'nikov, G.A. Ostroumov, and M. Yu Stoyak Formation of electrical breakdown in aqueous sodium chloride solutions Sov.Phys.Tech.Phys. Vol.9 No.5 p.730 Nov.1964	A W	P NLL

(Continued .....)

Significance Level	No.	Reference	Class	Source
	129	Mechanical behaviour of materials under dynamic loads Symposium San Antonio Texas Sept.6-8 1967	J I K L	NLL
	130	R.J. Thomas and J.R. Hearst An electronic scheme for measurement of exploding wire energy Univ. of California E O Lawrence Radiation Lab. U.C.R.L. 12065	Y	P NLL
	131	Grabwsky and Durran Gauge for measuring impulsive pressure in a container subjected to large time varying applied voltages Rev. Sci. Inst. Vol.39 No.1 Jan.1963	Z C	P NLL
	132	J. Skowronski New system of spark-gap electrodes for measurement of dielectric strength of insulating liquids Proc.I.E.E. June 1966, Vol.113 No.6	W Q	P E
	133	J. Crawley and L. Angerer Investigation of the electrical breakdown of transformer oil in Skowronski's cup sphere spark gap Proc.I.E.E. June 1966 Vol. 113 No.6	W Q	P E

(Continued .....)

Significance Level	No.	Reference	Class	Source
	134	H.McL. Ryan and C.A. Walley Field auxiliary factors for simple electrode geometries Proc.I.E.E. Vol.114 No.10 October 1967	T	P E
	135	P.P. Budnikow and N.I. Nerkistch Moskav Die Zerkleinerungsabeit inder Pulvertechnologies Silikat Technik, 10 Oct. 1961	Z	NLL
**	136	E. Yigit Dept. of Mining and Min. Tech. I.C., D.I.C. thesis, 1967	L Z P J	RSM P
*	137	J.S. Rinehart On fractures caused by explosions and impacts Colorado School of Mines Quarterly Vol.55 No.4 October 1960	I J L ?	RSM
	138	Rinehart and Pearson Explosive working of metals Pergammon 1963	? O	NLL
	139	D.B. Lombard Hugoniot Eq'n of state for rocks Livermore Site Radiation Labs. Univ. California	J M ? F	NLL

(Continued .....)

Significance Level	No.	Reference	Class	Source
	140	Epshteyn, Arsh and Vitort New methods of crushing rock AD 288 713	Z M	NLL
	141	K.C. Kao and J.P.C. McMath The effect of the rate of rise of applied field and hydrostatic pressure on the electric strengths of fluid dielectrics 1968 Conference on Electrical Insulation	I Q W	P
	142	Ihor M. Vitkovitsky Similarities in spark and exploding wire discharges Exploding wires Vol.4	W Z Y X	P
**	143	H.K. Kutter The electrohydraulic effect, potential application in rock fragmentation U.S. Bureau Mines RI 7317 December 1969	C L M Z Y	P
	144	Z. Krasucki Effect of dielectric thickness on the onset of discharges in liquid-solid dielectrics E.R.A. Report 5197 1967	W Q U	P

(Continued .....)

Significance Level	No.	Reference	Class	Source
	145	Leif BJØRNØ A comparison between measured pressure waves in water arising from electrical discharges and detonation of small amounts of chemical explosives A.S.M.E. Paper No.69 Unt 1 (Underwater technology conference San Diego California 9-12 March, 1969)	? Z C A	P
	146	D.F. Kelsall, K.J. Reid and C.J. Restarick Continuous grinding in a small wet ball mill Powder technology 1 291-300 No.5 Feb.1968	P *	P
*	147	E.I. Parknomenko Electrical properties of rocks Plenum Press N.Y. 1967	M	P
	148	Meloy and Gumtz The fracture of single, brittle Hetetogeneous particles - statistical derivation of the mass distribution equation Powder Technology Vol.12 1968-69	L M P	P
*	149	Lynch and Bull U of Queensland Aug.1966 Winter School on Mineral processing	*	P

(Continued .....)

Significance Level	No.	Reference	Class	Source
	150	Symposium on Optimum Control 14 April-16 April 1964 Imperial College	*	P
	151	Dorr and Anable Free grinding and classification in Rocky Mountain Fund Volume on "Milling Methods" Trans.A.I.M.E. 1934	* P	RSM
	152	R.T. Hukki An analysis of mill and classifier performance in a closed grinding circuit Trans A.I.M.E. Vol.238 Sept.1967	* P	RSM
	153	D.F. Kelsall, P.S.B. Stewart and K.J. Reid Confirmation of a dynamic model of closed circuit grinding with a wet ball mill Trans I.M.M. Sec.C Vol.77 March 1967	* P	RSM
**	154	T.G. Callcott Solution of comminution circuits Trans I.M.M. Sec.C Vol.76 March 1967	* P	RSM

(Continued .....)

Significance Level	No.	Reference	Class	Source
*	155	D. Eisenberg and W. Kauzmann The structure and properties of water Oxford Clarendon Press 1969	A	LP
**	156	W.G. Chace et al A bibliography of the electrically exploded conductor phenomenon A D 662 345	Z Y X ?	P
*	157	W.J. Guman et al Studies on an electric discharge underwater sound source A D 681 862	Z B	P
*	158	W.J. Guman et al Study of a pulsed underwater sound projector A D 648 003	Z	P
*	159	W.J. Guman et al Study of a pulsed underwater sound projector A D 648 216	Z	P
*	160	J.R. McGrath Some mathematical aspects of underwater explosions caused by exploding wires A D 659 297	Y K	P

Significance Level	No.	Reference	Class	Source
	161	J.R. McGrath Underwater exploding wires A D 663 085 Nov. 1967	Y	P
*	162	H.A. Wright Underwater electrodeless spark sound source A D 636 168 July 1966	Y Z	P
*	163	H.A. Wright Underwater electrodeless spark sound source A D 659 534 Oct. 1967	A Z	P
*	164	L.A. Coleburn et al Regular reflection of oblique shock waves in water A D 687 094	I J K	P
	165	J.O. Outwater et al On the fracture energy of glass A D 640 848	L	P
	166	Y.A. Kotov and M.A. Melnikov Recording shock waves and exploding wire electrical characteristics A D 685 489	Z Y C	P

(Continued .....)

Significance Level	No.	Reference	Class	Source
*	167	N.C. Chase et al I. Studies of electrically exploding wires and films. II. Studies of crossed field plasma accelerators and plasma diagnostic techniques A D 628 034	Y	P
*	168	N. Bobrov The surprises of E.G.E. A D 676 160	P Z H	P
***	169	I.D. Smith Improvements in or relating to capacitative stores for electrical energy UK Pat No. 1,161,347	A Q T U W	P
	170	D. White and D.I. Bell Improvements in or relating to fuel elements for nuclear reactors UK Pat No. 991,424	Z O !	P
*	171	Improvements in or relating to gears and methods of manufacturing the same UK Pat No. 1,019,196	Z O !	P
	172	Improvements in the manufacture of multilayer vessels UK Pat No. 1,020,912	Z O !	P

(Continued .....)

Significance Level	No.	Reference	Class	Source
	173	Method and apparatus for forming a workpiece UK Pat No. 1,032,834	Z O !	P
	174	Improvements in or relating to a process and apparatus for the manufacture of Prosthetic accessories UK Pat No. 1,068,551	Z O ! D	P
	175	Tool equipment for electro hydraulic forming machines UK Pat No. 1,086,395	Z O !	P
	176	Methods of and apparatus for shaping workpieces by electro-magnetic forming UK Pat No. 1,104,495	O T Z !	P
	177	Improvements in or relating to electrohydraulic forming apparatus UK Pat No. 1,109,146 UK Pat No. 1,109,147	Z O!	P
	178	Improvements in electro-hydraulic systems UK Pat No. 1,113,750	Z O !	P
	179	Electromagnetic forming UK Pat No. 1,116,242	R O !	P

(Continued .....)

Significance Level	No.	Reference	Class	Source
*	180	Forming and/or shearing UK Pat No. 1,163,704	Y Z O R !	P
	181	Metal forming device and method US Pat No. 2,976,907	R O !	P
	182	Shock aided extrusion US Pat No. 3,181,328	Z O !	P
	183	Metal forming devices using direct electrode contact US Pat No. 3,187,532	R O !	P
	184	Electrical discharge apparatus for forming US Pat No. 3,188,844	Z O !	P
	185	Devices for metal forming by magnetic tension US Pat No. 3,196,649	R O !	P
	186	Electrical explosion forming US Pat No. 3,200,626	Z O !	P
	187	Explosive forming by electrical discharge - method and apparatus US Pat No. 3,203,212	Z O !	P

(Continued .....)

Significance Level	No.	Reference	Class	Source
	188	Electrohydraulic forming method and apparatus US Pat No. 3,222,902	Z O !	P
	189	Method and apparatus for utilizing electrical discharge pressure waves US Pat No. 3,225,578	Z O !	P
	190	Hydrospark forming apparatus US Pat No. 3,248,917	Z O !	P
	191	Electrohydraulic impulse scoring and/or weakening of thin materials US Pat No. 3,267,780	Z R O !	P
	192	Process for the manufacture of a gear US Pat No. 3,286,329	Z O !	P
	193	Method of seamless explosive plating or cladding of thick-walled vessels US Pat No. 3,292,253	? Z O !	P
	194	Control of stresses during shock aided hydrostatic extrusion US Pat No. 3,306,089	Z O !	P

(Continued .....)

Significance Level	No.	Reference	Class	Source
	195	Forming apparatus U.S. Pat No. 3,338,080	Z O !	P
	196	Forming apparatus U.S. Pat No. 3,345,843	Z O !	P
	197	Electrohydraulic forming apparatus U.S. Pat No. 3,558,487	Z O !	P
	198	High pressure generating apparatus U.S. Pat No. 3,208,254	Z O !	P
	199	Underwater sound producing system U.K. Pat No. 1,120,601	Z A B !	P
	200	Spark discharge elements for continuous seismic soundings U.K. Pat No. 1,154,394	A Z B !	P
	201	Multiple electrode spark source U.S. Pat No. 3,245,032	Z A B !	P
	202	Apparatus for an electro-hydraulic system U.S. Pat No. 3,283,294	Z A B !	P

(Continued .....)

Significance Level	No.	Reference	Class	Source
	203	Underwater spark discharge sound producing system U.S. Pat No. 3,286,226	Z A B !	P
	204	Generation of signals by rapid vaporization of metallic elements U.S. Pat No. 3,332,510	Z A B Y !	P
	205	Spark gap system U.K. Pat No. 754,508	V !	P
	206	Blown discharge gap switch U.K. Pat No. 779,585	V !	P
	207	Improvements relating to electrical spark gap discharge apparatus U.K. Pat No. 781,378	V !	P
	208	Improvements relating to spark gap apparatus U.K. Pat No. 822,000	V !	P
	209	Improvements in or relating to an electrical impulse current installation U.K. Pat No. 852,445	V S R !	P
	210	Improvements in or relating to impulse current installations U.K. Pat No. 855,584	V S R !	P

(Continued .....)

Significance Level	No.	Reference	Class	Source
	211	Pulse generator U.S. Pat No. 3,225,223	S Q !	P
	212	Electrical spark gap with insulation which maintains its high insulative character throughout its operation U.S. Pat No. 3,287,590	V !	P
	213	Electrical discharge devices U.S. Pat No. 3,317,777	V !	P
	214	Spark Gaps U.S. Pat No. 3,346,762	V !	P
	215	Improvements in or relating to the production of Antigenic material U.K. Pat No. 1,108,524	Z D !	P
	216	Method and device for electrically sterilizing and cleaning milking machines and the like U.K. Pat No. 879,945	Z D !	P
	217	Apparatus and method for electrically treating materials U.K. Pat No. 1,122,181	Z P I !	P

(Continued .....)

Significance Level	No.	Reference	Class	Source
	218	Electrohydraulic processes and apparatus for initiating chemical and physical reactions U.K. Pat No. 1,056,074	Z P I !	P
*	219	CCCP Pat No. 118,692 50_c17_{40}	Z P !	P
**	220	Method of crushing ores with explosive energy released in a liquid medium and apparatus therefore U.S. Pat No. 3,207,447	Z P !	P
***	221	Improvements in or relating to electrohydraulic crushing techniques U.K. Pat No. 1,121,786	Z P !	P
	222	Crushing apparatus with sonic wave action U.S. Pat No. 3,284,010	P K !	P
	223	Method of splitting non metallic brittle materials and devices for carrying out such methods U.S. Pat No. 3,219,280	M L P !	P
	224	Method for loosening frozen ore beds U.S. Pat No. 3,181,799	Z !	P

(Continued .....)

Significance Level	No.	Reference	Class	Source
	225	Shock sintering process U.K. Pat No. 1,148,608	Z O !	P
	226	Method and apparatus for shaping objects from ceramic raw material U.K. Pat No. 1,148,112	Z O !	P
	227	Electrohydraulic system and working fluids therefore U.K. Pat No. 1,073,739	Z W !	P
	228	Electrical circuit for electrohydraulic systems U.S. Pat No. 3,234,429	Z S !	P
	229	A method and apparatus for storing electrical energy U.K. Pat No. 1,108,237	Z S !	P
	230	Improvements in spark discharge electrodes for electrohydraulic systems U.K. Pat No. 1,068,440	Z !	P
	231	W. Johnson The explosive forming of tube 9th Commonwealth Mining and Metallurgical Congress, 1969	O ? Z R	P

(Continued .....)

Significance Level	No.	Reference	Class	Source
	232	V.N. Pastukhov Calculating the initial stages of an electrical discharge in water 1968 Journal of Tech. Phys. Sov. Phys. Vol.38 No.2	Z W	P
	233	Improvements in or relating to electrohydraulic forming apparatus U.K. Pat No. 1,109,146	Z O !	P
	234	R.C. Wrede Introduction to vector and tensor analysis Wiley 1963	*	LP
	235	G.W.C. Kaye and T.H. Laby Tables of physical and chemical constants Longmans Green 1966	R J K	P
	236	K.R. Spangenberg Fundamentals of electron devices McGraw Hill 1957	Q W X	P
	237	E.A. Erdélyi and E.F. Fuchs Non linear magnetic field analysis of D.C. machines I.E.E.E. Trans on Power Apparatus and Systems Vol. PAS 89 No.7 1970	T	P

Significance Level	No.	Reference	Class	Source
	238	P.E. Haskell and C.H.J. Beaven Computer simulation of the transient performance of a closed circuit grinding system Trans.I.M.M. Section C Vol.79 1970 p.C238	*	P
	239	W. Johnson The explosive forming of tube 9th Commonwealth Mining and Metallurgical Conference I.M.M. 1969	O ?	P
	240	F.J. McCoy and W.R. Bell Electrostatic generators for power production 1967 Conference on Electrical Insulation and Dielectric Phenomena	Q	P
	241	British Standard 1984 Single sized gravel aggregates for roads 1953	M *	RSM

Cross Index

A Underwater

12 13 14 35 40 42 43 44 49 51 71
72 73 74 75 97 98 99 100 111 128 145
155 163 169 202 203 204

B Oceanography

72 74 157 199 200 201 202 203 204

C Instruments

3 4 5 6 7 8 9 10 11 59 60
67 109 131 143 145 166

D Bio Science

42 43 111 174 215 216 217

E Lasers

35 53 61

F Nuclear Devices

-

G Rapid Excavation

45 46 47 56

H Materials Handling

45

(Continued .....)

I High Pressures

3 4 5 6 12 13 14 15 16 17 18
19 20 21 22 23 24 25 26 27 28 29
30 31 32 33 52 59 60 67 96 101 102
103 104 105 111 124 129 218

J Stress Analysis

6 12 13 17 50 52 62 63 64 77 80
81 82 94 95 96 124 129 139 235

K Acoustics

6 12 13 14 15 51 71 72 73 74 75
76 77 78 79 81 82 83 96 111 124 129
160 164 222 235

L Fracture

6 64 77 84 85 94 95 96 124 129 136
137 143 158 165 233

M Rock

6 36 37 41 44 50 52 62 64 77 78
79 94 95 139 140 143 147 148 168 223 241

N Erosion

14

O Metal Forming

98 111 138 170 171 172 173 174 175 176 177
178 179 180 181 182 183 184 185 186 187 188
189 190 191 192 193 194 195 196 197 198 225
226 231 233 239

(Continued .....)

P Crushers

36 37 41 44 57 58 97 136 146 148 151
152 153 154 168 218 219 220 221 222

Q High Voltage Systems

10 11 54 55 66 68 92 109 111 123 126
127 132 133 141 144 211 236 240

R Magnetics

34 68 69 70 106 107 109 111 112 119 120
125 180 181 183 185 191 209 210 231 235

S Circuits

68 70 92 109 111 125 209 210 211 228 229

T Fields

106 107 108 109 110 111 112 113 114 115 116
117 118 119 120 121 122 123 134 169 176 237

U Capacitors

54 55 70 109 111 123 144 169

V Switches

2 93 109 111 205 206 207 208 209 210 212
213 214

W Breakdown

2 34 35 53 93 99 100 109 111 114 115
116 117 118 120 121 122 123 128 132 133 141

(Continued .....)

W Breakdown (ctd)

142 144 169 227 232 236

X Sparks

1 2 8 34 35 66 93 99 106 107 109

111 114 142 169 236

Y Exploding Wires

16 39 86 87 88 89 90 91 111 130 142

143 156 160 161 162 166 167 180 204 239

Z Electrohydraulics

14 16 35 36 37 38 39 40 41 42 43

44 74 75 76 95 97 98 99 100 111 131

135 136 140 142 143 145 156 157 158 159 162

163 166 168 169 170 171 172 173 174 175 176

177 178 180 182 184 186 187 188 189 190 191

192 193 194 195 196 197 198 199 200 201 202

203 204 215 216 217 218 219 220 221 224 225

226 227 228 229 230 231 232 233

! Patents

Nos. 169 through to 230 233

* Process Modelling and Control

146 149 150 151 152 153 154 234 238 241

? Explosives

16 48 49 50 51 69 70 101 102 137

138 139 145 156 193 231 239

Appendix 9 - List of Figures

Part 2

2/1	Breakdown time-lag versus voltage
2/2	Time-lag versus standard deviation of time-lag
2/3	Distribution of breakdown time-lags at 40KV
2/4	" " " " " " 35KV
2/5	" " " " " " 30KV
2/6	" " " " " " 25KV
2/7	Predicted breakdown time-lags

Part 3

3/1	Momentum range experiment
3/2 - 3/5	Impulse versus pellet length
3/6	Time constant, impulse and pressure versus $\sqrt{LC}$

Part 4

4/1	Release wavefront diagram
4/2	Failure by reflected stresses
4/3 - 4/18	Distortion grids
4/19	Trajectories of points on a dynamically loaded square
4/20 - 4/39	Stress isometrics
4/40	Impulse, stress ratio, and stress ratio per impulse versus time constant
4/41	Fracture criterion
4/42	Computed fracture pattern

Part 5

5/1	Crushing efficiency versus point load strength
5/2	Kick's Constant versus point load strength
5/3	Bond's Index versus compressive strength
5/4	Kick's Constant versus compressive strength
5/5	Crushing power consumption versus water conductivity
5/6	Size distribution of crushed Aberdeen Granite
5/7	" " " " Bathstone
5/8	" " " " Cambourne Granite
5/9	" " " " Carrera Marble
5/10	" " " " Darley Dale Sandstone
5/11	" " " " Dolorite
5/12	" " " " Pennant Sandstone
5/13	" " " " Derbyshire Granite
5/14	" " " " Turkish Chromite
5/15	" " " " Nickel Ore
5/16	" " " " South African Gold Ore
5/17	" " " " Beryllium Ore

Part 6

6/1	Separating crusher
6/2	Length jig
6/3 - 6/5	Development of the aperture concept
6/6	Basic aperture set for shape experiments
6/7	Final primary space for shape experiment
6/8	Axes for shape isometrics

(Continued .....)

6/9 - 6/26 Shape operators

6/27 Process Topology

6/28 Topological diagram of a rod mill

6/29 Signal as a sum of unit impulses

6/30 Rectangular aperture set

6/31 Irregular aperture set

6/32 Plant flow sheet

6/33 Grinding circuit

6/34 - 6/43 Dynamics of grinding

6/44 - 6/52 Dynamics of grindability

Appendix 1

A1/1 Block diagram of charging control unit

A1/2 High voltage circuit

A1/3 Electrode system

A1/4 Measuring circuit

A1/5 Typical oscillogram

Appendix 2

A2/1 Water programme flow chart

A2/2A Grid for water programme

A2/2B Section of grid

A2/3 Area of grid element

(Continued .....)

Appendix 3

A3/1 Interlaced mesh

A3/2 Boundary of mesh

A3/3 Flow chart for stress analysis programmes

A3/4 Effect of numerical method on pulse shape

Appendix 4

A4/1 Resistive charging

A4/2 Inductive charging

Appendix 6

A6/1 Electrohydraulic crusher

A6/2 Crusher circuit diagram